UNIVERSIDAT POLITÉCNICA DE VALENCIA

Institute for Energy Engineering

Department of Nuclear and Chemical Engineering

COUPLED LAGRANGE-EULER MODEL FOR SIMULATION OF BUBBLY FLOW IN VERTICAL PIPES CONSIDERING TURBULENT 3D RANDOM WALKS MODELS AND BUBBLES INTERACTION EFFECTS

Ph.D. Thesis

Presented by:

Mohamed Ali Abdelaziz Essa

Supervisors

Dr. José-Luis Muñoz-Cobo

Dr. Sergio Chiva Vicente

COUPLED LAGRANGE-EULER MODEL FOR SIMULATION OF BUBBLY FLOW IN VERTICAL PIPES CONSIDERING TURBULENT 3D RANDOM WALKS MODELS AND BUBBLES INTERACTION EFFECTS

by

Mohamed Ali Abdelaziz Essa

Submitted to the Department of Mechanical Engineering and Design in Partial Fulfillment of the Requirements for the Degree of

Doctor of PHILOSOPHY

At the

Polytechnic University of Valencia

November 2012

Certified by Dr. José-Luis Muñoz-Cobo. Thesis supervisor

Certified by Dr. Sergio Chiva Vicente. Thesis supervisor

Accepted by…
Accepted by…
Accepted by…
Accepted by…
Accepted by…

Abstract

A novel Two-way coupled Euler-Lagrange mode, including bubble-bubble collision, coalescence, with variable bubble radius, and bubbles breakup was applied to simulate air-water bubbly flow in vertical pipes. This approach uses the Continuous Random Walks CRW models for creating the velocity fluctuations according to the given state of turbulent kinetic energy k and Dissipation rate ε at the location of the bubbles which is solved by the $k-\varepsilon$ turbulence model. This dissertation i) describes the development of the Euler-Lagrange Approach under study, ii) presents a study for the two-way coupling effect on both the continuous and dispersed phases properties, iii) studies the effect of both the lift force coefficient and bubble induced turbulence BIT relations on the gas void fraction distributions, iv) studies the effect of the bubbles coalescence and breakup on bubble sizes and gas void fraction distributions. And presents the results of the simulations performed under each of these considerations.

The two-way coupling process takes the effect of the dispersed phase on the continuous one through inserting source terms in the conservation equations of momentum and Turbulence. Also it modifies the volume of the computational cells in the Euler solver available for the continuous phase according to the void fraction of each cell. During the two-way coupling process, some studies needed to be performed like the adjustment of the lift force coefficient and the $S_{k,BIT}$ relation due to the change of the liquid velocity profiles as a result of the two-way coupling.

The bubble-bubble collision was applied in the two-way coupling process. It was found that considering the collision appears on the void fraction distribution only in the high velocity and high gas holdup cases with very small effect. The bubble-bubble coalescence was applied as a complementary part of the collision process using the film drainage model of Chesters (1991). This model compares the film drainage time with the contact time to calculate the coalescence efficiency. The coalescence model was tested first before applying the breakup, so the bubbles size increased only and this affected on the void fraction distribution badly. Then the breakup model of Martínez-Bazán (1999a, b) was applied to perform the equilibrium in the bubble sizes. These two processes of the coalescence and breakup found to consume long computational time, the reason that did not give us a chance for testing many cases with considering both coalescence and breakup.

The main investigation point through the development of this work was the BIT kinetic energy term and its effect on the used CRW model. This was considered in nearly every phase of the model development to study the effect of the BIT under the different considerations of the bubbles interaction mechanisms. It could be concluded a final

expression for the BIT relation that is used successfully with the CRW models under consideration.

Resumen

Una nueva aproximación euleriana-lagarangiana, en su forma de acople en dos vías, para la simulación de flujo de burbujas, agua-aire es presentada en la tesis, en la que se incluyen los efectos de las colisiones entre burbujas, así como las posibles roturas o coalescencia de burbujas. Esta aproximación utiliza el modelo Continuous Random Walk, CRW, para tener en cuenta las fluctuaciones de la velocidad. Esta aproximación se enmarca dentro de un modelo de turbulencia k-epsilon para la fase continua del líquido. En esta tesis se estudiarán los métodos para realizar el acople entre ambas aproximaciones, el efecto de la fuerza lift y de la dispersión turbulenta sobre la distribución de la fracción de huecos, así como los modelos de coalescencia y rotura de burbujas que puedan ser empleados en este tipo de aproximación.

Se ha partido de un código euleriano para simular la parte continua, y sobre él se ha acoplado la aproximación lagrangiana. Para que ese acople afecte a la fase continua sobre su solver ser han añadido fuentes de momento y turbulencia. Además se ha modificado el volumen computacional de cada celda para que tenga en consideración el volumen ocupado por la fase dispersa. El acople en doble vía hace que los perfiles de velocidad y turbulencia de la fase continua se modifiquen notablemente y que se aproximen a los reales, lo que resulta básico para la correcta simulación de las fuerzas interfaciales.

La colisión entre burbujas, y burbujas y pared se ha incluido. Este efecto es necesario como paso previo a incluir los procesos de rotura o coalescencia de burbujas, aunque la colisión en sí tenga efectos limitados en la distribución de la fracción de huecos. El proceso de coalescencia se basa en el modelo de Chester (1991), el modelo compara el tiempo de colisión con el tiempo de drenaje de la película entre burbujas para determinar si existe o no coalescencia. El modelo de rotura se basa en el modelo de Martínez-Bazán.

Uno de los principales hitos de la tesis es el desarrollo realizado para incluir la fuente de turbulencia inducida en la fase continua debido a la presencia de burbujas y su inclusión el CRW. Esto permite evitar la utilización de los modelos de de fuerza d dispersión turbulenta y disponer así de un modelo mucho más realista. Diferentes metodologías han sido probadas, y una expresión es propuesta que ofrece resultados muy acordes con los experimentales. En la tesis se hace uso de resultados experimentales para testear las soluciones aportadas en cada caso.

Resum

Una nova aproximació euleriana-lagarangiana, en la seva forma d'acoblament en dues vies, per a la simulació de flux de bombolles, aigua-aire és presentada a la tesi. També s'inclouen els efectes de les col.lisions entre bombolles, així com les possibles trencaments o coalescència de bombolles. Aquesta aproximació utilitza el model Continuous Random Walk, CRW, per tenir en compte les fluctuacions de la velocitat. Aquesta aproximació s'emmarca dins d'un model de turbulència k-epsilon per a la fase contínua del líquid. En aquesta tesi s'estudiaran els mètodes per realitzar l'acoblament entre les dues aproximacions, l'efecte de la força lift i de la dispersió turbulenta sobre la distribució de la fracció de buits, així com els models de coalescència i trencament de bombolles que puguin ser emprats en aquest tipus d'aproximació.

S'ha partit d'un codi eulerià per simular la part contínua, i sobre ell s'ha acoblat l'aproximació lagrangiana. Perquè aquest acoblament afecti al solver de la fase contínua s'ha de afegir fonts de moment i turbulència. A més s'ha modificat el volum computacional de cada cel.la perquè tingui en consideració el volum ocupat per la fase dispersa. El acoblament en doble via fa que els perfils de velocitat i turbulència de la fase contínua es modifiquin notablement i que s'aproximin als reals, el que resulta bàsic per a la correcta simulació de les forces interfacials.

La col.lisió entre bombolles, i bombolles i paret s'ha inclòs. Aquest efecte és necessari com a pas previ a incloure els processos de ruptura o coalescència, encara que la col.lisió en si tingui efectes limitats en la distribució de la fracció de buits. El procés de coalescència es basa en el model de Chester (1991), el model compara el temps de col.lisió amb el temps de drenatge de la pel.lícula entre bombolles per determinar si existeix o no coalescència. El model de ruptura es basa en el model de Martínez-Bazán.

Un dels principals fites de la tesi és el desenvolupament realitzat per incloure la font de turbulència induïda en la fase contínua a causa de la presència de bombolles i la seva inclusió el CRW. Això permet evitar la utilització dels models de força de dispersió turbulenta i disposar així d'un model molt més realista. Diferents metodologies han estat provades, i una expressió és proposta que ofereix resultats molt d'acord amb els experimentals. En la tesi es fa ús de resultats experimentals per testejar les solucions aportades en cada cas.

Acknowledgements

First of all, praise to Allah the greatest, the most merciful, the all beneficent, the omniscient, who guided the man to know which he did not know.

Then, as recognition of gratitude, I introduce my great respect and thanks for my parents for their continuous material and moral assistance in hole my life until being in the current position.

I'd like also to thank my wife who was beside me at the good and bad moments in this work with sharing me both of them with complete happiness and satisfaction. My thanks also to all my family and my friends, how was beside me during this work.

I'd like to express also my great gratitude to my supervisors José-Luis and Sergio Chiva. With whom I learned a lot especially for Sergio Chiva for his continuous guidance and continuation in this work. We found many times of tensions and problems but finally we could solve the problems with patience and discussion.

I'd like to express my thanks also to Dirk Lucas, Eckhard Krepper, Yixiang Liao from the HZDR who aided me during the development of my code in my stage in Dresden, Germany. Many thanks also to Filippo en München, Germany with who I had beneficial discussions during the last period of this work.

Contents

List of Tables

List of Figures

Nomenclature

a	The dimension of the ellipsoid in the directions parallel to the wall (m)
A	Surface are (m^2)
As_{De}	The collision cross sectional area between bubble and eddy (m^2)
BIT	Bubble induced turbulence
BIT_c	BIT effect according to bubble density concentration.
C	Constant or coefficient
CRW	Continuous Random walk
C_{tb}	Coefficient of Bubble Induced Turbulence kinetic energy
D,d	Diameter (m)
DBM	Discrete bubble model
Dp	Pipe diameter (m)
e	The kinetic energy of an eddy
$\hat{e}_r, \hat{e}_\theta, \hat{e}_z$	Unit vectors at (r,θ,z) cylindrical coordinates directions.
E	Aspect ratio (-)
E_c	The surface energy of the bubble
Eo	Eötvös number (-)
er	Restitution coefficient
F	Force (N)
$f(D_b)$	Breakup frequency of bubble of size D (1/s)
$fa(\alpha)$	Turbulence damping factor due to the dispersed phase eqn. (2.109)
$f_{D,coll}$	The collision rate of bubbles with eddies eqn. (2.99).
Ff	Fluctuating force, eqn. (3.8) (N)
$fu_g(\alpha)$	Void fraction function at BIT kinetic energy eqn. (3.38)
f_V	Ratio between daughter bubble diameter and mother bubble diameter
g	Gravitational acceleration (m/s^2)
h	Liquid film thickness (m/s)
h_col	Collision frequency between bubbles (1/s)
h_f	Critical thickness of the liquid film separating two colliding bubbles (m).
h_i	Initial thickness of the liquid film separating two colliding bubbles (m).
I	Turbulence intensity= $\sqrt{\left(\overline{(u')^2} + \overline{(v')^2} + \overline{(w')^2}\right)/3}/\bar{u}$ (-).
i,j,k	Unit vectors in Cartesian coordinates x, y, and z direction respectively
J	Superficial velocity (m/s)
k	Turbulent kinetic energy (m^2/s^2)
k_g	A constant coefficient for the Martínez-Bazán breakup frequency model
m	Mass (kg)
Mo	Morton number (-)
mo	The interfacial mobility between the contact surfaces of two colliding bubbles (-)
n	Mid width of the mapping window used in eqn.(5.2)
n	Position vector normal to the colliding surface of two bubbles
N_bre	Collected number of bubbles breakup during the simulation period
N_coa	Collected number of bubbles coalescences during the simulation period
n_e	Concentration of eddies in the size range of interest eqn. (2.99)

p	Pressure (Pa)
Pr	Probability of forming two baughter bubbles from a breakup process
PSC	Particle source in cell
q	Time (s)
r	Radial position of cylindrical coordinates (m)
R	Radius (m)
R_W	Neighbor window width of bubble for colliding neighbors (m)
r_{ab}	Relative distance between bubbles a and b (m)
Re	Reynolds number (-)
Re_∇	Reynolds number based on average shear (-)
S	Source term
Sc	Schmidt number (-)
SC	Scaling factor for void fraction distribution, eqn. (4.7)
St	Stokes number (-)
t	Time (s)
Tf(l)	Template function of the bubble l
t_phy	Physical time for the computation (s)
U,V,W	Mean velocity components at x, y and z direction (m/s)
u,v,w	Instantaneous velocity component at x, y and z direction (m/s)
ú, ý, ẃ	Fluctuating velocity component at x, y and z direction (m/s)
V	Volume (m^3)
Vf	Void fraction (-).
Vg	Gas velocity at vertical direction (m/s).
Vgr	Radial gas velocity (m/s).
W	Work (N.m)
W_0	Relative velocity vector for two colliding bubbles at the contact point
We	Weber number (-)
Wn	Wav number (1/m)
x_i, x_j	Cartesian coordinate x,y,z as i=1,2,3,or j=1,2,3 respectively (-)
y	y direction at Cartesian coordinates
Y_{wall}	The distance from the wall to the bubble center (m)
z	z direction at Cartesian and cylindrical coordinates

Greek

ξ_{12}	Bubble diameter ration between bubbles 1 and 2
α	Void fraction
β	A constant coefficient for the Martínez-Bazán breakup frequency model, also used as a geometrical parameter as illustrated at figure 2.1.
δ	Probability density function of the daughter bubble size in bubble breakup
δ_D	Dirac delta function eqn. (3.11)
Δt_c	Contact time step (s)
Δt_E	Eulerian time step (s)
Δt_l	Lagrangian time step (s)

ε	Turbulent dissipation rate (m^2/s^3)
ζ	Ratio between the eddy diameter and the bubble diameter, eqn. (2.113)
η	Kolmogorov length scale (m),
η_{br}	Breakup efficiency (-),
θ	Angular vector at cylindrical coordinates
$\lambda(D_{b,1},D_{b,2})$	Coalescence efficiency between bubbles of diameters d1 and d2 (-)
Λ	Ratio between the critical bubble diameter of breakup and the bubble diameter
μ	Dynamic viscosity ($N.s/m^2$)
ν	Kinematic viscosity (m^2/s)
$\xi(t)$	Random Gaussian white noise variable (-)
ρ	Density (kg/m^3)
σ	Surface tension coefficient (N/m)
σ_{dr}	Standard deviation when considering coalescence and contact time as random variables equation (2.68)
σr	Reynolds stress tensor
σ_{sr}	Strain rate tensor
σ_u	Lagrangian Standard deviation of velocity fluctuations defined at equation (3.21)
τ	Time scale (s)
τ_b	Bubble response time scale (s),
τ_c	Time response of the continuous phase in existence of the dispersed one (s),
τ_{ij}	Reynolds stress tensor
τ_L	Lagrangian time scale(s),
τs	Confinement stress on the bubble (N/m^2).
τt	Deformation stress on the bubble (N/m^2).
τ_t	Integral time scale of turbulence (s)
τ_w	Wall shear stress (N / m^2)
τ_λ	Tailor time scale of the turbulent flow (s),
ϕ	Property of bubbles passing through a cell to be averaged at the cell equation (5.5)
Φ	Property of a cell averaged from all the bubbles passing through it equation (5.5)
ψ	Property of a bubble averaged from the surrounding cells
Ψ	Property of cells around the bubble to be averaged at the bubble
ω	Vorticity vector (1/s)
Ω_j	Boundary of cell j
$\Gamma(D_{b,1},D_{b,2})$	Coalescence rate between two colliding bubbles of sized d_1 and d_2

Sub indexes

0	Initial value
a	Particle a
ab	Relative between particles a and b

b	Bubble ,or Particle b
br	Breakup
bu	Buoyancy
c	Continuous phase
con	Contact
d	Dispersed phase
Dr	Drag
dr	Drainage
e	Eddy property
eff	Effective
f	final
g	gas
hb	Horizontal bubble dimension
hd	Horizontal direction for bubble
i	initial
l	liquid
LF	Lift
low	Lower level
m	Mixture
mid	Middle level
min	Minimum value
mag	Magnitude value
max	Maximum value
n	normal
p	Particle
r	Radial component
rel	Relative between the two phases
T	Transverse lift
t	Turbulent
tc	Tangential component at the point of contact
TD	Turbulent dispersion
tD	Terminal property of bubble of diameter D
te	Terminal property of eddy
ter	Terminal property
upp	Upper level
vb	Vertical bubble dimension
VM	Virtual mass
w	Wall
wat	Water
WL	Wall lubrication
x	X direction
y	y direction
z	Axial component or z direction
θ	Angular component

Super indexes

int	Interaction of bubbles on the continuous phase in source terms
nr	Normalized value

Symbols

$\bar{}$	Average value, or component
$'$	Fluctuating component.
$\vec{}$	Vector
$\hat{}$	Unit vector
$\dot{}$	Variable first derivative by time
$\ddot{}$	Variable second derivative by time

1. Introduction

Multiphase flow plays an important role in most industrial applications, such as power generation, energy conversion and safety technology in power plants, paper manufacturing, food processing, as well as processes in the automobile, aeronautical and space industries. Multiphase flow is considered as a heterogeneous mixture of multiple fluids or phases, which are not homogeneously mixed at a molecular level but can be identified as macroscopic structures, such as solid particles, droplets, and bubbles, in a certain region. The variety of the types of multiphase flows is illustrated, of which two-phase flow is of particular significance. Depending on the constituents of the flow, Ishii (1975) suggested that two-phase flow was classified into four groups: solid-gas flow, gas-liquid flow, solid-liquid flow, and liquid-liquid flow consisting of two immiscible fluids.

Gas-liquid two-phase flow is not only crucial to many industrial problems but also important in some natural processes, as in the ocean-atmosphere interactions. Typical gas-liquid two-phase flow problems consist of void and pressure wave propagation, bubble-driven circulation systems, as well as some well-known thermal-hydraulic and safety problems in nuclear reactor systems. Issues relevant to nuclear reactor systems include critical heat flux (CHF) problems, direct contact condensation from emergency core cooling system (ECCS) injection, flow oscillations in boiling water reactors (BWRs), and heat transfer through boiling. Knowledge of two-phase flow is essential when we deal with economical and technological constraints, as well as safety and environmental issues involving two-phase flow. However, many important fluid dynamic and thermal aspects of the prevailing gas-liquid two-phase flows are still poorly understood.

At the next sections, a brief description for the numerical methods used for simulating the two-phase flow is presented. Then, a literature review for the past work in the PTM method is explored. After that, the main objectives of this research work are mentioned. Then a brief description for the experimental data used for validating our model is presented. And finally an outline that describes the rest chapter in the present thesis is explored.

1.1 Two-phase flow Numerical methods

Multi-phase flows exist in many natural and technological systems. Owing to the many challenges that are being faced by many applied scientists, practicing engineers, undergraduate and graduate students or researchers engaging in the subject of multi-phase flows, the advancement of digital computers has apparently re-focused the

reliance on computational predictions to better understand and predict the multi-phase phenomenon. With increasing prevalence, the feasibility of application of computational models is certainly gaining significant traction. Modeling multi-phase flows, in general, encompasses a wide spectrum of different length scales, a broad range of engineering disciplines, and a multitude of different computational approaches. One of the types of Two-phase flow is the dispersed gas-liquid flow or bubbly flow. Applications of this type can be found in many industrial fields like bubble columns, stirred vessels, Nuclear reactors cooling lines, and boiling and condensation applications. There are three main approaches used for bubbly flow numerical solution, i.e. an averaging method (Tomiyama et al., 1995a), an interface tracking method (Hirt and Nichols, 1981) and a particle tracking method (Žun et al., 1993). Most of the simulations so far have been conducted using the averaging method which is based on a drift-flux or a two-fluid model. Although this method can be applied to practical problems and work with high void fractions, it cannot take the bubble size distribution into account and limited in very dilute zones. The interface tracking method provides detailed information of the flow field around bubbles without using any empirical constitutive laws. However, it requires a lot of CPU time and memory so that the problems we can solve are limited to simple ones including only a few bubbles (Tomiyama et al., 1994a,b). These defects of the averaging and interface tracking methods can be easily overcome if the particle tracking method (PTM) or the Euler-Lagrange coupling model is used. The particle tracking model has advantages over the front tracking method that it can solve relatively higher number of bubbles at shorter computational time, work better more complex problems. However, it cannot describe the change in the bubble surface like the front tracking method. And it have advantages over the Euler-Euler model that it can describes easily the size distributions of bubbles, numerically straightforward to implement physical phenomena like heat and mass transfer, wall-bubble interactions. However it consumes a lot of CPU time in locating the bubbles in the computational cells and is difficult in parallel implementation. For the advanced reasons, we think that it is possible developing the Euler-Lagrange method to give better performance and minimize its drawbacks. In the Euler-Lagrange modeling, the continuous phase is solved by Euler framework by solving the Navier-Stocks equations in the computational domain. The dispersed phase is simulated considering particles affected by forces from the continuous fluid, applying these forces on each particle using the Newton's second law we get the acceleration of the dispersed phase particle through the continuous phase. When only the effect of the continuous phase is considered on the dispersed phase, it is called one-way coupling regime. When both the effect of dispersed phase on the continuous one and vice versa is considered then it is called Two-way coupling regime. If bubble interactions like bubbles collisions, coalescence and breakup are considered with the effect of each phase on each others, then it is called four-way coupling. For this advantage of the Particle tracking or discrete bubble model, (also called Euler-Lagrange modeling) over the other two methods, it shared many advances and investigation for improvement in the last years.

1.2 Review for the past work

In this section, the past works presented using the PTM is explored. This will start with the works used one-way coupling. Then Works used two-way coupling including the source terms description to account for the back effect of the bubbles on the continuous phase. Then the works used the four-way coupling considering bubbles collision, coalescence and breakup in the PTM. After that, the methods used the CRW in their PTM modeling are presented.

1.2.1 One-way coupling

Some works have been introduced with one-way coupling which takes only the effect of the continuous phase on the dispersed one. The effect of the continuous phase is taken by calculating the relative forces from the continuous phase acting on the dispersed one. These forces are drag force, Lift force, virtual mass force, Wall lubrication force, wall deformation forces and others. Applying these forces in Newton's second law for each bubble, the acceleration of the bubble each time step of the Lagrange simulations can be expressed as follows:

$$(\rho_d + C_{VM}\rho_c)V_b \frac{d\vec{u}_b}{dt} = \sum_i \vec{F}_i \qquad (1.1)$$

Where C_{VM} is the coefficient of the virtual mass force which is assumed to equal to 0.5, V_b is the volume of the bubble, $\rho_d$and ρ_c are the densities of the gas acting as the dispersed phase, and the liquid acting as the continuous phase respectively, $\sum_i \vec{F}_i$ is the summation of the forces acting on the bubble, and $d\vec{u}_b/dt$ is the acceleration of the bubble. The equation is introduced in the vectorial form.

This coupling is acceptable for the cases of low void fraction of the dispersed phase. Some of the works which had used this coupling are Žun et al (1993), Wang and Maxey (1993a,b), Maxey et al. (1994), Yang and Lei (1998), Meneveau et al. (1996), Spelt and Biesheuvel (1997), and Muñoz-Cobo et al (2012), Mattson et al (2012).

1.2.2 Two-way coupling

Many works considering the two-way coupling between the Euler and Lagrange frameworks have been introduced recently. The two-way coupling means the consideration of the continuous phase effect on the dispersed one and vice versa. The effect of the continuous phase on the dispersed one is considered by the same way used in the One-way coupling method.

The effect of the bubbles on the continuous phase is considered by introducing a source terms in the Navier-Stockes equations and changing the volume available for the continuous phase in the computational cells according to the void fraction in the cell.

Also source terms in the turbulence equations is introduced to account for the bubble induced turbulence effect. Mortensen and Trapp (1992) developed a two-way one-dimensional particle tracking method based on a two-fluid model for the liquid phase and an equation of motion for each bubble. Many others applied the two-way coupling in their modeling like Squires and Eaton (1990), Elghobashi and Truesdell (1993), Climent and Magnaudet (1999), Garg et al (2007), John (2009), Sungkorn et al (2011), Tomiyama et al (1997), Patankar et al (2001), Laín et al (2002), pang et al (2010)

1.2.2.1 Source terms in the momentum equation

Various averaging methods have been introduced for collecting the effect of the bubbles passing through the cell in the source term of the cell. Examples of these are the works introduced by

Guan et al (2010)

In this model, the particle source in cell (PSC) approach introduced by Crowe et al. (1977) is used to consider that the particle is smaller than the cell size. The source terms in the momentum equation are:

$$S_u^{int} = n\overline{\langle -m_b\left(\frac{Du_b}{Dt} - g_x\right)\rangle} \qquad (1.2-1)$$

$$S_V^{int} = n\overline{\langle -m_b\left(\frac{Dv_b}{Dt} - g_y\right)\rangle} \qquad (1.2-2)$$

$$S_W^{int} = n\overline{\langle -m_b\left(\frac{Dw_b}{Dt} - g_z\right)\rangle} \qquad (1.2-3)$$

Such that S_u^{int}, S_V^{int}, S_W^{int} are the interaction source terms considered in the momentum equations at the directions x,y, and z respectively, the $\langle\ \overline{\ }\ \rangle$ is an averaging process over the n particles passing through the cell under calculation, m_b is the bubble mass, g_x, g_y, g_z are the gravity accelerations at the x,y, and z directions respectively, $\frac{Du_b}{Dt}$, $\frac{Dv_b}{Dt}$, $\frac{Dw_b}{Dt}$ are the acceleration of the bubble in the three directions x,y, and z respectively.

Darmana et al (2006)

In this model, the source terms in the momentum equation is considered as the reaction of the summation of forces acting on the bubble, but for averaging this forces on the cell, he used the idea of the template function introduced by Deen et al, (2004) that approximate the effect of the bubble on the cells depending on the relative position of the bubbles form the cell. The momentum transfer rate from the bubbles to the liquid in a computational cell j, Φ(j), can be calculated as:

$$\Phi(j) = \frac{\sum_i \phi(l) \int_{\Omega j} \omega(l)\, d\Omega}{V_{cell}} \tag{1.3}$$

Where Φ is the reaction of the momentum transfer exerted on the bubbles, $\phi(l) = -\sum F$. V_{cell} is the volume of the cell, $\int_{\Omega j} \omega(l) d\Omega$, is the integration of the template function over the cell, $\sum_i$ means summation over all the bubbles passing through this cell.

Other models were used for this approximation like that of Andrews and O'Rourke (1996), that used in the work of Patankar et al (2001). Other approximating model is introduced by Delonij et al (1996) based on an area-weighted averaging technique. Also the approximation introduce by Laín et al (2002) based on the model of Particle source in cell (PSC) introduced by Crowe et al. (1977).

1.2.2.2 Bubble induced turbulence effect.

The effect of the bubbles on the continuous phase turbulence is taken by inserting a source term in the turbulence equations, or modifying the turbulent viscosity. The two methods works are introduced here.

Source terms in turbulence k-ε model

Guan et al (2010)

The source terms introduce in the turbulence kinetic energy K, and turbulence dissipation rate ε equations are

$$S_k^{int} = C_{k1}\alpha_c\alpha_d P_c + C_{k2}C_f\alpha_c\alpha_d k_c \tag{1.4}$$

$$S_\varepsilon^{int} = C_{\varepsilon 3}\frac{\varepsilon_c}{k_c}\alpha_c\alpha_d P_c + C_{\varepsilon 4}C_f\alpha_c\alpha_d\varepsilon_c \tag{1.5}$$

$$C_f = \frac{3}{4}\frac{C_{Dr}}{D_b}|U_d - U_c| \tag{1.6}$$

This is characterized by the drag effect. The first additional terms in the equations (1.4) and (1.5) describe the increased generation of turbulence in the liquid due to momentum exchange between the phases, which are based on the proposal by Malin (1983) and Malin and Spalding (1984). The second additional terms are due to the proposal by Simonin and Viollet (1988) accounting for the migration of gas bubbles through the liquid. According to Smith (1998), the additional model coefficients take the values of

C_{k1}=6.0, C_{k2}=0.75, $C_{\varepsilon 3}$=4.0, $C_{\varepsilon 4}$=0.6

Yao and Morel (2004)

Yao and Morel have however proposed alternative source terms for modeling the turbulence production in the wakes of bubbles according to

$$S_k^{int} = -\left(F_{d,drag} + F_{d,VM}\right)(U_d - U_c) \tag{1.7}$$

$$S_\varepsilon^{int} = C_{\varepsilon 3}\frac{S_k^{int}}{\tau}, \quad \tau = \left(\frac{D_b^2}{\varepsilon_c}\right)^{1/3} \tag{1.8}$$

Where τ is the characteristic time for the bubble-induced turbulence and $F_{d,drag}$, and $F_{d,VM}$, are the interfacial force densities due to drag and virtual mass exerted on the disperse phase in the momentum equations. The constant $C_{\varepsilon 3}$ can take values ranging from 0.6 to 1.0 depending on the particular gas–liquid systems in question.

Modification of the turbulent viscosity

Sato et al (1975)

Sato et al (1975) suggested that the effect of the bubble induced turbulence can be considered by adding a eddy viscosity due to the bubbles such that the total eddy viscosity is the summation of the eddy viscosity produced by the k-ε model, and the eddy viscosity of bubbles as follows:

$$\mu_{t,c} = C_\mu \rho_c \frac{(k_c)^2}{\varepsilon_c} + \frac{1}{2} C_{\mu b} \rho_c \alpha_d D_b |U_d - U_c| \tag{1.9}$$

Where $C_{\mu b}$ has a value of 1.2. The second term in equation (1.9) is the asymptotic form suggested by Sato et al (1975). Through the use of the effective viscosity, the source or sink terms S_K^{int} and S_ε^{int} are set to zero in most investigations of gas–liquid flows.

1.2.3 Four-way coupling

The four way coupling name is taken from the two-way coupling plus the inteaction between bubbles as another two-way coupling as menstioned by Guan et al (2010). In this approach, in addition to considering the two-way coupling, the interaction between bubbles like the collision, coalescence and breakup effects are considered as well. Examples of works following this approach are Delonij et al (1996), R*ü*ger et al (2000), Sommerfeld et al (2003), Darmana et al (2006), Shams et al (2010), Farzpourmachiani et al (2011), Movahedirad et al (2012).

1.2.3.1 Collision modeling

Sommerfeld (2000) stated that considering bubble-bubble interactions is important when the volume void fraction of the gas exceeds 10%. Bubble-bubble interactions

mean the collision between the bubbles, coalescence and breakup of the bubbles. Which in turn change the bubble size distribution and hence the resulting void fraction profile.

Some works were introduced to take in account the collision effect of the bubbles using the hard-sphere model proposed by Hoomans et al. (1996) that consider collision with conservation of kinetic energy and constant force during collision like Delnoij et al. (1996), Laín et al. (2002), and Darmana et al. (2006). Some works have applied a stochastic collision model proposed by Sommerfeld (2001) like that in the work of Sommerfeld et al. (2003) and Rüger et al (2000). Other works used the soft sphere collision model of Cundall et al (1979) that consider changing force during the collision like Huilin et al (2006) and Wachem et al (2010).

1.2.3.2 Coalescence modeling

Some works also considered the coalescence of the colliding bubbles using binary coalescence model of Prince and Planch (1990) that depends on comparing between the time consumed to drain the film contained between the two colliding bubbles and the contact time between them. If the film drainage time is less than the contact time, the coalescence occurs, if not, then the two bubbles are bounced away from each others. Examples of works with this model are Tsouris et al. (1994), Sommerfeld et al. (2003), Darmana et al. (2006), Michael et al. (2009), and Lau et al (2010). Other coalescence models are used also. The coalescence models of Chesters (1991) and Lee et al (1987a) are used in the work of the discrete bubble model (DBM) introduced by Van Den Hengel et al (2005). In these coalescence models, the coalescence rate is modeled as the product of the collision frequency and the coalescence efficiency. In this work, the collision model is responsible for the coalescence efficiency, so only the coalescence efficiency is needed. In the model of Chesters (1991), the coalescence efficiency was calculated using the film drainage model introduced by Prince and Planch (1990). If we considered the film drainage time t_{dr} and the contact time τ_{con}. Then the coalescence $\lambda(D_1, D_2)$ efficiency is calculated as follows:

$$\lambda(D_1, D_2) = \exp\left(-\frac{t_{dr}}{\tau_{con}}\right) \tag{1.10}$$

In the model of Lee et al (1987a), the coalescence time is equal to the time required for thinning plus the time of rupture. And the contact time is based on the theory of isotropic turbulence which is calculated by a different relation.

1.2.3.3 Breakup modeling

Recently, the breakup model was applied in the Lagrangian simulations. For example, the work of Lau et al (2010) that introduced a breakup model for the discrete particle methods based on the breakup theory of Hinze (1955) that introduced a dimensionless ration between the force which cause deformation of the bubble and the surface tension which restore the bubble sphericity. This ratio was called Weber number. Depending on the flow conditions, there is a critical Weber number over which the breakup occurs

for the bubbles. A different work was introduced by Van den Hengel (2005) based on the breakup model of Luo and Svendsen (1996) which considered that the breakup occurs as a result of collision of the bubble with an eddy that is able to break the bubble. the breakup efficiency is given by the probability that a bubble will break after it gets "hit" by a liquid phase eddy of size dependent on the state of eddies in the place of the bubble.

1.2.4 Works used stochastic modeling for bubbles diffusion.

Some works used the stochastic modeling in molding the fluctuating particle motion. These methods consider the liquid velocity used for calculating the forces acting on the bubble as a sum of the average localized liquid velocity and fluctuating components that is generated from this stochastic model. Two famous types are used for the stochastic modeling which are the continuous random Walk (CRW), and the discrete random walk (DRW) model. The DRW model assumes that the random value of the fluctuating velocity component is kept constant over an interval of time given by the characteristic lifetime of turbulent eddies. In the CRW model, the fluctuating velocity components are obtained by solution of the Langevin equation. This provides a more realistic description of the turbulent eddies, at the expense of increased computational effort (due to the requirement for smaller time steps for the integration of particle trajectory equation). Many works used the DRW in modeling the turbulent diffusion of the bubbles or particles for its little consumption for computational resources. Examples fro these are Buwa et al (2006), Farzpormachiani et al (2011), and Han Luchang et al (2010). A little number of works was presented using the CRW model for its long computational time like Pozorski et al (1998) using the Langevin equation. In the present work, we used Langevin equation to generate the liquid fluctuations that will be used in the particle momentum equation. We believed that this is a physical method to model the turbulent dispersion of the bubbles in the continuous phase as it is more realistic and able to model even the anisotropy of the turbulence.

1.3 Objectives of the present research

The Simulation of bubbly flow using the Lagrange-Euler modeling needs much development. As was mentioned before, it has advantages over the two methods used for multiphase flow simulations. This work had started with a Lagrange code for solving the bubbles motion coupled to a 2D computational Fluid Dynamics (CFD) code that solves the motion of the continuous phase in a one way coupling approach.

In the present research one objective is to enhance the Lagrangian-Eulerian simulation tool under study to apply the different models for getting distributions of both the continuous phase and the dispersed phase comparable to the experimental data.

The objectives of this research are divided into two parts. The first is to apply the models already existing in the field of the Lagrangian Eulerian simulations which are:

1. Replacing the 2D CFD solver by a 3D CFD solver to consider better modeling for turbulence and as a primary step for the further development steps which cannot be handled without 3D CFD Euler solver.

2. To apply the two-way coupling process that considers the back effect of the bubbles on the continuous phase. This back effect will be considered in the void fraction of the cell, the momentum, and the turbulence kinetic energy and dissipation rate. And the effect of the two-way coupling process on both the continuous and the dispersed phases is studied.

3. Consider the different bubble-bubble interaction mechanisms including collision, coalescence and breakup modeling. And the effect of each of these mechanisms on the simulation data is studied.

The second part of the objectives designed for the present work is a new addition for the field of the Lagrangian Eulerian modeling of the two-phase flow which are:

1. To develop a new formula for the Bubble Induced Turbulence (BIT) that affects the turbulence of the continuous phase. This BIT formula will be coupled with the continuous phase as a source in the equations of both turbulence kinetic energy and dissipation rate.

2. The turbulence dispersion effect on the bubbles is handled by a stochastic modeling for the fluctuating part of the liquid velocity which is created as a function of the local state of turbulence for the continuous phase. In that way, both using a cheap method created for simulating the turbulence diffusion of the particles in the turbulent flow, and considering the effect of the particles on the continuous phase is considered.

3. Validating the developed Lagrangian Eulerian model with experimental data.

1.4 Experimental database

The experimental data used in the present work was produced in the “Instituto de Ingeniería Energética” in the “Universidad Politécnica de Valencia”. Upward isothermal co-current air-water flow in a vertical pipe (52 mm inner diameter) has been experimentally investigated. Figure 1.1 displays the outline of the experimental facility used to perform the experimental work. It is a thermo-hydraulic loop, with a test section, a lower plenum where air bubbles and water are mixed in a chamber that produces bubbly flow or cap/slug flow, and an upper plenum where the air is separated from the liquid. The test section is a round transparent tube made up of Plexiglas® with constant area, the inner diameter is 52 mm and the length of the section is 3340 mm. purified water is used as working fluid, and the water circulation is provided by two centrifugal pumps controlled by a frequency controller. The air is supplied by an air

compressor and it is introduced to the test section through a porous sinter element with an average pore size of 40 μm installed below the mix chamber at the lower plenum. The air and water temperature is kept constant during the test assay. The air mass flow rate is measured by two thermal mass flow meters and controllers (Bronkhorst ® , EL-FLOW model, range 5 -200 Nl/min, range 50 – 1400 Nl/min), and the liquid flow rate by an electromagnetic flow meter (Badger Meter ® , range 0-30 m^3/hr).

Local measurements of void fraction, interfacial area concentration (IAC), interfacial velocity and Sauter mean diameter were measured using a four sensor conductivity probe. Liquid velocity was measured using Laser Doppler Anemometry (LDA). For further information about the experimental instrumentation and set up, please refer to Mendez (2008).

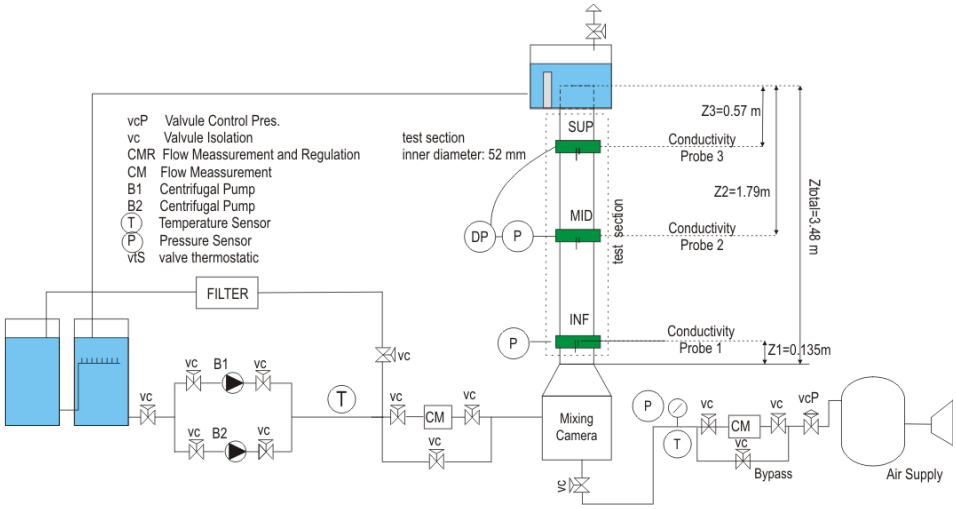

Figure 1.1. Outline of the experimental facility.

Different air-water flow configurations were investigated for a liquid flow rate ranged from 0.491 m/s to 3 m/s and a void fraction up to 25 % .For each two-phase flow configuration fifteen radial position and three axial locations were measured by the conductivity probe methodology, and several radial profiles were also measured with LDA at different axial positions.

The experimental data used for comparison in the present research is indicated with the conditions of each case in table 1.1.

In the present work, the experiments of the liquid velocity in the range from 0.5 to 2.0 m/s and for the average void fraction range from 5% to 15% are considered. This range validates the condition of bubble flow for which the form of the bubble can be distorted but is not in the form of cap or slug flow as can be seen from the flow pattern map for this series of experiment in figure 1.2.

Table 1.1. Experimental cases and conditions.

Case name	J_c [m/s]	J_g [m/s]	<α> [-]
F01AG01	0.5	0.075	5.14
F01AG02	0.5	0.075	10.38
F01AG03	0.5	0.077	15.73
F02AG01	1.0	0.121	4.84
F02AG02	1.0	0.135	9.36
F02AG03	1.0	0.144	14.97
F03AG01	2.0	0.209	3.69
F03AG02	2.0	0.231	8.18
F03AG03	2.0	0.268	14.90

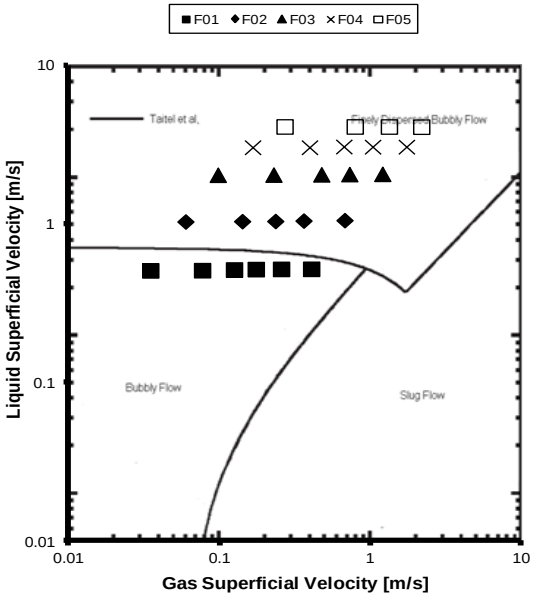

Figure 1.2. Flow pattern map for the experiments F0XA.

The experimental data for gas void fraction distribution, gas velocity, Interfacial area concentration and bubbles Sauter mean diameter are shown at figure 1.3., 1.4, 1.5, and 1.6 respectively. In the experimental data illustrated at figures 1.3:1.6, the symbols F01A, F02A, F03A refer to the values of the liquid superficial velocity of 0.5, 1.0, and 2.0 m/s respectively. And the gas void fractions G01, G02, G03 refer to the three gas void fractions 5%, 10%, and 15% respectively. These data are measured at three different pipe heights Z_{low}, Z_{mid}, Z_{upp} such that $Z_{low} = 2D_p$, $Z_{mid} = 36D_p$ and $Z_{upp} = 56D_p$.

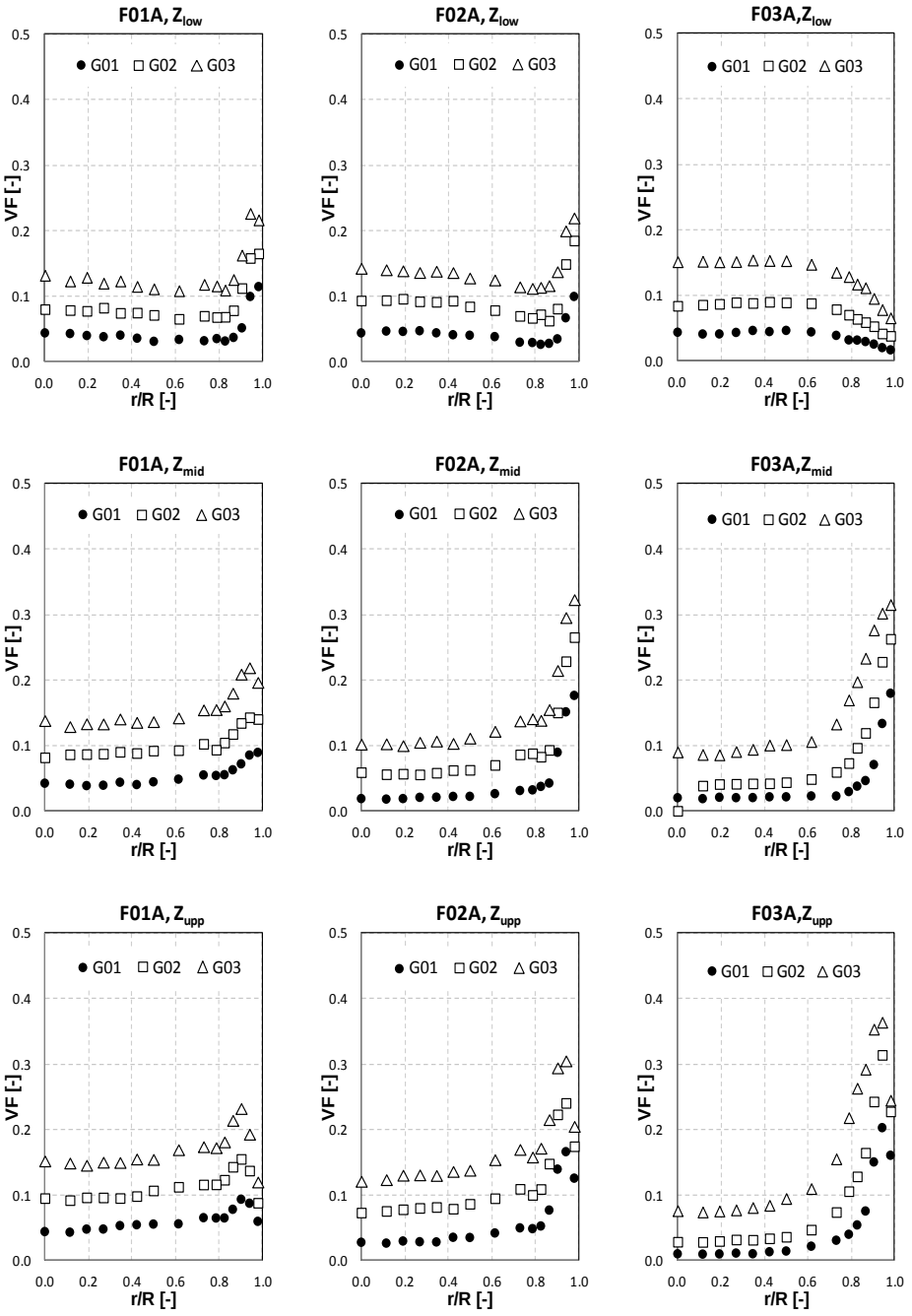

Figure 1.3. Void fraction radial distribution for experimental cases at three different heights Z_{low}, Z_{mid}, Z_{upp}.

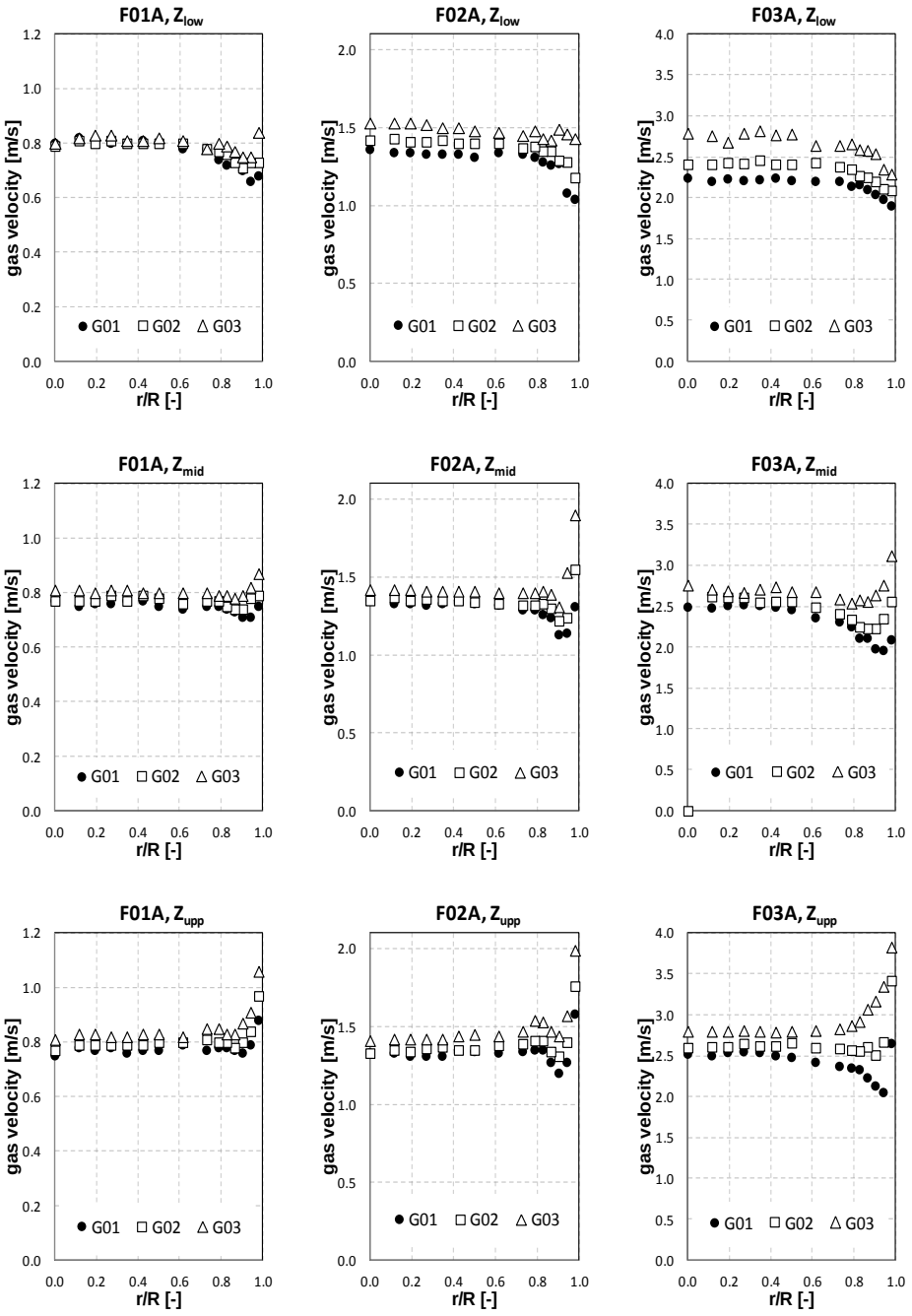

Figure 1.4. Gas velocity radial distribution for experimental cases at three different heights Z_{low}, Z_{mid}, Z_{upp}.

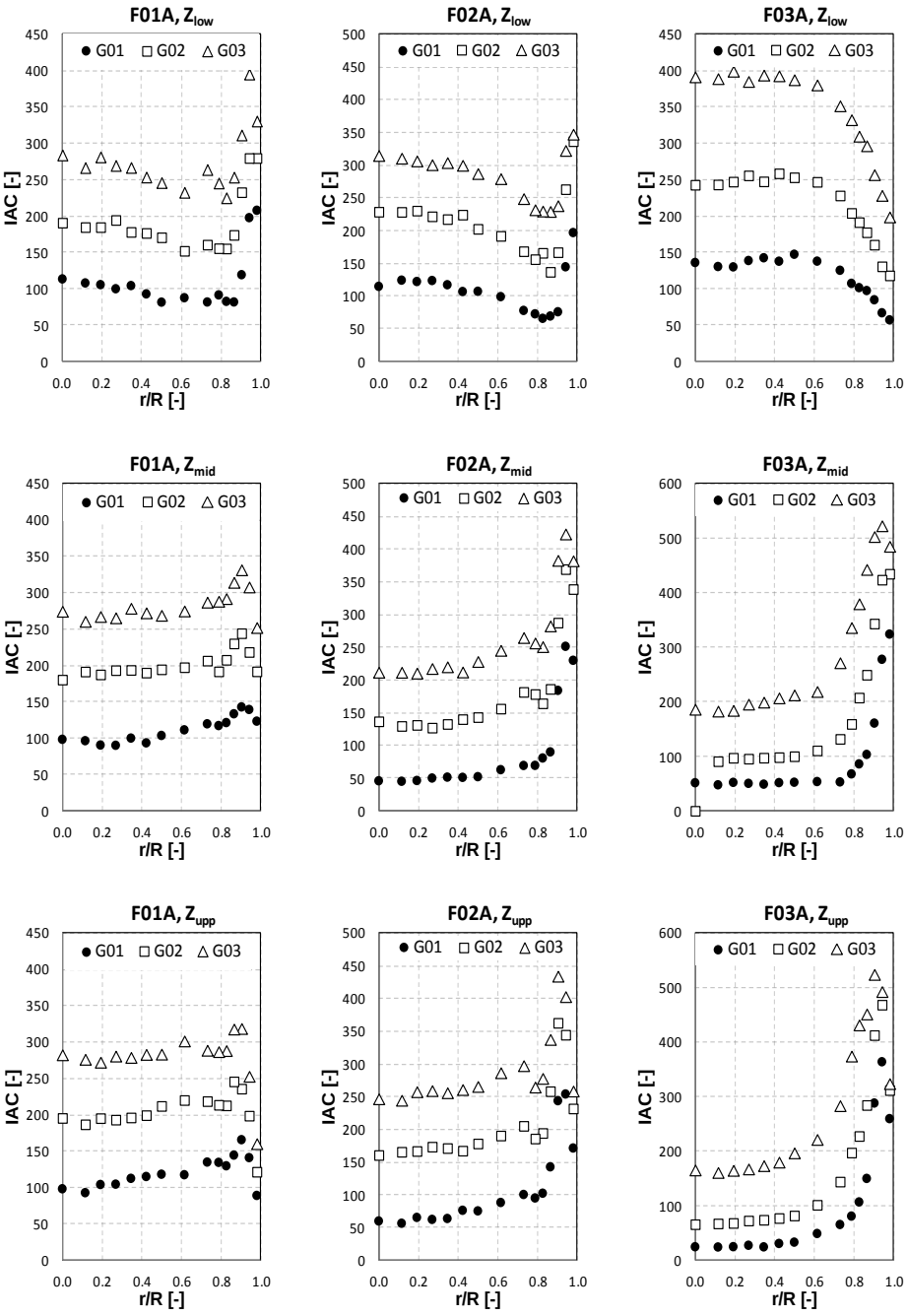

Figure 1.5. Interfacial area concentration radial distribution for experimental cases at three different heights Z_{low}, Z_{mid}, Z_{upp}.

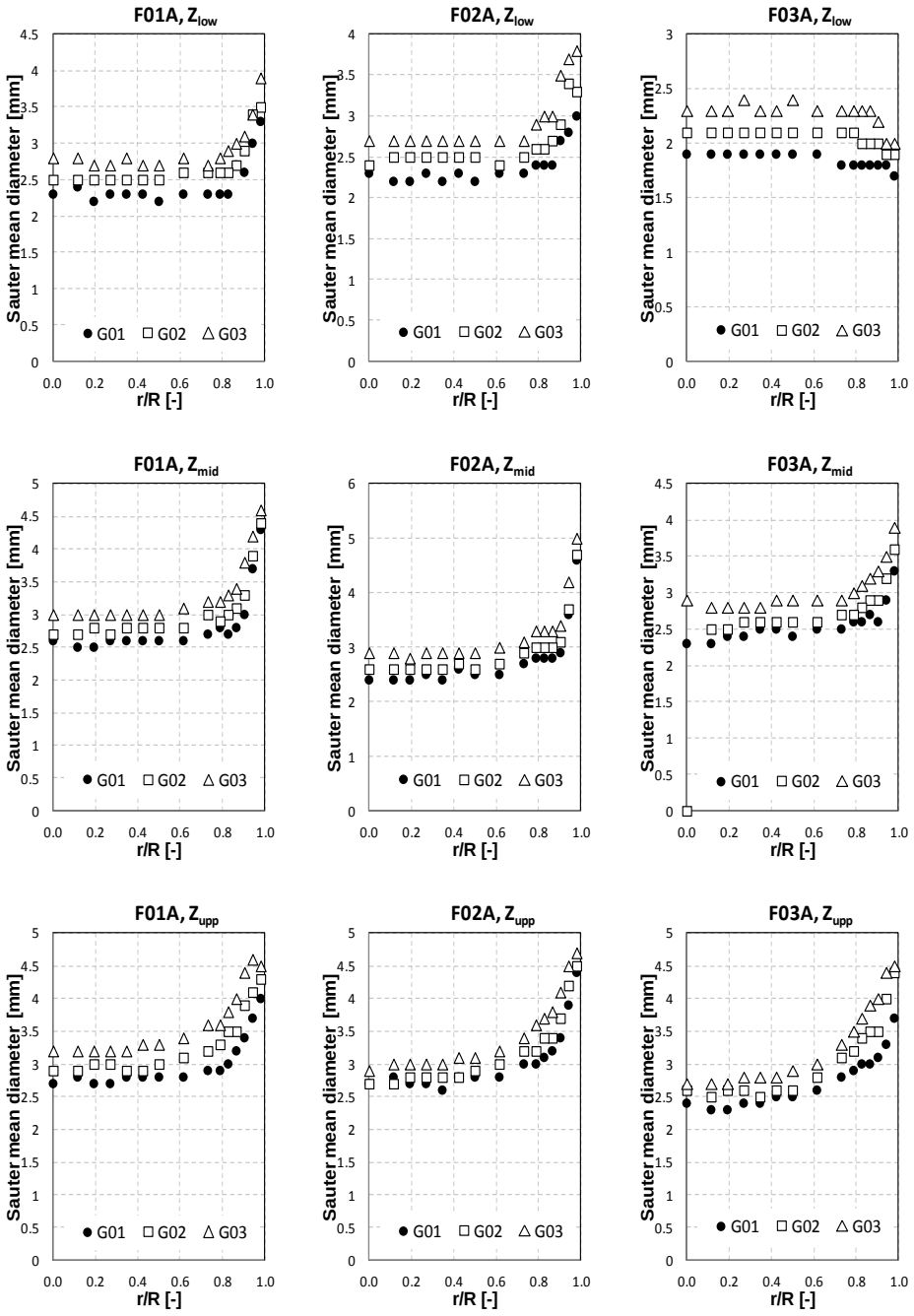

Figure 1.6. Sauter mean diameter radial distribution for experimental cases at three different heights Z_{low}, Z_{mid}, Z_{upp}.

It can be observed at figure 1.4 in the gas velocity distributions that close to the wall , experimental data shows higher values of the gas velocity. In fact this is not true as the bubbles follow the liquid velocity and affected by the wall friction, the gas velocity close to the wall should be lower than that at the center for the effect of wall friction. This problem appears as a main problem in the conductivity probe measurements as the bubbles close to the wall suffer from many collisions and circulations that make the measurement of the probe insensitive beside the wall for gas velocity. As the profiles of IAC and Sauter mean diameter are not measured directly and are calculated from the measured data of the velocity and void fraction, the same problem of the profiles of IAC and Sauter diameter appear beside the wall that gives illogic values as appears at figures 1.5 and 1.6.

1.5 Thesis outline

The next chapters of the thesis are organized as follows. Chapter 2 describes the numerical modeling used in the present research. First, it describes the bubbles hydrodynamics that are considered in the present work including the forces acting on the bubbles, Collision, Coalescence and Breakup modeling with brief reviews for the important works near to our application of the bubbly flow systems. Then, it describes the Euler and Lagrangian solvers used in this research starting with overview about the Euler solver used including the numerical methods and modeling used in the Euler solver. Then it presents a description of the Lagrangian model governing equations and the numerical methods used for particle location in the Euelrian grid and the used algorithms.

Chapter 3 presents a brief introduction for the turbulence problem in the one-phase flow and that model of turbulence used for the Euler solver. Then it describes the Stochastic modeling of particles diffusion in this work. After that it presents a brief discussion for the bubble induced turbulence (BIT) modeling and the model that is suggested for the present work. Finally it presents an indication for the effect of the BIT on the results of generated velocities fluctuations of the CRW model.

Chapter 4 presents the One-way coupling processes used in this work. It first presents the method used for approximating the Euler quantities at the particle location. Then it describes the time stepping method used in the one way coupling. After that, it explains the code algorithm and flow chart that is used for applying the one-way coupling. Then it presents a Study for the effect of the Bubble Induced Turbulence formula on the void fraction distribution in order to find the best fit of the BIT formula on the relative velocity and gas void fraction. Then it presents a study for the effect of lift force coefficient on the void fraction distribution. Finally, it presents the simulation results of applying the one-way coupling process.

Chapter 5 presents the process of applying the two-way coupling mechanism with the different interaction mechanisms. First it describes how to apply the two-way coupling

without considering any bubbles interactions. This contains the time stepping method, the methods for interpolating bubbles data at computational cells, how the Euler solver conservation equations are modified to account for the two-way coupling method. Then it presents the code algorithm in case of two-way coupling process. After that, it presents the simulation results including the effect of the two-way coupling process in both the continuous phase and the dispersed phase properties. Then a study for the effect of the lift force with considering two-way coupling is presented. After that the two-way coupling process with considering the bubbles collision will be presented, with description of, the time stepping method used, the change in the code algorithm, the effect of considering the bubble collision on the void fraction profiles, and a study for the effect of the BIT coefficient on the void fraction distribution. After that the consideration of the bubbles coalescence applied with bubbles collision is studied in the change of the time stepping, code algorithm and the simulation results. Then, the application of the breakup mechanism with both the collision and coalescence mechanisms is applied, in that case, it will be explored the time stepping method, the changes in the code algorithm, and the effect of that on the simulation results.

Finally chapter 6 presents the conclusions from the present work in four main points. The one-way coupling development, the two-way coupling development, the CRW model used, and finally the new features presented by this new model. Then it descries some investigation lines that need further research in the future.

2. Numerical modeling

In this chapter, the numerical methods developed and implemented during the course of this work is described. At first, the bubbles hydrodynamics modeling including, the acting forces on the bubbles, collision modeling, coalescence modeling and breakup modeling are presented. Then an overview for the Euler solver which includes a brief description of the Euler solver used during this work, governing equations, boundary condition presentation and other facility used in this solver are explored. Then an overview about the Lagrange solver model including the different acting forces with its modeling, indication of the models applied, methods for locating the particle in the grid, and boundary conditions are explored.

2.1 Bubbles hydrodynamics

In Lagrangian simulations for particulate flows, it is more physical the consideration of the interaction among bubbles, and between bubbles and the flow boundary, even if the void fraction is very low, it can exist an overlapping of the bubbles if the bubbles interaction was not considered. As stated by Sommerfeld (2000), at gas hold up ratios below 10% the bubbles hydrodynamics can be neglected for its small effect in this small void fraction. If the gas void fraction exceeded this value, bubbles interactions should be taken into account in the simulation. Also as stated by Laín et al (2002) and Sungkorn (2011) void fraction up to 2% can be simulated by one-way coupling because the bubbles hydrodynamics effect on the continuous phase will be neglected.

In this work, the bubbles interaction mechanisms including collision modeling, coalescence modeling and breakup modeling have been applied. In the next it is presented first, the Forces acting on the bubbles with indication of the effect of the forces for different cases. Then a description for the collision modeling with a brief overview is presented. After that the coalescence modeling and breakup modeling with the presentation of some of the past works.

2.1.1 Acting forces

There are many forces acting on the motion of the bubbles inside the liquid. The forces which have a major effect on the moving bubbles are;

- Buoyancy force,
- Drag force,

- Lift force,
- Wall lubrication force,
- Bubble deformation force,
- Turbulent dispersion forces,
- Virtual mass force.

There are other forces like basset force, and pressure gradient force that do not have considerable effect in our case. The form of these forces will be described in some details in the models presented here for each individual force. And the adequate model will be selected.

Buoyancy force

The buoyancy force is generated in the vertical direction as a result of the difference in the densities between the two phases. It is calculated in cylindrical coordinates as follows:

$$F_{bu,r} = 0.0 \qquad (2.1-1)$$

$$F_{bu,\theta} = 0.0 \qquad (2.1-2)$$

$$F_{bu,z} = V_b(\rho_c - \rho_d)g_z \qquad (2.1-3)$$

Drag force

The Drag force $\vec{F}_{Dr}$ acting on the bubble depends on the relative velocity between the bubble and the continuous phase (liquid), its components are given by the following expression:

$$\vec{F}_{Dr} = -\frac{3}{8}C_{Dr}\,\frac{1}{R_b}\rho_c V_b|\vec{u}_{rel}|\vec{u}_{rel} \qquad (2.2)$$

Where $\vec{u}_{rel} = \vec{u}_b - \vec{u}_l$ is the relative velocity that feels the bubble at a given position in the liquid field such that $\vec{u}_l$ is the sum of the average liquid velocity obtained from the RANS approximation $\overrightarrow{U_l}$, and the fluctuating component generated from the CRW model $\overrightarrow{u_l}$, R_b is the radius of the bubble, and V_b is the volume of the bubble. Many empirical correlations have been used for modeling the Drag coefficient C_{Dr} for bubbles flow in liquids. In the next lines, some of the models used with air-water systems are explored.

Schiller and Nauman model

Schiller, L. and Nauman, A., (1933) introduced an expression for the drag coefficient that is valid for particles with $Re_b < 800$ that keep the spherical shape, as follows:

$$C_{Dr} = \frac{24}{Re_b}\left(1.0 + 0.15 Re_b^{0.687}\right) \quad (2.3)$$

Where Re_b is the bubble Reynolds number defined as $Re_b = \rho_c |u_{rel}| d_b / \mu_c$.

Grace model

Grace et al. (1976) considered the distortion of the bubble for an ellipsoid shape for which the bubble drag coefficient is expressed as follows;

$$C_{Dr} = \frac{4}{3}\frac{g d_b}{U_{ter}^2}\frac{(\rho_c - \rho_d)}{\rho_c} \quad (2.4)$$

Where U_{ter} is the terminal velocity of the bubbles. Grace revisited the previous experimental studies by Hu and Kintner (1955) and Johnson and Braida (1957) and, based on their data, derived a useful correlation for the terminal velocity of ellipsoidal bubbles and drops. They concluded that the experimental data may be expressed by the following correlation, which is valid for Re_b>0.1, Eo<40 and Mo<0.001:

$$U_{ter} = \frac{\mu_c}{\rho_c d} Mo^{-0.149}(J - 0.857) \quad (2.5)$$

Such that

$$J = \begin{cases} 0.94H^{0.757} & \text{for } 2 < H < 59.3 \\ 3.42H^{0.441} & \text{for } H > 59.3 \end{cases} \quad (2.6)$$

Where the parameter H is defined as:

$$H = \frac{4}{3} Eo.\, Mo^{-0.149}\left(\frac{\mu_c}{\mu_{wat}}\right)^{-0.14} \quad (2.7)$$

Where μ_{wat} is the dynamic viscosity of water, and Eo, Mo are the Eötvös and Morton Numbers respectively which are defined as follows:

$$Eo = \frac{g.(\rho_c - \rho_d).D_b^2}{\sigma} \quad , \quad Mo = \frac{g\mu_c^4(\rho_c - \rho_d)}{\rho_c^2 \sigma^3} \quad (2.8)$$

Ishii and Zuber model

The drag coefficients based on the correlations by Ishii and Zuber (1979) for different flow regimes are normally employed for gas–liquid flows. The function $C_{Dr}(Re_b)$, known as the drag curve, can be correlated for individual bubbles across several distinct bubble Reynolds number regions:

Stokes region ($0 \leq Re_b < 0.2$)

$$C_{Dr} = \frac{24}{Re_b} \qquad (2.9-1)$$

Viscous region ($0 \leq Re_b < 1000$)

$$C_{Dr} = \frac{24}{Re_b}\left(1 + 0.1Re_b^{0.75}\right) \qquad (2.9-2)$$

Turbulent region ($Re_b \geq 1000$)

$$C_{Dr} = 0.44\ \text{E:} \qquad \text{Newtons Regime} \qquad (2.9-3)$$

$$C_{Dr} = \frac{2}{3}\sqrt{E_o \text{E}}\text{:} \qquad \text{Distorted regime} \qquad (2.9-4)$$

$$C_{Dr} = \frac{8}{3}\ \text{É:} \quad \text{Churn turbulent Regime} \qquad (2.9-5)$$

However, for large Reynolds number, this model does not consider the bubble Reynolds number but consider the deformation that can occur to the bubble as a function of the Eötvös number and the void fraction at the location of the bubble. From above, the Ishii and Zuber modification for the Newton and distorted regimes takes the form of a multiplying factor E, which is given in terms of the void fraction as

$$E = \left[\frac{1 + 17.67(1-\alpha_d)^{6/7}}{18.67(1-\alpha_d)}\right]^2 \qquad (2.10)$$

where α^d is the volume fraction of the disperse phase. For churn turbulent, however, the multiplication factor $\acute{E}$ takes the form:

$$\acute{E} = (1-\alpha_d)^2 \qquad (2.11)$$

The Lagrangian Framework under study considers each bubble individually; this model is not adequate for our application.

Laín model

Laín proposed an experimental correlation for the bubble drag coefficient for a wide range of Reynolds number for fluid sphere in Laín et al (2002) as follows;

$$C_{Dr} = \begin{cases} 16\mathrm{Re}_b^{-1} & \mathrm{Re}_b < 1.5 \\ 14.9\mathrm{Re}_b^{-0.78} & 1.5 < Re_b < 80 \\ 48\mathrm{Re}_b^{-1}\left(1 - 2.21\mathrm{Re}_b^{-0.5}\right) + 1.86 \times 10^{-15}\mathrm{Re}_b^{4.756} & 80 < Re_b < 1500 \\ 2.61 & 1500 < Re_b \end{cases} \quad (2.12)$$

As shown in his expression of drag coefficient, Laín considered only the dependence on the bubble Reynolds number without considering any distortions, so this model is preferred for small bubbles that keep the spherical shape.

Tomiyama models

Tomiyama (1998) proposed other relation for the bubble drag coefficient C_D for bubble flow in water for three cases, pure water, slightly contaminated water, and contaminated water systems which are respectively given by:

$$C_{Dr} = \max\left[\min\left\{\frac{16}{\mathrm{Re}_b}(1 + 0.15\mathrm{Re}_b^{0.687}), \frac{48}{\mathrm{Re}_b}\right\}, \frac{8}{3}\frac{\mathrm{Eo}}{\mathrm{Eo} + 4}\right] \quad (2.13)$$

$$C_{Dr} = \max\left[\min\left\{\frac{24}{\mathrm{Re}_b}(1 + 0.15\mathrm{Re}_b^{0.687}), \frac{72}{\mathrm{Re}_b}\right\}, \frac{8}{3}\frac{\mathrm{Eo}}{\mathrm{Eo} + 4}\right] \quad (2.14)$$

$$C_{Dr} = \max\left[\frac{24}{\mathrm{Re}_b}(1 + 0.15\mathrm{Re}_b^{0.687}), \frac{8}{3}\frac{\mathrm{Eo}}{\mathrm{Eo} + 4}\right] \quad (2.15)$$

The range of experimental data that agreed with these relations are $10^{-3}<\mathrm{Re}<10^{5}$, $10^{-2}<Eo<10^{3}$ and $10^{-14}<\mathrm{Mo}<10^{7}$.

Tomiyama also got expressions for C_{Dr} in the case of distorted bubbles in high Reynolds number flows. In Tomiyama (2004) he proposed the following correlation for distorted bubbles that take oblate or prolate spheroidal front:

$$C_{Dr} = \begin{cases} \frac{8}{3}\frac{\gamma^{1/3}\mathrm{Eo}}{(\gamma \mathrm{E_n})^{2/3}(1 - \mathrm{E_n^2})^{-1}\mathrm{Eo} + 16\mathrm{E_n^{4/3}}}\mathrm{F}(\mathrm{E_n})^{-2} & \text{for } \mathrm{E_n} < 1 \\ 6\gamma^{-1/3} & \text{for } \mathrm{E_n} = 1 \\ \frac{8}{3}\frac{\gamma^{1/3}\mathrm{Eo}}{(\gamma \mathrm{E_n})^{2/3}(\mathrm{E_n^2} - 1)^{-1}\mathrm{Eo} - 16\mathrm{E_n^{4/3}}}\mathrm{G}(\mathrm{E_n})^{-2} & \text{for } \mathrm{E_n} < 1 \end{cases} \quad (2.16)$$

For a perfect spheroid bubbles ($\gamma = 1$) the expression is simplified to

$$C_{Dr} = \begin{cases} \frac{8}{3}\frac{Eo}{E^{2/3}(1-E^2)^{-1}Eo + 16E^{4/3}}F(E)^{-2} & \text{for } E < 1 \\ 6 & \text{for } E = 1 \\ \frac{8}{3}\frac{Eo}{E^{2/3}(E^2-1)^{-1}Eo - 16E^{4/3}}G(E)^{-2} & \text{for } E < 1 \end{cases} \quad (2.17)$$

Such that

$$E_n = \frac{b}{a} \quad (2.18)$$

$$F(E_n) = \frac{\cos^{-1}E_n - E_n\sqrt{1-E_n^2}}{1-E_n^2} \quad (2.19)$$

$$G(E_n) = \frac{E_n\sqrt{E_n^2-1} - \tanh^{-1}\left(E_n^{-1}\sqrt{E_n^2-1}\right)}{E_n^2-1} \quad (2.20)$$

The dimentions a, b and the value of γ can be specified refering to figure 2.1.

As a comparison among the different models presented above with watching the difference between the calculated drag coefficients in figure 2.2, it is observed that Grace considered in his model that the terminal velocity of the particle is a function of the two phases and Eötvös number which consider a fixed velocity for each bubble and this is not true in the Lagrangian simulation as the velocity of the bubble is specified according to the forces affecting on the bubble up on which the bubble accelerates or decelerates. And as a result, this produce a constant drag coefficient as shown in figure 2.2.

Laín model considered only the change in Reynolds number and considered that the bubble will be perfect sphere and did not consider the bubble distortion as he did not include Eötvös number in his calculations. As can be seen in figure 2.2, the behavior of the Laín drag coefficient is very rare as it does not maintain a fixed proportionality with Reynolds number.

On the other hand, it can be observed that in Tomiyama (1998) model, he considered the bubble distortion effect and included Eötvös number in his calculation and as it can be seen at figure 2.2 the smooth change of the drag coefficient with increasing Reynolds number. As a conclusion, it was decided to use the model of Tomiyama (1998) in the present work as it considers wide range of experiments that include our application and for good agreement with experimental data as shown in Tomiyama (1998).

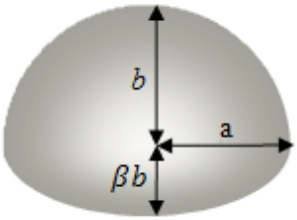

$E_n < 1$ *Oblate spheroidal front*

$E_n > 1$ *Prolate spheroidal front*

$$\gamma = \frac{2}{1+\beta}, \quad \beta > -1$$

Figure 2.1. Distorted bubbles with dimensions specification.

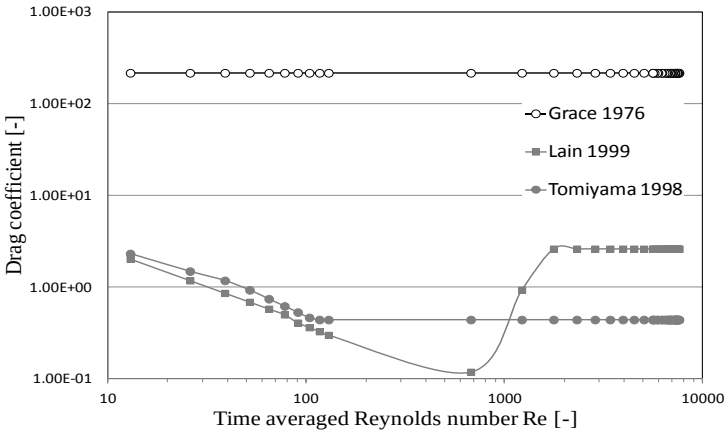

Figure 2.2. Drag coefficient comparison among different models as a function of Re_b and for Eo= 0.7893.

Lift Force

When bubbles flow in liquid which have velocity gradient, the bubble moves laterally with relative velocity related to the velocity gradient of the fluid. This motion is due to the change of the pressure on the sides of the bubble which exert a force called Lift force.

Hibiki and Ishii (2007) presented a good overview for the lift force models proposed up to the date. They commented that in the 1980s and 1990s, extensive experiments were performed to identify important parameters to determine the lateral bubble migration characteristics. The experiments showed that relatively small and large bubbles tend to

migrate toward a channel wall and center, respectively (Žun, 1998; Liu, 1993; Hibiki and Ishii, 1999; Hibiki et al., 2001, 2003). A numerical simulation of single bubbles (Tomiyama et al., 1993, 1995b) suggested that the bubble migration toward the pipe center was related closely to a slanted wake behind a deformed bubble. Thus, it has been indicated that the bubble size and complex interaction between a bubble wake and a shear field around the bubble play an important role in the lateral bubble migration (Serizawa and Kataoka, 1988, 1994). Tomiyama et al. (2002) measured bubble trajectories of single air bubbles in simple shear flows of glycerol–water solutions to evaluate transverse lift force acting on single bubbles. Based on the experimental result, they assumed the lift force caused by the slanted wake had the same functional form as that of the shear-induced lift force, and proposed an empirical correlation of the lift coefficient, see Table 2.1. Very recent experiment done by Tomiyama et al. (2004) implies that a slight bubble deformation might change the direction of the lift force acting on a bubble even at Re <5 and this results agree with the numerical simulation results by Takagi and Matsumoto (1995). As described above, the lift force is still poorly understood, and thus experimental and numerical efforts have further to be made to understand the lift force (Sridhar and Katz, 1995; Loth et al., 1997; Ervin and Tryggvason, 1997).

On the other hand Moraga (1999) stated that at high values of the multiplication of $(Re * Re_{\nabla})$, wake effects dominate and the lateral force is toward the low velocity region. At smaller values of $(Re * Re_{\nabla})$ inviscid lift reverses the direction of the lateral force. Such that Re is the Reynolds number based on relative velocity and Re_{∇} is based on average shear. He stated also that the non-dimensional parameter $(Re * Re_{\nabla})$ is by itself insufficient to describe the behavior of the lift coefficient since the Reynolds number, Re, plays an important role too. Also he stated that many possible explanations of the sign reversal of the lift force have been explored. Perhaps the most obvious possibility for bubbly flows is bubble deformation. Serizawa and Kataoka (1987) and Žun (1985) found evidence that bubble size and shape affect the discrete phase's distribution profile and plays an important role in the transition from bubbly to slug flow. Kariyasaki (1987) attributed the change in sign to the fact that bubbles adopted an airfoil shape which was responsible for the observed aerodynamical lift.

As a conclusion, it can be stated that there are three main reasons for the lateral migration of particles. The first reason is the shear flow around the bubble. The second is the rotation of the bubbles. The third is the deformation of the bubble that causes a slanted wake behind the bubble which is asymmetric and increase the lateral lift on the bubble.

Auton Model

The first analytical expression for the lift force was suggested by Auton (1987) for the case of a spherical particle moving in a velocity gradient of an inviscid fluid. The expression proposed by Auton was as follows:

$$\vec{F}_{LF} = -C_T V_b \rho_c (\vec{u}_{rel}) \times \vec{\omega} \tag{2.21}$$

Where C_T is the lift coefficient, V_b is the bubble volume and $\vec{\omega}$ is the the vorticity of the liquid velocity field, $\vec{\omega} = \text{rot}\,\vec{u}_c$ (Auton 1987). In his work, Auton considered a constant value of the lift coefficient C_T of 0.5. many other researchers considered also a constant value for C_T as Drew and Lahey (1979) which used the same value as Auton of 0.5, Lopez de Bertodano (1992) and Takagi and Matsumoto (1998) suggested a value of C_T=0.1. And a value of C_T=0.01 was suggested by Wang et al (1987) for viscous flows. Actually this previous expression of the lift force have been generalized to all the researchers after that.

Tomiyama Model

Using the same form of the lift force expression introduced by Auton, Tomiyama (1998) proposed a form of the lift coefficient that take in account the interaction between the distorted bubble and the shear field of the liquid phase and is given by

$$C_T = \begin{cases} \min[0.288\tanh(0.121Re_b), f(Eo_{hd})], \text{for } Eo_{hd} < 4 \\ f(Eo_{hd}), \text{for } 4 < Eo_{hd} < 10 \\ -0.27, \text{for } Eo_{hd} > 10 \end{cases} \tag{2.22}$$

Where Eo_{hd} is an Eötvos modified number, given in terms of the maximum horizontal dimension of the bubble d_{hb} which is developed by Wellek et al (1966).

$$Eo_{hd} = \frac{g(\rho_c - \rho_d)d_{hb}^2}{\sigma} \quad , \quad \text{with } d_{hb} = D_b \sqrt[3]{1 + 0.163Eo^{0.757}} \tag{2.23}$$

And the function $f(Eo_{hd})$ is the same function defined by Tomiyama(1998):

$$f(Eo_{hd}) = 0.00105{Eo_{hd}}^3 - 0.0159{Eo_{hd}}^2 - 0.0204Eo_{hd} + 0.474 \tag{2.24}$$

The correlation of Wellek et al (1966) used for defining the maximum horizontal bubble diameters was deduced for liquid-liquid two phase flows but it was checked and confirmed by Tomiyama et al (2002) for bubbly flow up to Eo of 3.4. Some correlations were presented for describing the bubble shape deformation as the bubble geometry mean aspect ratio E which is the ratio of the vertical diameter to the horizontal one of the deformed bubble.

$$E = d_{vb}/d_{hb} \tag{2.25}$$

For more systems like Ziqi et al (2010) presented the following correlation:

$$E = 4.67 * Re^{0.625} Eo^{-1} Mo^{0.291} \tag{2.26}$$

It is clear that the expression of Wellek (1996) fits the experimental data for the air-water system more than this relation of Ziqi et al (2010) as can be shown in figure 2.3

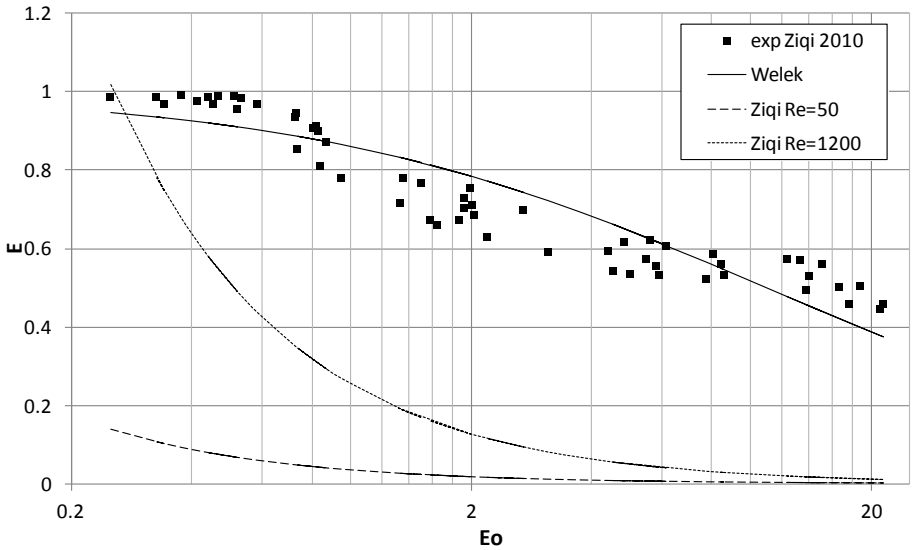

Figure 2.3. Bubble deformation aspect ratio comparison for different models for air-water systems.

It can be observed from figure 2.5 that the coefficient C_T defined by Tomiyama in equation (2.22) becomes negative when the bubble diameter becomes bigger than 5.8 mm for the case of air-water systems. As this value depends on the properties of the fluids and diameter of bubbles, it will differ for different pressures and fluids. And this can explain why the big bubbles migrate towards the center of the pipe and the small ones migrate towards the pipe wall.

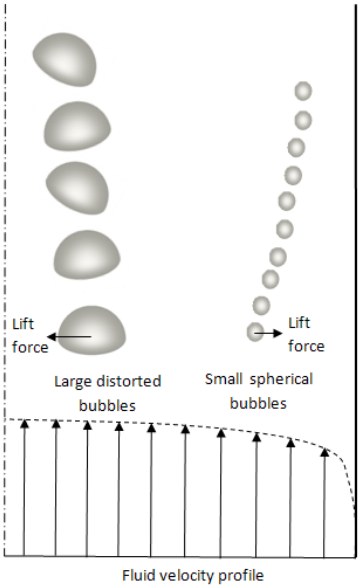

Figure 2.4. Radial bubbles migration according to lift force.

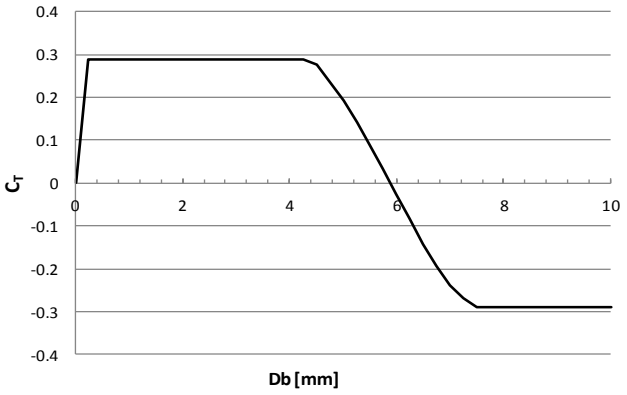

Figure 2.5. Tomiyama Lift Coefficient for air water systems.

Hibiki model

Hibiki and Ishii (2007) presented a modified model for the lift force coefficient after performing an extensive study of the literature on lift force modeling. They presented a definition for the lift coefficient in case of no particle deformation which can be modified for deformation effects by multiplying this coefficient by a modification factor. In case of no deformation the lift coefficient is :

$$C_T = \sqrt{\{C_T^{Low\ Re}(Re_b, G_S)\}^2 + \left\{C_T^{High\ Re}(Re_b, G_S)\right\}^2} \tag{2.27}$$

Where

$$C_T^{Low\ Re}(Re_b, G_S) = \frac{6}{\pi^2(2Re_b \times G_S)^{\frac{1}{2}}} \frac{2.255}{\left(1 + \frac{0.1Re_b}{G_S}\right)^{\frac{3}{2}}} \tag{2.28}$$

$$C_T^{High\ Re}(Re_b) = \frac{1}{2}\left(\frac{1 + 16{Re_b}^{-1}}{1 + 29{Re_b}^{-1}}\right) \tag{2.29}$$

Such that Re_b is the bubble Reynolds number and G_S is a dimensionless velocity gradient number which is defined as follows

$$Re_b = \frac{\rho_c |v_r| d_b}{\mu_c} \quad G_S = \frac{0.5 D_b \omega}{u_{rel}} \tag{2.30}$$

And ω is the magnitude of velocity gradient.

In case of bubble deformation, the lift coefficient is multiplied by a factor ξ which takes in account the deformation of the bubbles, this factor is expressed as follows:

$$\xi = 2 - \exp(0.136 Eo^{1.11}) \tag{2.31}$$

It can be observed that the deformation factor values goes to 1 as the Eötvös number vamishes (not deofmed bubble).

The new lift coefficient for distorted bubbles will be as follows:

$$C_T = \xi \sqrt{\{C_T^{Low\ Re}(Re_b, G_S)\}^2 + \left\{C_T^{High\ Re}(Re_b, G_S)\right\}^2} \tag{2.32}$$

It should be noted that from the definition of the current model, the critical bubble diameter for air water systems is 5.7mm at which the sign of the lift coefficient changes, which is very similar to that of Tomiyama model 5.8mm.

For multi particle systems Hibiki extended the relation 2.31 by defining the Renolds number Re and the dimensionless velocity gradient number G_S as follows:

$$Re_b \equiv \frac{\rho_c |u_{rel}| D_b}{\mu_m} \quad G_S \equiv \left| \frac{0.5 D_b}{u_{rel}} \frac{du_c}{dx} \right| \tag{2.33}$$

And the definition of the Lift force per unit volume will be as follows:

$$\vec{F}_{LF} = -\alpha_d \, C_T \rho_c \, \vec{u}_{rel} \times \vec{\omega} \tag{2.34}$$

the $C_L^{Low\ Re}$ and $C_L^{High\ Re}$ values are defined as in equation 2.28 and 2.29 respectivelt. And the lift force coefficint C_L is defines as equation 2.32 with the ξ coefficient defined as follows:

$$\xi = 2 - \exp\left(2.92 D_d^{*\,2.21}\right) \tag{2.35}$$

Such that D_d^* is the nondimensional bubble diameter defined as :

$$D_d^* = \frac{\sqrt{Eo}}{4} \tag{2.36}$$

Unfortunately, up to now, no one could give a universal expression for the lift force coefficient that can be used for all systems. The model of Tomiyama (1998) gave good agreements with experimental results but it was designed for single bubble and did not have in account the effect of the void fraction on the lift force coefficient. On the other hand, Hibiki fixed this problem and proposed a correlation for multi particle systems but the range of experiments with which the correlation is evaluated is limited. Some researchers used constant values for the lift force coefficient ranging from 0.01 recommended for viscous flows up to 0.5.

In the present work, the Euler solver could give us the velocity gradients in Cartesian coordinates, so it was decided to calculate the lift force in Cartesian coordinates and then transform it to the cylindrical coordinates to be used in the Lagrangian solver.

The lift force is defined in equation 2.34, the vorticity can be calculated in Cartesian coordinates as follows:

$$\vec{\omega} = \text{curl}(\vec{u}_l) = \begin{vmatrix} \hat{i} & \hat{j} & \hat{k} \\ \frac{\partial}{\partial x} & \frac{\partial}{\partial y} & \frac{\partial}{\partial z} \\ u_{l,x} & u_{l,y} & u_{l,z} \end{vmatrix} =$$

$$= \hat{i}\left(\frac{\partial u_{l,z}}{\partial y} - \frac{\partial u_{l,y}}{\partial z}\right) - \hat{j}\left(\frac{\partial u_{l,z}}{\partial x} - \frac{\partial u_{l,x}}{\partial z}\right) + \hat{k}\left(\frac{\partial u_{l,y}}{\partial x} - \frac{\partial u_{l,x}}{\partial y}\right) \quad (2.37)$$

As a result, the cross product of the relative velocity vector and the curl of the liquid velocity will give:

$$(\overrightarrow{u_b} - \overrightarrow{u_c}) \times \vec{\omega} = \begin{vmatrix} \hat{i} & \hat{j} & \hat{k} \\ (u_{b,x} - u_{l,x}) & (u_{b,y} - u_{l,y}) & (u_{b,z} - u_{l,z}) \\ \left(\frac{\partial u_{l,z}}{\partial y} - \frac{\partial u_{l,y}}{\partial z}\right) & -\left(\frac{\partial u_{l,z}}{\partial x} - \frac{\partial u_{l,x}}{\partial z}\right) & \left(\frac{\partial u_{l,y}}{\partial x} - \frac{\partial u_{l,x}}{\partial y}\right) \end{vmatrix} \quad (2.38)$$

Finally, the lift force can be expressed as follows:

$$F_{LF} = -C_t \times V_b \times \rho_c \times$$

$$\begin{bmatrix} \left[(u_{b,y} - u_{l,y})\left(\frac{\partial u_{l,y}}{\partial x} - \frac{\partial u_{l,x}}{\partial y}\right) + (u_{b,z} - u_{l,z})\left(\frac{\partial u_{l,z}}{\partial x} - \frac{\partial u_{l,x}}{\partial z}\right)\right] \\ -\left[(u_{b,x} - u_{l,x})\left(\frac{\partial u_{l,y}}{\partial x} - \frac{\partial u_{l,x}}{\partial y}\right) - (u_{b,z} - u_{l,z})\left(\frac{\partial u_{l,z}}{\partial y} - \frac{\partial u_{l,y}}{\partial z}\right)\right] \\ \left[-(u_{b,x} - u_{l,x})\left(\frac{\partial u_{l,z}}{\partial x} - \frac{\partial u_{l,x}}{\partial z}\right) - (u_{b,y} - u_{l,y})\left(\frac{\partial u_{l,z}}{\partial y} - \frac{\partial u_{l,y}}{\partial z}\right)\right] \end{bmatrix} \quad (2.39)$$

Wall lubrication force

This force is originated as a result of the drainage of liquid around a bubble that is moving in the vicinity of the pipe wall. The non-slip condition at the wall should slow the drainage rate between the bubble and the wall, at the bubble-wall side, while the drainage of liquid is increased on the opposite side of the bubble. Therefore we have a asymmetrical drainage of liquid for a bubble moving close to the wall. As a consequence the bubble suffers a hydrodynamic force known as wall lubrication force.

Antal model

The expression for this force was first deduced by Antal et al (1991b) for Re<1500 and gas fraction less than 10%. The expression is as follows per unit volume:

$$\vec{F}_{WL} = -\frac{\alpha_d \rho_c \left[(\vec{u}_{rel}) - \left((\vec{u}_{rel}).\vec{n}_w\right)\vec{n}_w\right]^2}{D_b} \times C_{wl} \tag{2.40}$$

Such that in Antal model, the coefficient C_{wl} is expressed as follows:

$$C_{wl} = \max\left(0, C_{w1} + \frac{C_{w2} D_b}{Y_{WALL}}\right) \tag{2.41}$$

Where $Y_{WALL}$is the distance from the bubble is center to the wall boundary, and $\vec{n}_w$ is the outward vector normal to the wall. The wall lubrication constants determined through numerical experiments of a sphere have been taken by different authors as follows:

	C_{w1}	C_{w2}
Antal	-0.01	0.05
Krepper et al (2005)	-0.0064	0.016

For the coefficients specified by Antal, he used experimental work of a very small bubble diameter of 0.87mm with 1.9% area average void fraction. So the model of Antal is valid for small bubbles in this range of bubble diameter at which the bubble is considered a complete sphere, with small gas void fractions. Also it is adviced using a very fine mesh when using the model of Antal to get grid convergence as stated in CFX-modeling guide.

The form of the wall lubrication force per unit volume can be modified to a more comfortable expression as follows:

$$\vec{F}_{WL} = -\alpha_d \rho_c \left[(\vec{u}_{rel}) - \left((\vec{u}_{rel}).\vec{n}_w\right)\vec{n}_w\right]^2 \times C_w \tag{2.42}$$

And the coefficient will be expressed as follows:

$$C_w = \max\left(0, \frac{C_{w1}}{D_b} + \frac{C_{w2}}{Y_{WALL}}\right) \tag{2.43}$$

With that modification, the coefficient is dimensionless and the expression of the wall force is easier to apply.

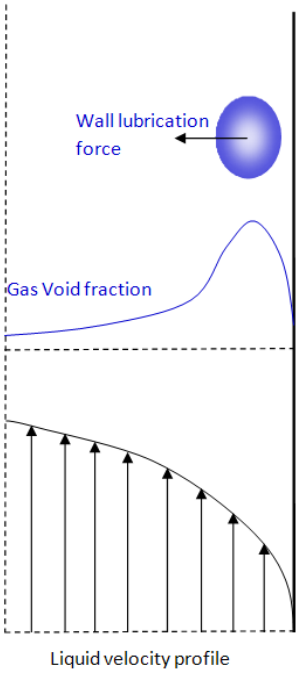

Figure 2.6. Wall lubrication force.

Tomiyama Models

Tomiyama (1998) proposed a model for the wall lubrication force dependent on Eötvös number of the bubble which is valid for air bubbles in Glycerol-water solution flows (log Mo=-2.8.) The force is expressed as follows:

$$\vec{F}_{WL} = -C_W f_{WL}(Y_{WALL})\rho_c |u_{rel,z}|^2 \hat{e}_r \tag{2.44}$$

Such that the wall lubrication coefficient is defied for Log Mo=-2.8 as follows:

$$C_W = \begin{cases} e^{-0.933Eo+0.179} & \text{for } 1 \le Eo \le 5 \\ 0.007Eo + 0.04 & \text{for } 5 \le Eo \le 33 \end{cases} \tag{2.45}$$

And the function $f_{WL}(Y_{WALL})$ is defined as follows:

$$f_{WL}(Y_{WALL}) = \frac{d_b}{2}\left\{\frac{1}{Y_{WALL}^2} - \frac{1}{(D_b - Y_{WALL})^2}\right\} \tag{2.46}$$

However, he stated that this model needs to be tuned for other Morton number systems.

Hosokawa, Tomiyama and others (2002) proposed a model for air-water systems valid for bubbles diameter ranging from 0.5mm up to 9mm as follows

$$C_W = \max\left[\frac{7}{Re_b^{1.9}}, 0.0217Eo\right] \tag{2.47}$$

Tomiyama et al (2002) in his simulation of single bubble, proposed the wall lubrication force as a function of the bubble volume in the place of the gas void fraction as follows:

$$\vec{F}_{WL} = -C_W V_b \rho_c \left|u_{rel,z}\right|^2 f_{WL}(Y_{WALL})\hat{e}_r \tag{2.48}$$

Frank et al models

In Frank et al (2008), they changed the function model of Tomiyama to be independent on the pipe diameter by changing the function $f_{WL}(y)$ to be as follows:

$$f_{WL}(Y_{WALL}) = \max\left\{0, \frac{1}{C_{WD}} \frac{1 - \frac{Y_{WALL}}{C_{wc} D_b}}{Y_{WALL}\left(\frac{Y_{WALL}}{C_{wc} d_b}\right)^{p-1}}\right\} \tag{2.49}$$

Such that the cut off coefficient $C_{wc} = 10.0$, the damping coefficient $C_{WD} = 6.8$, and the exponential coefficient $p = 1.7$ for this correlation gives the same correlation as that of Tomiyama model.

In Frank et al (2004) he proposed a modification for the wall coefficient for the model of Tomiyama 1998 by suggesting values for the wall lubrication coefficient in cases of $Eo < 1$ and $Eo > 33$ which does not exist in Tomiyama model, with slit change in the range $5 \le Eo \le 33$. The new expressing is as follows:

$$C_W = \begin{cases} 0.47 & Eo < 1 \\ e^{-0.933Eo+0.179} & 1 \le Eo \le 5 \\ 0.00599Eo - 0.0187 & 5 \le Eo \le 33 \\ 0.179 & Eo > 33 \end{cases} \tag{2.50}$$

As shown in Figure 2.7, the difference between the introduced models for calculating the wall lubrication coefficient is clear. It can be observed that the model of Antal gives the smallest value as it was designed for very small bubbles, the models of Tomiyama (1998) and Frank et al (2004) are very similar as the modification of Frank was only removing the dependence on the pipe diameter in the wall distance function f_{WL}.

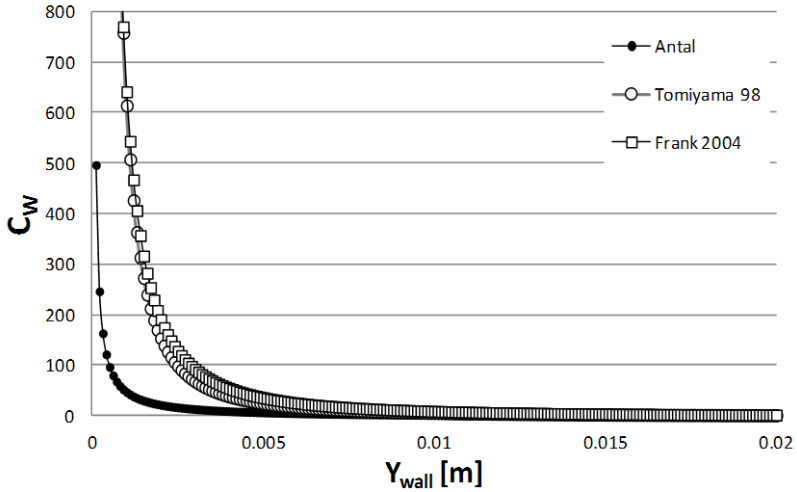

Figure 2.7. Comparison between different models for wall lubrication coefficient for D_b=2.8mm, Eo=1.074, and D_p=0.052m.

It was found that the model which fits our requirements in the present work is that of Hosokawa and Tomiyama et al (2002) as it takes in account the Reynolds number changes, which is a logic suggestion according to the nature of this force that should depend on the bubble Reynolds number, designed for air-water systems and valid for wide range of bubbles diameter which include the range applied in the simulations of the present thesis.

Bubble deformation force

According to Zaruba et al (2007), it is needed to consider a bubble deformation force that makes the bubble bounce when shocking with the pipe wall to prevent the bubble centre of mass displacement to be unrealistically close to the wall. Some researchers do not use this force depending on the effect of the wall lubrication force and consider that it is included in the wall lubrication force. In the current work, this force was considered according to the different nature of this force which depends on the bouncing effect on the wall and that the wall lubrication force generates from the difference of the velocity of liquid on the two sides of the bubbles when moving in the vicinity of the wall.

To compute this force it was assumed a bubble that when approaching and touching the walls deforms and adopts an oblate shape as displayed at figure 2.8 (a). It was assumed that the deformation of the bubble conserves the volume so it can be written as:

$$\frac{4}{3}\pi R_b^3 = \frac{4}{3}\pi a^2 Y_{wall} \Rightarrow a = \frac{R_b^{3/2}}{Y_{wall}^{1/2}} \tag{2.51}$$

Where y is the distance from the wall to the bubble center, and a denotes the dimension of the ellipsoid in the directions parallel to the wall. This ellipsoid is obviously oblate with y<a . The area of this ellipsoid can be calculated as the surface of a revolution spheroid with symmetry axis orthogonal to the wall. After some calculus it is obtained that this area is given by the following expression:

$$A(Y_{wall}) = 2\pi a^2 + 2\pi a Y_{wall}\frac{\sinh^{-1}\mu'}{\mu'},\ \mu' = \left(\frac{a^2}{Y_{wall}^2} - 1\right)^{\frac{1}{2}} = \left(\frac{R_b^3}{Y_{wall}^3} - 1\right)^{1/2} \tag{2.52}$$

The work that is needed to deform the bubble from the spherical form with radius R_b to the oblate one with distance y from the wall to the bubble centre is:

$$W(Y_{wall}) = \sigma\Delta A = \sigma\big(A(Y_{wall}) - A(Y_{wall} = R_b)\big) \tag{2.53}$$

Therefore the corresponding deformation force $\vec{F}_{Def}$ acting on a single bubble with $y = R - r$ is given on account that $\hat{e}_y = -\hat{e}_r$ by:

$$\vec{F}_{Def} = -\frac{\partial W(Y_{wall})}{\partial y}\hat{e}_y = 2\pi R_b \sigma \left(\frac{R_b}{Y_{wall}}\right)^2 f_D\left(\frac{R_b}{Y_{wall}}\right)\hat{e}_r \tag{2.54}$$

Such that f_D is given as follows:

$$f_D\left(\frac{R_b}{Y_{wall}}\right) = -1 + \frac{1}{2}\frac{\sinh^{-1}\mu'}{\mu'}\left(\frac{R_b}{Y_{wall}}\right)^{-\frac{3}{2}} + \frac{3}{2}\left(\frac{R_b}{Y_{wall}}\right)^{\frac{3}{2}}\frac{1}{\mu'^{\frac{5}{2}}}$$

$$\times\left(\sinh^{-1}\mu' - \frac{\mu'}{(1+\mu'^2)^{1/2}}\right) \tag{2.55}$$

The wall deformation force profile near the wall will be as shown in figure 2.10.

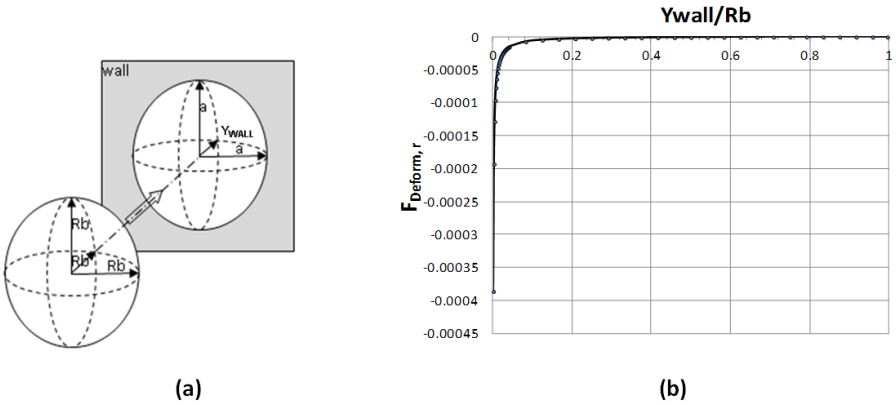

Figure 2.8. (a) Bubble deformation near the wall, (b) Bubble deformation force for 2.4mm bubble.

Turbulent dispersion Effect

The turbulent dispersion effect exist due to the turbulence of the phases and helps to make the distribution of the dispersed phase softer by redistributing the dispersed phase from the regions of high concentration of void fraction to the regions of low concentration. This effect is modeled in the numerical programs as a force and there is variety of models proposed for that force. This turbulent dispersion effect is a main factor that modifies the radial distribution of the gas void fraction profile. It controls the peak of the profile of gas void fraction and mainly softens the profile not to have sharp increments in the gas void fraction distribution. For example in case of the small bubbles, the lift force pushes the bubble in the direction of the wall, the force which resist this effect with the drag is the turbulence dispersion (TD) force and the same in the case of the large bubbles.

One of the models proposed for this force is the model of Antal et al (1991a) which suggested the following form of the TD force:

$$F_{TD,r} = -C_{TD}\rho_c k_c \nabla\alpha_c \tag{2.56}$$

Values of the coefficient C_{TD} ranging from 0.0: 0.5 have been employed successfully for bubbly flow with diameters of the order of millimeters. Lopez de Bertodano (1998) gives a formula for calculating the coefficient C_{TD} as follows:

$$C_{TD} = c_\mu^{1/4} \frac{1}{St(1+St)}, \qquad St \equiv \frac{\tau_b}{\tau_c} \tag{2.57}$$

Such that St is the Stokes number, τ_b is the bubble response time and τ_c is the time response of the continuous phase in existence of the dispersed one (Moraga et al 2003) and both of them are defined as follows:

$$\tau_b = \frac{8}{3}\frac{R_b}{C_{Dr}|u_{rel}|}, \qquad \tau_c = c_\mu^{1/4}\, k/\varepsilon \tag{2.58}$$

Such that the value of c_μ is 0.09 for the k-ε model, C_{Dr} is the bubble drag coefficient, R_b is the bubble radius, u_{rel} is the bubble relative velocity, K is the turbulent Kinetic energy of the continuous phase, and ε is the dissipation rate of turbulence. According to Lopez de Bertodano (1998) and Moraga et al (2003), values of C_{TD} up to 500 have been required for in some situations. Burns et al (2004) have derived an alternative approach based on the consistency of the favre averaging, which is expressed as follows:

$$F_{TD,r} = -C_{TD}C_{Dr}\frac{\mu_{t,d}}{\rho_d Sc_b}\left(\frac{\nabla\alpha_d}{\alpha_d} - \frac{\nabla\alpha_c}{\alpha_c}\right) \tag{2.59}$$

Where in this model$C_{TD} = 1$, $\mu_{t,d}$ is the turbulent viscosity of the dispersed phase and Sc_b is the bubble turbulent Schmidt number with an adopted value of 0.9, the constant C_{Dr} is the drag coefficient which describes the interfacial drag force. So, this model depends on the drag characteristics of the gas liquid system.

In the present work, the CRW modeling that generates velocity fluctuations which cause this effect of turbulent dispersion is considered. So it is not needed to apply any modeling for the turbulence dispersion effect.

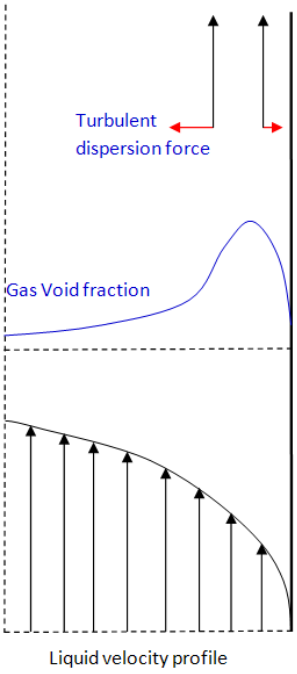

Figure 2.9. Turbulent Dispersion Force.

Virtual Mass Force

The Virtual mass force is defined as the force required by the bubble as it have a very small mass comparing with the mass of the same volume of the liquid, to move the same volume of liquid when acceleration or deceleration, or simply, force required for resisting the inertia of the liquid when accelerating or decelerating the bubble. It is called virtual mass because it is related to a mass of the liquid of the same volume of the bubble that is considered virtually. The virtual mass effect can be considered by the virtual mass coefficient written in equation 3.1. A value of 0.5 for the virtual mass coefficient C_{VM} is used in the present work as used by many authors in the application of bubbly flows (Tomiyama et al 1998, Delonij et al 1996, and Darmana et al 2006). Tomiyama (2004) presented a new approach for calculating the virtual mass coefficient. He considered the coefficient to be a tensor that changes its value depending on the shape of the spheroid that considered as the shape of the bubble and its aspect ratio.

2.1.1.1 Indication of Forces for Different Cases

In this section, the effect of each force on the trajectory of the bubble will be introduced. Three different cases of single bubble simulations were made with the same condition to observe the effect of the different forces on the radial bubble migration in a vertical pipe. Figure 2.10 shows the behavior of three different cases of a single bubble moving in an upward water pipe flow. The three cases were simulations of a single bubble for three different bubble diameters which are 2mm, 5mm, and 8mm injected at a radial distance r= D_p /4 such that D_p=0.052m is the diameter of the pipe. On the left hand side, it is presented a column for plots of the trajectories of the bubbles during its rise in the flow. On the right hand side column, it is shown the different instantaneous radial forces acting on the bubble with the total radial force.

In the first case of the 2mm bubble diameter, it can be observed the direct migration of the bubble to the wall side and that can be deduced from the radial forces diagram at which the total force is positive on the majority of the trajectory. It can be observed also that the lift force is always positive and the drag force change the sign to be in the opposite direction of the bubble motion. Also, it can be observed that the wall lubrication force is zero at all the trajectory and start to have a negative value when the bubble approaches the wall as it does the deformation force. In the second case of the 5mm bubble the bubble start to migrate in the direction of the pipe center and then changes to the direction of the wall, this change can be observed from the radial forces diagram. In this case the lift force also is positive according to Tomiyama model and the wall lubrication force start to have very small values different from zero as the bubble go in the wall direction. It can be observed that in this case the drag force is higher than the last case of 2mm diameter bubble. In the last case of 8mm bubble diameter, the most observable effect is the change of the direction of the effect for the lift force that now act in the negative direction which agree with the Tomiyama model as the bubble diameter is larger than 5.8mm. it can be seen that the wall lubrication force have a very small effect on the total radial force. In the three cases as these forces act very much when the bubble is close to the pipe wall. The motion of the bubble along the entire trajectory is in the direction of the pipe center which causes a positive drag force.

As a final observation, it can be seen that the lift force and the drag forces are the forces having the larger effect on the total force especially for small bubbles. The wall lubrication force starts to have bigger values for bigger bubbles due to the deformation effect and the increase of the velocity of the bubble. The deformation force as it is activated only when the center of the bubble start to be very near to the bubble wall with a distance less than the bubble radius, its effect can be observed only on the bubbles in the wall region

If we consider the radial forces acting on each bubble at a fixed height z=1.17m to see the order of magnitude for these forces. It is shown in table 2.1, the values of the different radial forces acting on each bubble. For the 2mm bubble as it is a small bubble, near the wall, it can be observed that the deformation force is the most effective one which make the bouncing effect as the bubble hit the wall and the resulting total force F_{total} is in the direction of the negative r direction as the wall lubrication force. For the 5mm bubble, the lift force is the more effective one in this case as the bubble size increase which increases the bubble relative velocity. For the 8mm bubble , the lift force changes its sign to be directed at the negative r direction In the three cases, the turbulence dispersion effect exist during the CRW model used for generating artificial fluctuating velocity components which generates the fluctuation of the bubble velocity and lead to the homogeneity of the void fraction distribution profile. In order to see this effect, is necessary to have a complete simulation of large number of bubbles. The turbulence dispersion effect is necessary to give a realistic void fraction profile distribution compared to the experimental one as shown in figure 2.11. If this effect does not exist, the bubbles of small size will accumulate on the wall of the pipe and that of the large size accumulate in the pipe center and the void fraction distribution will be much distorted.

Table 2.2. Different radial forces affecting on bubbles related to the total radial force at height z=1.17m.

Bubble diameter	F_{lift} /| F_{total} |	F_{wall} /| F_{total} |	F_{drag} /| F_{total} |	F_{deform} /| F_{total} |	F_{total}
2 mm	0.953	-0.227	0.085	-1.812	-3.5e-4
5 mm	12	-2.9	-8.1	0	1e-6
8 mm	-14.052	-1.47	16.52	0	1.53e-5

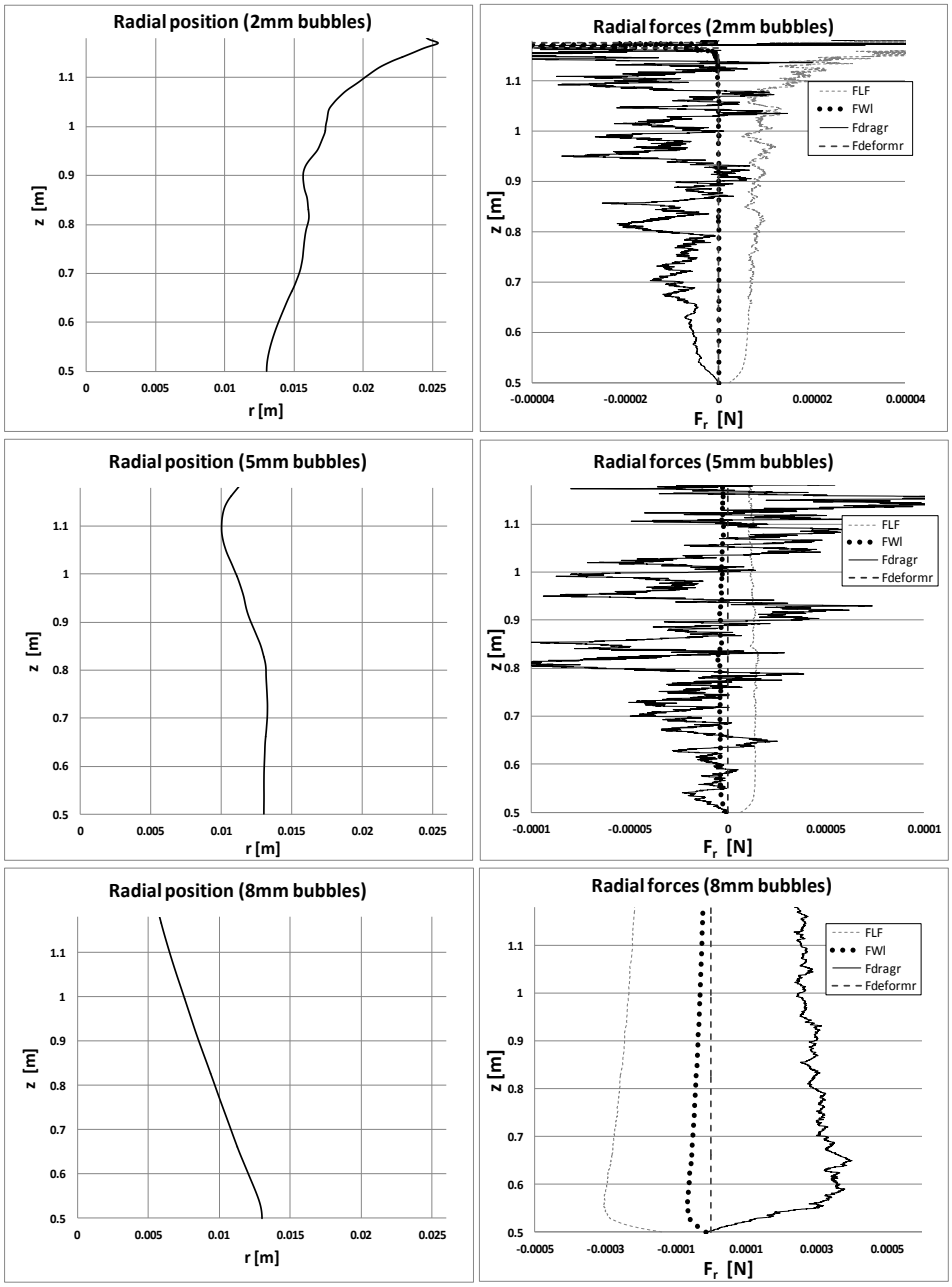

Figure 2.10. Radial migration of single bubble in 2m/s velocity water upward flow, in 0.026m radius pipe.

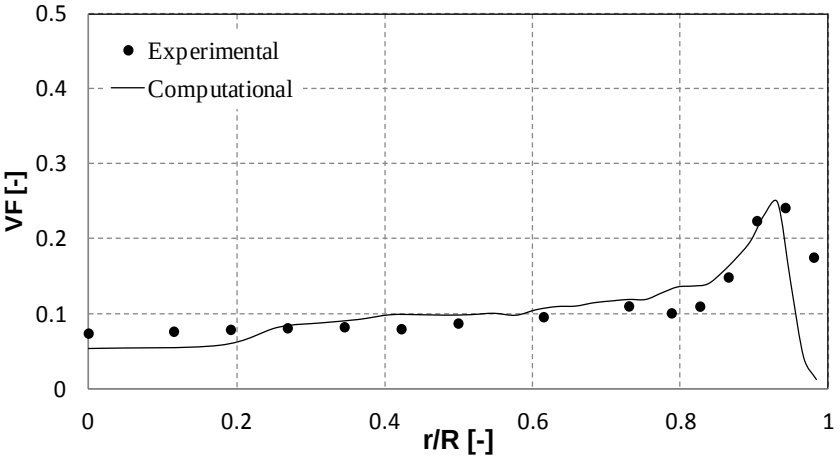

Figure 2.11. Radial gas void fraction profile for case J_c=2m/s and α_g=10%.

2.1.2 Collision modeling

In the present work, only dual collision is considered. The bubbles are very small (2.0 mm to 3.5 mm) which give us the ability to consider them as spherical bubbles without much deformation. The majority of the collision models considered in bubbly flow simulations neglects the deformation of the bubbles at the moment of collision and considers them as solid spherical bodies, these models will be explored with a brief description, stating the differences between them, and then one adequate model will be considered.

Hoomans et al (1996) model

Hoomans et al (1996) have proposed a collision model using a Hard-sphere approach with putting some assumptions. In his model, Hoomans considered in his model the restitution during the collision. This gave for the equation of the final normal velocity the following expression

$$u_{a,n}^{*} = u_{a,n} - (1 + er)\frac{(u_{a,n} - u_{b,n})m_b}{m_a + m_b} \tag{2.60}$$

With the definitions of the different velocities described at figure 2.12 being “er” the restitution coefficient.

Michaelides (2006) Model

Michaelides (2006) in his book has deduced the relation in a vectorial form considering the sliding effect of the particles during the collision. If the particles was sliding during the collision process with a friction factor of f_f, then the form of the final velocity will be as follows:

$$\vec{u}_a^* = \vec{u}_a - (1 + er)\left(\vec{n} \cdot \vec{W}_0\right)\frac{m_b}{m_a + m_b}\left(\vec{n} - f_f\vec{t}\right) \qquad (2.61)$$

Such that the vector $\vec{W}_0$ is the relative velocity vector between the two particles, $\vec{n}$ is a unit vector in the direction of center line between the two colliding bubbles, and $\vec{t}$ is a tangential unit vector normal to $\vec{n}$.

In case of particles no sliding during the collision process, the final velocity will be as follows:

$$\vec{u}_a^* = \vec{u}_a - \frac{m_b}{m_a + m_b}\left[(1 + er)\left(\vec{n} \cdot \vec{W}_0\right)\vec{n} + \frac{2}{7}\left|\vec{W}_{0,tc}\right|\vec{t}\right] \qquad (2.62)$$

Where $\vec{W}_{0,tc}$ is the initial tangential relative velocity between the two colliding particles at the point of contact.

Deen et al (2004) model

Deen et al., (2004), has proposed an approach of hard sphere collision by considering a complete elastic collision and neglecting energy loss as a result of the particle collision and friction. This model is based on the model of Hoomans et al (1996) with some simplifications. In this model, it is considered that the tangential components do not change due to the collision while the normal components will change according to the conservation of momentum and kinetic energy of the collision process in the normal direction, which produces the following equations:

$$m_a u_{a,n} + m_b u_{b,n} = m_a u_{a,n}^* + m_b u_{b,n}^* \qquad (2.63)$$

$$m_a u_{a,n}^2 + m_b u_{b,n}^2 = m_a {u_{a,n}^*}^2 + m_b {u_{b,n}^*}^2 \qquad (2.64)$$

The normal component is changed according to the following relation (elastic bouncing)

$$u_{a,n}^{*} = 2\frac{m_a u_{a,n} + m_b u_{b,n}}{m_a + m_b} - u_{a,n} \tag{2.65}$$

The velocities of the particles are as shown in figure 2.12.

It can be observed that the model of Deen is the same as the two former models when considering a complete elastic collision, which means a coefficient of restitution of value 1.

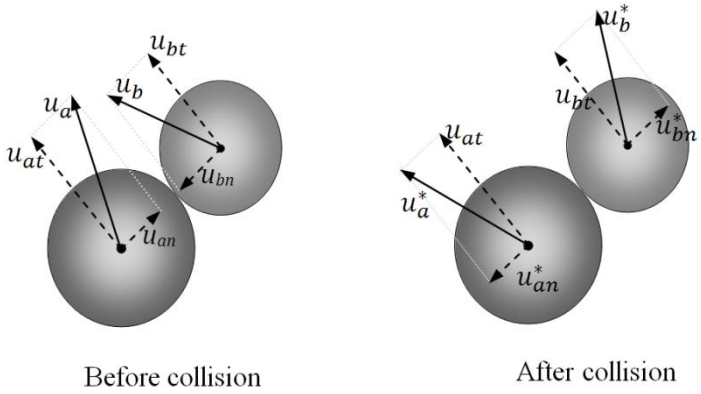

Figure 2.12. Configuration of bubble bounce following a collision event**.**

Applied model

In the present work, as small diameter of bubbles (2.0 to 3.5 mm) was used, and the bubbles are considered spherical, the collision process can be considered completely elastic for which the restitution coefficient is considered 1. And it can be considered frictionless collision between the two colliding particles and the friction coefficient is zero. For these reasons, the model developed by Deen et al (2004) was considered in the present work. Other reason for selecting this model was the necessity for gaining time during computation. Generally, the simulation of collision models for bubbles is considered elastic collisions as in Delnoij et al (1997), and Darmana et al (2006).

The collision time defined by Allen and Tildesley (1987) was used. This introduced the following formula for calculating the collision time between two spheres of different diameters:

$$d_{tc} = \frac{-\vec{r}_{ab}.\vec{u}_{ab} - \sqrt{(\vec{r}_{ab}.\vec{u}_{ab})^2 - \vec{u}_{ab}^{\,2}\left(\vec{r}_{ab}^{\,2} - (R_a + R_b)^2\right)}}{\vec{u}_{ab}^{\,2}} \tag{2.66}$$

Such that the a and b indexes denote the two colliding bubbles, $\vec{r}_{ab}$ is the relative position vector between them, $\vec{u}_{ab}$ is the relative velocity vector, and R_a, R_b are the radii of the bubbles a and b respectively

The model was applied according to fixed steps that will be explained in details in the following text:

At first, a neighbor list for each bubble is belt, which contains the bubbles around the desired one by a fixed distance R_w which form a spherical space around the considered bubbles i as shown at figure 2.13. For considering only one collision time for each pair of colliding bubbles, only the bubbles with indexes higher than the one under consideration of index I are counted as shown at figure 2.13. Then a loop is used for calculating the collision time using equation (2.66) and calculating the minimum collision time to be considered.

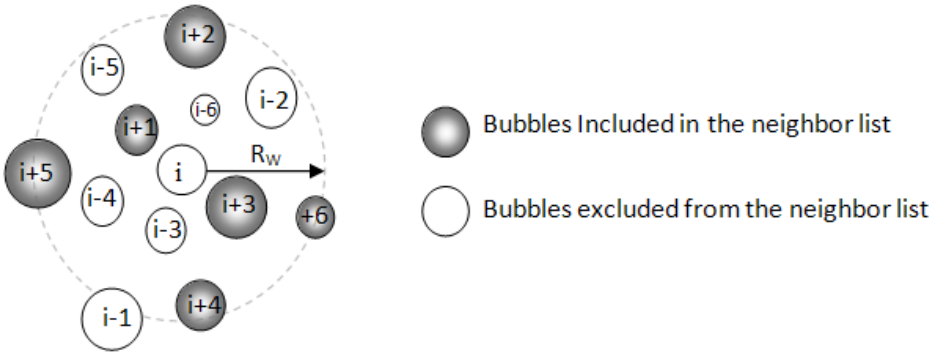

Figure 2.13. The neighbor list window for each bubble.

2.1.3 Coalescence modeling

As introduced in the literature work by Liao and Lucas (2010) at section 2 "mechanisms of fluid particle coalescence", three theories or criteria have been proposed for the coalescence process. The most popular theory is the film drainage model. Shinnar and Church (1960) state that, after their collision, two bubbles may cohere together and be prevented from coalescing by a thin film of liquid trapped between them. Attractive forces between them drive the film to drain out until it collapses, and coalescence follows. For simplicity, the coalescence is usually divided into three manageable sub processes: (1) two bubbles collide, trapping a small amount of liquid between them; (2) bubbles keep in contact till the liquid film drains out to a

critical thickness; (3) the film ruptures resulting in coalescence. In reality, the duration of collisions is limited due to the prevailing fluctuations and coalescence will occur only if the interaction time is sufficient for the intervening film to drain out down to the critical rupture thickness.

On the other hand, Howarth (1964) believes that the attraction force between two colliding interfaces, usually of molecular nature, is too weak in comparison with the turbulent force to control the coalescence probability. He argues that whether coalescence will occur or not depends on the impact velocity of the colliding bubbles. During energetic collisions, when the approach velocity of two colliding bubbles exceeds a critical value, immediate coalescence without liquid film capturing and thinning will be the dominant mechanism.

In the more recent work, Lehr et al. (2002), Lehr and Mewes (1999) introduced the critical approach velocity model, which is an empirical theory based on the experimental observation of Doubliez (1991) and Duineveld (1994) that small approach velocities lead to high coalescence efficiency.

In all cases, contact and collision is the premise of coalescence. The collision between bubbles is usually caused by their relative velocity. The relative motion may occur due to a variety of mechanisms and at least five sources can be distinguished in a turbulent flow: (i) motion induced by turbulent fluctuations in the surrounding continuous phase; (ii) motion induced by mean-velocity gradients in the flow; (iii) different bubble rise velocities induced by buoyancy or body forces; (iv) bubble capture in an eddy; (v) wake interactions or helical/zigzag trajectories.

For the collision resulting from the various relative velocities, different models for the corresponding frequency should be derived. It is usually assumed that collisions from these various mechanisms are cumulative (Swift and Friedlander, 1964; Prince and Blanch, 1990). Since not all collisions lead to coalescence, the concept of efficiency or probability is introduced. Therefore, the coalescence frequency Γ is determined by both the collision frequency $h\_col(D_{b,1}, D_{b,2})$, and the coalescence efficiency $\lambda(D_{b,1}, D_{b,2})$. $h\_col(D_{b,1}, D_{b,2})$ is determined by the mechanism of bubble collision as discussed in the section that follows, while the form of $\lambda(D_{b,1}, D_{b,2})$ depends on the three theories above for coalescence process.

These approaches can be classified according to their nature to, physical models, that provide a theory of the physical behavior of the phenomena, and empirical models that approximates the coalescence behavior with empirical relations from experimental work.

There are many limitations of the empirical models. For example, they depend on the experimental set-up or geometrical parameters and as a result cannot be extended to other cases. Furthermore, they can hardly explain the physical underlying law because they are based on an arbitrary function form and with a number of adjustable parameters which are tuned to fit a certain set of experimental data, Liao and Lucas (2010).

Physical models calculate the coalescence frequency from the collision frequency and the coalescence efficiency. They derive models based on physical quantities to define the mechanisms of each collision.

$$\Gamma\left(D_{b,1}, D_{b,2}\right) = h\_col\left(D_{b,1}, D_{b,2}\right)\lambda\left(D_{b,1}, D_{b,2}\right) \tag{2.67}$$

In Discrete Particle Modeling (DPM), as the Lagrangian tracking of the particle provides the collision of the particles (collision frequency) $h\_col\left(D_{b,1}, D_{b,2}\right)$, only to calculate the coalescence efficiency is needed. So, in the next text the film drainage model for calculating the coalescence efficiency is explored. More information about the other two models is presented at Liao and Lucas (2010).

In the next sub sections, a brief description for the Film Drainage model which depends on the comparison between the film drainage time and the contact time will be presented. Then the difference among various models presented for both the film drainage time and the contact time will be discussed.

Film Drainage Model

In the film drainage model, the coalescence efficiency of the collision depends on two time scales, the contact time t_{con} and the film drainage time t_{dr}. When two bubbles collide, the contact time means the time required for the two bubbles to coalesce, and the film drainage time is the time required for the thin film between the two colliding bubbles to drain. The starting point of the model is the work of Ross (1971). By assuming that the coalescence and contact time are random variables, Ross applied the probability density function of a normal distribution for the computation of coalescence efficiency

$$\lambda\left(D_{b,1}, D_{b,2}\right) = \frac{1}{2}\exp\left(-\frac{t_{dr}}{t_{con}}\right)\exp\left(\frac{1}{2}\frac{\sigma_{t_{dr}}^2}{t_{con}^2}\right) \times \operatorname{erfc}\left(\frac{\sqrt{2}}{2}\frac{\sigma_{t_{dr}}^2 - t_{dr}t_{con}}{t_{con}\sigma_{t_{dr}}}\right) \tag{2.68}$$

$\lambda(D_{b,1}, D_{b,2})$ defined at equation (2.68) was simplified by Coulaloglou (1975) assuming that the coalescence time is not distributed although the contact time remains a random variable, that is, $\sigma_{t_{dr}} = 0$, to be $\lambda(D_{b,1}, D_{b,2}) = \exp(-t_{dr}/t_{con})$.

Although a few criticisms appear in the literature on the validity of the two timescales, the assumption of random variables as well as normal distribution (Das and Kumar, 1987), the film drainage model is up to now the most popular one and has become the starting point of almost all subsequent models Liao et al (2010). The main difference amongst different models lies in the expression for the drainage and contact times.

Drainage Time t_{dr}

As stated by Lee and Hodgson (1968), various regimes of film drainage can be classified according to the particle surfaces state of rigidity (deformable, non-deformable, see figure 2.14, and the contact interfaces mobility (immobile, partially mobile, fully mobile, see figure 2.15. A good deal of analysis on these regimes is to be found in Liao et al (2010) which will be described in the next section .

(a) Non-deformable rigid spheres

When drops/particles are very viscous compared to the continous phase, or very small (D<1mm). The surface is not deformed much and they can be considered as a rigid spherical particles. For two non-deformable spheres with equal sizes, the drainage time was derived by Chesters (1991) by using the Poiseuille relation

$$t_{dr} = \frac{3\pi\mu_c}{2F} R_b^2 \ln\left(\frac{h_i}{h_f}\right) \tag{2.69}$$

Where h_i and h_f are the initial and critical film thicknesses respectively, and F is the applied force.

If replacing the bubble radius R_b with an equivalent one $R_{b,eq}$;

$$R_{b,eq} = \frac{2R_{b,1}R_{b,2}}{R_{b,1} + R_{b,2}} \tag{2.70}$$

Equation (2.69) can be extended to describe the case of unequal bubble sizes (Chesters and Hofman,1982). Then it becomes identical to the drainage time as given by Jeffreys and Davies (1971), Davis et al. (1989) with the form

$$t_{dr} = \frac{6\pi\mu_c}{F}\left(\frac{R_{b,1}R_{b,2}}{R_{b,1} + R_{b,2}}\right)^2 \ln\left(\frac{h_i}{h_f}\right) \tag{2.71}$$

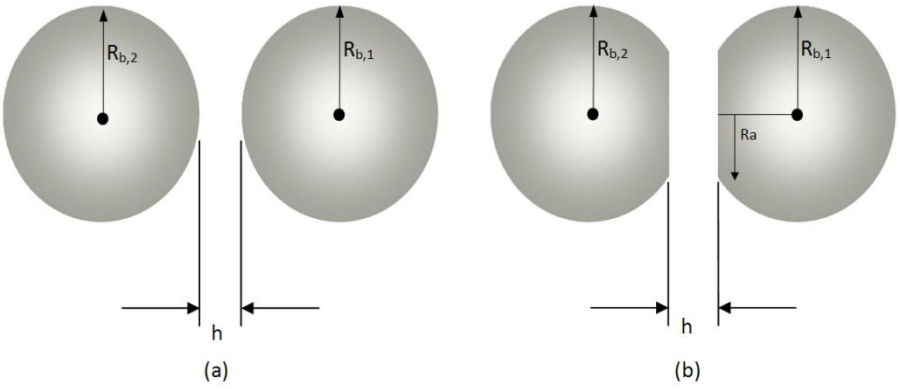

Figure 2.14. (a) Non deformable surfaces; (b) Deformable Surfaces.

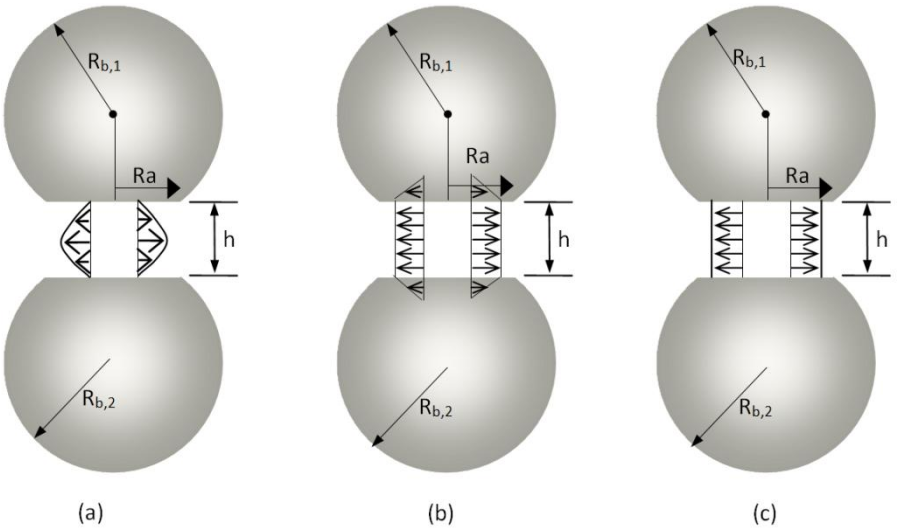

Figure 2.15. (a) Immobile interfaces, (b) Partially mobile interfaces, (c) Fully mobile interfaces.

However, the assumption of non-deformable particles is only reasonable for very small bubbles ($D_b \approx 1.0$mm). In most applications where large bubbles exist, the deformation of bubble surface during the collision has to be considered (Simon, 2004).

(b) Deformable particles with immobile interfaces

The classification of drainage regimes in the case of deformable particles depends on the mobility of colliding interfaces. For immobile interfaces, the film drainage is controlled by a viscous thinning. The liquid is expelled from the inter-spacebetween these rigid surfaces by a laminar flow. The velocity profile in the film is parabolic with no slip at the surface. The interaction between the film drainage and the circulation inside particles is not coupled; see figure 2.15 (a).

Based on the preceding model of Mackay and Mason (1963), Chesters (1991) derived the drainage time for the case of constant forces as

$$t_{dr} = \frac{3\mu_c F}{16\pi\sigma^2} R_b^2 \left(\frac{1}{h_f^2} - \frac{1}{h_i^2}\right) \tag{2.72}$$

Which is the same one as in the model of Chappelear (1961) if the bubble radius R_b is replaced by the equivalent radius $R_{b,eq}$ for the case of two unequal-sized particles,

$$t_{dr} = \frac{3\mu_c F}{16\pi\sigma^2} \left(\frac{D_{b,1} D_{b,2}}{D_{b,1} + D_{b,2}}\right) \left(\frac{1}{h_f^2} - \frac{1}{h_i^2}\right) \tag{2.73}$$

Simplifying Eq. (2.73) by treating the initial and critical film thickness h_i and h_f as constants, Coulaloglou and Tavlarides (1977) developed their coalescence model, which is one of the most famous models. The approximation of immobility of the film surface is applicable only to systems with extremely high dispersed phase viscosities or to one containing a surfactant soluble in the continuous phase as stated by Chesters (1991).

(c) Deformable particles with partially mobile interfaces

In many liquid–liquid systems drainage is predominantly controlled by the motion of the film surface, the contribution of the additional flow within the film due to the prevailing pressure gradient is much smaller.

By assuming a quasi-steady creeping flow, Chesters (1991) calculated the drainage time for partially mobile interfaces using the following relation:

$$t_{dr} = \frac{\pi\mu_d F^{1/2}}{2(2\pi\sigma/R_b)^{3/2}} (h_f^{-1} - h_i^{-1}) \tag{2.74}$$

Lee et al. (1987a) used the model of Sagert and Quinn (1976) for the partially mobile case

$$t_{dr} = -3mo\mu_c Ra^2 \int_{h_i}^{h_f} \frac{dx}{8x^3[2\sigma/R_b + A/(6\pi x^3)]} \tag{2.75}$$

By investigating the resisting hydrodynamic force during film drainage, Davis et al. (1989) concluded that the relationship between the force F and the drainage velocity dh/dt was given by

$$-F = \frac{6\pi\mu_c}{h}\left(\frac{R_{b,1}R_{b,2}}{R_{b,1}+R_{b,2}}\right)^2 \frac{dh}{dt}\frac{1+0.38mo}{1+1.69mo+0.43mo^2} \tag{2.76}$$

Where $mo = \mu_c/\mu_d\sqrt{Ra/h}$ characterizes the interfacial mobility. Based on the Eq. (2.76) Tsouris and Tavlarides (1994) proposed their new model.

(d) Deformable particles with fully mobile interfaces

The drainage regime with fully mobile interfaces is the most complicated closure model. It is considered when the viscosity of the dispersed phase is sufficiently small as stated by Chesters (1991). Bubble in pure systems is the case where the drainage process is controlled by both inertia and viscous force. Using the parallel-film model for fully mobile interfaces, Chesters (1975) proposed the following drainage equation:

$$\frac{dH}{dt} = \left[\frac{\sigma}{3\mu R_b}\frac{dH}{dt}\right]\exp\left(-\frac{12\mu_c t}{\rho_c Ra^2}\right) - \frac{\sigma}{3\mu_c R_b}, \qquad H = \frac{1}{2}\ln h \tag{2.77}$$

Since there is no analytical solution for the general expression equation (2.77), two limits are usually considered in the literature. For highly viscous liquids, the film is thinning viscously and the drainage velocity is independent of the film size, and hence the force. At this limit, one get

$$t_{dr} = \frac{3\mu_c R_b}{2\sigma}\ln\left(\frac{h_i}{h_f}\right) \tag{2.78}$$

In the inertia-controlled limit, which is the case of gas bubbles in turbulent flow, Eqn. (2.77) is shown to reduce to

$$t_{dr} = 0.5\frac{\rho_c u_t R_b^2}{\sigma} \tag{2.79}$$

The model was extended by Luo (1993) to unequal bubbles with sizes $d_{b,1}$, $d_{b,2}$

$$t_{dr} = 0.5\frac{\rho_c u_{12} D_{b,1}^2}{\left(1 + D_{b,1}/D_{b,2}\right)^2 \sigma} \tag{2.80}$$

From Eqn.(2.80), one can see that the drainage time for the inertia thinning is proportional to the approach velocity. That means the drainage time is small, i.e. the coalescence efficiency is high, when the approach velocity is low. That is consistent with the idea of the critical velocity model.

Lee et al. (1987a) suggested that the inertial thinning is predominant for pure inviscid fluid (mco10mPa s). They applied a different model, which is proposed by Sagert and Quinn (1976)

$$t_{dr} = \frac{Ra}{4}\left(\frac{\rho_c D_b}{2\sigma}\right)^{1/2} \ln\left(\frac{h_i}{h_f}\right) \tag{2.81}$$

Prince and Blanch (1990) simplified the model of Oolman and Blanch (1986) by neglecting the effect of Hamaker force and got,

$$t_{dr} = \left(\frac{R_{b,eq}^3 \rho_c}{16\sigma}\right)^{1/2} \ln\left(\frac{h_i}{h_f}\right) \tag{2.82}$$

Compressing Force F

To apply the above expressions for the description of the film drainage process during the coalescence, an interaction force F at collisions is needed in some of them. F is normally not a constant. Disturbances can be caused by the drag between the fluid particles and the continuous medium, change of the contact area during approach and the oscillation of the bubble itself. The force F is usually assumed to be proportional to the mean-square velocity difference at either ends of the eddy with a size of the equivalent diameter (Coulaloglou and Tavlarides, 1977; Hasseine et al., 2005; Tsouris and Tavlarides, 1994):

$$F \sim \rho_c \varepsilon^{2/3} \left(D_{b,1} + D_{b,2}\right)^{2/3} \left(\frac{D_{b,1} D_{b,2}}{D_{b,1} + D_{b,2}}\right)^2 \tag{2.83}$$

The collision force and duration was given by Chesters (1991) for both viscous and inertial collisions in turbulent flows. For the viscous regime corresponding to particles much smaller than the Kolmogorov scale, a typical force between two colliding particles can be expected to be proportional to the turbulent shear rate $\sqrt{\varepsilon/\nu_c}$

$$F \sim 6\pi\mu_c R_b^2 \sqrt{\varepsilon/\nu_c} \tag{2.84}$$

On the other hand, for inertial collisions, Chesters (1991) pointed out that because of inertia, the interaction force F, exerted by one particle on the other, is greater than that calculated by Eq. (2.84), which is essentially the force exerted by the external flow. They used the following relation:

$$F \sim \pi R a^2 \left(\frac{2\sigma}{R_b}\right) \tag{2.85}$$

The Contact Time t_{con}

For the calculation of the interaction time in a turbulent system, most of the previous studies used the relationship developed by Levich (1962), which is based on dimensional analysis.

$$t_{con} \sim \frac{D_b^{2/3}}{\varepsilon^{1/3}} \tag{2.86}$$

Chesters (1991) argued that the collision force and duration is controlled by the external flow in the bulk. By making an analogy to solid particles in viscous simple shear, they concluded that the contact time of particles at viscous collisions in turbulent flows should be inversely proportional to the strain rate of flow in the smallest eddies

$$t_{con} \sim (\varepsilon/\nu_c)^{-1/2} \tag{2.87}$$

During inertial collisions, there is a conversion process between kinetic energy and surface energy. From this point of view, Chesters (1991) stated that the actual contact time for inertial system was smaller than that obtained from equation (2.86). He derived the contact time from the energy balance with consideration of the virtual mass and he deduced the following equation:

$$t_{con} \approx [(4\rho_d/3\rho_c + 1)\rho_c R_b^3/2\sigma]^{1/2} \tag{2.88}$$

By criticizing the simplicity of Levich's expression and the suitability of Eqn.(2.87) and (2.88) for unequal sized fluid particles, Luo (1993) derived a more reasonable and fundamental expression for the interaction time based on a simple parallel film model

$$t_{con} = (1 + \xi_{12}) \left(\frac{(\rho_d/\rho_c + C_{vm})\rho_c D_{b,1}^3}{3(1 + \xi_{12}^2)(1 + \xi_{12}^3)\sigma}\right)^{1/2} \tag{2.89}$$

where C_{vm} is the added mass coefficient and ξ_{12} is the bubble diameter ratio of bubbles 1 and 2. Although it was found to be variable during the approach process (Kamp and

Chesters, 2001), C_{VM} is normally taken to be a constant between 0.5 and 0.8 (Jeelani and Hartland, 1991).

Kamp and Chesters (2001) extended their previous expressions to unequal-sized particles. They defined the contact time as the interval between the onset of film formation and the moment at which the bubbles begin to rebound. By assuming a balance between the increasing surface free energy and the corresponding reduction in the kinetic energy of the system, they concluded the contact time as

$$t_{con} = \frac{\pi}{4}\left(\frac{\rho_c C_{VM} D_{b,eq}^3}{3\sigma}\right)^{1/2} \tag{2.90}$$

Most of the introduced models considered only the inertial collision caused by turbulent fluctuations and were derived based on classical theories of isotropic turbulence, while Chesters (1991) divided the collisions in a turbulent flow into viscous and inertial collisions. At the same time, other than turbulence, Prince and Blanch (1990), Carrica et al. (1999) and Wang et al. (2005a, b) take also into account the buoyancy, shear rate and wake interaction.

In bubbly flow systems a drainage time model based on fully mobile interface and inertial collision should be used to consider the physical behavior. Considering the turbulent induced coalescence, Chesters (1991) combined the contact time in equation (2.88) with neglecting the $(4\rho_d/3\rho_c)$ term and the drainage time in equation (2.79) to calculate the coalescence efficiency as a function of Weber number We as follows:

$$\lambda\left(D_{b,1}, D_{b,2}\right) = \exp\left[-C_c\left(\frac{We}{2}\right)^{\frac{1}{2}}\right] \tag{2.91}$$

Such that C_c is a constant of order unity, and We is Weber number which is defined as follows:

$$We = \frac{\rho_c u_{rel}^2 D_b}{2\sigma} \tag{2.92}$$

This model was proposed by Chesters (1991) fundamentally for bubbles in turbulent flow which is the one that is used in the present work.

When the coalescence models are applied, the calculation of the resulting velocity of the resulting bubble will be calculated according to the conservation of kinetic energy of the bubbles after and before the coalescence process.

2.1.4 Break up modeling

The breakup or fragmentation of fluid particles in two-phase flows is an important matter that controls the dispersed phase size distribution with the coalescence process. The bubble size distribution affects in turn on the void fraction distribution of the dispersed phase, and to the interfacial area concentration distribution. Generally, the breakup mechanism can be expressed as a balance between external stresses from the continuous phase, which attempt to destroy the fluid particle, and the surface tension of the particle plus the viscous stress of the fluid inside it, which restores its form. Therefore, the breakup of a fluid particle is determined by the hydrodynamic conditions in the surrounding liquid and the characteristic of the bubble itself.

An overview for the theoretical breakup models for drop and bubble breakup was presented by Liao et al (2009) that gave a good classification for the suggested models. As stated by Liao et al (2009) at section 2.1 "Breakup due to turbulent fluctuations and collisions", this can be classified into five main categories which are:

(a) The turbulent kinetic energy of the particle is greater than a critical value. Examples of works presented upon this criteria are, Coulaloglou and Tavlarides (1977), and Chatzi et al., (1983, 1989, 1992).

(b) Velocity fluctuations around the particle surface greater than a critical value. As in the works of Alopaeus et al., (2002a,b) and Narsimhan and Gupta, (1979).

(c) Turbulent kinetic energy of the hitting eddy greater tan a critical value. As in the works of Lee et al., (1987a,b), Luo and Svendsen, (1996), Prince and Blanch, (1990), Tsouris and Tavlarides, (1994), and Martinez-Bazan et al., (1999a, b).

(d) Inertial force of the hitting eddy greater than the interfacial force of the smallest daughter particle. As in the works of Lehr and Mewes, (1999), and Lehr et al., (2002).

(e) Combination of the criterion (c) and (d), such as in Wang et al., (2003), and Zhao and Ge (2007).

Martinez-Bazan et al. (1999a) stated that most of the models in the literature were derived from an extension of the classical kinetic theory of gases. And these models assume the fact that turbulence consists of an array of discrete `eddies' and they also rely on physically questionable assumptions for the collision, such as collision cross-section, size and number density of eddies, . .

Liao et al (2009) declared that most of the models in the literature are based on the particle-eddy collision mechanism which relies on the assumption that the turbulent continuous flow consist of an array of discrete eddies that are treated like molecules in classical gas kinetic theories. The imaginary eddy concept is impossible to validate regarding the number density, shape, size of eddies and particle-eddy interactions. And the only model which avoids the eddy concept is that of Martínez-Bazán et al. (1999a). The models presented in the literature are still restricted to homogeneous and isotropic turbulent flows.

As a general comment of Liao et al (2009) on the works available in the literature, is that the breakup frequency increases with the turbulent dissipation rate and decreases with the increase of the disperse phase volume fraction. They commented also that some models predict the increase of breakup frequency monotonously with parent bubble size, while others give a peak. The daughter size distributions have completely different properties, i.e. bell-shape, U-shape and M-shape.

An overview for the breakup frequency models of an immiscible fluid immersed into a fully developed turbulent flow was presented by Lasheras et al., (2002). They presented a comparative analysis of some of the more commonly used turbulent fragmentation models [Coulaloglou and Tavlarides (1977), Konno et al. (1980), Prince and Blanch (1990), Tsouris and Tavlarides (1994), Luo and Svendsen (1996), Martínez-Bazán et al. (1999a)]. Then they commented the presented models with comparisons and recommendations. In the next sub sections, a short overview about these models is eplored.

Coulaloglou and Tavlarides model

Coulaloglou and Tavlarides (1977) defined the break-up frequency of a particle of size D as

$$f(D_b) = \left(\frac{\text{fraction of drop breaking}}{\text{breakup time}}\right) = \frac{1}{t_b}\frac{\Delta N(D_b)}{N(D_b)} \tag{2.93}$$

Where $N(D_b)$ is the total number of bubbles of size D_b. They modeled the fraction of particle breaking as

$$\frac{\Delta N(D_b)}{N(D_b)} = \exp\left(-\frac{E_c}{\bar{k}}\right) = \exp\left(-\frac{c_{1b}\sigma D_b^2}{c_{2b}\rho_c D_b^3 \overline{\Delta ú^2}(D_b)}\right) \tag{2.94}$$

With E_c the surface energy, $\bar{k}$ is the mean turbulent kinetic energy, and $\overline{\Delta ú^2}(D_b)$ is the mean squared value of the velocity fluctuations between two points separated by a distance D_b expressed in homogeneous and isotropic turbulence, and if D_b is within the

inertial sub range, this term can be written as $\overline{\Delta \acute{u}^2}(D_b) = c_{3b}\varepsilon^{2/3}{D_b}^{2/3}$ (Batchelor, 1956). Coulaloglou and Tavlarides assumed that the break-up time is given by the turbulent (eddy) turnover time,

$$t_{br} \propto \varepsilon^{-1/3}{D_b}^{2/3} \tag{2.95}$$

Substituting equations (2.94) and (2.95) in (2.93) , the resulting breakup frequency will be:

$$f(D_b) = C_{b1}{D_b}^{-2/3}\varepsilon^{1/3}\exp\left(-\frac{C_{b2}\sigma}{\rho_c\varepsilon^{2/3}{D_b}^{5/3}}\right) \tag{2.96}$$

Where C_{b1} and C_{b2} are two constants to be found experimentally.

Konno et al., model

Branching from the model of Coulaloglou and Tavlarides, Konno et al. (1980) used the basic formulation of Coulaloglou and Tavlarides to determine the particle break-up frequency, representing the probability density distribution of relative velocity $\acute{u}_{rel}(D_b)$ by a Maxwell distribution. They proposed the breakup frequency as

$$f(D_b) = C_k\frac{\sqrt{\overline{\Delta \acute{u}^2}(D_b)}}{D_b}\int_{u\cdot}^{\infty} 3\sqrt{\frac{6}{\pi}}x^2\exp\left(-\frac{3x^2}{2}\right)dx \tag{2.97}$$

Where the lower limit of integration is $u\cdot = u_{cr}/\sqrt{\overline{\Delta \acute{u}^2}(D_b)}$ and u_{cr} is a critical velocity.

Prince and Blanch model

Prince and Blanch (1990) followed arguments from the kinetic theory of gases, and postulated that particle break-up is the result of collisions between particles and turbulent eddies. Their break-up frequency, therefore, is given by a collision rate $f_{D,coll}$ multiplied by break-up efficiency η_{br}:

$$f(D_b) = f_{D,coll} * \eta_{br} \tag{2.98}$$

They defined the collision rate as:

$$f_{D,coll} = n_e A s_{De}\left(\overline{\Delta \acute{u}^2_{tD}} + \overline{\Delta \acute{u}^2_{te}}\right)^{1/2} \tag{2.99}$$

Where n_e is the concentration of eddies in the size range of interest, $\overline{\Delta \acute{u}_{tD}^2}$ and $\overline{\Delta \acute{u}_{te}^2}$ are the mean square of the turbulent velocity of particles and eddies, respectively, and As_{De} is the collision cross-sectional area between particles of radius $D_b/2$ and eddies of size $R_e = \pi/Wn$, given by

$$As_{De} = \frac{\pi}{4}\left(\frac{D_b}{2} + R_e\right)^2 \tag{2.100}$$

The density of eddies within a given size range is obtained by integrating the energy spectrum,

$$\frac{dn_e(Wn)}{dWn} = 0.1Wn^2 \tag{2.101}$$

Prince and Blanch point out that Eq. (2.101) gives an infinite number of eddies as the wave number Wn goes to infinity (small-size eddies). To avoid this problem, they arbitrarily chose a minimum eddy size equal to 20% of the particle diameter.

The break-up efficiency is similar to that given by Coulaloglou and Tavlarides and it is defined as:

$$\eta_{br} = \exp\left(-\frac{u_{b,cr}^2}{\overline{\Delta u_{te}^2}}\right) \tag{2.102}$$

Such that the critical bubble velocity is defined as:

$$u_{b,cr} = 1.52\left(\frac{\sigma}{\rho_c D_b}\right)^{1/2} \tag{2.103}$$

Using $\sqrt{\overline{\Delta \acute{u}_{te}^2}} = 1.4(\varepsilon D_b)^{1/3}$ the breakup efficiency will be defioned as follows:

$$f(D_b) = \int_0^{10\pi/D} \frac{0.14\pi}{16}\left(D_b + \frac{2\pi}{Wn}\right)^2 \left({D_b}^{2/3} + \left(\frac{2\pi}{Wn}\right)^{2/3}\right)^{1/2} \varepsilon^{\frac{1}{3}} \times \exp\left[-\frac{1.18}{(2\pi)^{2/3}}\frac{\sigma Wn^{2/3}}{\rho_c D_b \varepsilon^{2/3}}\right] Wn^2 dWn, \tag{2.104}$$

the lower limit of integration in Eq. (2.104) did not defined by Prince and Blanch, and they arbitrarily took $Wn_{max} = 10\pi/D_b$ to be the maximum wave number. Although they claimed that eddies with lengths less than 20% of the particle diameter do not have

enough energy to break up the particle, Lashers et al (2002) showed that their model is very sensitive to the upper limit of integration, and therefore, it cannot be chosen arbitrarily.

Tsouris and Tavlarides model

Lasheras et al (2002) proved that the Prince and Blanch, and Konno models predicted a critical diameter whose break-up frequency is maximized, and because of that, Tsouris and Tavlarides (1994) criticized their original model. Tsouris and Tavlarides considered this nonmonotonic behavior to be erroneous, and proposed a new model which predicted a monotonic increase of the break-up frequency with the drop diameter. Their new model was based on a particle-eddy collision model slightly different from that proposed by Prince and Blanch,

$$f(D_b) = C_{t1}\int_{n_e} As_{De}\left(\overline{\Delta ú_{tD}^2} + \overline{\Delta ú_{te}^2}\right)^{1/2} \exp\left[-\frac{C_{t2}E_C}{e_e}\right] dn_e \qquad (2.105)$$

Where $As_{De} = \pi(D_e + D_b)^2$ is the cross-section area,

And the average of the square of turbulent velocities of a aparticle of diameter D_b and a turbulent eddy of length $D_e = 2/Wn$ respectively are defined as:

$$\overline{\Delta ú_{tD}^2} = 1.07 D_b^{2/3}\varepsilon^{2/3} \qquad (2.106)$$

$$\overline{\Delta ú_{te}^2} = 8.2 Wn^{-2/3}\varepsilon^{2/3} \qquad (2.107)$$

And the average energy of an eddy of size D_e is defined as :

$$e_e = \frac{1}{2}\frac{\rho_c \pi D_e^3}{6} 8.2\varepsilon^{2/3}\left(\frac{D_e}{2}\right)^{2/3} = 0.43\rho_c \pi D_e^{11/3}\varepsilon^{2/3} \qquad (2.108)$$

The main difference between the Tsouris and Tavlarides model and the Prince and Blanch model is the value of the activation energy used. The form of the breakup frequency of the Tsouris and Tavlarides model is defined finally as follows:

$$f(D_b) = C_{t1} fa(\alpha_d)\varepsilon^{1/3}\int_{2/D_b}^{2/D_{min,e}} Wn^2\left(D_b + \frac{2}{Wn}\right)^2\left(1.07 {D_b}^{2/3} + \frac{8.2}{Wn^{2/3}}\right)$$

$$\times \exp\left[-\frac{C_{t2}\pi\sigma}{2}\frac{\left[2\left(\frac{D_b}{2^{1/3}}\right)^2 + D_{b,max}^2 + D_{b,min}^2 - 2{D_b}^2\right]}{0.43\rho_c\pi(2/Wn)^{11/3}\varepsilon^{\frac{2}{3}}}\right] dWn \qquad (2.109)$$

Where $D_{b,min}$ is a minimum bubble size and $D_{b,max} = (D_b^3 - D_{b,min}^3)^{1/3}$ is the diameter of a particle of complementary volume, $fa(\alpha)$ is a turbulence damping factor due to the presence of the disperse phase, α_d is the volume fraction of the dispersed phase and $D_{min,e}$ is an arbitrarily defined minimum eddy size.

Luo and Svendsen model

Luo and Svendsen (1996) also proposed a kinetic theory-type model, where the breakup frequency is calculated as a collision frequency between eddies and particles multiplied by a collision efficiency, they defined the collision frequency of eddies between eddy size as D_e and $D_e + dD_e$ with a particle of size D_b as

$$f_{D,coll} = \frac{\pi}{4}(D_b + D_e)^2\left(\overline{\Delta ú_{De}^2}\right)^{1/2}\frac{dn_e}{dD_e} \tag{2.110}$$

Where

$$\overline{\Delta ú_{De}^2} = \beta^{\frac{1}{2}}(\varepsilon D_e)^{\frac{2}{3}} \quad , \quad \beta = 2.045 \ , \qquad \frac{dn_e}{dD_e} = \frac{0.822(1-\alpha_d)}{D_e^4} \tag{2.111}$$

Where α_d is the void fraction of the dispersed phase.

The breakup efficiency is defined as:

$$\eta_{br} = \exp\left(-\frac{\overline{E}_c(D_b)}{\bar{e}(D_e)}\right) \tag{2.112}$$

Where $\bar{e}(D_e)$ is the mean kinetic energy of an eddy of size D_e defined as:

$$\bar{e}_e(D) = \rho_c\frac{\pi}{6}D_e^3\frac{\overline{\Delta ú_{De}^2}}{2} = \frac{\rho_c\pi\beta}{12}D_e^{11/3}\varepsilon^{2/3} = \frac{\rho_c\pi\beta}{12}\zeta^{11/3}D_b^3(D_b\varepsilon)^{2/3} \tag{2.113}$$

where $\zeta = D_e/D_b$. and $\overline{E}_c(D)$ is the increase in surface energy when a bubble of Diameter D_b is broken into two bubbles of size $D_{b,1}$ and $(D_b^3 - D_{b,1}^3)^{1/3}$. $\overline{E}_c(D)$ is expressed as:

$$\overline{E}_c(D_b) = C_f\pi\sigma {D_b}^2 \tag{2.114}$$

Where

$$C_f = f_V^{2/3} + (1-f_V)^{2/3} - 1 \ , \qquad f_V = \frac{D_{b,1}^3}{D_b^3} \tag{2.115}$$

Such that the value of C_f ranges from 0 to 0.26 depending on the daughter bubble diameter. The breakup frequency will be as follows

$$f(D_b; D_{b,1}) = 0.923(1-\alpha_d)\left(\frac{\varepsilon}{D_b^2}\right)^{\frac{1}{3}} * \int_{\zeta_{min}}^{1} \frac{(1+\zeta)^2}{\zeta^{11/3}} \exp\left(-\frac{12C_f\sigma}{\beta\rho_c\varepsilon^{2/3}D_b^{5/3}\zeta^{11/3}}\right) d\zeta \quad (2.116)$$

Such that

$$\zeta_{min} = D_{e,min}/D_b, \quad \frac{D_{e,min}}{\eta} \approx 11.4 - 31.4 \quad (2.117)$$

Where η is the Kolmogorov microscale. The global brekup frequency is calcualted as

$$f(D_b) = \frac{1}{2}\int_0^1 f(D_b; D_{b,1})\, df_V \quad (2.118)$$

Luo and Svendsen argued that their model does not have any unknowns or empirical parameters, However Lasheras et al (2002) proved that their model does depend on the upper limit of the integration in equation (2.116).

Martínez-Bazán model

Martínez-Bazán et al. (1999a) proposed a model based on purely kinematic ideas, and this model was suggested as a general case for liquid-liquid systems (Eastwood et al., 2000) although it is mainly developed for the breakup of air bubble immersed in turbulent water flow. The basic request for breakup in this model is that for a bubble to breakup its surface must deform, and furthermore, this deformation must be caused by the surrounding fluid.

The surface energy $E_c(D_b)$ is the minimum energy needed to deform a bubble of size D_b

$$E_c(D_b) = \pi\sigma {D_b}^2 \quad (2.119)$$

Neglecting the effect of the viscous force if compared to the surface tension force, the confinement stress defined as $(E_c(D_b)/\text{Volume of partilce})$ is expressed as

$$\tau s(D_b) = 6\frac{\sigma}{D_b} \tag{2.120}$$

For bubbles having a size within the inertial subrange, the average deformation stress is

$$\tau t(D_b) = \frac{1}{2}\,\rho_c \overline{\Delta \acute{u}^2}(D_b) \tag{2.121}$$

Where $\overline{\Delta \acute{u}^2}(D_b)$ is the mean value of the velocity fluctuations between two points separated by a characteristic distance D_b. This can be defined for homogeneous and isotropic turbulent flow using Kolmogorov universal theory as:

$$\overline{\Delta \acute{u}^2}(D_b) = \overline{|\acute{u}(x + D_b, t) - \acute{u}(x, t)|^2} = \beta(\varepsilon D_b)^{2/3} \tag{2.122}$$

When both of the confinement stress and the deformation stress are equal, a critical particle diameter $D_{b,cr} = \left(12\sigma/(\beta\rho)\right)^{3/5}\varepsilon^{-2/5}$ can be defined such that the particles of size smaller than $D_{b,cr}$ will never breakup (Kolmogorov,1949; Hinze, 1955). And the particles of size greater than $D_{b,cr}$ have a deformation stress larger than the confinement stress and will breakup in a time t_{br}. The bubble break up time can be estimated as:

$$t_{br} \propto \frac{D_b}{u_{br}} = \frac{D_b}{\sqrt{\overline{\Delta \acute{u}^2}(D_b) - 12\frac{\sigma}{\rho_c D_b}}} \tag{2.123}$$

Where u_{br} is the particle breakup velocity. The breakup frequency will be expressed as:

$$f(D_b) = \frac{1}{t_{br}} = k_g \frac{\sqrt{\beta(\varepsilon D_b)^{2/3} - 12\frac{\sigma}{\rho_c D_b}}}{D_b} \tag{2.124}$$

Where the constant $\beta = 8.2$ was given by Batchelor (1956), and $k_g = 0.25$ was found experimentally for the air bubbles in water by best fitting the transient volume probability density functions while solving the inverse problem of calculating the daughter p.d.f., see Martínez-Bazán et al. (1999b). Varying the value of k_g is equivalent to modifying the breakup frequency.

Martínez-Bazán et al (2010) presented non dimensional expression for the breakup frequency defined in equation (2.124) as a function of the turbulent Weber number We_t as:

$$f^{nr}(We_t) = \frac{f(D_b){D_b}^{2/3}}{\varepsilon^{1/3}} = k_g\beta^{1/2}\sqrt{1-\frac{1}{We_t}} \quad (2.125)$$

Where

$$We_t = \frac{\rho_c\beta\varepsilon^{2/3}{D_b}^{5/3}}{12\sigma} \quad (2.126)$$

With the value $k_g\beta^{1/2} \approx 0.673$. Martínez-Bazán defined even more general expression for the normalized breakup frequency for different definitions of W_{et} as:

$$f^{nr}(We_t) = C_g\sqrt{1-\frac{We_{t,cr}}{We_t}} \quad (2.127)$$

Where $We_{t,cr}$ is the critical Weber number and C_g is a constant.

Lasheras et al (2002) stated as a comment on the presented literature that, both the expression for breakup frequency and the daughter bubble distribution PDF in the model of Martínez-Bazán et al are based on the kinematics existing at the surface of each bubble. Although this model is conceptually and mathematically simpler than the others, it predicts the experimental results much more accurately. For that agreement of the Martínez-Bazán et al models with the experimental data, it is decided to use this model in the present work.

To complete the modeling of the breakup phenomena, breakup frequency is not sufficient, further information about the size distribution of the daughter bubbles after the breakup process is needed. In the next lines, the model of the daughter bubble distribution presented by Martínez-Bazán et al (1999b) will be explored.

Martínez-Bazán et al (1999b) proposed a model for air bubble breakup in a fully developed turbulent flow. In their model, the mother bubble of diameter D_b is considered to breakup into two daughter bubbles of diameters $D_{b,1}$ and $D_{b,2}$ which are related through by the conservation of mass as follows:

$$D_{b,2} = D_b\left[1-\left(\frac{D_{b,1}}{D_b}\right)^3\right]^{1/3} \quad (2.128)$$

They claimed that the splitting process cannot be purely random as the pressure fluctuations in homogeneous and isotropic turbulence are not uniformly distributed over all scales. This means that $\tau t(D_b)$, given in Eq. (2.121), is not uniformly distributed and therefore the splitting process cannot be purely random. They

considered that there is a distance, $D_{b,min}$ over which $\tau t(D_{b,min}) = \tau s(D_b)$. At this distance, the turbulent pressure fluctuations are exactly equal to the confinement forces for a mother particle of size D, and the probability of breaking off a daughter particle with $D_{b,1} < D_{b,min} = \left(12\sigma/(\beta\rho_c D_b)\right)^{3/2}\varepsilon^{-1}$ should be zero.

The fundamental theory suggested by Martínez-Bazán et al stated that the probability of bubble breaking off such that $D_{b,min} < D_{b,1} < D_b$ is proportional to the difference between the turbulent stresses over a length $D_{b,1}$ and the confinement forces holding the mother particle of size D_b together. So, for the formation of a daughter bubble of size $D_{b,1}$ the difference in the affecting stresses will be

$$\Delta\tau t_1 = \frac{1}{2}\rho_c\beta\left(\varepsilon D_{b,1}\right)^{2/3} - 6\frac{\sigma}{D_b} \tag{2.129}$$

And as the formation of the bubble $D_{b,1}$ will be coupled with the formation of the complementary volume bubble of size $D_{b,2}$, the probability of forming the two daughter bubbles of sizes $D_{b,1}$ and $D_{b,2}$ will be

$$\Pr(D_{b,1}, D_b) \propto \left[\frac{1}{2}\rho_c\beta\left(\varepsilon D_{b,1}\right)^{2/3} - 6\frac{\sigma}{D_b}\right]\left[\frac{1}{2}\rho_c\beta\left(\varepsilon D_{b,2}\right)^{2/3} - 6\frac{\sigma}{D_b}\right] \tag{2.130}$$

Using equation (2.128) for relating $D_{b,1}$ and $D_{b,2}$, the expression (2.130) can be expressed as

$$\Pr(D^{nr}) \propto \left(\frac{1}{2}\rho_c\beta(\varepsilon D_b)^{2/3}\right)^2 \left[D^{nr\,2/3} - \Lambda^{5/3}\right]\left[\left(1 - D^{nr3}\right)^{2/9} - \Lambda^{5/3}\right] \tag{2.131}$$

Where

$$D^{nr} = \frac{D_{b,1}}{D_b}, \qquad \Lambda = \frac{D_{b,cr}}{D_b} = \left(\frac{D_{b,min}}{D_b}\right)^{2/5} \tag{2.132}$$

$D_{b,cr}$ is the critical diameter defined as

$$D_{b,cr} = \left(12\sigma/(\beta\rho_c)\right)^{3/5}\varepsilon^{-2/5} \tag{2.133}$$

No assumption needs to be made about the minimum and maximum eddy size that can cause particle break-up. All eddies with sizes between the Kolmogorov scale and the integral scale, are taken into account. The daughter bubble probability density function can be obtained from equation (2.131) assuming that $\int_{D^{nr}_{min}}^{D^{nr}_{max}} \Pr(D^{nr})d(D^{nr}) = 1$. The pdf of D^{nr} then can be written as

$$\delta^{nr}(D^{*}) = \frac{\left[D^{nr\,2/3} - \Lambda^{5/3}\right]\left[\left(1 - D^{nr\,3}\right)^{2/9} - \Lambda^{5/3}\right]}{\int_{D_{min}^{nr}}^{D_{max}^{nr}}\left[D^{nr\,2/3} - \Lambda^{5/3}\right]\left[\left(1 - D^{nr\,3}\right)^{2/9} - \Lambda^{5/3}\right] d(D^{nr})} \quad (2.134)$$

Such that $f(D_{b,1}, D_b) = f^{nr}(D^{nr})/D_b$

Martínez-Bazán et al (2010) stated that the relation (2.134) have a misleading in the normalization step which implies that the pdf provided does not conserve volume. As the probability functions proposed in (2.131) should be function of volume V^{nr} rather than diameter D^{nr}. So he modified the p.d.f to be as follows:

$$\delta^{nr}(D^{nr}) = \frac{D^{nr\,2}\left[D^{nr\,2/3} - \Lambda^{5/3}\right]\left[\left(1 - D^{nr\,3}\right)^{2/9} - \Lambda^{5/3}\right]}{\int_{D_{min}^{nr}}^{D_{max}^{nr}} D^{nr\,2}\left[D^{nr\,2/3} - \Lambda^{5/3}\right]\left[\left(1 - D^{nr\,3}\right)^{2/9} - \Lambda^{5/3}\right] d(D^{nr})} \quad (2.135)$$

2.2. The Euler Solver Overview

General speaking, Euler framework uses the Reynold averaged equations for conservation of mass, momentum and Energy basis through the computational cells for solving any problem of fluid dynamics and heat transfer. In the present work, we are concerned only with the two phase flow mater at ambient temperature without phase change, and without considering the compressibility or any viscous energy transformation. It is not necessary to solve the energy conservation equation.

2.2.1 Conservation Equations

The conservation equations in the present case differ a little from the normal fluid dynamics equations as there are two phases in the same cell. So, the effect of the dispersed phase when writing the conservation equations should be considered. This will be clarified when explaining the two-way coupling process and dealing with the source terms

The Reynolds averaged conservation equations of mass and momentum, or as known by (RANS) equations For a Newtonian incompressible fluid flows, with a steady state simulation will be as follows:

Conservation of mass

$$\frac{\partial(\rho_c U_c)}{\partial x} + \frac{\partial(\rho_c V_c)}{\partial y} + \frac{\partial(\rho_c W_c)}{\partial z} = 0.0 \quad (2.136)$$

Conservation of momentum

$$\frac{\partial(\rho_c U_c U_c)}{\partial x}+\frac{\partial(\rho_c V_c U_c)}{\partial y}+\frac{\partial(\rho_c W_c U_c)}{\partial z}=$$

$$-\frac{\partial p}{\partial x}+\frac{\partial}{\partial x}\left(\mu_{c,eff}\frac{\partial U_c}{\partial x}\right)+\frac{\partial}{\partial y}\left(\mu_{c,eff}\frac{\partial U_c}{\partial y}\right)+\frac{\partial}{\partial z}\left(\mu_{c,eff}\frac{\partial U_c}{\partial z}\right)+\rho_c g_x+S_u \quad (2.137-1)$$

$$\frac{\partial(\rho_c U_c V_c)}{\partial x}+\frac{\partial(\rho_c V_c V_c)}{\partial y}+\frac{\partial(\rho_c W_c V_c)}{\partial z}=$$

$$-\frac{\partial p}{\partial y}+\frac{\partial}{\partial x}\left(\mu_{c,eff}\frac{\partial V_c}{\partial x}\right)+\frac{\partial}{\partial y}\left(\mu_{c,eff}\frac{\partial V_c}{\partial y}\right)+\frac{\partial}{\partial z}\left(\mu_{c,eff}\frac{\partial V_c}{\partial z}\right)+\rho_c g_y+S_v \quad (2.137-2)$$

$$\frac{\partial(\rho_c U_c W_c)}{\partial x}+\frac{\partial(\rho_c V_c W_c)}{\partial y}+\frac{\partial(\rho_c W_c W_c)}{\partial z}=$$

$$-\frac{\partial p}{\partial z}+\frac{\partial}{\partial x}\left(\mu_{c,eff}\frac{\partial W_c}{\partial x}\right)+\frac{\partial}{\partial y}\left(\mu_{c,eff}\frac{\partial W_c}{\partial y}\right)+\frac{\partial}{\partial z}\left(\mu_{c,eff}\frac{\partial W_c}{\partial z}\right)+\rho_c g_z+S_w \quad (2.137-3)$$

The terms S_u, S_v and S_w are the momentum source terms in the three Cartesian coordinates directions X, Y, and Z respectively. $\mu_{eff,c}$ is the effective viscosity which is a summation of the laminar viscosity of the fluid μ_c and the turbulent viscosity calculated through the turbulence model $\mu_{c,t}$.

2.2.2 Turbulence modeling

In this work, the standard k-ε model was used for turbulence modeling. In a separate chapter the turbulence modeling and turbulence modifications due to coupling processes will be explained in detail.

The Euler solver used in the present research for solving the continuous phase is the free code Dolfyn http://www.dolfyn.net/index_en.html created by Cyclone Fluid Dynamics BV. It is based in its theory of CFD on the book for J.H. Ferziger & M. Peric (2002) and programmed in Fortran 90,95. Dolfyn is a face based implicit Finite Volume Method code, employing primitive variables on 3D unstructured polyhedral meshes targeted towards these industrial types of problems. It uses unstructured grid generated by GMSH grid generator in Cartesian coordinates system. It uses the

SIMPLE algorithm for solving the Navier-Stockes equations based on the collocated grid strategy and segregated solver. The turbulence model provided with Dolfyn is the standard k-ε model.

Dolfyn is accompanied by a preprocessor. The preprocessor writes a geometry file in a format suitable for Dolfyn. The input is a set of three files which describe the cells, vertices and the boundaries for Dolfyn. Dolfyn reads the geometry file and a separate input file. In this input file the user sets numerical and modeling parameters, boundary conditions etc. The input file can be edited with any simple ASCII text editor. The Dolfyn file map is shown in figure 2.16. The numerical code Dolfyn uses a 'segregated solver' which means that the transport equations are solved sequentially. Because the coupled non-linear equations have been linearised implicitly, several iterations are needed in order to get a converged solution. Using the currently known fluid properties and mass fluxes the three momentum transport equations are solved.

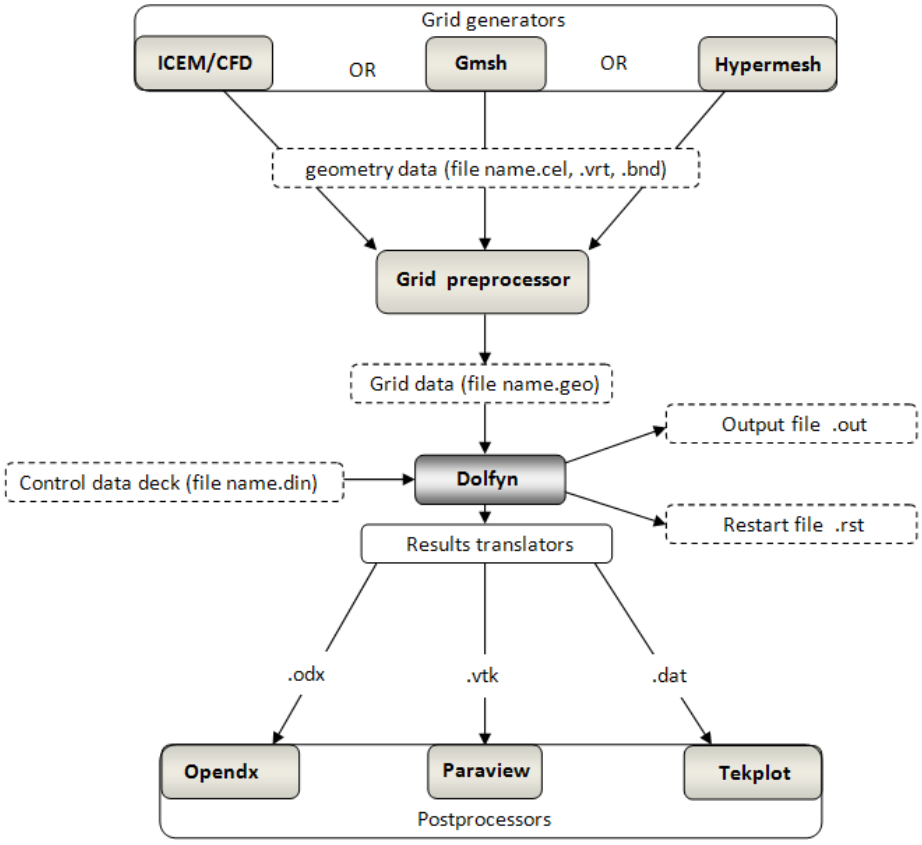

Figure 2.16. Dolfyn file map.

At this stage the continuity equation may not be satisfied and a pressure correction is set up. This correction is solved to obtain the correct pressure and velocity fields and the mass fluxes at the faces satisfy the continuity equation. After this stage the transport equations for the turbulence models, energy or species are solved. Finally the fluid properties are adjusted and the process is repeated until convergence.

The grid or mesh used by Dolfyn is based on 'face based unstructured polyhedral cells'. Unstructured does not mean tetrahedral cells only (in 3D, or triangles in 2D), but refers to the way the topology is implemented. In using polyhedral any type of mesh can be used, even 'structured hexahedral'. It only depends on the kind of preprocessor, or 'grid generator' one is using. The same applies to the postprocessor to visualize the final results; a postprocessor which only can handle hexahedral cells is of no use when one employs tetrahedral cells. Thus Dolfyn is never the limiting code in the process and it all depends on the kind of, favorite, pre- and postprocessors at hand.

2.2.3 Control input file

To make a simulation with Dolfyn, it needs beside the geometry (.geo) file, another file that describe the conditions of the flow and the simulations parameters. This is done with a .din control input file which is written with text editor in ASCII format. The .din file contains five parts, each part have defines some parameters for Dolfyn about the current run. These parts are as follows:

- General command parameters like title of the file, laminar or turbulent flow, specification and the turbulence model required, simulation type, steady state or transient, frequency at which results data written if it is required, and others.

- Control parameters like monitoring a variable value during the simulation at a specific position, differencing schemes and blending factors, relaxation factors for the variables, gradients calculation method and slop limiters, initialization of the domain, and others.

- Fluid properties like density, viscosity and temperature.

- Boundary conditions for the domain boundaries like inputs, outputs, walls and symmetry plans.

- Post processing parameters like type of results data type .VTK, .ODX, or .DAT. extra results required like point based or cell based variables. Also all the results file types can be written.

For further information about the control file and parameters dictionary, please refer to Dolfyn input Guide which can downloaded from this link http://www.dolfyn.net/index_en.html.

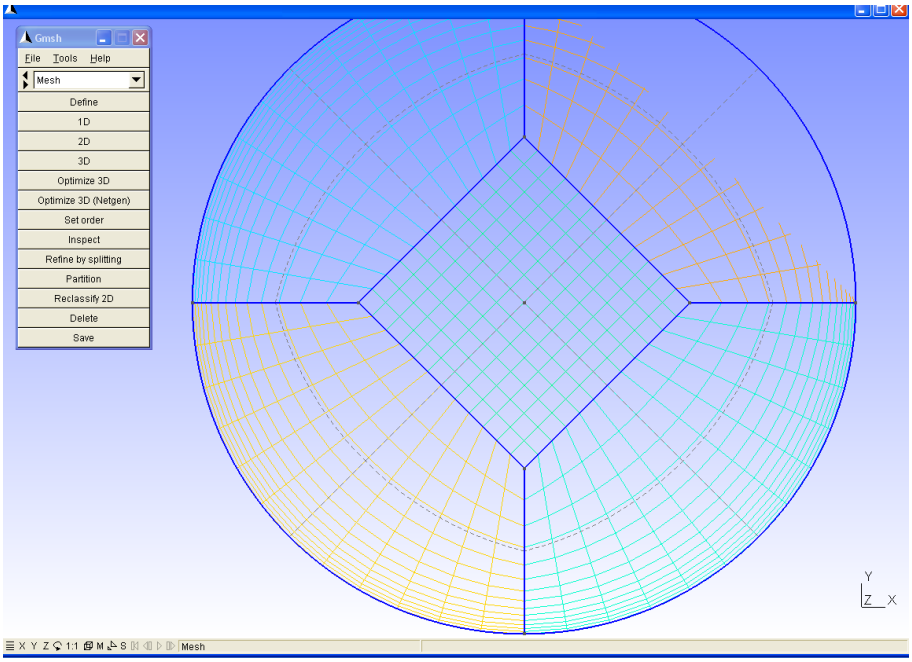

Figure 2.17. Gmsh interface.

2.3. The Lagrangian Solver Overview

In this section, it is described how the Lagrangian model is applied for each bubble. And the different forces considered acting on the motion of the bubbles in the continuous phase. Different modeling of each force will be presented with recommendation about the models that can be used in this work and the difference among the models. Finally some results for single bubble simulations using the recommended forces to show an order of magnitude for the acting forces is presented.

2.3.1 Equation of motion

The Lagrangian framework is applied for tracking the bubbles flowing through the liquid field by applying the Newton's second law of motion. In this work, the equation of motion for the bubbles was applied in cylindrical coordinates system as the

geometry of our simulation is a vertical pipe for which the Cartesian coordinates system is more convenient. The equation of motion will be presented as follows:

$$(\rho_d + C_{VM}\rho_c)V_b \frac{d\vec{u}_b}{dt} = \sum_i \vec{F}_i \tag{2.138}$$

Where C_{VM} is the coefficient of the virtual mass force which is assumed equal to 0.5. In cylindrical coordinates (r,θ,z), this equation is equivalent to the following set of equations:

$$(\rho_d + C_{VM}\rho_c)V_b(\ddot{r}_b + r_b\dot{\theta}_b{}^2) = \sum_i F_{i,r} \tag{2.139-1}$$

$$(\rho_d + C_{VM}\rho_c)V_b(r_b\ddot{\theta}_b + 2\dot{r}_b\dot{\theta}_b) = \sum_i F_{i,\theta} \tag{2.139-2}$$

$$(\rho_d + C_{VM}\rho_c)V_b\ddot{z}_b = \sum_i F_{i,z} \tag{2.139-3}$$

The velocities in the cylindrical coordinates (u_r, u_θ, u_z) in the (r, θ, z) directions are $\dot{r}_b, r_b\dot{\theta}_b, \dot{z_b}$ respectively, hence the derivation of these components once again with respect to the time gives the three acceleration velocities $\left(\ddot{r}_b + r_b\dot{\theta}_b{}^2\right)$, $(r_b\ddot{\theta}_b + 2\dot{r}_b\dot{\theta}_b)$, $\ddot{z}_b$ respectively. The time derivative vector of the velocity can be written as a function of time derivatives of velocities in the three directions as follows:

$$\frac{d\vec{u}_b}{dt} = \left(\frac{du_{b,r}}{dt} - \frac{u_{b,\theta}^2}{r}\right)\hat{e}_r + \left(\frac{du_{b,\theta}}{dt} + \frac{u_{b,r}u_{b,\theta}}{r}\right)\hat{e}_\theta + \frac{du_{b,z}}{dt}\hat{e}_z \tag{2.140}$$

The derivation of this equation is explained in details in appendix A. To discretize the acceleration term, Tailor series expansion is used which gives a solution of second order accuracy as follows:

$$u_b(t+dt) = u_b(t) + \frac{\partial u_b}{\partial t}\frac{dt}{1!} + o(dt)^2 \quad \Rightarrow$$

$$\frac{\partial u_b}{\partial t} = \frac{u_b(t+dt) - u_b(t)}{dt} + o(dt)^2 \tag{2.141}$$

2.3.2 Methods for locating particles in elements of arbitrary shape

In this section, it is explored some of the algorithms that are used for locating the particles in the field mesh. For structured grid, locating particles in a generalized-coordinate structured code is straightforward Marta Garcia (2009). For example in a two-dimensional case with uniform grid spacing, the cell (ic, jc) where a particle is located can be easily calculated as:

$$i_c = \mathrm{Int}\left\{\frac{(x_p - x_{min})}{x_{max} - x_{min}} N_x\right\} + 1, \quad j_c = \mathrm{Int}\left\{\frac{(y_p - y_{min})}{y_{max} - y_{min}} N_y\right\} + 1 \qquad (2.142)$$

Where x_p is the current location of the particle, x_{min} and x_{max} denotes the range of coordinate values for the current mesh, and N_x, N_y the number of cells in the x and y directions. Int { } denotes truncation to the lowest integer part.

With this simple equation, it is known know that the particle is located inside a cell and also the cell where it is located. However, this is not applicable for the case of unstructured grid because of the arbitrary shape of the grid elements which makes difficult to get a simple criterion to locate particles.

For unstructured grids, In the literature several authors have already tried to solve this problem: Seldner and Westermann (1988), Westermann (1992), and Löhner (1995). They describe approaches to locate particles in particle-in-cell codes. In the next sub sections, it is explored some particle locating techniques that can be used in our Lagrangian framework which are partial volumes areas method, shape function method and face normal vector comparison method.

Calculation of areas of partial volumes

This approach is based on the calculation of areas or partial volumes. The nodes of the grid element are joined to the particle location, and the volume of the resulting sub cells is compared to that of the control volume. If the particle lies inside the control volume, the sum of the sub cell volumes will be equal to the total volume. If the particle is outside the control volume the sum of the sub cell volumes will be greater than the total volume, this is illustrated in figure 2.18.

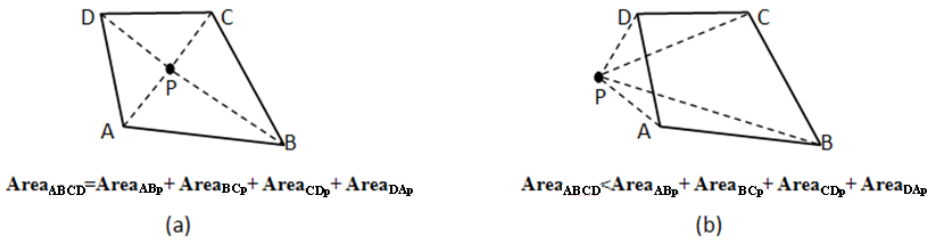

Figure 2.18. Calculation of areas to detect if (a) The particle lies inside the quadrilateral ABCD, (b) The particle is outside the quadrilateral.

As can be seen from figure 2.18, these methods will need the division of each area to sub-areas and will need many calculations till taking the decision that the particle is located inside the cell or not. And it is simpler to implement in 2D grids as the calculation of partial volumes in 3D grids will need more computational effort.

Evaluation of shape-functions

A second approach is to evaluate the shape-function values of the particle with respect to the coordinates of the points belonging to the element:

$$X_p = \sum_i N^i X_i \tag{2.143}$$

For triangles in 2D and tetrahedron in 3D, there are two equations for three shape-functions and three equations for four shape-functions, respectively. The sum-property of shape- functions,

$$\sum_i N^i = 1 \tag{2.144}$$

yields the missing equation, making it possible to evaluate the shape-functions from the following system of equations for a 3D tetrahedron:

$$\begin{Bmatrix} x_p \\ y_p \\ z_p \\ 1 \end{Bmatrix} = \begin{Bmatrix} x_1 & x_2 & x_3 & x_4 \\ y_1 & y_2 & y_3 & y_4 \\ z_1 & z_2 & z_3 & z_4 \\ 1 & 1 & 1 & 1 \end{Bmatrix} \cdot \begin{Bmatrix} N_1 \\ N_2 \\ N_3 \\ N_4 \end{Bmatrix} \tag{2.145}$$

Then, the point is inside the element if and only if

$$\min(N^i, 1 - N^i) \geq 0, \quad \forall i. \tag{2.146}$$

So this method is more convenient for triangular cells in 2D mesh or tetrahedron cells in 3D mesh. However, for other types of elements (quadrilateral, hexahedra, etc) more nodes than equations are encountered. Therefore, in order to determine if a particle is inside an element, the easiest way is to split the element into triangles or tetrahedron and evaluate each of these sub-elements. If the particle happens to be in any of them, it is inside the element.

The drawback of this procedure is that it is computationally expensive since it requires the evaluation of all sub-elements before particle detection.

Comparison of face-normal vectors

The third approach projects the particle location onto the faces of the grid element and compares these vectors with face-normals for all faces (Figure 2.19). If the particle lies inside the cell, the projected vectors point the same direction as the face-normals. This technique is very accurate even for highly skewed elements. In addition, if the condition is not verified on a face, there is no need to continue checking the rest of the faces inside this cell, which reduces dramatically the overall CPU time of the algorithm.

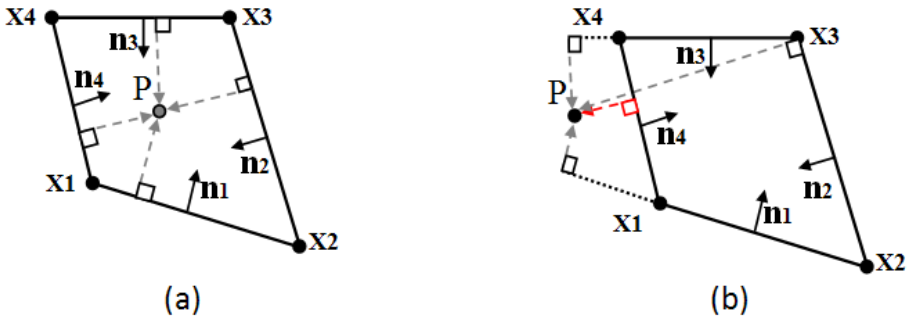

Figure 2.19. Comparison of particle location vector and face-normal vectors of the grid element (a) Particle inside the cell (b) Particle outside the cell.

This method has already been used in other simulations of Lagrangian particle-laden flows on unstructured grids (Apte et al. (2003), Haselbacher et al. (2007) call it the "in-cell test")

For the advantages of the face-normals comparison method over the two other methods, this method is used as a particle locating technique in our Lagrangian Framework. On one hand, this method can deal with any kind of element shape due to its face treatment, and on the other hand, there is no need to check the whole element to know if a particle is located inside it.

2.3.3 Algorithms for locating particles

As stated above, the face normals comparison method will be used to test the location of the particle inside a given cell. As the algorithm of implementing this technique will depend on the pre- knowledge of the particle location, there will be two different algorithms; the first is locating the bubble when it is injected as in this case there is no known cell for the particle at the last time step. The second is locating the particle during the simulation which means that the last cell at which the particle is located is already known, these algorithms will be discussed in the next two subsections.

Searching Particles at the Beginning of Injection

In the current work, a structured extruded mesh type is used as shown in figure 2.20. As we look for the particle inside a pipe, it was more convenient to look for the cell in which the particle is located. This is handled by choosing a list of cells around the particle which validate the condition that in the horizontal plane (x,y plane) the cell center is near to the particle by a distance of D/5 such that D is the diameter of the pipe. For calculating the cells range in the vertical plane, we choose the distance as one or more cell height. This will depend on the cell height and the average velocity of

particles. This in turn narrow the search space to only two or three levels of cells in the z direction and to a disk of diameter D/5 around the particle.

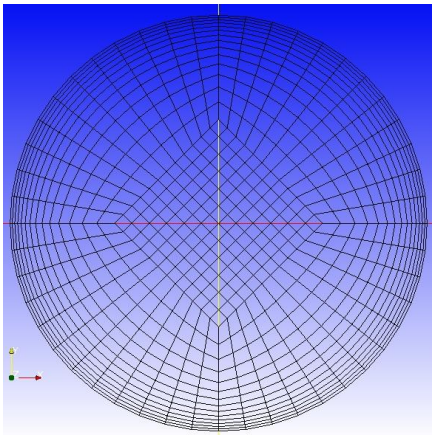

Figure 2.20. Grid top view.

Searching particles during the simulation

During the simulation, a cell number associated to each particle is stored in the integer-data array. This number corresponds to the cell where the particle is located before it changes its position. Therefore, given a particle location and the associated cell, the search algorithm determines the cell that contains the new particle position. The procedure is divided into several steps described below.

The first step consists of checking the current cell to know if the particle is still inside it, which is usually the case since particles displacements are small due to CFL time step restriction, In case of failure, the algorithm extents its search to the first level neighbor cells that have at least one vertex with the old cell . This is the second step and only cells that contain at least one node in common with the current particle cell are considered, reducing the search to a first level of cells. To that end, a pointer containing the number of elements connected to a given node has been created at the beginning of the simulation. This procedure is based on the known-vicinity algorithm which allows a significant improvement in speed by only checking the elements that cover the immediate neighborhood. Should this search fails, the third step consists of looking for the particle in a second level neighbor cells list. The second level neighbors cell is not used often except for high relative velocity flows. Should this also fail, the particle is considered lost in the last step and a message is displayed to notify a problem in the search algorithm.

Figure 2.21 illustrates the second step of this particle-location problem. Assuming that a particle is no longer located in the current cell (dark gray cell), the first operation consists of the detection of the surrounding cells (light gray cells). Then, a loop over these cells is performed to detect the new cell containing the particle by evaluating the

localization criterion (see Section 2.3.2). Several improvements are possible for this algorithm. In a first pass, one may evaluate the closest point to the given cell and only consider the elements surrounding that point instead of considering all the elements surrounding all the nodes, as pointed out by Löhner. R., (1995). Another possibility consists of detecting the face of the cell intersected by the particle trajectory, jumping from neighbor to neighbor until the particle is found. This last option performs very well and also does not limit particles to small displacements [Löhner. R., (1995), Apte et al., (2003), A. Haselbacher (2007)]. Future developments of the Lagrangian module should focus on the implementation of these functionalities.

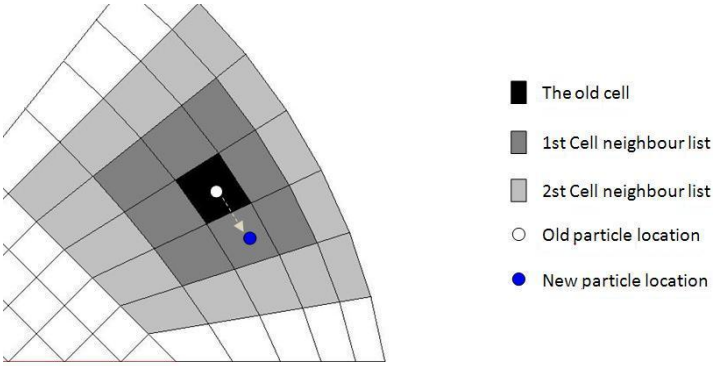

Figure 2.21. Top view of the grid and the searching algorithm during simulation.

3. Turbulence Modeling

Single phase turbulence is complex and still considered as a not resolved issue in science. Multiphase flow turbulence is much more complex and of course still far from its final accurate mathematical description. As a coupling process between the Euler and Lagrange frameworks in this work, turbulence modeling in the continuous phase should take in account the effect of the dispersed phase and vice versa. In this chapter it is presented an introduction for the turbulence and how it is affected in case of two phase flows. The Turbulence model used in the Euler solver for solving the Continuous phase is presented. Then it is introduced the Continuous Random Walk (CRW) model used in this coupled simulation to calculate the velocity fluctuations of the continuous phase and its effect on the motion of the bubbles in the dispersed phase. Then the bubble induced turbulence modeling used during this work and how its effect is considered in the turbulence of the continuous phase is described.

3.1 Introduction

In single phase flow, there are many length and time scales of eddies that cause turbulence. And to get the instantaneous velocity of the fluid at any point in the domain we have to solve all the time and length scales in the domain from the largest scale which is usually of the order of the floe geometry down to the smallest scales which are called Kolmogorov length and time scales. This is done by solving the instantaneous Navier Stokes equations on a very fine grid for which the cells size are of order of the Kolmogorov length scale and the solution time step is the Kolmogorov time scale of the specified problem. This method is called Direct Numerical Simulation DNS and it is the most expensive in computational effort and the most time consuming method for the CFD solution. Also this method is used only for simple problems with limited Reynolds numbers. An easier method suggested is to solve only the larger scales of turbulence because the large eddies of the large scales are responsible for the greatest part of the flow energy as illustrated in figure 3.1. This method is called Large Eddy Simulation LES. As shown in fig 3.1, the energy spectrum for a turbulent flow consists of three main regions. The first one is the energy containing eddies which have the minimum wave number (large eddies) and receives the energy from the flow. The second region is the inertial subrange region which nearly has equilibrium in receiving and losing energy. The third region is the viscous range for which the eddies are the smallest and it dissipate the kinetic energy of turbulence in form of internal energy. This last region has isotropic characteristics.

The idea of the large eddy simulation is solving only the large scales of turbulence and modeling the small scales as the small scales have isotropic properties. However, it requires a very fine grid with small time step such that the value of the cell Courant

number= u dt/dx to be in order of unity at each direction as stated in CFX modeling guid. So LES still consume much computational time. Reynolds proposed his famous averaging method for Navier-Stokes equations dividing the instantaneous velocity in two different components, a mean component U and a fluctuating component u' as shown in figure 3.2.

$$u(t) = U + \acute{u}(t) \tag{3.1}$$

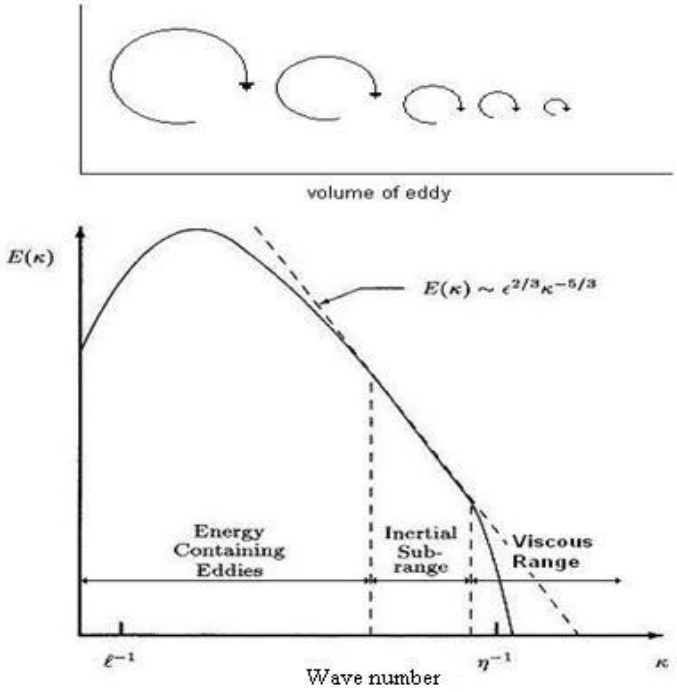

Figure 3.1. Energy spectrum of turbulence.

According to this averaging, the averaged Navier Stokes equations will have the form:

$$\rho\frac{\partial U_i}{\partial t} + \rho U_j\frac{\partial U_i}{\partial x_j} = -\frac{\partial p}{\partial x_j} + \frac{\partial}{\partial x_j}\left(2\mu\sigma_{sr,ij} - \rho\overline{\acute{u}_j\acute{u}_i}\right) + S_i \tag{3.2}$$

Such that $\sigma_{sr,ij}$ is the strain rate tensor defined as:

$$\sigma_{sr,ij} = \frac{1}{2}\left(\frac{\partial U_i}{\partial x_j} + \frac{\partial U_j}{\partial x_i}\right) \tag{3.3}$$

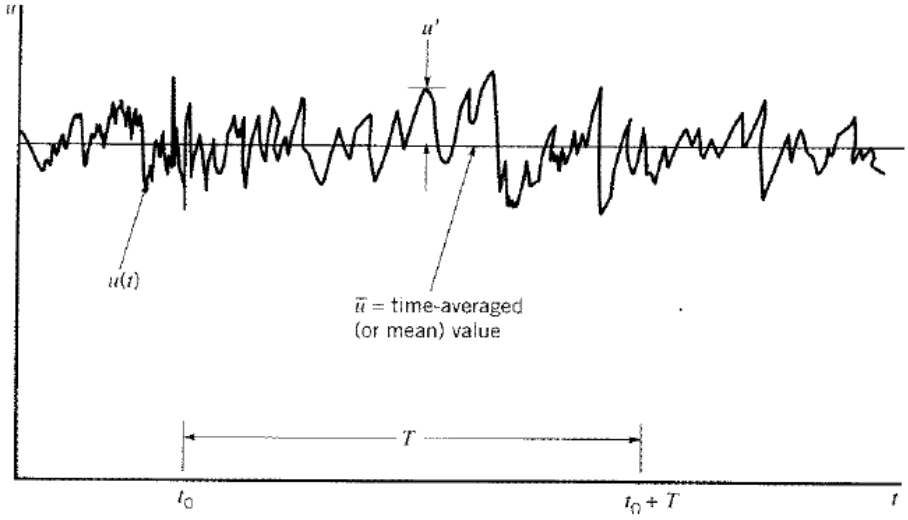

Figure 3.2. Averaging of an Instantaneous velocity u(t).

And the S_i is the source term. It can be observed from the Reynolds Averaged Navier Stokes equation (RANS) that in this equations the unknowns are the components of the velocity, the pressure and the Reynolds stresses $\overline{\acute{u}_j \acute{u}_i}$, and the equations available for solving these variables are the continuouity equation, the three directions momentum equations illustrated above. All the turbulence RANS models depend on modeling the term $\overline{\acute{u}_j \acute{u}_i}$to insert its effect in the RANS equation replacing the molecular viscosity μ by an effective viscosity μ_{eff}. This effective viscosity is a summation of the molecular viscosity μ and the turbulent viscosity μ_t that is calculated from the turbulence model used. This principle is called the Boussinesq eddy viscosity approximation that approximates this unknown term as a turbulent viscosity μ_t in the fluid due to turbulence and is added to the molecular viscosity of the fluid using Prandtl's Mixing-length Hypothesis; Prandtl (1925). By these hypothesis the term is defined as :

$$\overline{\acute{u}_j \acute{u}_i} = \left| l_{mix} \frac{\partial U}{\partial y} \right| \tag{3.4}$$

Such that the l_{mix} is the mixing length at the same location which is already unknown. Many models have been presented for modeling the eddy viscosity term according to

the RANS approximations. Some of these models are incomplete which needs adjustment of the length scale for each flow type like the Algebraic models and one equation models. Other models are complete that can adjust the length scales of turbulence during the process of solving conservation equations. The most famous Two equation model used is the k-ε model that is used in this work and will be explained in the next section, also the k-ω model is a complete two equation model that can be integrated even inside the boundary layer perfectly. Many other two equations models have been presented and have some success, further information about these models can be obtained from Wilcox (1994).

In case of the two-phase flow, the turbulence matter is more complicated and need modifications in the single-phase turbulence models to be applied in the two-phase flow problems. In the next sections, the one-phase turbulence model used in this simulation is explored, and it is discussed how it can be modified to account for the existence of the dispersed phase.

3.2 Turbulence Modeling for the Euler Solver

The Euler solver used in the present work uses the standard k-ε two equation turbulence model presented by Launder and Spalding (1972) for turbulence modeling. The conservation equations of the turbulence kinetic energy K and the turbulence dissipation rate ε in the standard k-ε model are expressed as follows:

Turbulence kinetic energy equation

$$\rho \frac{Dk}{Dt} = \tau_{ij} \frac{\partial U_i}{\partial x_j} - \rho\varepsilon + \frac{\partial}{\partial x_j}\left[(\mu + \mu_t/\sigma_k)\frac{\partial k}{\partial x_j}\right] + S_k \tag{3.5}$$

Turbulence dissipation rate

$$\rho \frac{D\varepsilon}{Dt} = C_{\varepsilon 1}\tau_{ij} \frac{\partial U_i}{\partial x_j}\frac{\varepsilon}{k} - \rho C_{\varepsilon 2}\frac{\varepsilon^2}{k} + \frac{\partial}{\partial x_j}\left[(\mu + \mu_t/\sigma_\varepsilon)\frac{\partial \varepsilon}{\partial x_j}\right] + S_\varepsilon \tag{3.6}$$

Eddy viscosity

$$\mu_t = \rho C_\mu \frac{k^2}{\varepsilon} \tag{3.7}$$

Closure Coefficients

$$C_{\varepsilon 1} = 1.44 \qquad C_{\varepsilon 2} = 1.92 \qquad C_\mu = 0.09 \qquad \sigma_k = 1.0 \qquad \sigma_\varepsilon = 1.3$$

The k- ε model is the most famous Practical and stable model for solving turbulence in turbulent flows especially in the free shear flows as it is not recommended in flows at which the behavior of the flow near the wall is important, it is also not recommended for complex geometries that may have adverse pressure gradients and flow separation. In this work, the geometry of modeling is a vertical pipe of upward flow, that is a simple geometry without adverse pressure gradient and the velocity of the flow is up to 3m/s of water flow so we was satisfied by the solution of this model as a tool for turbulence solution.

3.3 Stochastic modeling of particles diffusion

As discussed in the introduction section, the Reynolds averaged Navier-Stokes equations (RANS) consider dividing the instantaneous velocity u into a mean component U and A fluctuating component ú. The RANS equations solve the mean component of the continuous phase. To consider the turbulence dispersion of the bubbles in the continuous phase, we should consider the fluctuation velocity of the continuous phase. This can be done by one of two approaches. The first is to solve the continuous phase using the Direct Numerical Simulation that can find all the scales of turbulence time and length scales by solving Navier-Stokes equations. This method (as was presented at the Introduction section) is very expensive computationally and limited to low Reynolds number and simple flows. An alternative approach is to simulate individual particle trajectories by assuming that the velocity fluctuations of this particle are random in space and time. This random motion of particles in fluid is called Brownian motion due to Robert Brown in (1827) how discovered this phenomenon while studying the motion of pollen grains in water. He described this motion as “Matter is composed of small particles which he called active molecules that exhibit a rapid irregular motion having its origin in the particles themselves and not in the surrounding fluid”. Some of the properties of this motion were investigated and are summarized by Coffey et al (2004) in these points;

1. The motion is very irregular, composed of translations and rotations, and the trajectory appears to have no tangent.
2. Two particles appear to move independently, even when they approach one another to within a distance less than their diameter.
3. The smaller the particles, the more active the motion.
4. The composition and density of the particles have no effect on the motion.
5. The less viscous the fluid, the more active the motion.
6. The higher the temperature, the more active the motion.
7. The motion never ceases.

A stochastic processes that describe this Brownian motion in physical applications is the Markov Chain which is a stochastic process in which the current state of the system is only determined from its state in the immediate past, and not by its entire history, and both the states and time are discrete.

Some works in that field was presented for describing this motion statistically, like the theory of the Brownian movement as formulated by Einstein and Fürth (1926) and Smoluchowski (1943). Although it was in agreement with experiment, it seemed far from the Newtonian dynamics of particles (Nelson 1967) as it sound to rely on the idea of the probability density distribution of Brownian particles and the Fokker-Planck equation which describes the time evolution of that distribution.

In order to model this Brownian motion mathematically, we need an equation that describes the change of the particle velocity with respect to time. There are two different approaches for modeling the velocity of particles in Brownian motion, one is called the Discrete Random Walk (DRW) at which the fluctuating velocity components are discrete piecewise constant functions of time and their random value is kept constant over an interval of time given by the characteristic lifetime of the eddies. The other is that called Continuous Random Walk (CRW): The fluctuating velocity components are obtained by solution of the Langevin equation, which behaves in time like filtered white noise. This provides a more realistic description of the turbulent eddies, at the expense of greater computational effort. Langevin (1908) introduced the concept for the equation of motion of a random variable (in this case the position of a Brownian particle). In addition, by his formulation of the theory, Langevin was the founder of the subject of stochastic differential equations.

Langevin began by simply writing down the equation of motion of the Brownian particle according to Newton's laws under the assumptions that the Brownian particle experiences two forces,

a) A systematic force (viscous drag) $-\zeta\dot{x}(t)$, which represents a dynamical friction experienced by the particle. x is the displacement and ζ is the coefficient of friction.
b) A rapidly fluctuating force F(t), which is generated as a result of the impacts of the molecules of the liquid on the particle, now called white noise. This is the residual force exerted by the surroundings.

Thus, his equation of motion, according to Newton's second law of motion, is for a particle of mass m expressed as:

$$m\frac{d^2x(t)}{dt^2} = -\zeta\frac{dx(t)}{dt} + Ff(t) \tag{3.8}$$

This can be simplified as follows:

$$\frac{du(t)}{dt} = -\frac{\zeta}{m}u(t) + \frac{Ff(t)}{m} \tag{3.9}$$

The fluctuation force $Ff(t)$ assumed to be centered Gaussian random variable having zero mean and it is independent, so it is called Gaussian white noise.

In fact, this equation was first studied in connection with Brownian motion (e.g., Wang and Uhlenbeck, 1945; Csanady, 1973, p. 28) and was only later applied to turbulent dispersion (e.g., Durbin, 1980) considering the similarity created by Boussinesq between the motion of the molecules and the motion of turbulent eddies. This section shows how the Langevin equation is related to existing Markov-chain models of turbulent dispersion.

One of the solutions presented for Langevin equation for diffusion of particles in homogenous isotropic turbulent flows is that presented by Legg and Raupach (1982). They presented the Langevin equation written at (3.9) as follows

$$\frac{du}{dt} = -a_1u(t) + b_1\xi(t) \tag{3.10}$$

With $\xi(t)$ is a Gaussian white noise, which is a stationary stochastic process with a Gaussian probability density function, zero mean, and a covariance at two times q and t of

$$\overline{\xi(q)\xi(t)} = \delta_D(t-q) \tag{3.11}$$

Such that δ_D is the Dirac delta function. Another property of $\xi(t)$ is that it is everywhere discontinuous but its integral is continuous not differentiable process.

Although Equation (3.10) is a stochastic differential equation, its solution can be obtained by formal application of the conventional method for an ordinary first-order linear differential equation. The solution presented as follows:

$$u(t) = u(t_0)e^{-a_1t} + b_1\int_{t_0}^{t} e^{-\alpha(q-t)}\xi(q)dq \tag{3.12}$$

After some mathematical and statistical manipulations, they deduced that the covariance function for the velocity will follow this expression:

$$\overline{\acute{u}(0)\acute{u}(t)} = \overline{\acute{u}^2(0)}e^{-a_1 t} \tag{3.13}$$

If the Lagrangian integral time scale of the particles velocity τ_L is defined as

$$\tau_L = \overline{(\acute{u}^2(0))^{-1}} \int_0^{\infty} \overline{\acute{u}(0)\acute{u}(t)}\, dt \tag{3.14}$$

We can deduce the value of a_1 from substituting equation 3.13 in equation 3.14 as follows

$$\tau_L = \overline{(\acute{u}^2(0))^{-1}\acute{u}^2(0)} \int_0^{\infty} e^{-a_1 t}\, dt = -\frac{1}{a_1}(e^{-\infty * t} - e^{-0*t}) = \frac{1}{a_1} \tag{3.15}$$

they deduced that the value of a_1 equals to$1/\tau_L$, such that τ_L is the Lagrangian integral time scale for the particle velocity. Also they deduced that there is a relation between a_1 and b_1 given by:

$$b_1 = \sigma_u\sqrt{2}a_1 = \sigma_u\sqrt{2}/\tau_L \tag{3.16}$$

Where $\sigma_u^2 = \overline{\acute{u}^2(0)} = \overline{\acute{u}^2(t)}$ is the Lagrangian velocity variance.

It can be observed that equation (3.12) can represent a Markov process as the value of $\acute{u}(t)$ depends only on $\acute{u}(t_0)$ at t_0 and not on the values of $\acute{u}$ at time before the time t_0. A main property of the Markov process is that it is continuous but not differentiable. Hence no Markov process can represent the change of velocity in turbulent flow, which must be everywhere differentiable. Otherwise, infinite accelerations would occur. Therefore, equation (3.12) can not represent the diffusion of particle in turbulent flows.

Equation (3.12) can only represents the turbulent dispersion if we considered that the particles velocities are defined at discrete times, $t_0, t_1, \ldots t_n$ where $t_{n+1} - t_n = \Delta t$. If the value of Δt is chosen to be much greater than the time scale T_λ over which the particle correlation remains correlated, then the sequence $u(t)$ at equation (3.12) will be a Markov chain which is like the Markov process but it is defined only at discrete times and differentiable everywhere.

The Markov sequence or chain is represented as follows:

$$\acute{u}_{n+1} = a_2\acute{u}_n + b_2\sigma_u\xi_n \tag{3.17}$$

Such that $\acute{u}_{n+1} = \acute{u}(t_{n+1})$, $\acute{u}_n = \acute{u}(t_n)$, and ξ_n is a random number from a Gaussian distribution with zero mean and unit variance. The coefficients a and b is selected to give the sequence $\acute{u}_n$ the correct standard deviation σ_u and the integral time scale τ_L. This can be done by comparing equation (3.17) with that of (3.12) with considering the integral interval (t_n, t_{n+1}). This shows that:

$$a_2 = e^{-a_1 \Delta t} = e^{-\Delta t/\tau_L} \tag{3.18}$$

And the value of b can be specified by equating of the fluctuating terms in the two equations (3.17) and (3.12) (explained in details at Legg et al 1982), the value of b will be as follows:

$$b_2 = (1 - a_2^2)^{1/2} = (1 - e^{-2\Delta t/\tau_L})^{1/2} \tag{3.19}$$

Now the Markov chain based on Langevin equation that represents the particles diffusion in turbulent flow can be expressed as follows

$$\acute{u}(t + \Delta t) = \acute{u}(t) \exp\left(\frac{-\Delta t}{\tau_L}\right) + \left[1 - \exp\left(\frac{-2\Delta t}{\tau_L}\right)\right]^{1/2} \sigma_u(t)\xi(t) \tag{3.20}$$

Such that ξ_n is a random number from a Gaussian distribution with zero mean and unit variance. $\sigma_u^2(t)$ is the velocity variance which is defined for isotropic turbulence case as follows (Bocksell et al 2006):

$$\sigma_u^2(t) = \overline{\acute{u}\acute{u}} = \overline{\acute{v}\acute{v}} = \overline{\acute{w}\acute{w}} = 2k/3 \tag{3.21}$$

In fact, the value of the time step Δt needed for solving equation (3.20) is not selected arbitrary. It was mentioned before that the value of Δt should be selected to be much greater than the time scale over which the particle acceleration still correlated τ_λ. The value of τ_λ is suggested by Legg et al (1982) to be equal to the Taylor time scale of the turbulent flow under consideration which is expresses as $\tau_\lambda = \sqrt{15\,\nu k/\varepsilon}$ (Wilcox 1994). It is clear that the value of Δt should be chosen to be much less than the Lagrangian Integral time scale τ_L also to catch the variation of turbulent fluctuations at the turbulent flow.

Legg and Raupach (1982) considered also the effect of the compressibility on the fluctuations when there is a gradient for the velocity variance in the different flow directions. Detailed description for this consideration can be found in Legg and Raupach (1982).

Bocksel et al (2006) presented investigation study for the Markov chain relation (3.16) presented by Legg and Raupach (1982). He further considered that the diagonal terms of the Reynolds stress tensor $(\sigma r_u, \sigma r_v, \sigma r_w)$ are not equal and presented a more general relation called the full CRW model as follows:

$$\begin{bmatrix} u(t+\Delta t) \\ v(t+\Delta t) \\ w(t+\Delta t) \end{bmatrix} = \begin{bmatrix} k_u & 0 & 0 \\ 0 & k_v & 0 \\ 0 & 0 & k_w \end{bmatrix} \begin{bmatrix} u(t) \\ v(t) \\ w(t) \end{bmatrix}$$

$$+ \begin{bmatrix} \sigma r_u \sqrt{1-kl_u^2} & 0 & 0 \\ 0 & \sigma r_v \sqrt{1-kl_v^2} & 0 \\ 0 & 0 & \sigma r_w \sqrt{1-kl_w^2} \end{bmatrix} \begin{bmatrix} \sqrt{1-b^2} & b & 0 \\ 0 & 1 & 0 \\ 0 & 0 & 1 \end{bmatrix} \begin{bmatrix} \xi_u \\ \xi_v \\ \xi_w \end{bmatrix} \qquad (3.22)$$

Where

$$kl_u = \exp\left(\frac{-\Delta t}{\tau_{L,u}}\right), \quad kl_v = \exp\left(\frac{-\Delta t}{\tau_{L,v}}\right), kl_w = \exp\left(\frac{-\Delta t}{\tau_{L,w}}\right),$$

$$b = \frac{R_{uv}\left[1 - \exp\left(\frac{-\Delta t}{\tau_{L,u}}\right)\exp\left(\frac{-\Delta t}{\tau_{L,v}}\right)\right]}{\left[1 - \exp\left(\frac{-2\Delta t}{\tau_{L,u}}\right)\right]^{\frac{1}{2}}\left[1 - \exp\left(\frac{-2\Delta t}{\tau_{L,v}}\right)\right]^{\frac{1}{2}}}, \qquad R_{uv} = \frac{\overline{\acute{u}\acute{v}}}{\sigma r_u \sigma r_v} \qquad (3.23)$$

And the types of simulations are considered for the expression (3.22) according to the considerations in table 3.1 below:

Table 3.1. Bocksel and Loth (2006) CRW model types.

Name	Turbulence type	Time-scale Type
Isotropic	$\overline{\acute{u}\acute{u}} = \overline{\acute{v}\acute{v}} = \overline{\acute{w}\acute{w}} = 2k/3$, $\overline{\acute{u}\acute{v}} = 0$	$\tau_{L,u} = \tau_{L,v} = \tau_{L,w}$
Diagonal	$\overline{\acute{u}\acute{u}} \neq \overline{\acute{v}\acute{v}} \neq \overline{\acute{w}\acute{w}}$, $\overline{\acute{u}\acute{v}} = 0$	$\tau_{L,u} \neq \tau_{L,v} \neq \tau_{L,w}$
Full	$\overline{\acute{u}\acute{u}} \neq \overline{\acute{v}\acute{v}} \neq \overline{\acute{w}\acute{w}}$, $\overline{\acute{u}\acute{v}} \neq 0$	$\tau_{L,u} \neq \tau_{L,v} \neq \tau_{L,w}$

The simulation presented by Bocksel and Loth (2006) according to the proposed models showed that the full CRW model gave the best agreement with DNS results, followed by the diagonal type and then the isotropic case. Details about the simulation results and discussions can be found at the work of Bocksel and Loth (2006).

In order to apply the full or diagonal case in equation (3.22) approximations needed for the values of Reynolds stresses $(\overline{\acute{u}\acute{u}}, \overline{\acute{v}\acute{v}}, \overline{\acute{w}\acute{w}})$ as in this case it will not be equal as in the isotropic case. Also the integration time scale of turbulence τ_L will not be the same in

the three coordinates and needs further approximations to solve the equation (3.22). This needs that the turbulence be modeled in the continuous flows by the Reynolds stress model or models that can simulate the anisotropic inhomogeneous turbulence cases.

In the present work, the standard k-ε model is used for solving the continuous phase turbulence. The turbulence state is considered isotropic in this model, so, the use of the diagonal or full case of equation (3.22) will not be necessary with the standard k-ε model. For that, the isotropic relation of the CRW presented mainly by legg and Raupach (1982) was used. The upgrade of the Lagrangian solver for the full CRW model presented by Bocksel et al (2006) may be used in the future when the turbulence model is updated to account for the anisotropy effects of turbulence.

In the present work equation (3.30) represents the change of the fluctuating component of the liquid with time, so we will consider it in our model as the fluctuating components of the liquid velocity. At the present case, the Langevin equation is used in cylindrical coordinates, so equation (3.20) can be written for the three cylindrical coordinates r, θ, z as follows:

$$\acute{u}_{l,r}(t+\Delta t) = \acute{u}_{l,r}(t)\exp\left(\frac{-\Delta t}{\tau_L}\right) + \sqrt{1-\exp\left(\frac{-\Delta t}{\tau_L}\right)}\,\sigma r(t)\xi_r(t) + \frac{\acute{u}_{l,\theta}^2}{r}\Delta t \qquad (3.24)$$

$$\acute{u}_{l,\theta}(t+\Delta t) = \acute{u}_{l,\theta}(t)\exp\left(\frac{-\Delta t}{\tau_L}\right) + \sqrt{1-\exp\left(\frac{-\Delta t}{\tau_L}\right)}\,\sigma r(t)\xi_\theta(t) - \frac{\acute{u}_{l,r}u_{l,\theta}}{r}\Delta t \qquad (3.25)$$

$$\acute{u}_{l,z}(t+\Delta t) = \acute{u}_{l,z}(t)\exp\left(\frac{-\Delta t}{\tau_L}\right) + \sqrt{1-\exp\left(\frac{-\Delta t}{\tau_L}\right)}\,\sigma r(t)\xi_z(t) \qquad (3.26)$$

Where τ_L is the characteristic time of the Lagrangian time scale correlation (Dehbi, 2008), and the variables ξ_r, ξ_θ, ξ_z denote a Gaussian white noise random process, with components that independent Gaussian random numbers. Further information about the representation of the acceleration terms in cylindrical coordinates can be found at Muñoz-Cobo et al. (2012).

The values of the fluctuating liquid velocities represented in equations (3.24) to (3.26) are added to the liquid mean velocity calculated by the RANS model to compose the instantaneous liquid velocity used for calculating the forces acting on the bubble as explained in chapter 2, and calculated at equation (2.139).

The model given by these equations assumes isotropic turbulence. The characteristic time τ_L is computed away from the boundary layer by the following relation:

$$\tau_L(r,\theta,z) = 0.14\frac{k(r,\theta,z)}{\varepsilon(r,\theta,z)} \text{for } y^+ > 100 \tag{3.27}$$

Where $k(r,\theta,z)$and $\varepsilon(r,\theta,z)$ denote the turbulent kinetic energy and dissipation rate at point (r,θ,z). Inside the boundary layer, we have used the following expression computed by DNS by Kallio and Reeks (1989):

$$\begin{aligned} &\tau_L^+(r,\theta,z) = 10 && \text{for } y^+ < 5 \\ &\tau_L^+(r,\theta,z) = 7.122 + 0.5731y^+ - 0.00129(y^+)^{\,2}, && \text{for } 5 \le y^+ < 100 \end{aligned} \tag{3.28}$$

Where the none dimensional Lagrange time scale is defined by $\tau_L^+ = \tau_L((u^*)^2/\nu_l)$ as u^* is the friction velocity.

A more general Markov/Langevin equation can be deduced for fluid particles in cylindrical coordinates (Veenman, 2004) but for the purpose of this work, equations 3.14:16 gave good results for the analyzed cases, and also these equations contain the non linear terms of the Markov-Langevin type equation deduced by Veenman.

3.4 Bubbles Induced Turbulence (BIT) Modeling

In the one-way coupling process between the Eulerian and Lagrangian solvers, the effect of the dispersed phase on the continuous phase is neglected and the RANS equations and turbulence equations of the Eulerian Framework is solved without any modifications. In case of the two-way coupling process, the back effect of the dispersed phase turbulence on the continuous phase should be considered in the governing equations as will be discussed at chapter 5 in the two-way coupling process.

Three approaches have been proposed for modeling of the bubble induced turbulence. The first and simplest one is the proposed by Sato and Sekoguchi (1975), as well as by Sato et al. (1981) where the effective viscosity in the RANS equations is considered as a sum of three components, the dynamic viscosity of the fluid, the turbulent viscosity produced by the turbulence model used, and the bubble induced turbulent viscosity which is modeled as follows in Sato et al (1975) model:

$$\mu_{t,BIT} = \frac{1}{2}C_{\mu b}\rho_l\alpha_g D_b|U_b - U_l| \tag{3.29}$$

Such that, $C_{\mu b} = 1.2$.

Another approach to the modeling of bubble-induced turbulence is due to Arnold et al. (1988). It is based on the assumption that the influence of the gas bubbles on the liquid turbulence results primarily from the velocity fluctuations, which originate from the displacement of liquid by the rising bubbles. Since, for continuity reasons, such a displacement takes place in the surrounding fluid even if the bubbles rise in a stagnant medium, these fluctuations cannot be interpreted as turbulence in the conventional sense. Therefore, the notion "pseudo-turbulence" is used instead. A theoretical estimate of the influence of these fluctuations can be derived under the assumption of a potential flow around a group of spheres. Like this model proposed by Lopez de Bertodano et al (1994) as follows:

$$S_{k,BIT} = \frac{1}{4}\alpha_g |u_b - u_l|^2 \tag{3.30}$$

And this bubble induced turbulent kinetic energy $S_{k,BIT}$ is introduced as a source term in the conservation equation of the turbulent kinetic energy.

The third approach to be discussed for the modeling of bubble-induced turbulence allows for the convective and diffusive transport of turbulent kinetic energy. This model incorporates the influence of the gas bubbles on the turbulence by means of additional source terms in the balance equations for both k and ε.

The additional source term in the k-equation is taken to be proportional to the product of the drag force and the slip velocity between the two phases, as proposed by Kataoka and Serizawa (1989). Under the assumption of equilibrium between the pressure force and the drag force, this term can be represented as follows

$$S_{k,BIT} = -C_k \alpha_d \nabla P. |u_b - u_l| \tag{3.31}$$

Since the slip velocity and the pressure gradient are oppositely directed, this term is always positive if the model constant C_k is greater than zero.

The corresponding source term in the ε-equation is usually modeled as

$$S_{\varepsilon,BIT} = C_\varepsilon \cdot \frac{\varepsilon}{k} S_{k,BIT} \tag{3.32}$$

and is also positive. This means that the contribution of the bubbles both to the production and to the dissipation of the turbulent kinetic energy is positive. The superposition of both effects can result in an increase, as well as in a decrease, of the turbulence intensity compared with the single-phase turbulence model.

One of the most famous models that follow this approach was presented by Yao and Morel (2004). They proposed a form for the source terms in the K and ε equations as follows:

$$S_{k,BIT} = -\left(F_{d,drag} + F_{d,vm}\right)(u_b - u_l) \tag{3.33}$$

$$S_{\varepsilon,BIT} = C_{\varepsilon 3}\frac{S_{k,BIT}}{\tau}, \quad \tau = \left(\frac{D_b^2}{\varepsilon_c}\right)^{1/3} \tag{3.34}$$

Where τ represents the characteristic time of the bubble induced turbulence. And $F_{d,drag}$ and $F_{d,vm}$ are the interfacial drag and virtual mass forces exerted on the bubble respectively. The constant $C_{\varepsilon 3}$ was adjusted to a value of 0.6 for boiling bubbly flow experiment and to a value of 1.0 for adiabatic bubbly flow experiments.

In the present research, the bubble induced turbulence term is used in the CRW model for generating the fluid velocity fluctuations which is affected by the bubble induced turbulence. In the one way coupling process, we considered that the BIT kinetic energy k_{BIT} that is used in the CRW model depends on the bubble Reynolds number and the gas void fraction. According to this assumption, the total turbulence kinetic energy used in CRW model is a sum of the continuous phase turbulence kinetic energy and the BIT kinetic energy as follows:

$$k(r,\theta,z) = k_l(r,\theta,z) + k_{BIT}(r,\theta,z) \tag{3.35}$$

Such that,

$$k_{BIT}(r,\theta,z) = C_{tb}.Re_b.fu_g(\alpha) \tag{3.36}$$

Such that Re_b is the bubble Reynolds number defined as follows:

$$Re_b = \frac{\rho_c|u_{rel}|\,D_b}{\mu_c} \tag{3.37}$$

And $fu_g(\alpha)$ is the function describes the dependence of k_{BIT} on the void fraction α. It was used a value of $fu_g(\alpha) = \alpha$ with $C_{tb} = 5.5e-5$, but it showed some strange values in the void fraction distribution. So finally we adjusted this relation and it was found that the expression for $fu_g(\alpha)$ that best fits the experimental data for the three liquid velocities 0.5, 1.0, 2.0 m/s and for the three gas fractions 5%, 10%, and 15% is as follows:

$$fu_g(\alpha) = \frac{|\nabla\alpha_g|}{\alpha_g} \tag{3.38}$$

With the value of $C_{tb} = 0.02$, this consideration gave good agreement with experimental data without considering bubble induced turbulent dissipation rate as was publicated in Muñoz-Cobo et al (2012). It should be noticed that the coefficient C_{tb} at equation (3.36) with the last definition of $fu_g(\alpha)$ at (3.38) will have dimensions of (m^3/s^2).

For the case of two way coupling process, the bubble induced turbulence model should be similar to the BIT models introduced in the literature of inserting source terms in the k and ε equations and at the same time follows the same dependence of the BIT term proposed to be convenient for the CRW model. To suggest an expression for the source term of turbulent kinetic energy equation produced by the bubbles, it is consiered that the BIT kinetic energy is proportional to the energy lost in the frictional stress produced by the flow of the bubble in the continuous liquid. Also the bubble induced turbulent kinetic energy is proportional to the relative velocity of the bubble and an expression for the void fraction $fu_g(\alpha)$, in that way the final expression of the bubble induced turbulence will be expressed as follows:

$$S_{k,BIT} \propto F_{d,drag}\, u_{rel}\, fu_g(\alpha) \tag{3.39}$$

For the drag force, from the expressions of the drag force in equation (2.2) and the drag coefficients, it can be assume the following proportionality of the dreg force and drag coefficient:

$$\vec{F}_{Drag} \propto C_D \rho_c\, u_{rel}^2 D_b^2 \tag{3.40}$$

And

$$C_D \propto \frac{1}{Re_b} = \frac{\mu_c}{\rho_c\, D_b\, u_{rel}} \tag{3.41}$$

Then

$$\vec{F}_{Drag} \propto \frac{\mu_c}{D_b\, u_{rel}}\, u_{rel}^2\, D_b^2 \tag{3.42}$$

Substitute from the proportionalities 3.39, 3.40, and 3.41 in 3.38 it is found that

$$S_{k,BIT} \propto \frac{\mu_c}{D_b\, u_{rel}} D_b^2\, u_{rel}^2 u_{rel} fu_g(\alpha) = \mu_c D_b\, u_{rel}^2 fu_g(\alpha) \tag{3.43}$$

So, this leads to the following:

$$S_{k,BIT} = C_{tb}.\, D_b\, u_{rel}^2 fu_g(\alpha) \tag{3.44}$$

As we work for the same continuous phase, we considered that the coefficient C_{tb} already has the term μ_c inside it and as a result, it will have dimensions of $(N.s/m^2)$. With some adjustments and tests for the turbulence dispersion models explained in chapter 2, the expression for $fu_g(\alpha)$ defined at equation (3.38) found to give some strange distributions at the pipe center. We found that with this expression, the effect of the gas void fraction is accounted for two times, one with the expression of $fu_g(\alpha)$ and another with the averaging made by the two-way coupling. So, we decided to delete the term $fu_g(\alpha)$ from the source term added to the turbulence kinetic energy equation $S_{k,BIT}$. And the final expression for the bubble induced turbulent kinetic energy that is considered as a source term in the k equation is expressed as follows.

$$S_{k,BIT} = C_{tb}.u_{rel}^2 * d_b \tag{3.45}$$

This relation is only used in the two-way coupling when considering the source term in the turbulence kinetic energy equation $S_{k,BIT}$.

For the value of the bubble induced dissipation, the same expression of Yaw and Morel (2004) in equation (3.34) was considered at the present work.

It should be highlight on the method of considering the bubble induced turbulence in both the one- and two-way coupling processes which are explained in chapter 4 and 5. In the one-way coupling process, we consider the increase of turbulence kinetic energy that is used in the Langevin equation for calculating the fluctuating part of the liquid velocity. The total k used in equations 3.35 is:

$$k = k_c + k_b \tag{3.46}$$

In this case we do not consider any change in the value of the dissipation rate ε. In case of the two-way coupling, there is no need to add the bubble induced component of the kinetic energy in the Langevin equation as it is already considered as a source term during the solution of the turbulence equations for the Eulerian solver. So the calculated turbulence data already contains the effect of the bubble induced turbulence on the k and ε values as source terms in k and ε equations.

3.5 Indication for the CRW model including the BIT effect

To indicate the order of magnitude of the velocity fluctuations that are obtained in the present work, a simple analysis for the resulting fluctuations produced by equations 3.24-3.26 was made. The case F03AG01 of the two-way coupling results for water velocity of 2.026m/s and gas hold up of 5% inside a vertical pipe of diameter 0.052m and 1m height was considered. The profiles of the turbulence kinetic energy k and turbulent dissipation rate ε at the id length of the simulated pipe are as shown in figure

3.3. These profiles of k and ε include already the effect of the bubble induced turbulence and for that reason, it can be seen the very large value of ε close to the pipe walls. We selected three different radial positions of r=0.025 m, 0.02 m, and 0.0m at pipe center. For these three positions, the values of k and ε are shown in table 3.2. For these three radial positions, the fluctuation velocity produced by the Langevin equation 3.22:24 considering a Lagrangian time step of dt=1.0e-4 seconds are shown in figure 3.4.

Table 3.2. Values of k and ε at selected radial positions.

r [m]	k [m^2/s^2]	ε [m^2/s^3]
0.0	0.19196	2.656
0.02	0.5396	22.3
0.025	0.6952	78.7836

From figures 3.3, And 3.4, it can be observed that at the center of the pipe, the fluctuations are very week and this is due to the smallest values of k and ε. As both of them specify the characteristic time τ_L defined in 3.20. Moving to the pipe wall at position r=0.02 m, the values of k and ε increase and as a result the fluctuations increase as shown in figure 3.4. Close to the wall, at the radial position r=0.025 m,

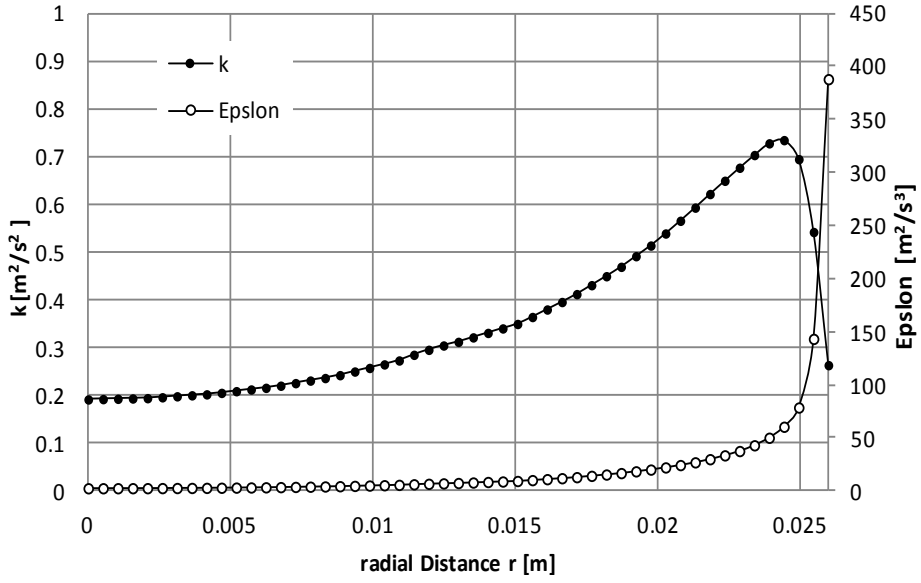

Figure 3.3. The radial k and ε profiles at the mid distance of the pipe height.

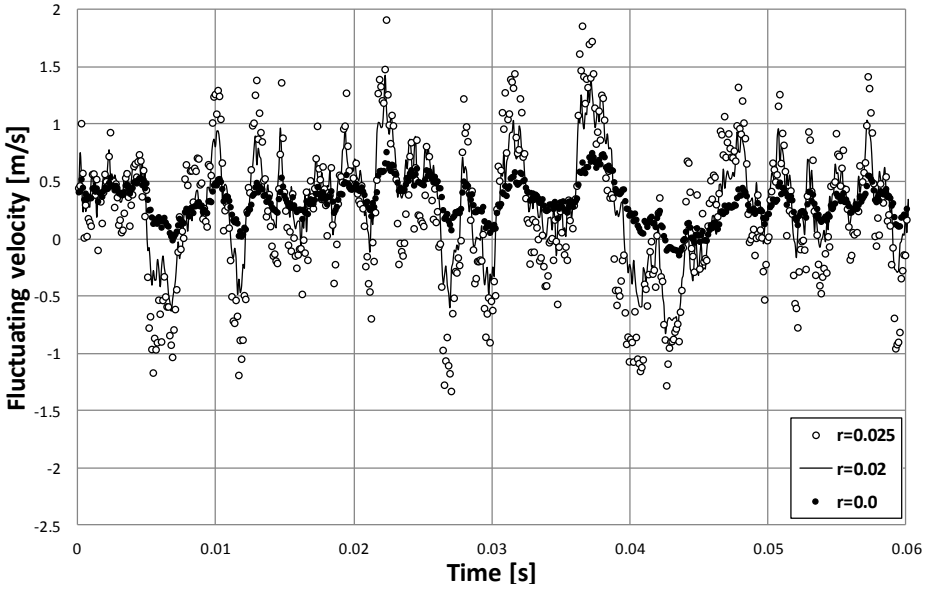

Figure 3.4. The velocity fluctuations at three different radial positions produced by the Langevin equation at time step dt=1.0e-4 s.

The values of k and ε become bigger especially ε, as a result the characteristic time τ_L decreases which increase the value of the fluctuations. It can be observed from the fluctuations at figure 3.4, the homogenous distribution of the fluctuations and that they have a mean value of zero which agrees with the isotropic turbulence model considered in the present work.

4. One-way Coupling Process Study and Discussion

In this chapter, the process of the One-way coupling between the two solvers will be described. At first, the methodology of the one-way coupling process that we used for describing the coupling procedure is explained. Then the time stepping mode used followed by the description of the code algorithm is presented. Then a study for the effect of the bubble induced turbulence BIT formula on the radial distribution of the gas void fraction is discussed, and a relation that can be used with our model is defined. Then a study for the effect of the lift force coefficient on the distribution of the gas void fraction will be introduced. Finally the results from the One-way coupling with the selected lift force coefficient and the selected BIT relation are presented.

In the one-way coupling for the two phases, the effect of the continuous phase on the dispersed phase is taken in account but the contrary is not true. This process can be true only for low gas void fractions. For high gas void fractions, the back effect of the dispersed phase on the continuous phase cannot be neglected. So the work in this chapter is considered as a pre step for the two way coupling process and also for the consideration of the bubble interaction mechanisms mentioned in chapter 2.

The sequence of the simulation for the one-way coupling is iterative. This is done by primarily generating randomly number of bubbles which in the current simulation was 20000 at the inlet of the pipe. Then applying the Newton's second law to each bubble and calculating the acting forces on the bubble, the change in the velocity and direction of the bubbles can be calculated. This follows tile all the bubbles get out at the top outlet of the pipe and at this moment, we have the first iteration of the void fraction distribution. this resulting void fraction distribution is used as an input for the second step making the same until getting a second void fraction distribution. The iterations are continued tile a convergence in the void fraction distribution is reached to be considered as the final distribution of the void fraction.

4.1 Approximating Eulerian quantities at bubble location

The data for the continuous phase are required at the bubble place considering that the bubbles are smaller than the computational cells and can be considered as point in the domain. These data are, velocity components U, V, W, velocity gradients, turbulence kinetic energy K and turbulence dissipation rate ε at the bubble location. These data are required for calculating the different forces acting on the bubble and that controls its motion as explained in acting forces section.

For the Lagrangian solver, the values need are, the velocities of the liquid, turbulence kinetic energy K, and turbulence dissipation rate ε at the location of the bubble. Many interpolation techniques are used. the methods that are used in this work is presented, further information about these techniques can be found in the classical text books on numerical analysis like at Press et al (1996) and (2003). We will discuss in the next subsection, the methods used in this work:

Weighted Inversed Distance Method

In this method, the cell at which the bubble is located is identified. The liquid variables like the velocity and turbulence k and ε are already known at the cell nodes or vertices.

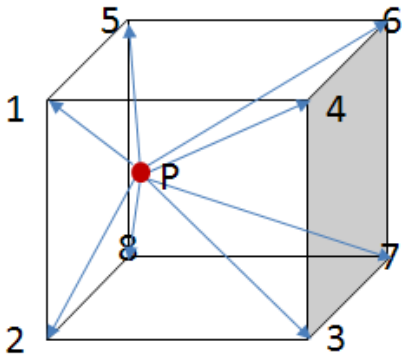

Figure 4.1. Inverse Distance Weight method.

So, knowing the distance between the bubble center location and the nodes the variables at bubble center location can be calculated using this relation:

$$\varphi_p = \sum_{i=1}^{n} \varphi_i / d_{ip}^n \Big/ \sum_{i=1}^{n} 1/d_{ip}^n \qquad (4.1)$$

Such that φ_i is the variable value at node i, d_{ip} is the distance between the node i and the bubble location p, φ_p is the variable value at bubble location, and n is a constant =2.0. This method was used because the majority of the cells are larger than the size of the bubble and they can be treated considering the particle source in cell technique Crowe et al (1997). If the bubble center is located on the face between two cells, the value of the variable is approximated at the bubble between the 12 corners of the two cells, and this rarely occurs.

4.2 Computational domain and boundary conditions

The computational domain used for simulation in the one-way coupling process is a vertical pipe of diameter 0.052 m and height of 3m. The locations of the boundaries are shown at figure 4.2.

The boundary conditions for the Euler solver are presented in the one way coupling process as follows. For the inlet, a uniform velocity profile was inserted with a value that depends on the liquid flow for each case as shown at table 1.1. The turbulence kinetic energy and dissipation rate was presented as fixed values of 10e-4 each. The wall presented with no slip condition. The outlet presented as the only outlet with the gradient of the entire variables equal to zero. On the other hand, the Lagrange solver needs also boundary conditions for the bubbles entering from the inlet. This was done by generating the bubbles at the inlet according to the void fraction distribution at the inlet. Also the velocity of the entering bubbles was interpolated form the radial distribution of the vertical velocity of the bubbles at the inlet. The wall was considered as a solid wall at which the bubble is reflected inside the pipe. More detailed description for the method of generating the bubbles will be shown at the code algorithm section.

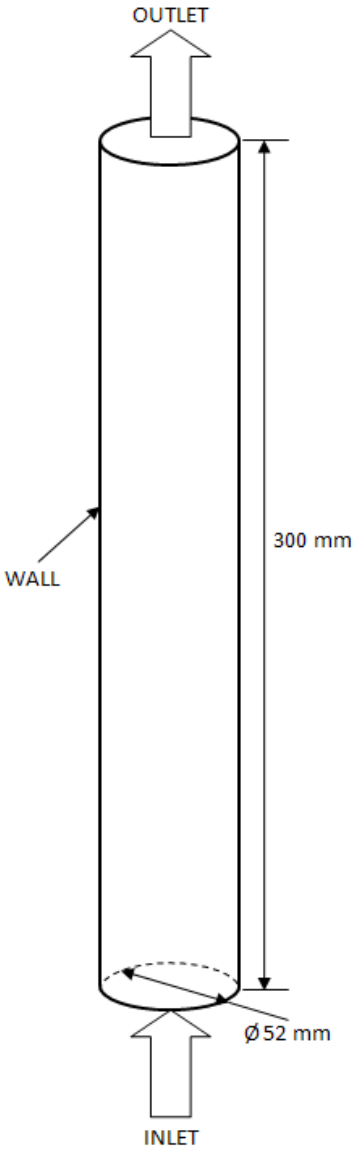

Figure 4.2. Computational domain layout.

4.3 Time stepping

In case of no consideration for bubbles collisions for small void fractions, only one time step is required to advance the motion of the bubbles according to the Newton's second law equations (2.138). The forces acting on the bubble are assumed to be constant during each time step. As stated by Laín et al (2002), the numerical solution of the Lagrangian equation requires that the time step to be sufficiently smaller than all relevant time scales for the bubble motion which are:

- The time required for a bubble to cross a control volume.
- The bubble response time scale, $\tau_b(C_{Dr}) = \frac{4}{3\mu_l}\frac{(\rho_g+0.5\rho_l)D_b^2}{Re_b C_{Dr}}$ as stated by Laín et al (2002),
- The integral time scale of turbulence which varies along the trajectory of the bubble due to changing the local values of k and ε is suggested by Laín et al (2002) to be on the form $\tau_t = 0.16\, k/\varepsilon$.

In the present work, the bubble was considered to be able to pass the cell in one time step but this is accounted for by the techniques used for bubble locating in the cell described in chapter 3, so the first conditions is not necessarily valid. In the present work, a fixed Lagrangian time step was used which was necessary for the CRW model (chapter 3) used for generating the velocity fluctuations, which in turn are dependent on the time step used.

4.4 Code Algorithm

In the one way coupling process without considering bubbles interactions, two nested loops are considered. The inner one is a Do loop to apply the time integration for each bubble from the entrance of the pipe tile the bubble getting out of the top outlet, and the outer loop for counting the bubbles. The algorithm of the code is as shown in figure 4.3. In the inner loop the real operations of the Lagrangian simulation is handled by calculating the forces exerted on each bubble, calculating the new velocity of the bubble and updating bubbles position. Also the inner loop contains the z limit of the bubble such that the bubble data including velocity, position, and size are stored as it gets out from the outlet. The code flow chart is shown in Figure 4.3.

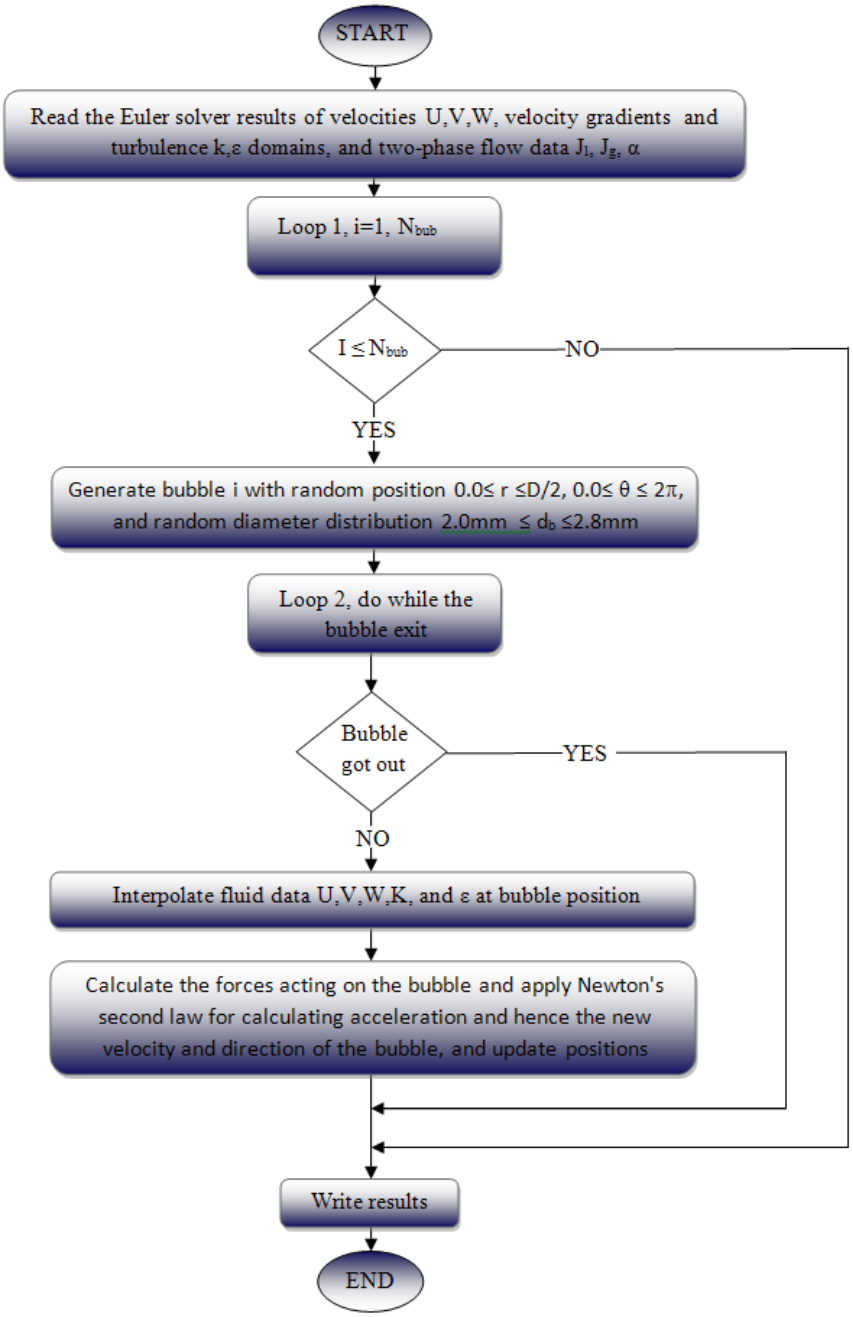

Figure 4.3. Code flowchart without considering bubbles collision.

4.5 Study for the Effect of the BIT formula on the void fraction distribution.

In this section, the study we have done for the formula of the gas void fraction $f(\alpha_g)$ to be consistent with the CRW model used and to follow the base described in section 3.4. In the test for getting the complete relation for K_{BIT} to be finally as introduced in chapter 3, many relations have been tested even for the dependence on the bubble relative velocity u_{rel} and diameter D_b. At first we used a simple relation of K_{BIT} as follows:

$$K_{BIT} = C_{tb} * \alpha_g * Re_b \tag{4.2}$$

From this relation it is calculated the average radial profile of the bubble Reynolds number and the gas void fraction for some test cases as shown in figure 4.4 and 4.5, also we have obtained that the radial profile of the multiplication of the void fraction by the Reynolds number is shown in figure 4.6. As it can be seen in figure 4.4, the Reynolds number is similar for fixed liquid flow rate even with different gas hold ups. So the dependence of the K_{BIT} formula on the Reynolds number will be for different liquid velocities only.

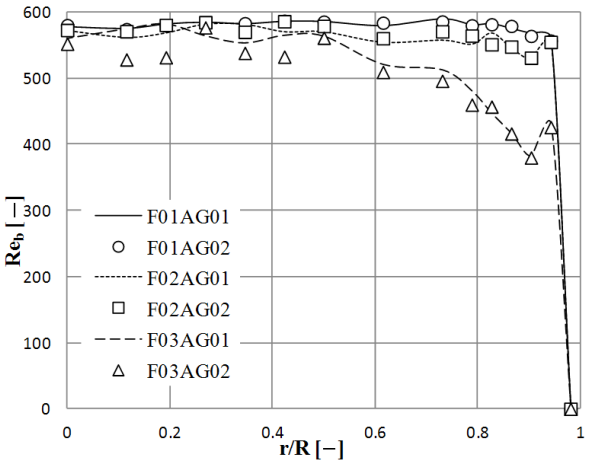

Figure 4.4. The averaged bubble Reynolds number radial distributions for the test cases.

In figure 4.5, it can be observed the difference between the different void fraction profiles for the test cases. This changes with the average void fraction for different hold up cases and will affect the bubble induced turbulence to be increased especially close to the wall as presented in the relation of K_{BIT}.

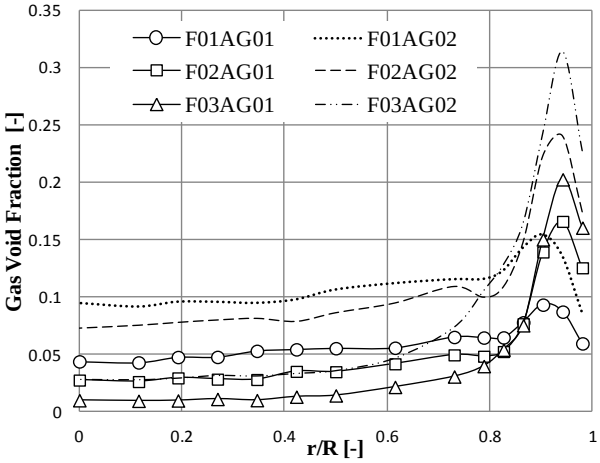

Figure 4.5. The radial distribution of the gas void fraction profile

It can be observed in figure 4.6 that the dependence of K_{BIT} will be affected more by the void fraction distribution than the Re_b.

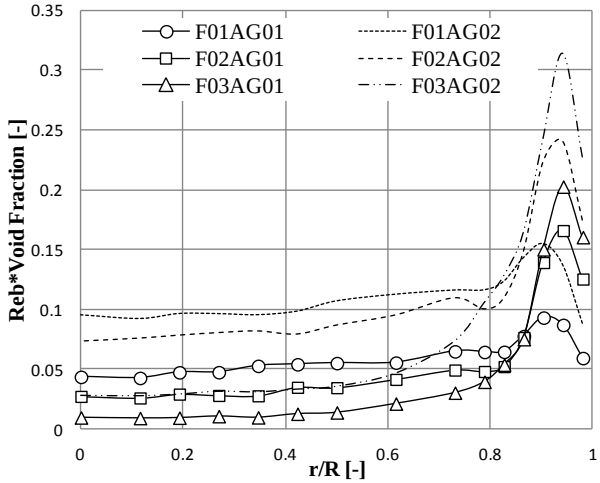

Figure 4.6. The radial profile of the void fraction multiplied by Re_b.

The void fraction distributions that resulted from the presented relation of the K_{BIT} are shown in figure 4.7. The name of the test case is written in the top of each graph. The solid circles represent the Experimental data and the continuous lines represent the simulation data. It can be seen that this relation gave good agreement with experimental data for the low gas hold ups in the top graph series. However, in the gas hold ups of G02 which represents 10% average void fraction, the relation gave a peak close to the wall for the case F01AG02 and the calculated distribution is not the same as the experimental void fraction because at the center have step distribution. This means that in this test case, the turbulence dispersion is low respect to the lift force and need to increase to distribute this peak beside the wall. In the other two cases F02AG02 and F03AG02 the distribution is not bad but need to be adjusted the K_{BIT} relation more to give a more smooth distribution.

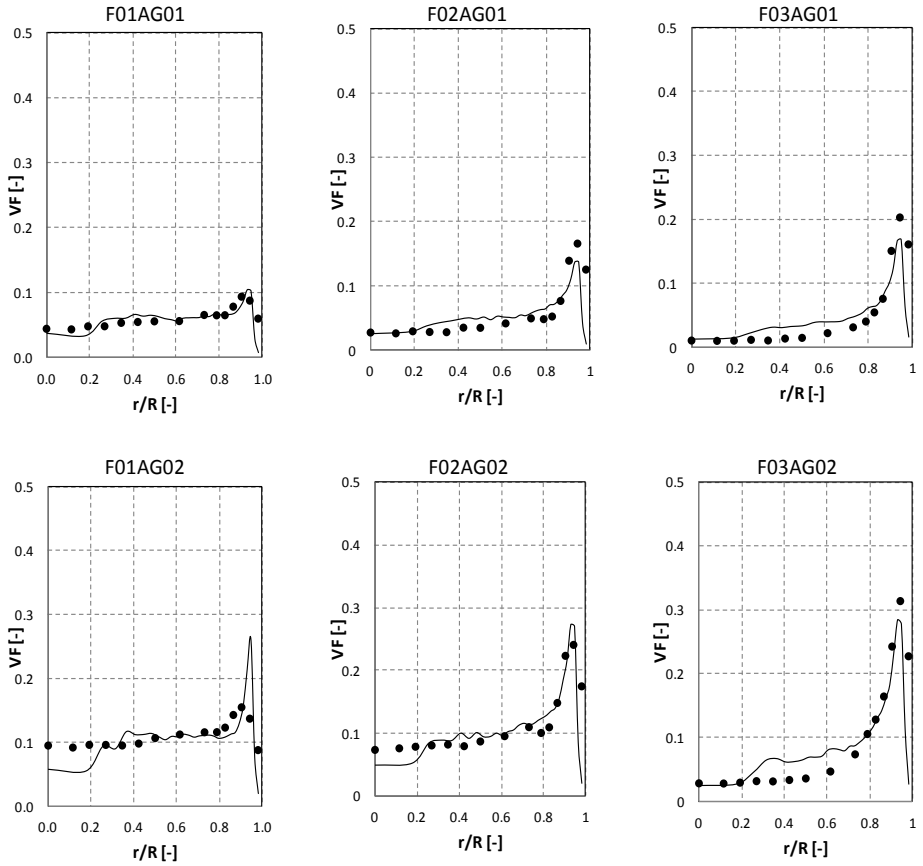

Figure 4.7. Void fraction profiles for the relation $k_{BIT} = C_{tb} * \alpha_g * Re_b$ with C_{tb}=5.5e-5.

To suggest another relation for the K_{BIT}, we tried to find a new dependence on the void fraction which is consistent with various test cases. As presented in the section of acting forces in chapter 2. The turbulence dispersion effect was described and the model presented for converting it to force that can make balance with other lateral force and give more smooth distribution of the void fraction profile. Burns et al (2004) suggested that the dependence will be on the gradient of the void fraction divided by the void fraction: $(\nabla\alpha_d/\alpha_d - \nabla\alpha_c/\alpha_c)$. This relation can be written as follows: $(\nabla\alpha_d/(\alpha_d - \alpha_d^2))$. In the present study, the term α_d^2 was neglected as it is very small and the dependence was suggested to be on $(\nabla\alpha_d/\alpha_d)$. The new relation of the K_{BIT} will be as follows:

$$K_{BIT} = C_{tb} * Re_b * (\nabla\alpha_d/\alpha_d) = C_{tb} * \left(\frac{u_{rel} D_b \rho_l}{\mu_l}\right) * (\nabla\alpha_d/\alpha_d) \qquad (4.3)$$

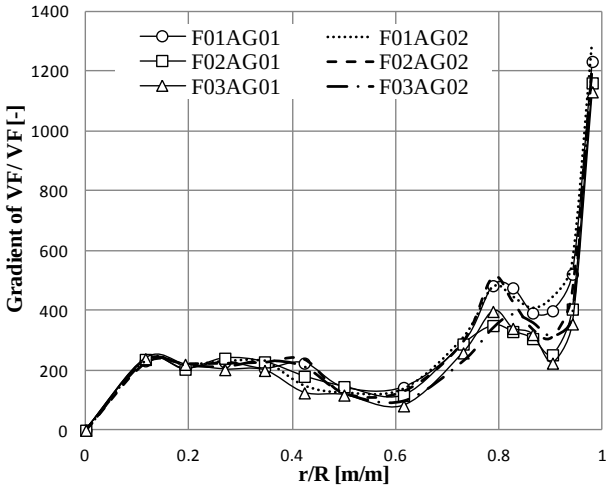

Figure 4.8. The radial profile of $(\nabla\alpha_d/\alpha_d)$ for different test cases.

Both of the liquid density ρ_l, and the liquid dynamic viscosity μ_l can be collected with the constant C_{tb} so that the relation can be as follows:

$$K_{BIT} = C_{tb}\, u_{rel}\, D_b * (\nabla\alpha_d/\alpha_d) \qquad (4.4)$$

The radial profile of $(\nabla\alpha_d/\alpha_d)$ is shown in figure 4.8. it can be observed from figure 4.8 that the wall peak of the value $(\nabla\alpha_d/\alpha_d)$ is very similar for all the test cases which means that there will not be big difference between the different cases because of this relation. The simulation results obtained using the K_{BIT} given by equation (4.4) are shown in figure 4.9. It can be seen at figure 4.9 that there is a wall peak for the calculated void fraction higher than the experimental results in all cases except the

cases of F03AG01 and F03AG02. If we gave a glance on the relation (4.4) we can see the dependence of the K_{BIT} on three main parameters.

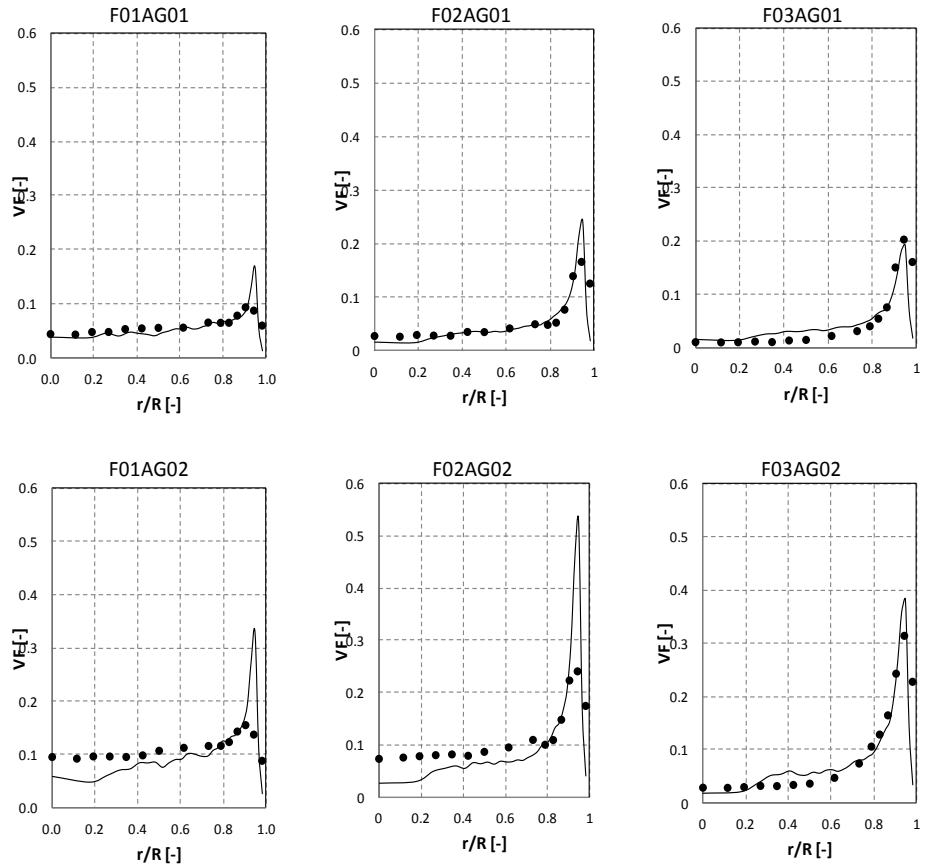

Figure 4.9. Void fraction obtained using the relation $K_{BIT} = Ctb\ u_r\ D_b(\nabla\alpha_d/\alpha_d)$ with C_{tb}=9.285e-3.

The first parameter is the void fraction relation $(\nabla\alpha_d/\alpha_d)$ which gave approximately the same distribution for the bubble induced turbulence and the difference will be very low depending on this parameter. The second is the bubble diameter which may affect because in the test experiments, the bubbles at lower liquid velocity are bigger than that at the higher liquid velocity. A graph which illustrates the range of bubble Sauter mean diameter at the inlet is shown in figure 4.10.

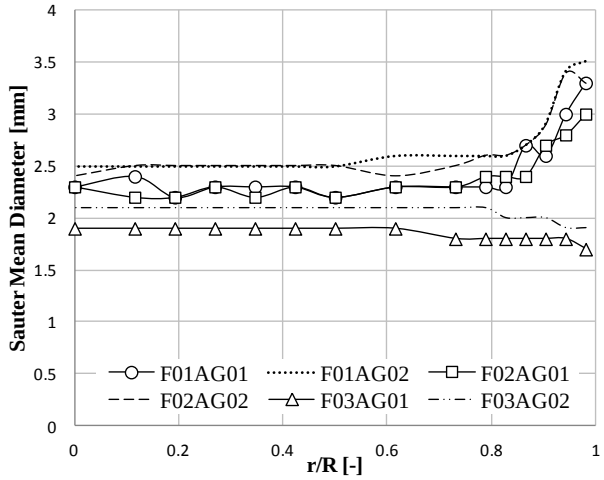

Figure 4.10. Sauter mean diameter at the inlet.

The third parameter is the relative velocity. As shown in figure 4.11, it can be observed that the test experiments F01A and F02A have approximately a fixed value of the relative velocity that does not change in the radial direction. Only the experiment F03A has a notable change of the relative velocity in the radial direction. This may lead us to assume the dependence of the K_{BIT} on the square of the relative velocity u_{rel}^2 as this leads to minimizing the effect of the relative velocity beside the wall for the experiments F03AG01 and F03AG02. This will lead to increasing the peak of the void fraction in these two cases as the rest of the cases to have the same tendency. The dependency on u_{rel}^2 is recommended also with the derivation that we made in section 3.4 theoretically.

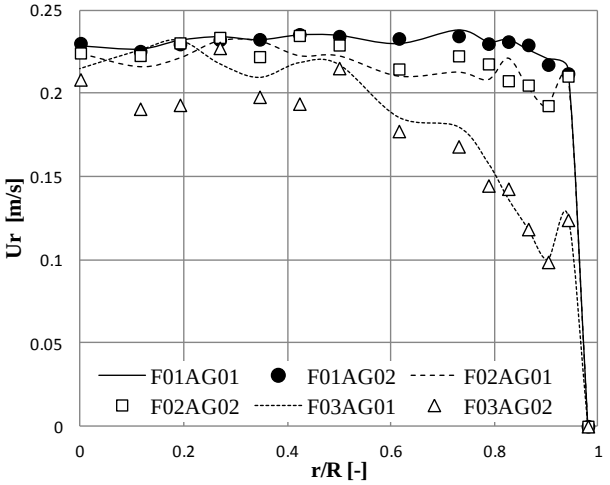

Figure 4.11. Radial profiles for the relative velocity.

Figure 4.12 shows the profile of u_{rel}^2 scaled by factor 4.26 to have the maximum value as the profile of u_{rel}. It can be observed that the difference in the profiles of the cases F03AG01 and F03AG02 at the center and wall of the pipe. This in turn decreases K_{BIT} at the wall and causes a void fraction peak near the wall for the two cases of F03A as stated before. The new K_{BIT} relation will be expressed as follows:

$$K_{BIT} = C_{tb}\, u_{rel}^2\, D_b(\nabla\alpha_d/\alpha_d) \tag{4.5}$$

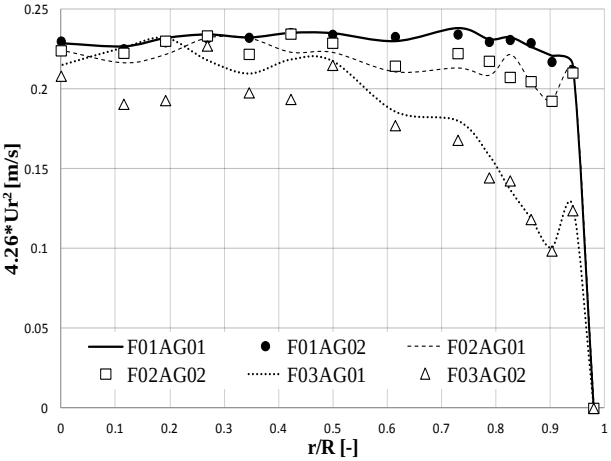

Figure 4.12. Radial profiles for the square of the relative velocity.

The calculated profiles according to this relation are shown in figure 4.13. As shown in figure 4.13, all the void fraction profiles have a wall peak that is higher than the experimental data. This is due to using the value of u_{rel}^2 in place of u_{rel} in the K_{BIT} relation (4.4). To adjust the model of K_{BIT} for minimizing this peak, the coefficient of C_{tb} can be smaller to be less than 0.02. This wall peak may be caused by two main effects. The first is that the lift force may be very large. The other cause is that the turbulence dispersion may be not strong enough to redistribute the void fraction and soften the distribution. First we like to investigate the lift force used in the model as this force acts always in the direction of the wall and the two-way coupling effect was not activated yet. So in the next section a study for the effect of the lift force coefficient on the void fraction distribution is presented.

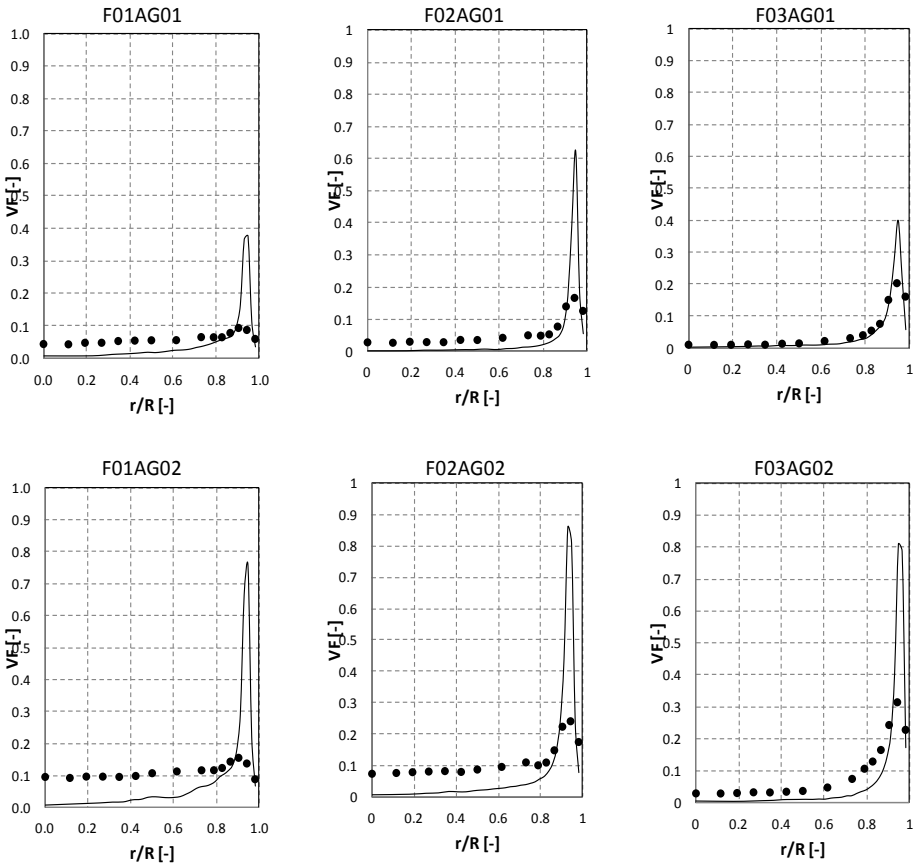

Figure 4.13. Void fraction profiles of the relation $K_{BIT} = C_{tb}\, u_{rel}^2\, D_b(\nabla\alpha_d/\alpha_d)$ with C_{tb}=0.02.

4.6 Study for the Effect of the lift coefficient on the void fraction distribution.

As was presented in the former section, it was found that the lift force applied is very high as the wall peak of the void fraction exists in the majority of the tested cases. In this section the study made to ensure the lift force coefficient used in the current model is presented. The lift coefficient used for all the test cases in the former study was that for Tomiyama (1998) which was explained in section 2.2.1 of the acting forces. In the range of the diameters used, the Lift coefficient resulting from Tomiyama relation will have a value of 0.28. As was stated before, the value of the lift coefficient is critical and there is variety of values suggested by many authors as discussed before in the acting forces section. At first, the relation of Tomiyama was tested and gave the distribution discussed in the former section shown at figure 4.13. As was seen, the lift coefficient

was too high as compared with the turbulent dispersion effect and caused wall peaks for the void fraction distributions. To investigate that, lower values for the lift coefficient was used, which was different in each test case to have good agreement with the experimental data. The void fraction profiles that resulted from this test are shown in figure 4.14 with the value of C_T for each case written beside the case name. This study was made to test the lift force coefficient used. As can be seen at figure 4.15, each case has a specific lift coefficient that is different from the others. The lift coefficients are in the range from 0.05 to 0.1. This is logic because the lift force is function of many parameters that differ from one case to another. In the present work a fixed unique value for the lift coefficient was used to give accepted results for all the cases. This value and the profiles resulting from using it will be presented at the next section.

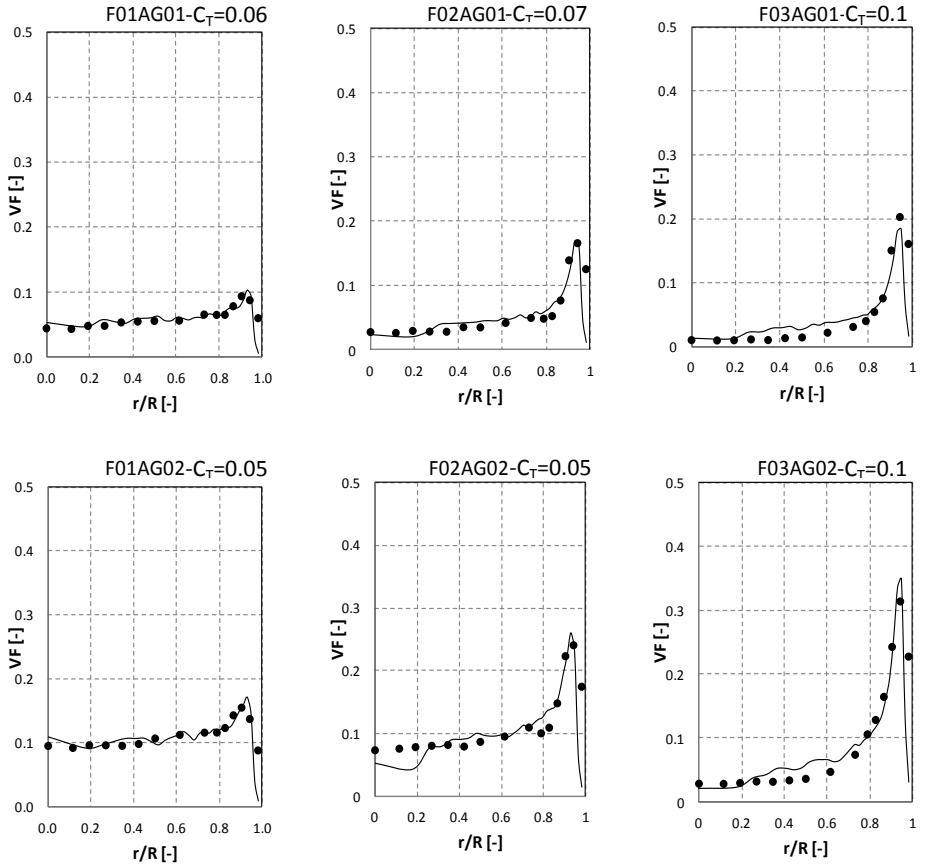

Figure 4.14. The void fraction profiles with the relation $BIT = C_{tb}\, u_{rel}^2\, D_b(\nabla\alpha_d/\alpha_d)$ with C_{tb}=0.02, with different lift coefficnt for each test case.

Regarding the lift coefficient value, the two-way coupling or the bubble interaction mechanisms were not activated. This can be a cause why the present simulations need only a small value of the lift coefficient. The lift force depends not only on the lift coefficient but also on the liquid vorticity that take in account the gradients of the liquid velocity as demonstrated in section 2.2.1. The gradients of the liquid velocity close to the wall without taking the back effect of the bubbles are too high. This is because the bubbles make some pushing effect on the liquid velocity and affect on the liquid velocity profile to be with higher gradient. The liquid velocity profile for the tested cases is shown in figure 4.15. So, it may be also a reason for the small value of the lift coefficient that it is needed. This is because the liquid vorticity is already higher than the supposed value. At the next chapter, these effects will be discussed in details when applying the Two-way coupling.

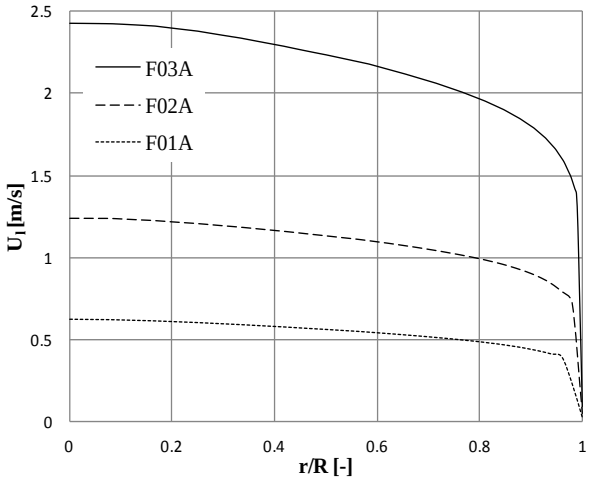

Figure 4.15. The liquid velocity profiles for the different test cases at height of 1.5m of the pipe.

4.7 Results and discussion

In this simulation the final results will be presented after the adjustment of the lift coefficient and the K_{BIT} relation discussed in the preceding sections. The experimental cases that will be studied in this section will be that of liquid velocity 0.5 m/s, 1.0 m/s and 2.0 m/s, with void fractions of 5%, 10% and 15%. In the current simulations, a number of 20000 bubbles was injected from the pipe inlet and follow the Lagrangian solver tile getting out and counting the different profiles of void fraction, gas velocity and Interfacial area concentration at the pipe outlet. As the number of bubbles used in the simulation is not the same as the real number in the experimental case, the outlet profiles are normalized and scaled when comparing with the experiments. For example to calculate the radial profile of the void fraction at the outlet, the cross section of the pipe was divided into a number of radial sectors with equal cross sectional area. Then we count the bubbles exiting from each sector, finally we divide the volume of the bubbles passing through each sector by the total volume of the bubbles to give us the normalized profile of the void fraction. To scale this profile by the real one, the normalized output profile is multiply by a scaling factor of:

$$SC = \alpha_{average} * N_{sect} \tag{4.6}$$

The profile of the gas velocity is calculated by collecting the bubbles in each sector and averaging the velocity of them to give the average bubbles velocity in each sector and hence the gas velocity profiles. The interfacial area concentration is normalized as the void fraction profile. The comparison of the void fraction profiles, gas velocity profiles and the gas interfacial area concentration profiles are shown in the figures 4.16, 4.17, and 4.18 respectively. In general, a good agreement between the simulation and the experimental data can be found. As explained in chapter 2 in the section of the acting forces, as the lift force coefficient is a critical matter that depends on many parameters and tile now there is no an universal expression to identify the lift force coefficient, a constant coefficient of 0.07 have been used for all the simulations in this section. Of course some cases will give agreement with this coefficient more than others but in general there is good agreement for all the cases with this value of the lift force coefficient. In the void fraction profiles, it can be observed that as the average void fraction increases, a wall peak that is greater than the experimental data appears, which means that the lift force is greater than the turbulence dispersion effect in the simulation. For void fractions G01 and G02 there is good modeling for both the lift forces and the turbulence dispersion effect, and the distribution is acceptable when compared with the experiments.

Figure 4.17 shows the comparison of the simulated radial gas velocity profiles with the experimental ones. It can be observed that there is a great accordance between them especially for the liquid velocities F01, and F02. As this is a simulation of only one way coupling that the liquid does not take the back effect of the bubbles momentum or turbulence on the continuous phase, this effect increases as the velocity of the liquid increases and the gas void fraction increase as in the case F03AG03 with the higher liquid velocity and gas fraction. This is because the momentum effect of the bubbles increases when increasing the liquid velocity and increasing the number of bubbles in the experimental case which is governed by the gas void fraction.

Figure 4.18 illustrates the comparison between the one-way simulation results for the gas IAC with that of the experimental cases. The interfacial area concentration is an illustrative parameter for the void fraction and the bubbles diameter in each radial sector. As in this simulation the bubble diameter remain the same without considering any change due to breakup and coalescence, then the best agreements can be found in the low void fraction cases F01AG01, F02AG01, F03AG01. As the void fraction increases as in cases of G02, the need for the application of the breakup and coalescence of the bubbles increases and the profiles starts to have more differences with the experimental data especially at the center and wall region which reveal the lower and upper limits of the bubbles diameters. This explains why the distribution of the IAC is the best in the G01 simulations and gets a little away from the experiment at G02 simulations, and goes away more from the experiments in the G03 simulations. As was hinted in chapter 1, the presented profiles of IAC are not directly measured and are approximated mathematically.

As a final comment, due to the studies and comparisons made in this chapter, we could conclude that the lift force expression used in this work does not work very well with the one-way coupling process. This may be due to the neglecting of the back effect of the bubbles on the continuous phase, and neglecting the bubble interaction mechanisms like bubbles collision, coalescence and breakup in the time that we are using relatively high void fraction (5% to 15%). The other reason may be the relation that we suggested for the K_{BIT} that it gives low dispersion effect or needs some adjustment in the coefficient C_{tb}. To solve this dispersion, we decided to keep the same relation of the the K_{BIT} suggested in equation (4.2) and the same lift coefficient of C_T=0.07, and apply the two way coupling and considering the bubble interaction mechanisms. After considering these effects, we will discover if the problem of the distributions is caused by the error in the K_{BIT} relation or by the lift coefficient, and this is the study that will be presented in the next chapter.

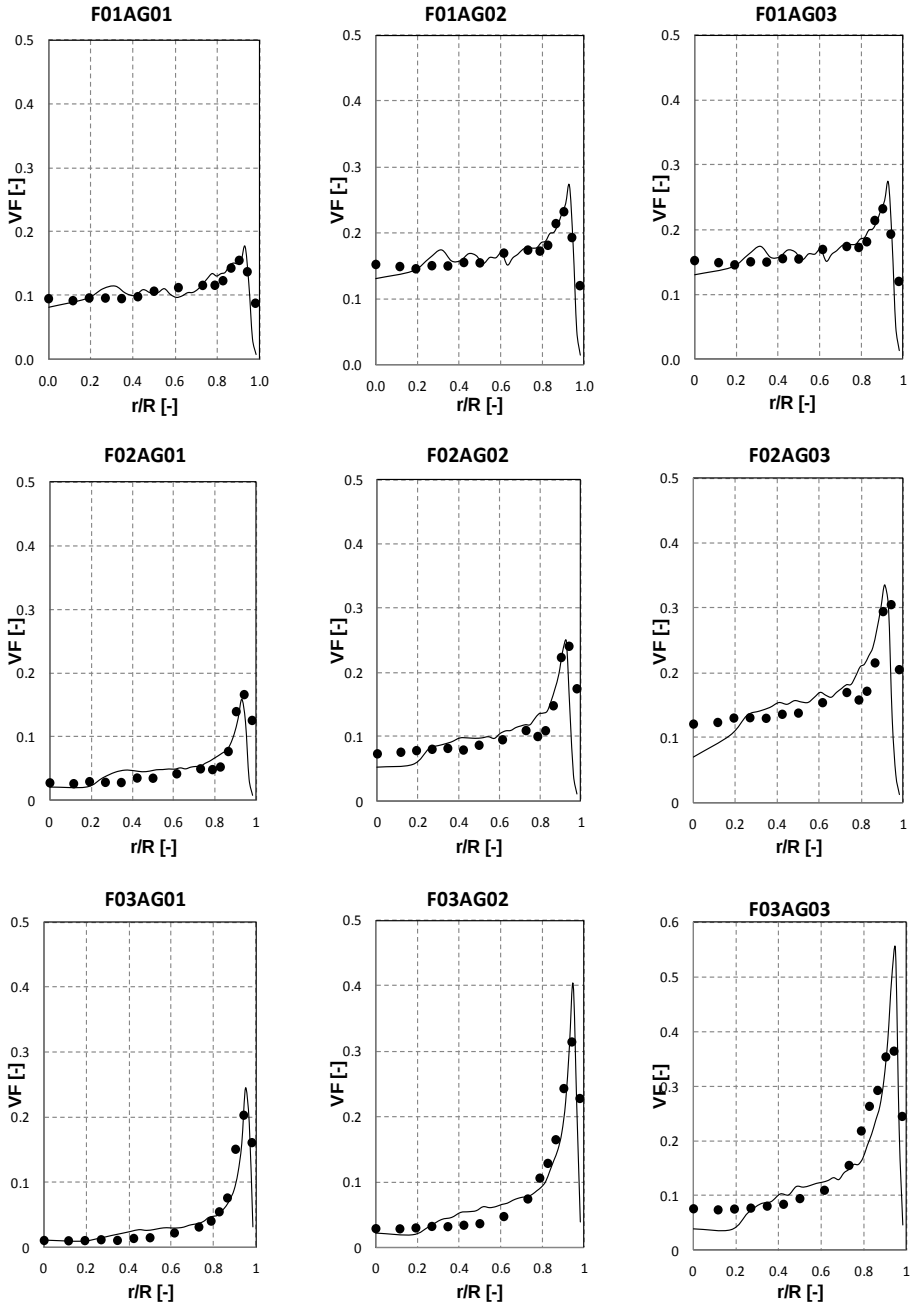

Figure 4.16. Void fraction profiles for the test cases. • Experimental data, — simulation results.

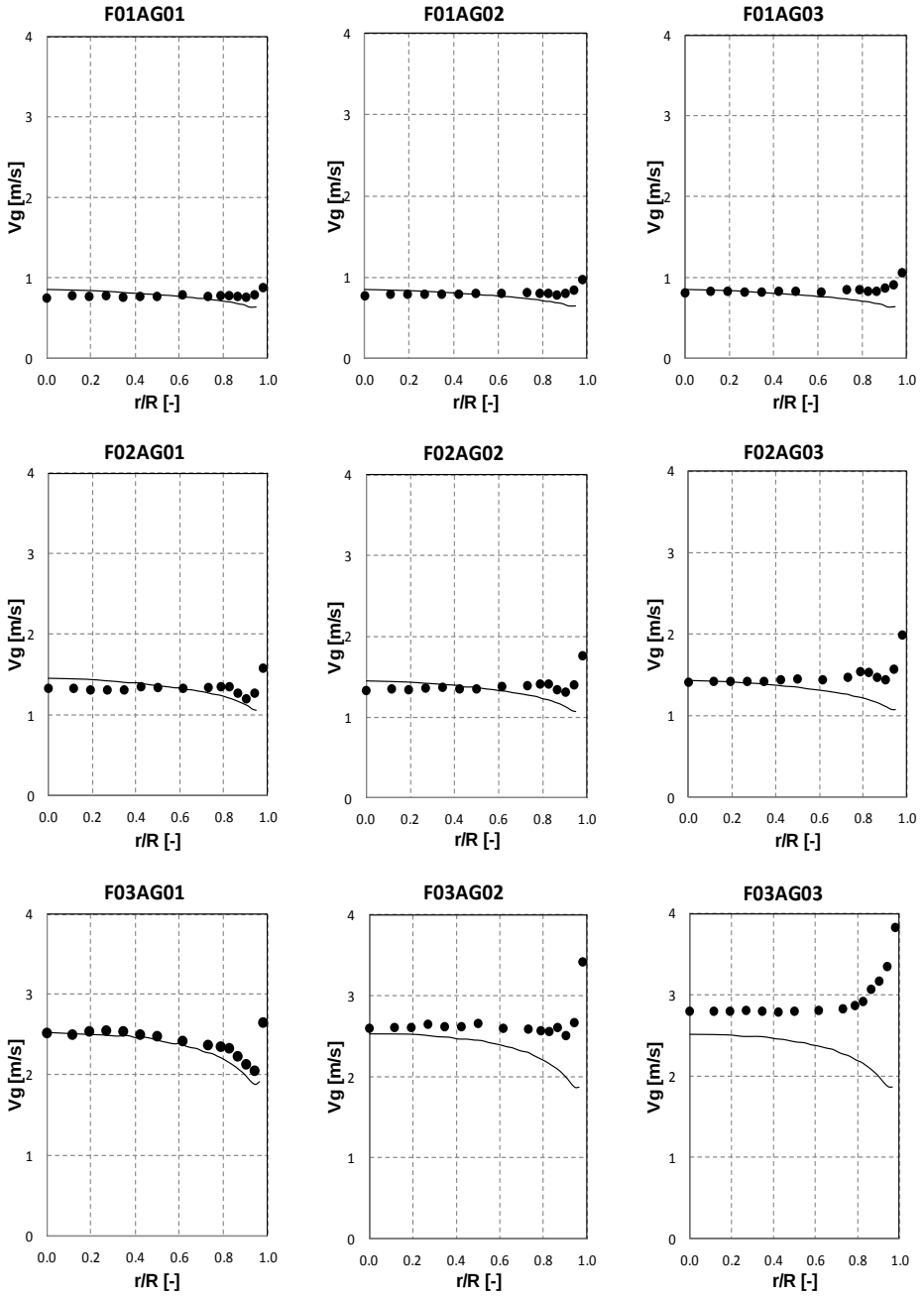

Figure 4.17. Gas velocity profiles for the test cases. • Experimental data, — simulation results.

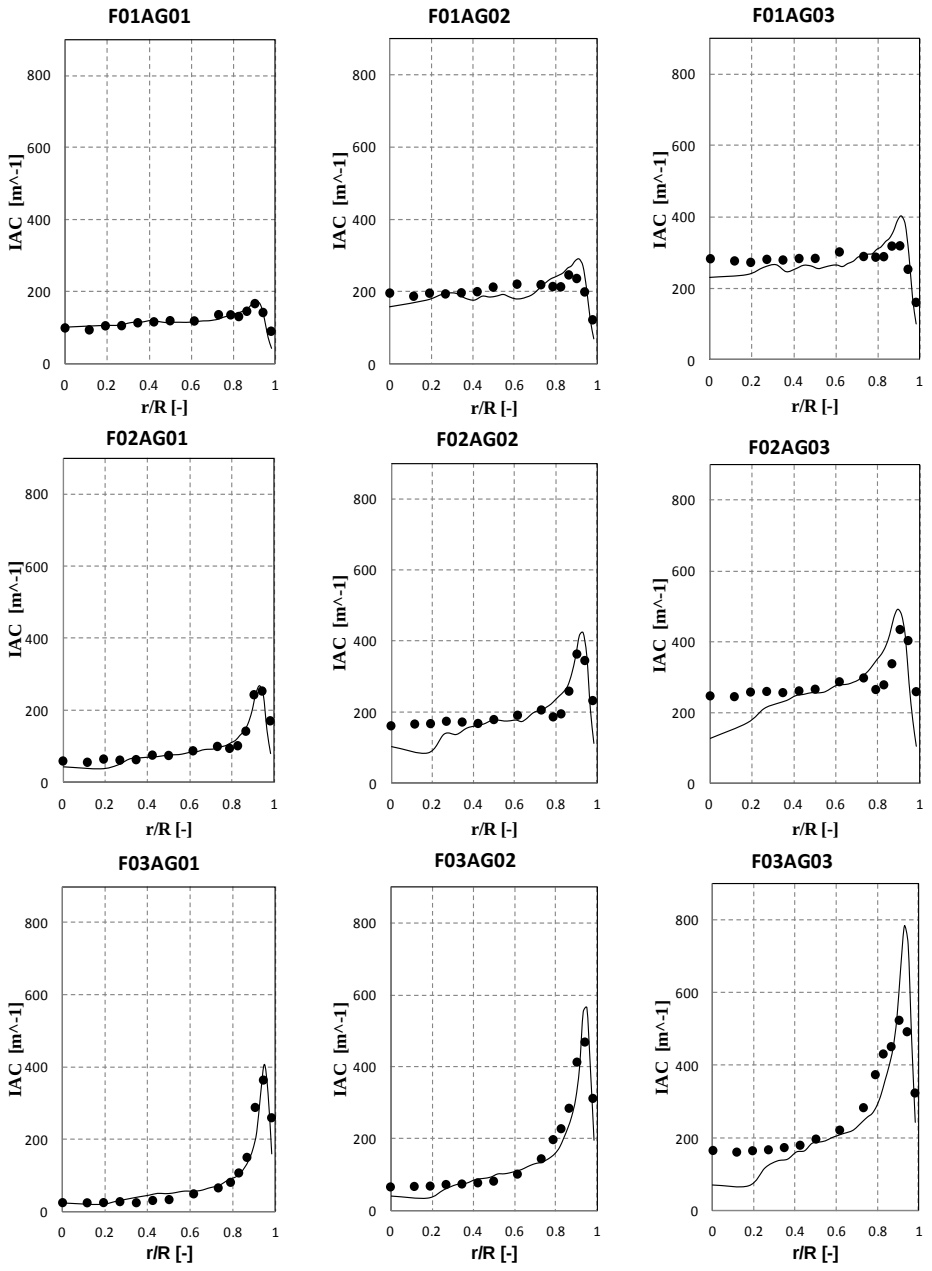

Figure 4.18. Gas interfacial area concentration (IAC) profiles for the test cases. • Experimental data, — simulation results.

5. Two-way Coupling Process Study and Discussion

Two-way coupling between the Eulerian and Lagrangian Solvers means to take the effect of each phase on the other. In the former chapter we presented the one-way coupling process which only considers the effect of the continuous phase on the dispersed one. In this chapter we will consider also the back effect of the dispersed phase on the continuous one. In this chapter at first, the process of the two-way coupling without considering the bubbles interaction mechanisms is presented. This includes the description of the time stepping, then the description of the method used for approximating the bubbles data in the Eulerian domain cells. Then the modifications in the Euler solver conservation equations of the continuity, momentum and turbulence to account for the bubbles effect on the continuous phase are described. Then the code algorithm is presented. And finally the simulation results are compared with the experimental data. The next section describes the two-way coupling process taking into account the bubbles collisions. In this section, the time stepping method, then the code algorithm, and then the results of the code compared with the experimental data are presented. Then the modeling is presented with considering bubbles coalescence mechanism. After that, the model considering the two-way coupling with bubble collisions, coalescence and breakup is presented. In this section, it is described the time stepping method, the code algorithm, and the results of the code compared with the experimental data. The next section presents a brief discussion about the calculation time for the different processes and consideration in the coupled model.

5.1 Two-way coupling without considering bubbles interactions

In the two-way coupling process, the back effect of the bubbles on the continuous phase is considered in the Euler solver. This needs the interpolation of the bubbles effect on the neighbor cells, modification in the Euler solver conservation equations of continuity, momentum and turbulence, and changing the algorithm of the code as we will see in the next sub sections.

5.1.1 Time stepping

In the present process, only two time steps are considered, the smaller one is the Lagrangian one over which the Lagrangian code solves its equations for each bubble. The other one is the Eulerian time step over which the Euler solver approximates the effect of the dispersed phase on the Euler solver equations and solves it. The two time steps are shown at figure 5.1 (a). The Lagrangian time step Δt_L have values of 1.0e-4,5.0e-4, and 1.0e-3 seconds for the cases F03A, F02A, And F01A respectively. The

Eulerian time step can equal to 50 to 100 scale of Δt_L as stated in Lain et al (2002). We considered in the present simulation values of Δt_E of 1.0e-2, 2.0e-2 and 4.0e-2second for the cases F03A, F02A and F01A respectively.

5.1.2 Bubble data interpolation at computational cells

In the two-way coupling process, to interpolate the data of the bubble at the location of the computational cells, there are some techniques used. One of them is the particle source in cell PSC introduced by Crowe et al. (1977). In this approach, the particle is considered as a local source of momentum, turbulence kinetic energy, and turbulence dissipation rate in the computational cells of the continuous phase. Using this approach, Laín et al (2002) introduced time- and ensemble- averaging in the following form for the source term:

$$\bar{S} = -\frac{1}{\Delta t_E}\sum_k \sum_n \Delta t_L * S_{b,n}^k \tag{5.1}$$

Where $S_{b,n}^k$ is the property of the bubble to be averaged. The sum over n indicates the averaging of the instantaneous contribution of the bubbles along the bubble trajectory (time averaging). And the sum over k is related to the number of bubbles that pass through the cell in the Eulerian time step Δt_E as shown in figure 5.1 (a).

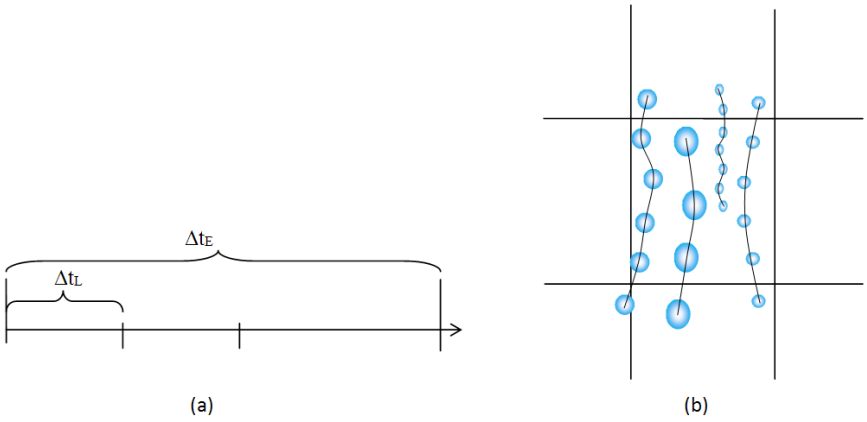

Figure 5.1. (a) Time stepping in the two-way coupling process, (b) Bubbles trajectories inside the cell.

Another approach was proposed by Kitagawa et al (2001). This approach introduced a Lagrangian template function which converts the dispersed phase quantities to be introduced in the continuous phase source terms and void fraction of liquid in the cell.

Using Gaussian and Goniometric functions they found that false numerical velocity fluctuations can be removed. Following the same idea, Deen et al., (2004) proposed to use a fourth order polynomial function which integration is cheaper compared to a Gaussian function or the function proposed by Peskin (1977). They found this technique; a grid independent solution can be obtained. The template function proposed by Deen et al (2004) is as follows:

$$\mathrm{Tf}(x - R_l) = \begin{cases} \frac{15}{16}\left[\frac{(x - R_l)^4}{n^5} - 2\frac{(x - R_l)^2}{n^3} + \frac{1}{n}\right] & -n \le (x - R_l) \le n \\ 0, & \text{otherwise} \end{cases} \quad (5.2)$$

Where Tf is the template function, $(x - r_l)$ is the distance between the desired cell and the location of the bubble r_l, $2n$ is the width of the mapping window. This template function moves with the bubble location and depending on the relative location of the bubble for an arbitrary cell j as shown in figure 5.2.

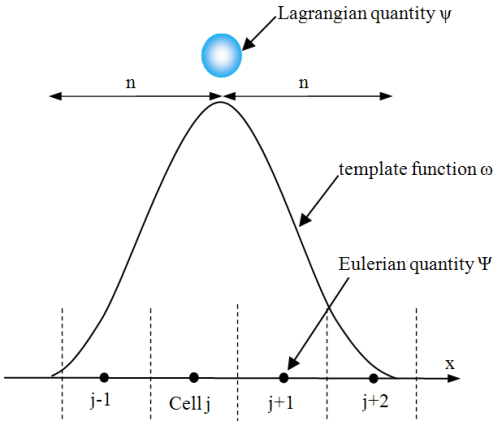

Figure 5.2. Template function used for Lagrangian and Eulerian two-way coupling

The integration of this function $\int_{\Omega j} \mathrm{Tf}(x - R_l)$ represents the influence of the bubble l on the cell j when calculating the Lagrangian property effect on the Euler cells. Or the influence of the Euler value in cell j on the bubble l when calculating the Eulerian property of the cell on the bubbles. In 3D space the integration of the function will be as follows:

$$\int_{\Omega j} \mathrm{Tf(l)}\, d\Omega = \int_{\Omega j} \mathrm{Tf(x - R_l)}\, d\Omega$$
$$= \int_{\Omega j,z} \int_{\Omega j,y} \int_{\Omega j,x} \mathrm{Tf}\left(x - R_{l,x}\right) \mathrm{Tf}\left(y - R_{l,y}\right) \mathrm{Tf}\left(z - R_{l,z}\right) dx\, dy\, dz \quad (5.3)$$

Given bubble l, and the width of the mapping window $2n$, the liquid volume fraction in computational cell j is calculated as follows:

$$\alpha(j) = 1 - \frac{\sum_i V_b(l) \int_{\Omega j} \mathrm{Tf(l)}\, d\Omega}{\mathrm{Vcell}} \quad (5.4)$$

The sum over i indicates all the bubbles that passes through this cell.

On the other hand, the quantity of bubble l like the momentum source can be calculated at the continuous phase computational cell j as follows:

$$\Phi(j) = \frac{\sum_{\forall l} \phi(l) \int_{\Omega j} \mathrm{Tf(l)}\, d\Omega}{\mathrm{Vcell}} \quad (5.5)$$

Also the sum over i indicates the bubbles passed through the cell j, and the quantity $\phi(l)$ is the reaction of the momentum transfer exerted on the bubble $\phi(l) = -\sum F$.
Also the quantities of the continuous phase can be approximated at the location of the bubble using the template function as follows:

$$\psi(l) = \sum_{\forall j} \Psi(j) \int_{\Omega j} \mathrm{Tf(l)}\, d\Omega \quad (5.6)$$

Such that the sum over j means the cells around the bubble for which the integration of the template function is not zero. $\Psi(j)$ is the value of the quantity at cell j, and $\psi(l)$ is the value of the quantity at the bubble l.

The integration presented above is equal to 1 if the limits of the integration were -n to n which means that if the integration limits lie completely inside the cell, then the effect of the bubble will go to this cell only and on the other hand the bubble will not affect on to other cells. The template function presented above is simply applied for perpendicular grids that have square or cubic cells for the ease of finding the integration limits. However, in the present work, some of the cells are not a perfect

square in the x,y directions, so the x,y coordinates of integration will be selected for each cell depending on the lines connecting the center of fronted faces, and the limits of the integration will be calculated depending on the distance between the bubble center and the centers of the faces as shown in figure 5.3. As can be seen at figure 5.3, the new x', y' coordinates are nearly perpendicular. In case (a) when the bubble center lies inside the cell, the x' direction integration is accomplished in the limits $-dx1 \leq x' \leq dx2$ the same for y' direction that the limits of the integration will be $-dy1 \leq y' \leq dy2$. In case (b) when the center of the bubble is outside the cell in the direction of y' as shown, the limits of integration will be $0 \leq y' \leq (dy2 - dy1)$ as the distance dy1 is outside the face.

In this work the bubbles may pass through more than one cell during one Eulerian time step, so, it is needed to apply the time and ensemble averaging proposed by Laín et al (2002). At the same time, the grid is not uniform and the cells differ in their size and shape which leads to approximating the bubble effect on the cell using the template function proposed by Deen et al (2004).

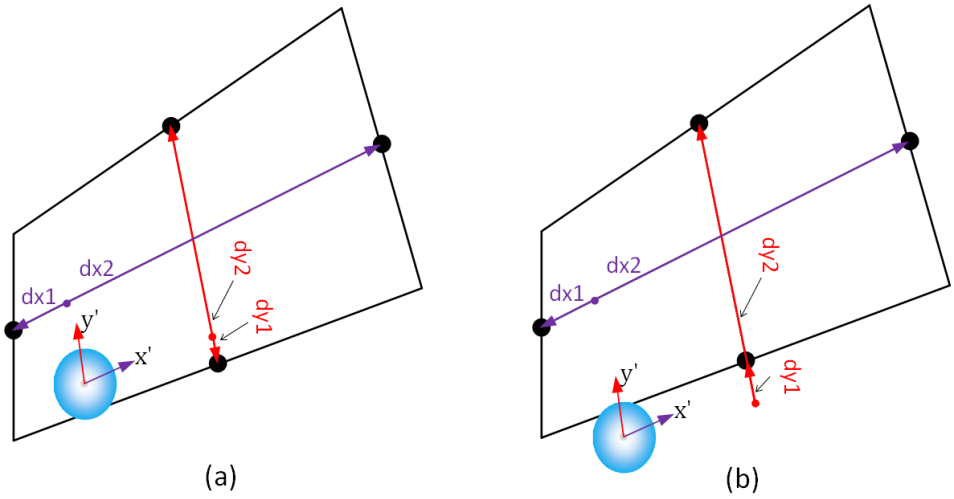

Figure 5.3. Template function integration limits and coordinates for non perpendicular cells (a) Bubble center inside the cell, (b) Bubble center outside the cell.

In order to combine the two approaches, the averaging process of the source terms proposed in eqn. (5.1) can be modified as follows:

$$\bar{S}(j) = -\frac{1}{\Delta t_E V_{cell}} \sum_k \sum_n \Delta t_L * S_{b,n}^k * \int_{\Omega j} Tf(k)\, d\Omega \qquad (5.7)$$

Where eqn. (5.7) is the same as eqn. (5.1) with adding the template function integration. This is done for each location of the bubble k during its trajectory for all the bubble passing through the cell j.

5.1.3 Modifications in the Euler solvers equations in the Two-way coupling

The equations that are solved for calculating the velocity and turbulence field in the Euler solver are the continuity equation, momentum equations and the turbulence k-ε equations. At first, the space available for the liquid inside the cell should be considered as it may contain a bubble or a part of it. So the first modification is the multiplication of the density by a term that calculates the quantity of the continuous phase inside the computational cell which is the local volume fraction of liquid α_l for the cell. This is applied for all the equations solved by the Euler solver.

5.1.3.1 Modification in the continuity and momentum equations

The continuity equation at the two-way coupling process is modified by inserting the liquid volume fraction in all the terms as follows:

$$\frac{\partial(\alpha_l \rho_l U)}{\partial x} + \frac{\partial(\alpha_l \rho_l V)}{\partial y} + \frac{\partial(\alpha_l \rho_l W)}{\partial z} = 0.0 \qquad (5.8)$$

Navier-Stokes equations in case of the two-way coupling are modified by multiplying the density of liquid, the pressure gradient term and the diffusion terms by the liquid volume fraction in the computational cell α_l, and adding a source term in the three flow directions x,y, and z , which accounts for the bubbles interaction as follows:

$$\frac{\partial(\alpha_l \rho_l U_l U_l)}{\partial x} + \frac{\partial(\alpha_l \rho_l V_l U_l)}{\partial y} + \frac{\partial(\alpha_l \rho_l W_l U_l)}{\partial z} = -\alpha_l \frac{\partial p}{\partial x} + \frac{\partial}{\partial x}\left(\alpha_l \mu_{l,eff} \frac{\partial U_l}{\partial x}\right) + \frac{\partial}{\partial y}\left(\alpha_l \mu_{l,eff} \frac{\partial U_l}{\partial y}\right) + \frac{\partial}{\partial z}\left(\alpha_l \mu_{l,eff} \frac{\partial U_l}{\partial z}\right) + \alpha_l \rho_l g_x + S_u + S_u^{int} \quad (5.9-1)$$

$$\frac{\partial(\alpha_l \rho_l U_l V_l)}{\partial x} + \frac{\partial(\alpha_l \rho_l V_l V_l)}{\partial y} + \frac{\partial(\alpha_l \rho_l W_l V_l)}{\partial z} = -\alpha_l \frac{\partial p}{\partial y} + \frac{\partial}{\partial x}\left(\alpha_l \mu_{l,eff} \frac{\partial V_l}{\partial x}\right) + \frac{\partial}{\partial y}\left(\alpha_l \mu_{l,eff} \frac{\partial V_l}{\partial y}\right) + \frac{\partial}{\partial z}\left(\alpha_l \mu_{l,eff} \frac{\partial V_l}{\partial z}\right) + \alpha_l \rho_l g_y + S_v + S_v^{int} \quad (5.9-2)$$

$$\frac{\partial(\alpha_l\rho_l U_l W_l)}{\partial x}+\frac{\partial(\alpha_l\rho_l V_l W_l)}{\partial y}+\frac{\partial(\alpha_l\rho_l W_l W_l)}{\partial z}=-\alpha_l\frac{\partial p}{\partial z}+\frac{\partial}{\partial x}\left(\alpha_l\mu_{l,eff}\frac{\partial W_l}{\partial x}\right)+$$

$$\frac{\partial}{\partial y}\left(\alpha_l\mu_{l,eff}\frac{\partial W_l}{\partial y}\right)+\frac{\partial}{\partial z}\left(\alpha_l\mu_{l,eff}\frac{\partial W_l}{\partial z}\right)+\alpha_l\rho_l g_z+S_w+S_w^{int}\quad(5.9-3)$$

The terms S_u, S_v and S_w are the source terms in each cell due to the boundary conditions. The sources with the superscript int mean the interaction source terms that are produced according to the interaction with the dispersed gas phase. The momentum source terms were simply taken as the inverse of the forces affecting on the bubbles as it act as the interaction of these forces, except for the vertical component that we subtract the buoyancy force from it not to be applied two times on the bubble as calculated by lain (2002). By applying the averaging technique that was explained in eqn. (5.7), the momentum source terms will be expressed as follows:

$$S_u^{int}=-\frac{1}{\Delta t_E V_{cell}}\sum_k\sum_n\Delta t_L*F_{x,n}^k*\int_{\Omega j}Tf(k)\,d\Omega\quad(5.10-1)$$

$$S_v^{int}=-\frac{1}{\Delta t_E V_{cell}}\sum_k\sum_n\Delta t_L*F_{y,n}^k*\int_{\Omega j}Tf(k)\,d\Omega\quad(5.10-2)$$

$$S_w^{int}=-\frac{1}{\Delta t_E V_{cell}}\sum_k\sum_n\Delta t_L*(F_{z,n}^k-F_{bu,z}^k)*\int_{\Omega j}Tf(k)\,d\Omega\quad(5.10-3)$$

And the local liquid void fraction of each cell is calculated by the same approximation technique as follows:

$$\alpha_l=1-\frac{1}{\Delta t_E V_{cell}}\sum_k\sum_n\Delta t_L V_b(k)*\int_{\Omega j}Tf(k)\,d\Omega\quad(5.11)$$

Such that the definitions of sums over k and n are as explained in eqn (5.1).

5.1.3.2 Modification in the turbulence equations

The turbulence equation used in the two way coupling process will be the same as it in the main program with adding a source term in each of the turbulence kinetic energy and dissipation rate equation as follows:

Turbulence kinetic energy equation

$$\frac{\partial(\alpha_l\rho_l U_l k_l)}{\partial x}+\frac{\partial(\alpha_l\rho_l V_l k_l)}{\partial y}+\frac{\partial(\alpha_l\rho_l W_l k_l)}{\partial z}=\alpha_l\mu_{l,t}\left(\frac{\partial U_i}{\partial x_j}+\frac{\partial U_j}{\partial x_i}\right)\frac{\partial U_i}{\partial x_j}-\alpha_l\rho_l\varepsilon_l+\frac{\partial}{\partial x_j}\left[\alpha_l\left(\mu_l+\frac{\mu_{l,t}}{\sigma_k}\right)\frac{\partial k}{\partial x_j}\right]+S_k+S_k^{int} \quad (5.12)$$

Turbulence dissipation rate

$$\frac{\partial(\alpha_l\rho_l U_l \varepsilon_l)}{\partial x}+\frac{\partial(\alpha_l\rho_l V_l \varepsilon_l)}{\partial y}+\frac{\partial(\alpha_l\rho_l W_l \varepsilon_l)}{\partial z}=\alpha_l C_{\varepsilon 1}\mu_{l,t}\left(\frac{\partial U_i}{\partial x_j}+\frac{\partial U_j}{\partial x_i}\right)\frac{\partial U_i}{\partial x_j}\frac{\varepsilon_l}{k_l}-\alpha_l\rho_l C_{\varepsilon 2}\frac{\varepsilon_l^2}{k_l}+\frac{\partial}{\partial x_j}\left[\alpha_l\left(\mu_l+\frac{\mu_{l,t}}{\sigma_\varepsilon}\right)\frac{\partial \varepsilon_l}{\partial x_j}\right]+S_\varepsilon+S_\varepsilon^{int} \quad (5.13)$$

The interaction source terms are defined as follows:

$$S_k^{int}=-\frac{1}{\Delta t_E V_{cell}}\sum_k\sum_n \Delta t_L * S^k_{K_{BIT},n} * \int_{\Omega j} Tf(k)\, d\Omega \quad (5.14-1)$$

$$S_k^{int}=-\frac{1}{\Delta t_E V_{cell}}\sum_k\sum_n \Delta t_L * S^k_{\varepsilon_{BIT},n} * \int_{\Omega j} Tf(k)\, d\Omega \quad (5.14-2)$$

Such that the K source term $S_{K_{BIT}}$ explained at section 3.4, and the relation between the $S_{\varepsilon_{BIT}}$ and $S_{K_{BIT}}$ is defined by Yao and Morel (2004) at equation (1.9). Many works proposed different modeling for the source terms in the k-ε equations (Malin 1983 , Malin and Spalding 1984, smith 1998, and Yao and Morel 2004). In the present research, the model proposed for the $S_{K_{BIT}}$ term at section 3.4 is applied as it acts as the turbulence kinetic energy added to the turbulence kinetic energy equation as a source term to account for the bubbles turbulence. This is explained in details at section 3.4. For the source term of the turbulence dissipation rate it was taken as that of Yao and Morel (2004) model as explained at the Turbulence modeling chapter.

5.1.3.3 Source terms and density definition in the Euler solver

Source terms

In the Euler solver used in the coupling process, the source terms is defined for all the cells in a subroutine called "fluxuvw" which calculates the convection and diffusion fluxes through the cell faces and add the effect of these fluxes in the cell source terms in the three directions Su(), Sv(), Sw(). In fact this subroutine is the one responsible for setting the source terms for the momentum equation. During the solution of the

Lagrangian framework, the forces acting on each bubble and the bubble location and the bubble template function integration is calculated. As one Euler time step is completed, the averaging process of the source terms and the liquid void fraction is accomplished and sent to the Euler solver using a module defined in both solvers. The source terms calculated by the Lagrangian solver for the computational cells are soru(),sorv(),sorw() for the equations of momentum for velocities u, v, and w respectively. These Lagrangian source terms are added to the source terms calculated by the subroutine "fluxuvw" of the Euler solver as follows before running the Euler solver. And in that way, the Euler solver takes the effect of the interaction momentum of the dispersed phase.

For the source terms of turbulence Kinetic energy k and turbulence dissipation rate ε, it is handled by the subroutine "fluxscalars" . This subroutine is responsible for setting the scalar fluxes through cell faces. These scalars can be the turbulence kinetic energy k, the turbulence dissipation rate ε. it uses the definition of su() as the source term for any of these scalars. So, we modify the source term of the k by adding the Lagrangian variable sork() which calculates the average k source term in the cell to the su() when the variable solved in "fluxScalars" is k. and the same is done for ε that add the Lagrangian variable sorEps() to su() when the variable solved is ε.

Density definition

If the cell contains a bubble or a portion of it, then the complete volume of the cell will not be available for the liquid. For that reason, we need to modify the volume by multiplying the density in the equations of momentum and turbulence by the local void fraction of liquid α_l calculated by the Lagrangian solver. At the Euler solver, the density is defined as an array for all the cells of the domain in the subroutine "InitializeVariables". As we created the liquid void fraction in an array called sorvf() in the Lagrangian solver, we simply multiply the value of the density in the subroutine "InitializeVariables" by the value of sorvf() to modify the density of the liquid in each cell.

5.1.4 Code algorithm for the two-way coupling without bubbles interactions

In the one-way coupling process, only the effect of the continuous phase on the dispersed one was considered. So, the bubbles were introduces in the pipe in an approximate manner that can give us the distribution of the void fraction profile in the pipe. In the present process of the two-way coupling, as we need to take also the back effect of the bubbles on the liquid, the method of introducing the bubbles in the one way coupling process will not be adequate for these reasons:

- The importance of the local effect of the bubbles on the continuous phase.
- The actual effect of the bubbles on the liquid velocity can only be simulated if all the pipe is filled with bubbles
- The unsteady nature of the two-way coupling process.

For these reasons, the method of injection of the bubbles was changed to be more physical. In this process the bubbles are generated in a complete imaginary pipe below the real one such that the distribution of bubbles validates the inlet condition of the void fraction distribution. This imaginary pipe of bubbles moves with a constant velocity equal to the injection velocity of bubbles. During the motion of the imaginary pipe upwards, the bubbles enter the real pipe with a velocity according to the gas velocity profile at inlet. The bubbles are treated as a bubble flowing in the liquid and their effect is considered on the liquid. To account for the instantaneous changes of the void fraction profile, the real pipe is divided into a number of vertical divisions such that each part has a void fraction distribution that depends on the distribution of the real bubbles in this part. The calculation of the void fraction distribution in each part is calculated at each Lagrangian time step or each number of Lagrangian time steps depending on the required precision. When sufficient number of bubbles get out from the pipe outlet, the simulation stops and the bubbles went outside the pipe from the outlet are counted by size, radial location, and velocity to be used in calculating the void fraction distribution, gas velocity profile, average bubble size, and interfacial area concentration at the outlet. This is shown in figure 5.4. This was designed such that the number of the bubbles that go outside not to be less than 6000 bubbles to ensure that sufficient number of bubbles is used in the calculation of the profiles.

The code algorithm of the two-way coupling process is shown in figure 5.5. At first the program reads the boundary conditions like the inlet gas velocity and void fraction distribution and the Euler solver results. Then a do loop generates bubbles in an imaginary length of the pipe below the inlet with a void fraction distribution equal to that introduce at the inlet. Then a do while loop start with the condition that if sufficient number of bubbles went out from the pipe top outlet which is called loop2. This loop is considered the loop responsible for time advance in the program. Then inside loop2 some complete loops run. The first nested loop is loop 3 which updates the positions of all the bubbles according to the Lagrangian time step with counting the bubbles that escaped from the top exit. The second nested loop is loop 4 which is responsible for re calculating the void fraction distributions in the divided vertical sectors. Then start loop 5 which calculates the forces acting on each bubble and apply the Newton's second law to calculate the acceleration of the bubble. Also loop 5 calculates the momentum and turbulence source terms caused by each bubble averaged over the domain cells. After ending Loop 5, test is made for the cumulated time, if it reached the Euler time step

then the Lagrangian solver calls the Euler solver to run. After the Euler solver finish running. The Euler solver results are reread. Then the test of loop 2 tests for the total number of exiting bubbles if it reached the limit, then the program write the Lagrangian results and stops. If not, the program starts again to update the location of all the bubbles in loop3.

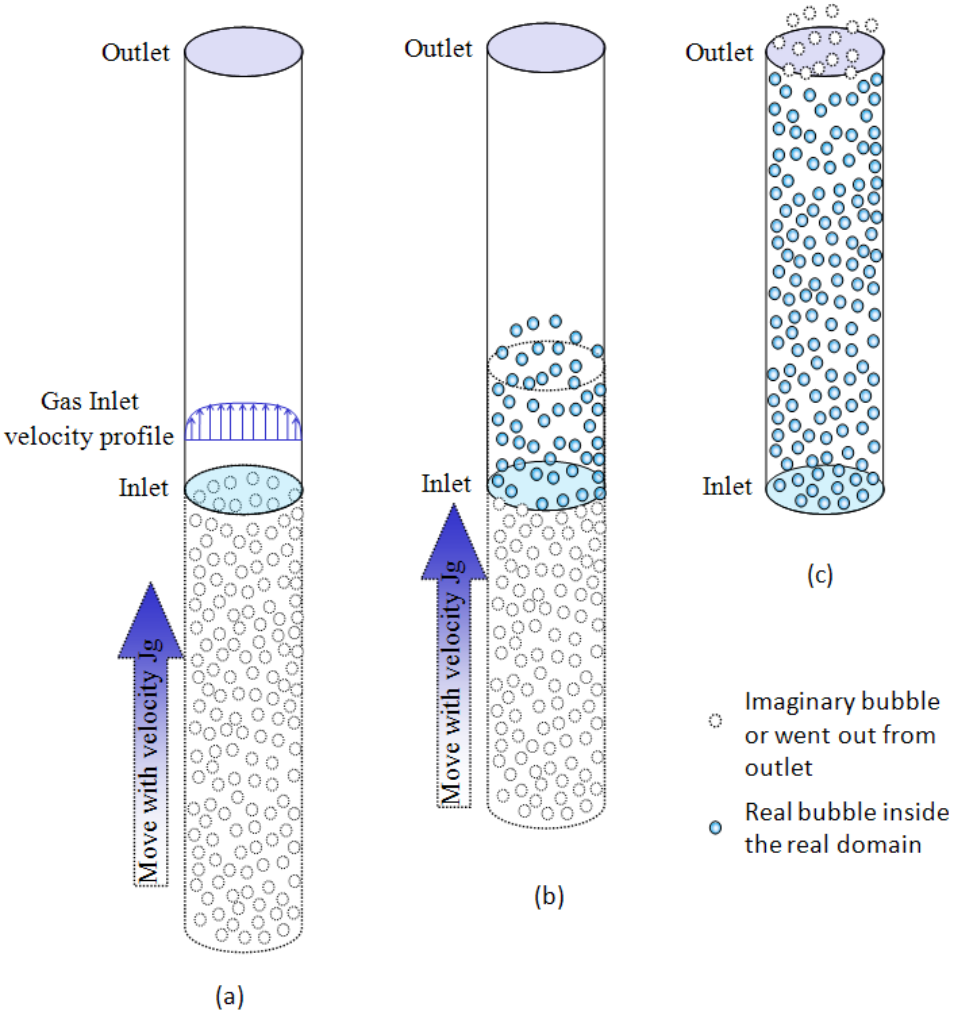

Figure 5.4. Descriptive diagram of the two-way coupling process (a) Start of the simulation, (b) Some bubbles entered the domain with velocity form the gas inlet velocity profile, (c) The end of simulation when the last imaginary bubble enter the real domain.

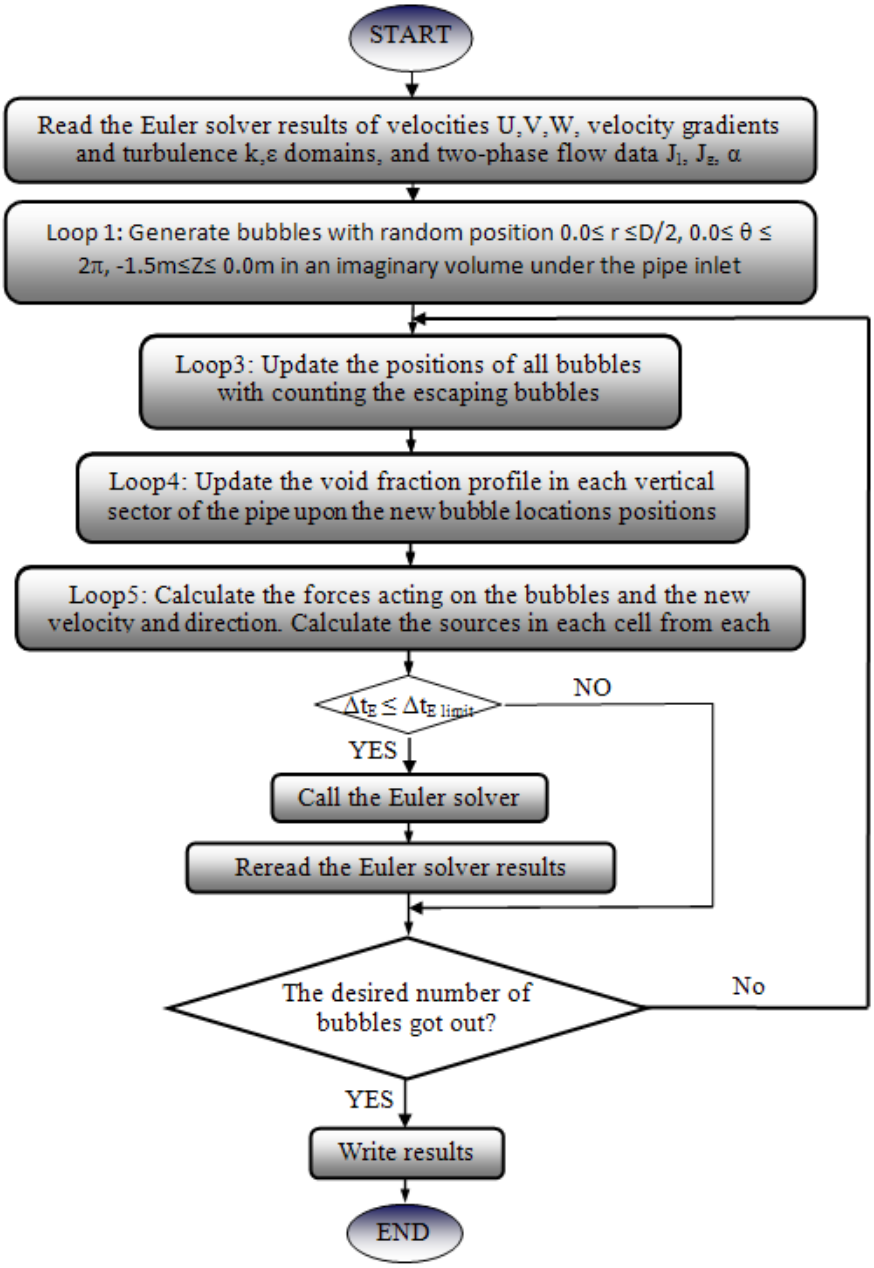

Figure 5.5. The flow chart for the Two-way coupling process without considering bubbles interactions.

5.1.5 Results and discussion

At this section, the simulation results of the two-way coupling compared with the previous results of the one-way coupling are presented. The effect of the two-way coupling process on the liquid properties is presented for the velocity, void fraction, and turbulence properties of k and ε. After that, the effect of the two-way coupling on the dispersed phase is presented for the void fraction and gas velocity. Then, the effect of changing the lift coefficient on the distribution of the void fraction is discussed. The test cases for the presented results will be F01AG01, F01AG03, F02AG01, F02AG03, F03AG01, and F01AG03. The calculations will maintain the same lift coefficient of C_T=0.07 tile other value is mentioned.

5.1.5.1 Effect of the Two-way coupling on liquid properties

As discussed in section 5.1.3, the effect of the dispersed phase on the continuous one is considered as a source terms in the different conservation equations of momentum, turbulence kinetic energy, and turbulence dissipation rate, and considering the volume of the cell available for liquid. In the present section, the change of the liquid velocity profile due to the source terms in the momentum equations is discussed. Also, the change of the liquid void fraction due to the dispersed phase is discussed. After that, the effect of the source terms added by the two-way coupling process on the turbulence kinetic energy and the dissipation rate of the liquid is discussed.

Liquid velocity and void fraction

The velocity of the liquid is affected by the existence of the bubbles in the domain. This is considered by first changing the volume of the computational cell available for the liquid, and also by inserting a source term in the momentum equation. Figure 5.6 illustrates the change of the radial liquid velocity profile at the mid distance of the pipe. The liquid velocity illustrated is the axial component as the other transverse components are neglected respect to the axial one. From figure 5.6, it can be observed that the velocity profile affected by the two-way coupling process has smaller gradient of velocity and has higher average value which is expected as the gas void fraction increases. This is clear from comparing between the profiles of the two-way coupling of the gas void fractions G01 and G03. This change in the velocity profile can be explained by the existence of the bubbles. As the bubbles act as layers over which the liquid flows which minimize the effect of the liquid viscosity that cause the profile of the one way coupling. It can act also as a distributor which is put in the pipe for distributing the velocity of the fluid to be uniformly distributed in the radial direction. This change in the liquid velocity profile will in turn affect on the forces acting on the bubbles that controls its motion through the liquid phase.

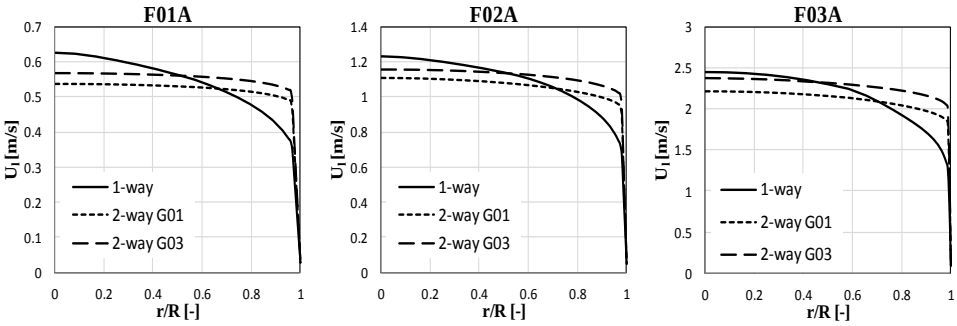

Figure 5.6. Radial velocity profiles for the axial velocity component of the liquid for the cases F01A, F02A and F03A.

An important change will occur to the lift force of the bubble as it accounts for the vorticity which is a function of the liquid velocity gradients at different directions. And as the gradient of the liquid velocity decreases with applying the two-way coupling, the effect of the lift force acting on the bubble will decrease dramatically.

Figure 5.7 shows the liquid void fraction radial distribution at a vertical distance in the mid of the vertical pipe.

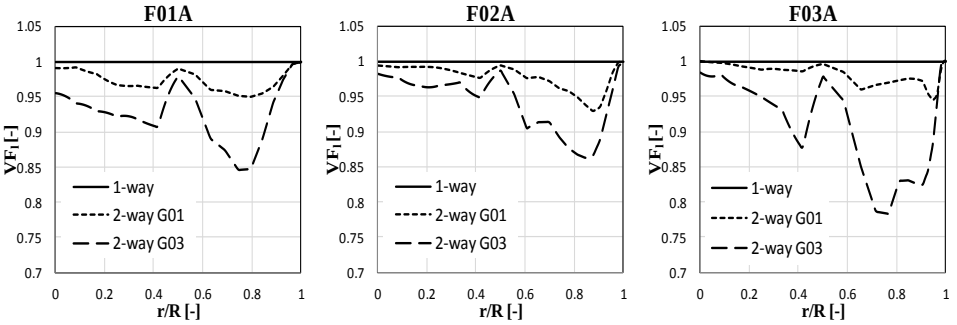

Figure 5.7. Radial liquid fraction distributions.

The liquid void fraction profiles shown at figure 5.7 were calculated by considering the volume of the computational cell available for liquid with respect to the total volume at a given instant. In the liquid fraction profiles, it can be observed that the lower fraction close to the wall decreases with increasing the liquid velocity which gives the minimum value at F03A. This will be emphasized by the gas void fraction profiles that increase the peak with increasing the gas hold up and the liquid velocity as will be shown later in this chapter. It can be observed that at distance r/R=0.5, there is a peak in the liquid volume fraction, it was found that this peak is caused by the difference in

the cell shape of the grid at this point as shown at figure 2.17. This change in the cell shape give difference in the calculated template function that describes the gas fraction in the cell. This can be fixed by using finer grid. However, finer grid will consume more computational time.

Liquid Turbulence Kinetic energy K and dissipation rate ε

In the two way coupling process, the source terms in the k and ε equations are applied according to the values discussed in chapter 3 of Turbulence modeling. This source terms cause the increase of both the values of k and ε in the liquid. A comparison between the one-way and two-way coupling for the k and ε radial profiles for the test cases are shown at figure 5.8.

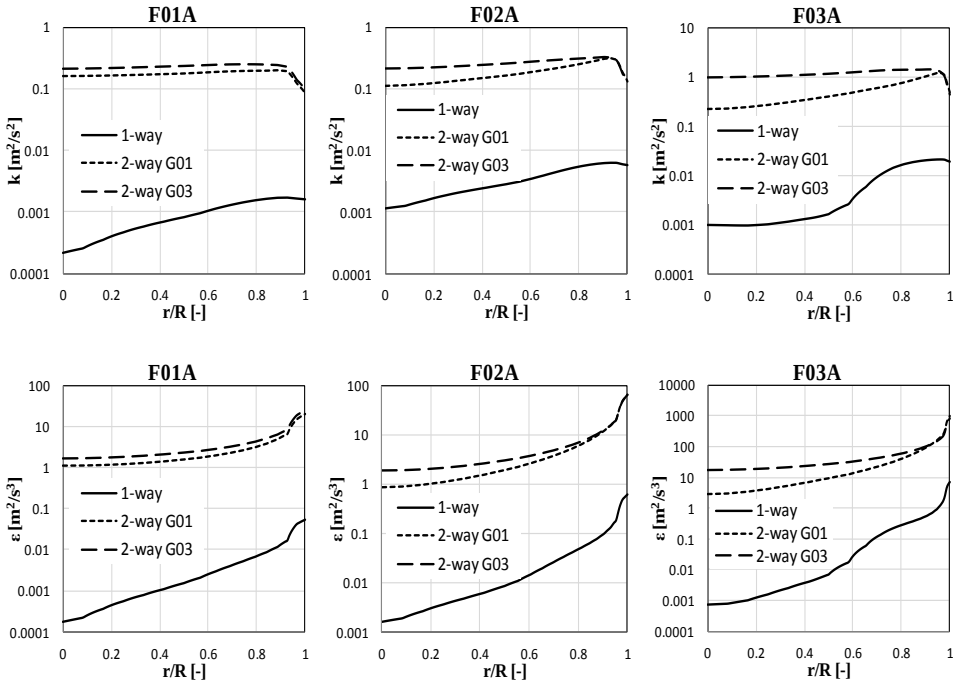

Figure 5.8. Radial turbulent kinetic energy k and turbulent dissipation rate ε profiles with the effect of the Two-way coupling process.

As illustrated at figure 5.8, the application of the two-way coupling process by the source terms in the turbulence kinetic energy and dissipation rate equations causes severe increase in the values of both k and ε. Also it can be seen that the values of both the k and ε increase with increasing the void fraction from G01 to G03. This change at the liquid flows F01 does not have much difference as the liquid velocity is low (0.5

m/s), but this difference is clear when the velocity of liquid increases as shown at F02 and F03 liquid flow rates (1.0 m/s and 2.0 m/s respectively). It can be observed also that the change of the profiles due to adding the effect of the two-way coupling is clear at the center of the pipe but it does not change at the pipe wall. This is explained by the existence of the bubbles a little bit away from the wall because of the effect of the bubble deformation force and the wall lubrication force. In the plots of the dissipation rate, it can be observed that the value of ε is very sensitive to the existence of the dispersed phase such that it is increased about 1000 times of the value of the one-way value. On the other hand the increase of the value of the turbulence kinetic energy is about 500 times of the one-way values. This seems to be very high values compared to the calculation made before like that of Krepper et al (2010). Other observation is that the profiles of K and ε in the two-way coupling are softer and have lower gradient which was the same for the case of the velocity profiles explained at the previous subsection. It can be concluded that the existence of the dispersed phase affect to the values of k and ε is more than the increasing in the dispersion phase percent. This is clear from the profiles of k and ε as the change of the profiles due to increasing the gas holdup from 5% to 15% is much less than the changes of the profiles due to inserting a second phase in the flow. This change in the turbulence properties of the liquid phase will in turn affect on the velocity fluctuations generated according to the CRW used and as a result will affect on the turbulence dispersion affecting the distribution of the bubbles.

5.1.5.2 Effect of Two-way coupling on the gas phase.

As was seen in the effect of the two-way coupling process on the continuous phase, the profiles of the velocity, turbulence kinetic energy and turbulent dissipation rate were changed. This in turn will lead to changes in the behavior of the dispersed phase and the forces affecting on it. In the present section, the effect of the Two-way coupling process on the distribution of the gas void fraction and velocity radial profiles is described.

Gas velocity distribution

The gas velocity radial profiles for the test cases at the pipe outlet are shown at figure 5.9. It can be observed from the gas velocity profiles that it follows the velocity of the liquid in being smoother with lower gradients. This results in that the gas velocity decreases at the pipe center and increases close to the wall. That is clear as the gas bubbles are affected by the external forces exerted on it by the liquid phase, which requires that any change in the liquid properties will affect the behavior of the gas bubbles. It can be observed that the change in the gas velocity profiles for the F01A case is very low, and the change in the F03A case is considerable. As was mentioned

before, the liquid velocity plays a leading role in the forces affecting on the gas bubbles which in turn controls the bubbles velocity and accelerations.

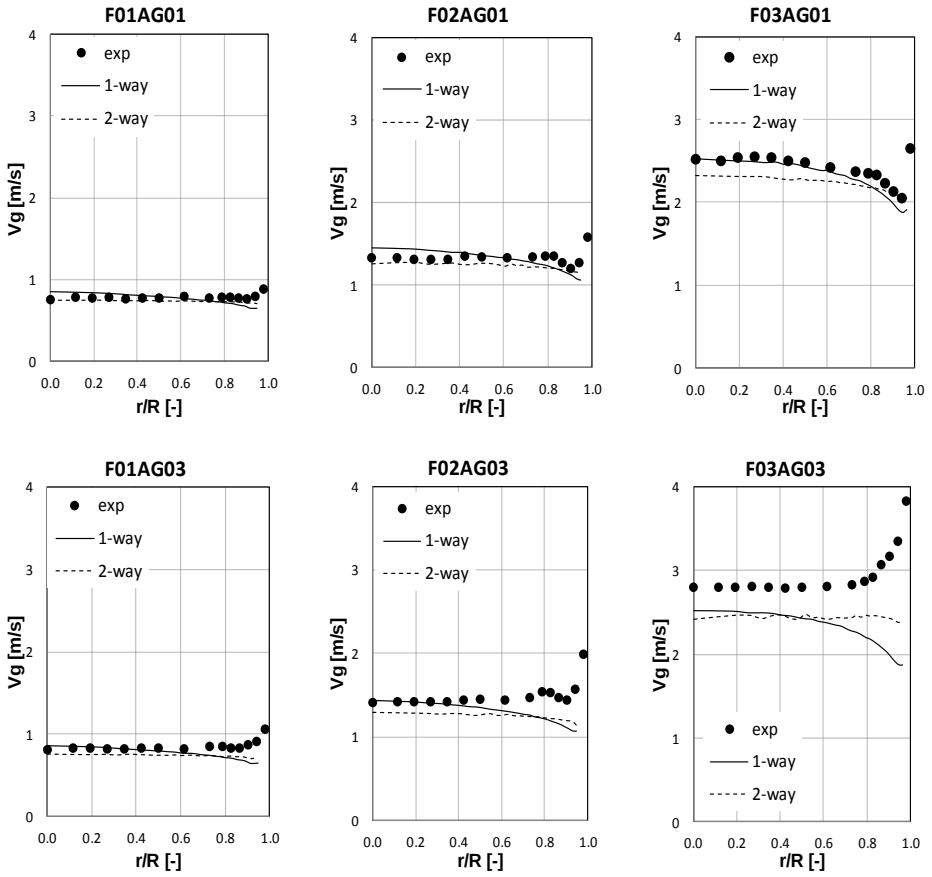

Figure 5.9. Gas velocity profiles for the Two-way coupling process without collisions.

Void fraction distribution

The distribution of the gas void fraction radial profiles for the test cases at the pipe outlet is shown at figure 5.10. as can be observed, the wall peak of the void fraction distribution moves a little away from the experimental data with the same lift coefficient of C_T=0.07 that was used for the one-way coupling and gave good results. In fact this was expected as the gradients of the liquid velocity decreased with applying the two-way coupling. The liquid velocity gradient in turn minimizes the lift force affecting on the bubbles which is the main component that moves the bubbles in the

wall direction. In order to recover the true distribution of the gas void fraction, we have to increase the lift coefficient in the lift force model. This will be investigated in the next section.

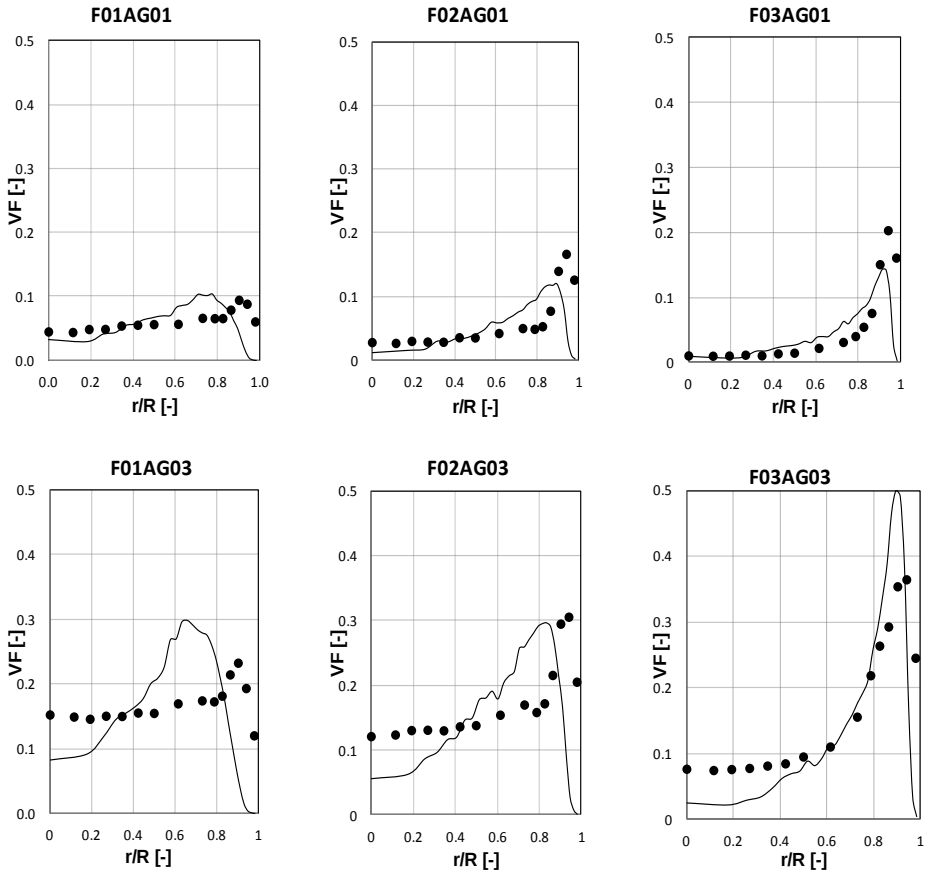

Figure 5.10. Gas void fraction profiles for the Two-way coupling process without collisions.

5.1.5.3 Study of the Lift coefficient effect on the void profiles

In the present section, the effect of changing the lift coefficient on the void fraction distribution for the two-way coupling process is studied. As was concluded from the results of figure 5.6, the lift coefficient should be increased in order to increase the lift force and as a result, increase the gas void fraction beside the wall. Two values were suggested for the lift coefficient which are C_T=0.15 and the other value will be that calculated according to Tomiyama (1998) relation presented at equation (2.22). the

results are illustrated at figure 5.11. At the legend of figure 5.11, C_T refers to the lift coefficient. The effect of changing the lift coefficient from 0.07 to 0.15 is very small for the cases of 5% gas void fraction.

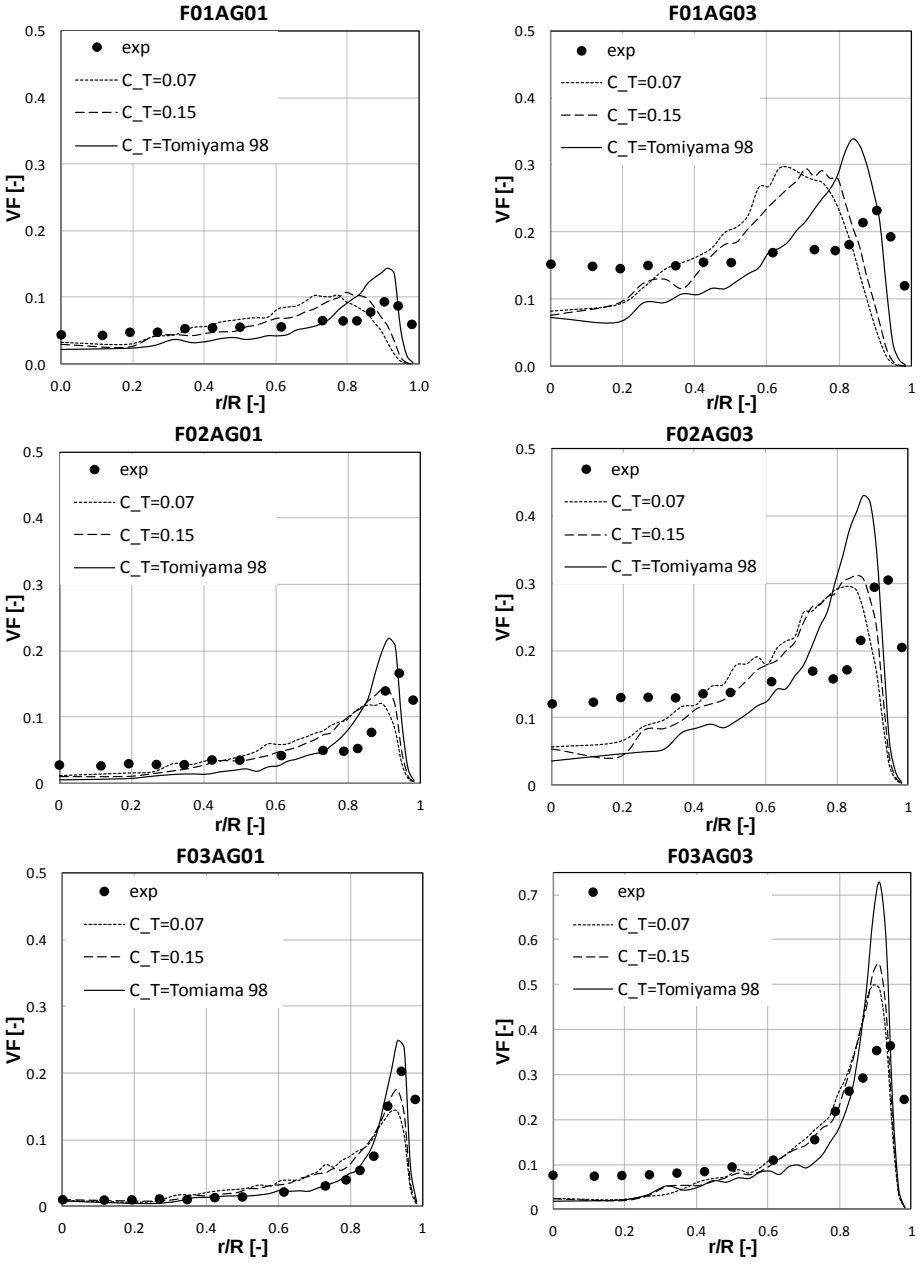

Figure 5.11. Gas void fraction profiles for different values of the lift coefficient C_T.

The lift coefficient of Tomiyama seems to give better results than the other two constant coefficient values C_T =0.07, and C_T=0.15 for two reasons. The first is that the results obtained with Tomiyama coefficient gave the wall peak value nearer to the experimental data. The second is that the value of the peak is a little higher than the peaks of the constant values coefficients which can be adjusted by increasing the turbulent dispersion effect suggested in the present work. For the results of 15% gas void fraction (G03), it can be noticed that the gas void fraction at the center is much lower than the experimental data. This could be caused by neglecting the effect of bubbles collisions that in turn redistribute the bubbles. This means that at high void fractions, the overlapping of the bubbles should not be permitted as it give non realistic higher values of void fraction at the regions of high concentrations of the gas, which should be redistributed to regions of low concentration if the collisions of bubbles were applied. Also it can be observed for high liquid velocities of 1.0 m/s in F02A, and 2.0 m/s in F03A that the effect of changing the lift coefficient does not affect much in changing the radial location of the void fraction wall peak. This is because the velocity of the liquid is high and the gradient of the velocity after applying the two-way coupling have considerable effect on the lift force, but in the F01 case, the velocity gradient distribution is very low, as can be observed clearly at figure 5.6.

As a conclusion, it can be stated that applying the two way coupling process changes the void fraction profile in all the cases. This is due to changing the liquid velocity profile which affects directly to the vorticity of the liquid and hence changes the lift force applied on the bubble. This could be fixed by adjusting the value of the lift force coefficient to that proposed by Tomiyama (1998) at equation (2.22). Although the expression of the lift coefficient of Tomiyama gave the best location of the void fraction wall peak, it still gives a void fraction wall peak higher that the experimental data, which needs to increase the effect of turbulence dispersion that cause lowering the void fraction peak and redistribute the bubble to the lower void fraction regions.

5.2 Two-way coupling with considering bubbles collision

Considering bubbles interaction mechanism is very important especially when the gas void fraction exceed 10% as stated by Sommerfeld (2000). In this section, the collision occurring between bubbles is considered to study this effect on the behavior of the bubbles. On the other hand it will be a start for applying the coalescence and breakup models in our work. In this section, the two-way coupling process considering the bubble's collision is presented. Also, the modifications needed for the Lagrangian solver to account for the bubbles collision in the time stepping method and the Lagrangian solver code is discussed. Then the effect of applying the bubble's coalescence mechanism with simulation data is presented with some discussion.

5.2.1 Time stepping

The time stepping method used when considering bubbles collisions will be the same as the preceding time stepping of the two way coupling without considering bubbles interactions but with further time step due to the collisions. The collision time step identify the next time of collision of two bubbles. This time is less than the Lagrangian one as shown at figure 5.12. Such that Δt_E is the Eulerian time step over which the Euler solver is called, Δt_L is the Lagrangian time step which is fixed during the simulation and Δt_c is the collision time step which calculates the duration tile the next collision of two bubbles. The next collision time is calculated according to the bubbles velocities and positions as expressed in equation (2.66) in collision models. Two types of collisions are considered, the first occurs among bubbles, and the second one occur between bubbles and the pipe wall. It was found during the simulation that the collisions of bubbles with the pipe wall have very high frequency and if we considered this time of collision, the resulting displacement of the bubble will be so small that will not affect very much on the bubble displacement. On the other hand the time consumed in the calculation will be very high. So, the wall collision of the bubble was simplified by considering a fixed distance from the pipe wall at which the bubble is reflected towards the pipe center with the same radial velocity. We believe that this is a logic consideration as normally a film of liquid exists beside the wall.

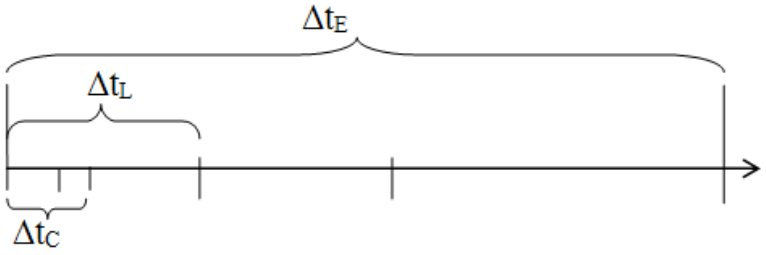

Figure 5.12. Time stepping method considering bubbles collisions.

5.2.2 Code Algorithm

In the case of considering the collisions of the bubbles in the calculation, the motion of each bubble at each time step, and its motion with respect to the neighbor bubbles are considered to calculate the next collision time. The loop system for the code will be similar to that of the two-way coupling at figure 5.5. Only the system of loops responsible for calculating the bubbles next collision time which are loops 3 and 4 were added at figure 5.13.

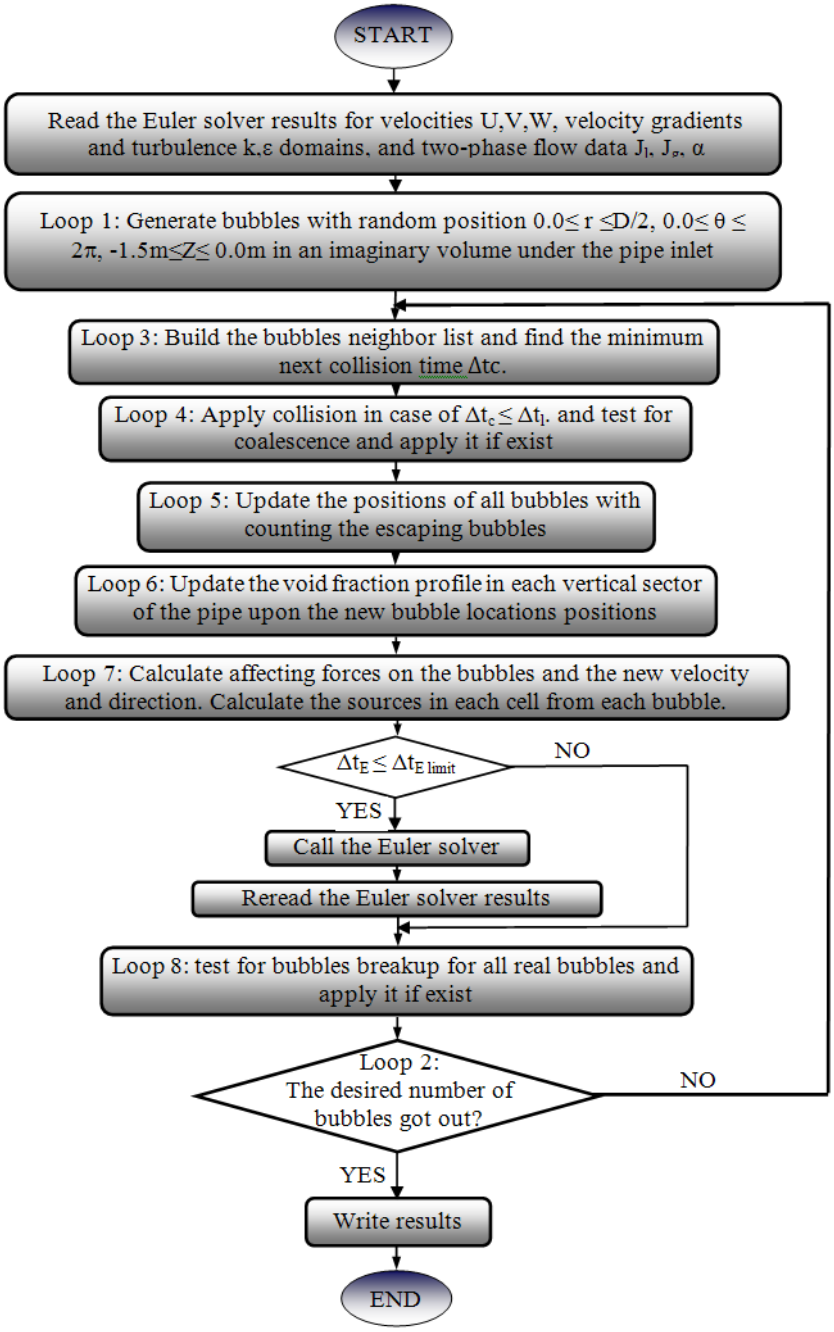

Figure 5.13. The flow chart for the Two-way coupling process considering bubbles collisions.

Loop 3 record the neighbor bubbles for the considered one in the loop, and calculates the time required for collision if occurs between the two bubbles and also get the minimum collision time. Loop 4 is a do while loop which apply the collision process. These loops continue working while the collision time Δt_c is less than the Lagrangian time step Δt_l. After loop 4 ends, the loops of the two-way coupling without collisions continue in operation.

5.2.3 Results and discussion

In this section, it is presented the primary simulation results from the two-way coupling process considering bubble's collisions, and its comparison with the former results of the two-way coupling without bubble's collision consideration. The gas void fraction distributions results are shown at figure 5.14.

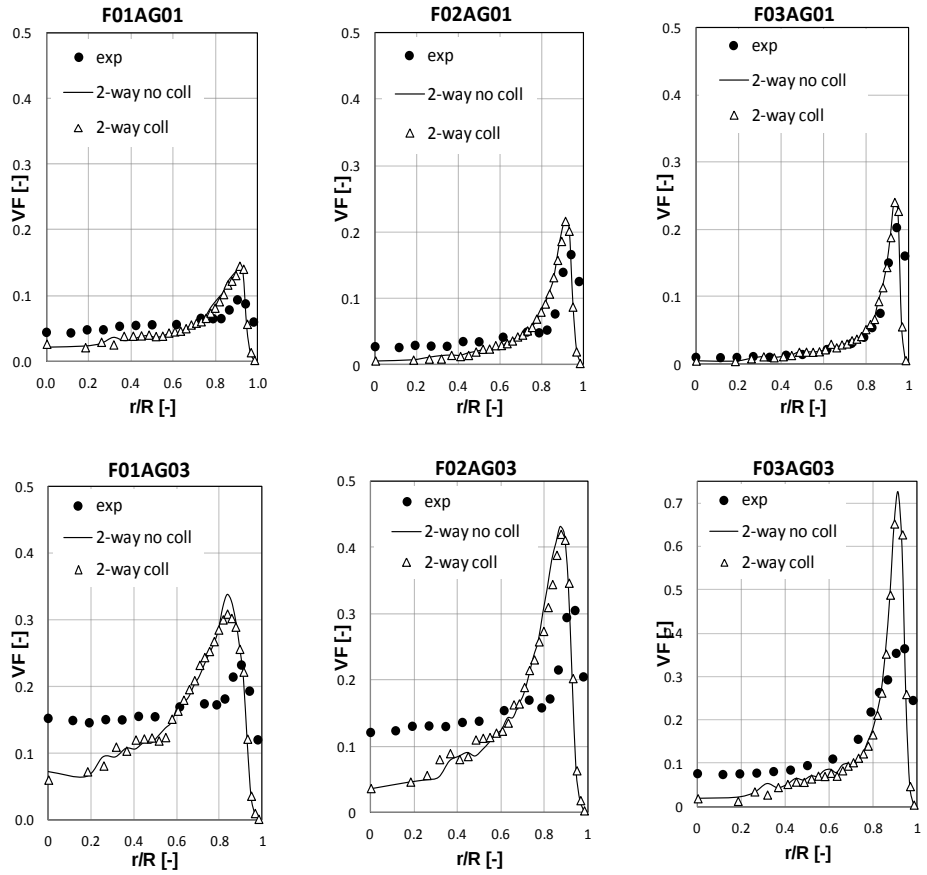

Figure 5.14. Gas void fraction radial distribution of two-way coupling for different cases.

At figure 5.14, the legend "2-way no coll" refers to the results of simulations with two-way coupling without considering bubbles collisions. The legend "2-way coll" refers to the results of simulations with two-way coupling when considering bubbles collisions. As can be observed from the void fraction distributions, the change of the profiles due to adding the collision effect is approximately neglected, especially for void fractions of G01 of 5%. For high void fractions of G03 15%, the change of the profiles was expected to differ when considering the bubbles collisions. This can be explained by two points. The first is that the collision rate increases and as a result the void fraction wall peak decreases a little. The second point is that in the present work, at each Lagrangian time step, the fluctuating velocity of the liquid is considered in the calculations of the forces acting on the bubbles. This also enhances the turbulent behavior of the bubbles as if we have the collision already applied. The problem in these profiles is that the void fraction has a peak that is higher than the experimental data especially at the 15% gas void fractions. As was hinted at the last section of the two-way coupling results without collision effect, the lift force of Tomiyama could give the best distribution of the void fraction but the peak beside the wall is higher than the experiments. For that reason, the adjustment of the S_{BIT} coefficient C_{tb} is studied at the next section to enhance the distribution of the bubbles as a result of increasing the turbulence effect.

5.2.4 Study for the effect of the BIT coefficient on the void fraction distribution

In this section, the study made for investigating the effect of the $S_{BIT,k}$ coefficient on the distribution of the void fraction profiles is presented of the test cases except for the case F03AG03 for calculation time constrains. That will be discussed later in this chapter. At the last section, we observed that the wall peak in the void fraction distribution did not change much when adding the bubbles collision effect. So the need for increasing the effect of the turbulence dispersion arises in order to redistribute the bubbles and decrease the void fraction wall peak. The last value used for the $S_{BIT,k}$ coefficient C_{tb} was 0.02. In the current study, higher values for the C_{tb} coefficient of 15.0 and 20.0 were tested but it was too high and created instability in the void fraction distribution. So, two further different values for the C_{tb} coefficient were suggested which are C_{tb}=0.025, and C_{tb}=0.035. The results of the simulations using these coefficients are shown at figure 5.15. It can be observed from the distribution of the void fraction in the different cases at figure 5.15 that for the low liquid velocity cases, F01AG01, and F01AG03 the change is not observed. This is due to the lower turbulence that follows the liquid velocity. On the other hand, the experiments of F02 and F03 both give a notable change in the profile due to the change of the C_{tb} value. And this is because the turbulence is higher in the higher liquid velocity cases, which leads to a considerable effect of the $S_{BIT,k}$ for small change in the C_{tb} coefficient as

shown. Also, It can be observed that the change of the C_{tb} coefficient did not affect the void fraction value at the pipe center in all the cases which means that the relation used for the $S_{BIT,k}$ does not change the void fraction at the pipe center even if the value of C_{tb} is changed.

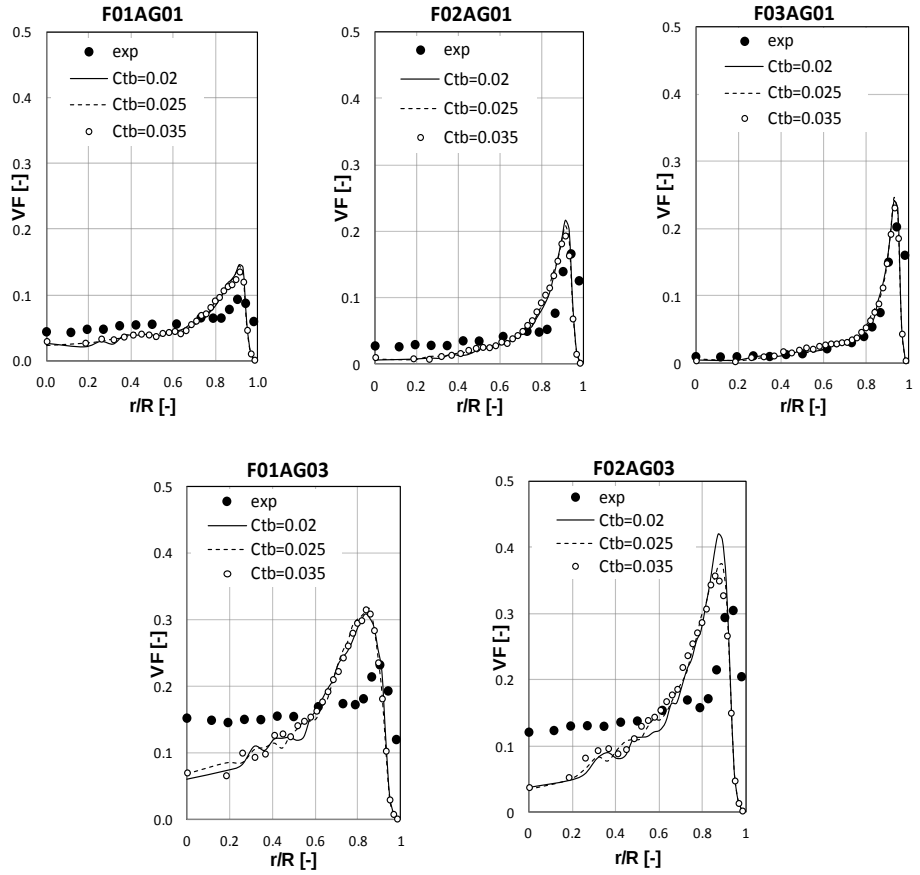

Figure 5.15. Gas void fraction radial distribution for the test cases for different values of the $S_{BIT,k}$ coefficient C_{tb}.

If we gave a glance on the equation (3.45) that expresses the $S_{BIT,k}$ as a source term in the kinetic energy equation, we can find out that the value of the $S_{BIT,k}$ in the pipe center may have a value of zero as the gradient of the void fraction is neglected at the pipe center. Also, the dependence of the S_{BIT} on the void fraction function was vital in the one-way coupling process as the continuous phase does not take in account the effect of the bubbles and bubble density on the continuous phase turbulence properties. On the other hand, in the two-way coupling process the existence of many bubbles was token in to account in the continuous phase due to the averaging process used for calculating the source terms considering the effect of the bubbles in the Euler solver

equations. Moreover, value of C_{tb} was increased to 0.06 but it gave high fluctuations problems. For these reasons, we decided to neglect the effect of the void fraction on the $S_{BIT,k}$ relation. The $S_{BIT,k}$ relation for the two-way coupling process will be as follows

$$S_{BIT,k} = C_{tb}.\, u_{rel}^2 * D_b \tag{5.15}$$

As we do not know initially the value for C_{tb}, we started with $C_{tb} = 20.0$. The test cases simulate was the same as that used for the advanced sections. The void fraction distribution resulting from the simulations using the new relation for the $S_{BIT,k}$ is shown at figure 5.16. "BIT with void" refers to the simulation results using the definition of equation (3.45) for $S_{BIT,k}$ and "BIT wot void" refers to the definition of $S_{BIT,k}$ presented at equation (5.13).

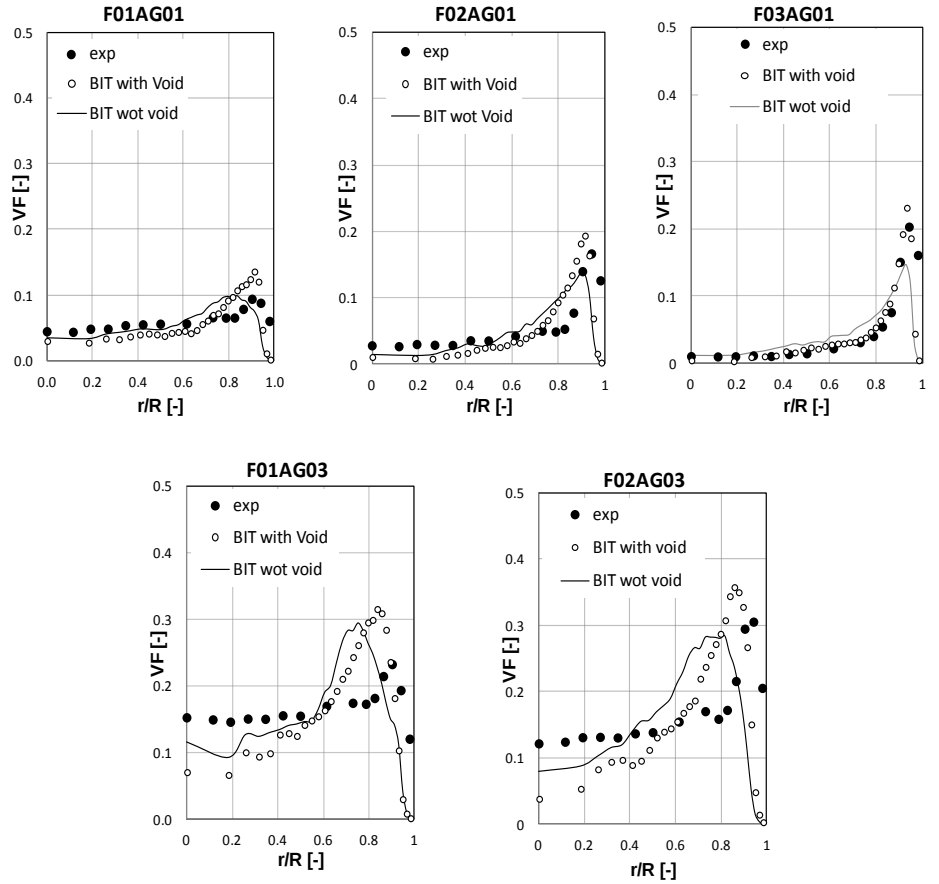

Figure 5.16. Gas void fraction radial distribution for the relation $S_{BIT,k} = C_{tb}.\, u_{rel}^2 * D_b$ with $C_{tb} = 20.0$.

As we can observe at figure 5.16, the value of the void fraction appears to be enhanced at the pipe center with the new $S_{BIT,k}$ relation defined in equation 5.15 and this is clearer at higher void fractions in cases F01AG03 and F02AG03. We can observe also that the wall peak value moved a little away from the experimental data. This can be explained as the initial vale of C_{tb} we used gave higher $S_{BIT,k}$ that it should be. So, we made another simulation with value for $C_{tb} = 15.0$ to minimize the $S_{BIT,k}$ effect. We found that applying a value of $C_{tb} = 15.0$ indeed decreases the effect of the turbulence dispersion but on the other hand, the void fraction of the gas decreases at the center of the pipe as shown at figure 5.17.

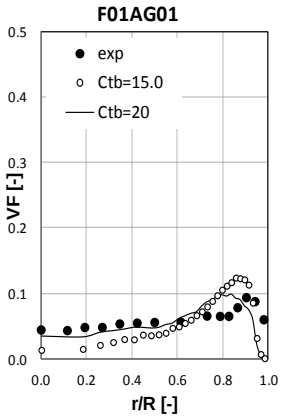

Figure 5.17. Gas void fraction radial distribution for the relation $S_{BIT,k} = C_{tb}.\, u_{rel}^2 * D_b$.

We could deduce from the distributions shown at figure 5.17 that $S_{BIT,k}$ of the two-way coupling have other dependence on the relative velocity of the bubble and the bubble diameter than that expressed in equation (5.15). It was decided to switch the $S_{BIT,k}$ relation to the turbulence kinetic energy equation source term expression proposed by Yao and Morel (2004) at equation (3.33) to compare the turbulence data in both models. The change in the distribution of the void fraction as a result of using equation (3.33) is shown at figure 5.18. As can be observed from figure 5.18, the source term expressed by Yao and Morel does not give sufficient turbulent dispersion effect for the bubbles and it is clear that the effect of the lift force is greater than the effect of the turbulence dispersion. As a result, the void fraction distribution gives a wall peak higher than experimental data in the simulated test cases. In order to investigate the reason of this difference, we analyzed both simulations that uses the Yao and Morel relation 3.33 and the one using the relation (5.15) with C_{tb}=20. We plotted the distribution of the turbulence kinetic energy for both simulations at figure 5.19.

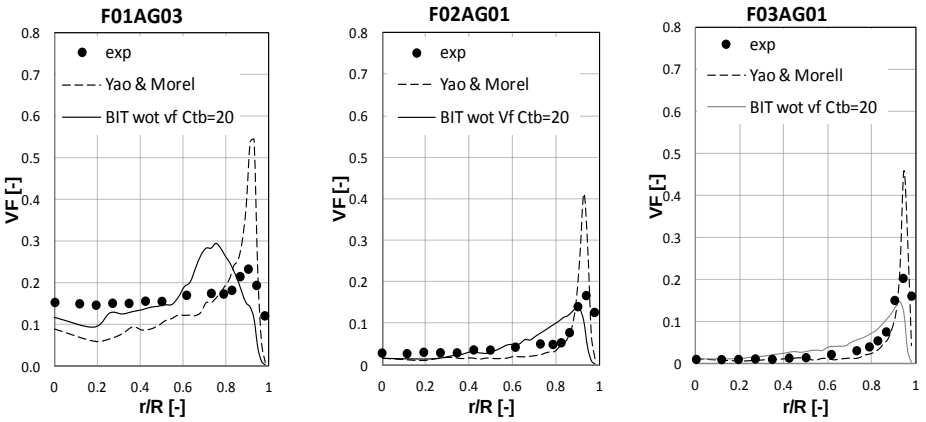

Figure 5.18. Gas void fraction radial distribution for the relation $S_{BIT,k} = C_{tb}.u_{rel}^2 * D_b$ with $C_{tb} = 20.0$ compared with the model of Yao and Morel (2004).

From figure 5.19, we can see that the model of Yao and Morel cause lower turbulence kinetic energy than that in equation 5.15 by a factor of 10^2. As hinted by Krepper et al (2010) the model of Yao and Morel gave good agreement with the experimental data for the turbulence kinetic energy. So we can deduce that our model gives excess turbulence in the turbulence kinetic energy equation. In order to modify our model for better behavior, we will decrease the C_{tb} coefficient. On the other hand, to test the dependence of the model on the relative velocity, we plotted the relation of equation (5.15) and the same relation with the relative velocity only without squaring, multiplied by scaling factor. This is shown at figure 5.20.

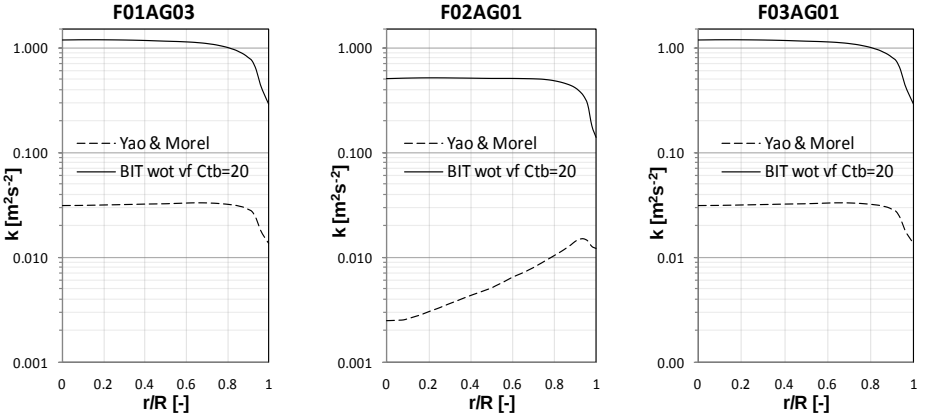

Figure 5.19. Turbulent Kinetic Energy radial distribution for the relation $S_{BIT,k} = C_{tb}.u_{rel}^2 * D_b$ with $C_{tb} = 20.0$ compared with the model of Yao and Morel (2004).

The collected BIT (BITc) at figure 5.20 expresses the effect of the source terms at each computational cell according to the bubbles density at the cell

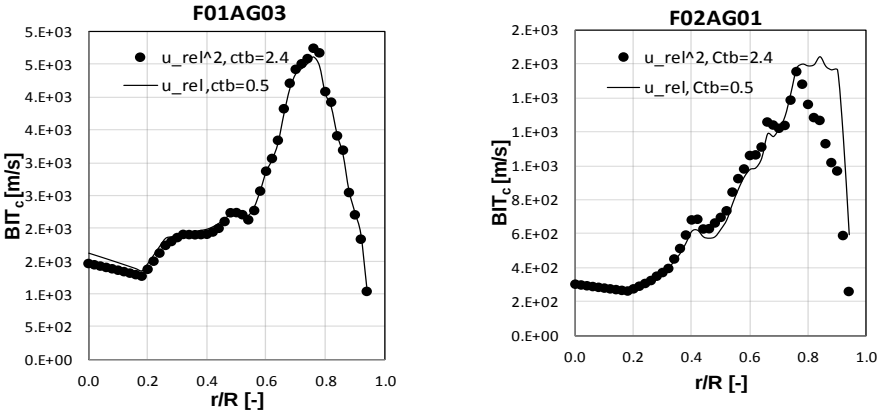

Figure 5.20. Collected BIT radial distribution for the relation $S_{BIT,k} = 2.4 * u_{rel}^2 * D_b$ compared with $S_{BIT,k} = 0.5 * u_{rel} * D_b$.

At this test, we decreased the C_{tb} coefficient from 20.0 to 2.4 and compared the relation 5.15 with the following one

$$S_{BIT,k} = C_{tb}.u_{rel} * D_b \tag{5.16}$$

With the C_{tb} value of 0.5. We notice that the coefficient C_{tb} should in that case have dimensions of dynamic viscosity multiplied by velocity, i.e. (N/m). From figure 5.20, we found out that at low liquid velocity cases , there is now big difference between the two relations as the relative velocity profile is nearly equal at all the points. For the case F02AG01 it was found that the relation (5.16) should give better behavior for the turbulence dispersion effect as it increases at the locations of higher bubbles density. So, finally we used the relation (5.16) as the $S_{BIT,k}$ which is used as a source term for the turbulence kinetic energy equation of the continuous phase. The resulting void fraction and gas velocity distributions when using equation (5.16) is shown at figures 5.21 and 5.22 respectively .at these figures, the results of equation (5.16) which is defined as "Bit Eqn u_rel" in the graph legend, are compared with the results from equation (5.15) which is defined as "Bit Eqn u_rel^2" at the graph legend, and the Model of Yao and Morel (2004). We can see at figure 5.21 that the new relation (5.16) could give the best behavior for the test cases compared to the relation of equation (5.15) and the relation of Yao and Morel at equation (3.33). At the gas velocity distributions figure 5.22, it can be seen that the difference between the three models is very low. And the results of simulations using the relation (5.16) gives moderate results for the velocity between the relation (5.15) and that of Yao and Morel. The last step to ensure the behavior of the last equation (5.16) is to test the turbulence Kinetic energy

profile compared to the other two relations of (5.15) and (3.33) which is plotted at figure 5.23.

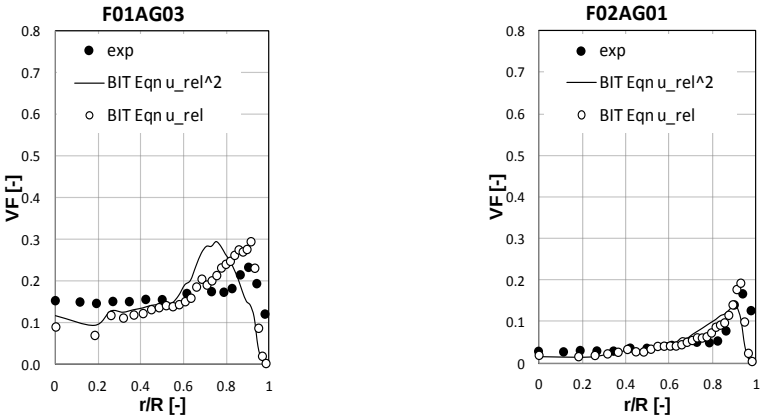

Figure 5.21. Gas void fraction distribution for the relation $S_{BIT,k} = 0.5 * u_{rel} * D_b$ compared with the relation $S_{BIT,k} = 20 * u_{rel}^2 * D_b$.

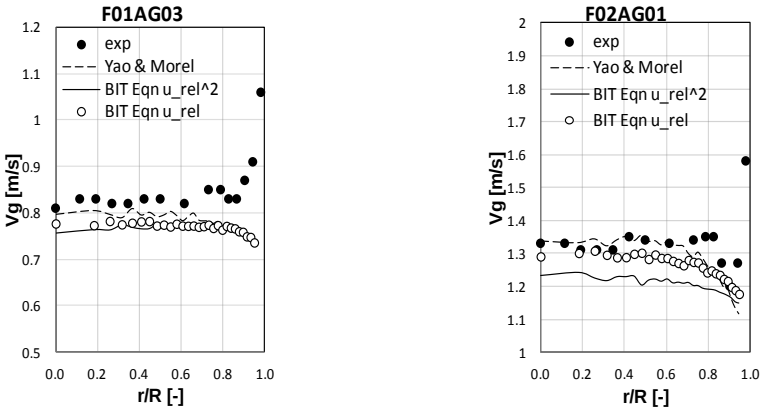

Figure 5.22. Gas velocity distribution for the relation $S_{BIT,k} = 0.5 * u_{rel} * D_b$ compared with the relation $S_{BIT,k} = 20 * u_{rel}^2 * D_b$.

As shown at figure 5.23, the turbulence kinetic energy resulting from the simulations with equation 5.14 is larger than that for the Yao and Morel model equation 3.33. However it is less than the model in equation 5.13. As we do not have measurements for the turbulence variables in the current Experimental data series, we suffice to have good agreements of the relation 5.14 with experimental void fraction distributions and gas velocity distribution. And we consider that it is valid as a source term in the turbulence kinetic energy equation of the Euler solver as $S_{BIT,k}$. At the same time the turbulence dispersion effect produced by this relation gives good agreement with experimental results with the lift coefficient defined by Tomiyama (1998)

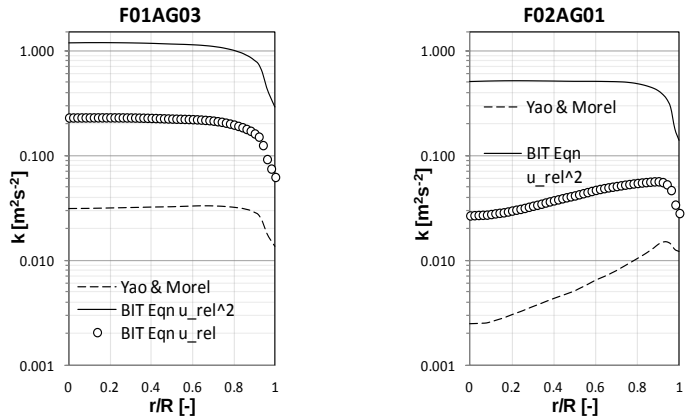

Figure 5.23. Turbulence kinetic energy distribution for the relation $S_{BIT,k} = 0.5 * u_{rel} * D_b$ compared with the relation $S_{BIT,k} = 20 * u_{rel}^2 * D_b$.

Here, the simulation results from equation (5.16) are presented for the void fraction distribution, gas velocity distribution, interfacial area concentration and averaged bubble diameter at figures 5.24, 5.25, 5.26 and 5.27 respectively. At the void fraction distributions in figure 5.24, we can see that the distributions due to equation (5.16) have good agreement with experimental data for the illustrated cases. Small liquid velocity simulations (F01A) gives distributions differ little form experiments. We can deduce that at low liquid velocity cases, our model of bubble induced turbulence needs to be enhanced to prevent this wall peak and to redistribute the bubbles to the pipe center. But generally the model gave acceptable results for all the cases. At figure 5.25, we can see also good agreement for the gas velocity radial profile between the simulation results with experimental data. When the velocity of the liquid increases as in the case F03A, we can find that the simulated gas velocity is lower than the experimental one. This is a common problem in measurements using the conductivity probe close to the wall because of the collisions of the bubbles with the wall, the measurements are not real. This computed low velocity can be caused by a higher simulated turbulence than in the real case, as the turbulence energy when increases cause loss of the averaged velocity values. At figure 5.26, it is illustrated the IAC radial profiles for the cases F03AG01, F03AG02, and F03AG03 as an example for the accordance of the simulations with the experimental data. As was mentioned at chapter 1, the IAC data are not directly measured so it was not considered much in our comparisons. The same for the Sauter mean bubble diameter as it is not measured directly and was mathematically approximated from experimental void fraction and IAC data. So, it is shown at figure 5.27 the experimental data of only the central part of the pipe because the data of the experimental Sauter mean diameter are not expressing a logic act for the diameters of the bubbles as illustrated in the experimental results at chapter 1.

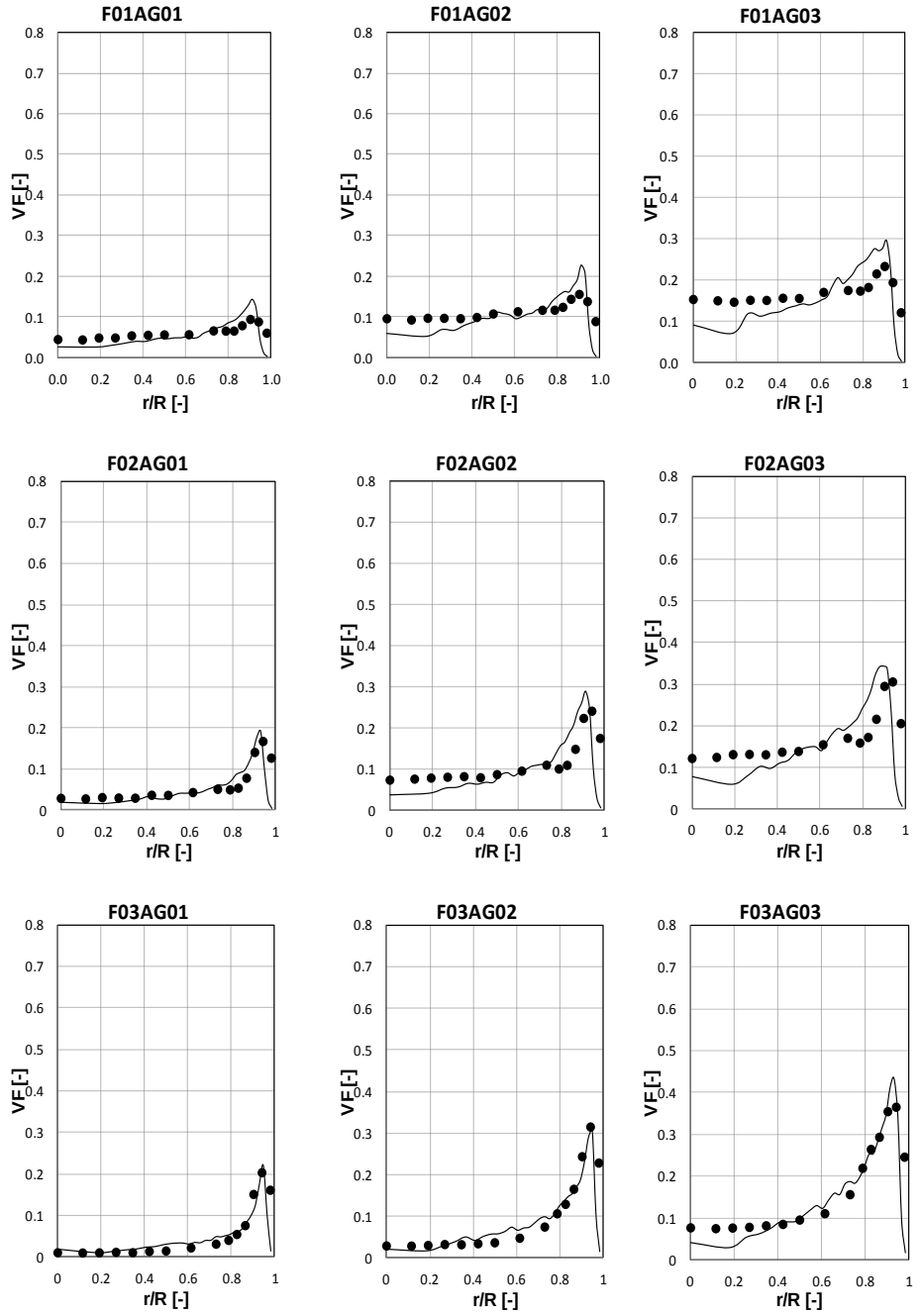

Figure 5.24. Gas void fraction distribution for the relation $S_{BIT,k} = 0.5 * u_{rel} * D_b$.

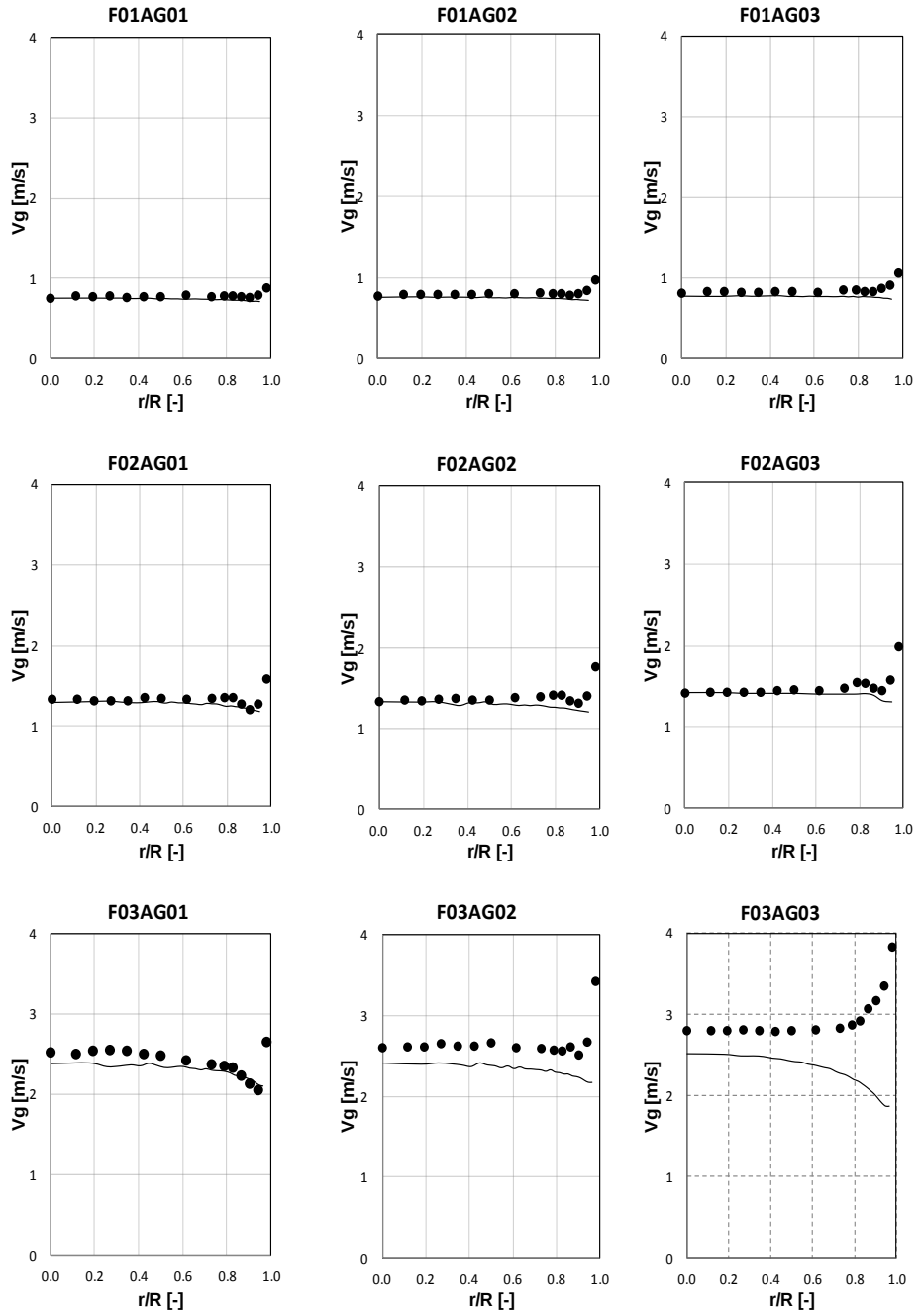

Figure 5.25. Gas velocity distribution for the relation $S_{BIT,k} = 0.5 * u_{rel} * D_b$.

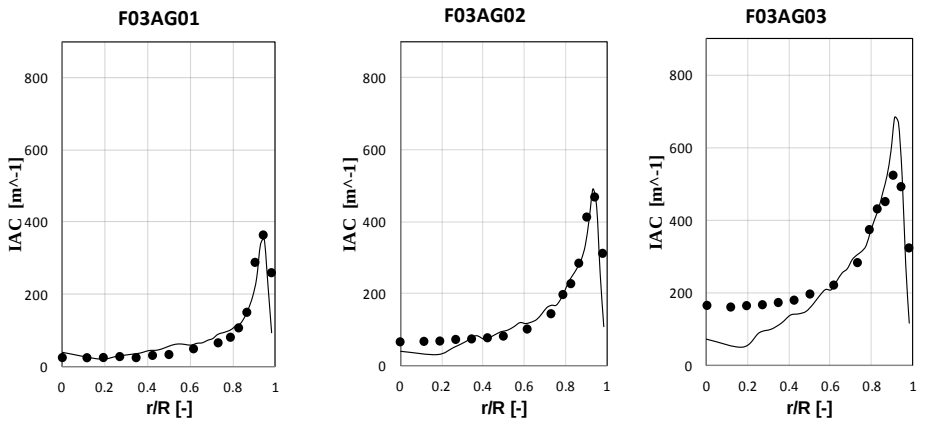

Figure 5.26. Gas IAC distribution for the relation $S_{BIT,k} = 0.5 * u_{rel} * D_b$.

At figure 5.27, good agreement can be considered with the experimental data especially for the cases F01AG01, F01AG02 and F02AG01 at which bubbles coalescence and breakup application is not necessary in order to represent the actual bubble size. for higher void fraction and liquid velocity test cases, the agreement with the experimental data is good as the calculations predicts the increase in the average bubble diameter as the increase in the Sauter mean diameter between the different cases when increasing the average gas void fraction. Finally it can be concluded that the proposed equation of the $S_{BIT,k}$ Eqn (5.16) gave good agreements in the void fraction distribution for all the test cases.

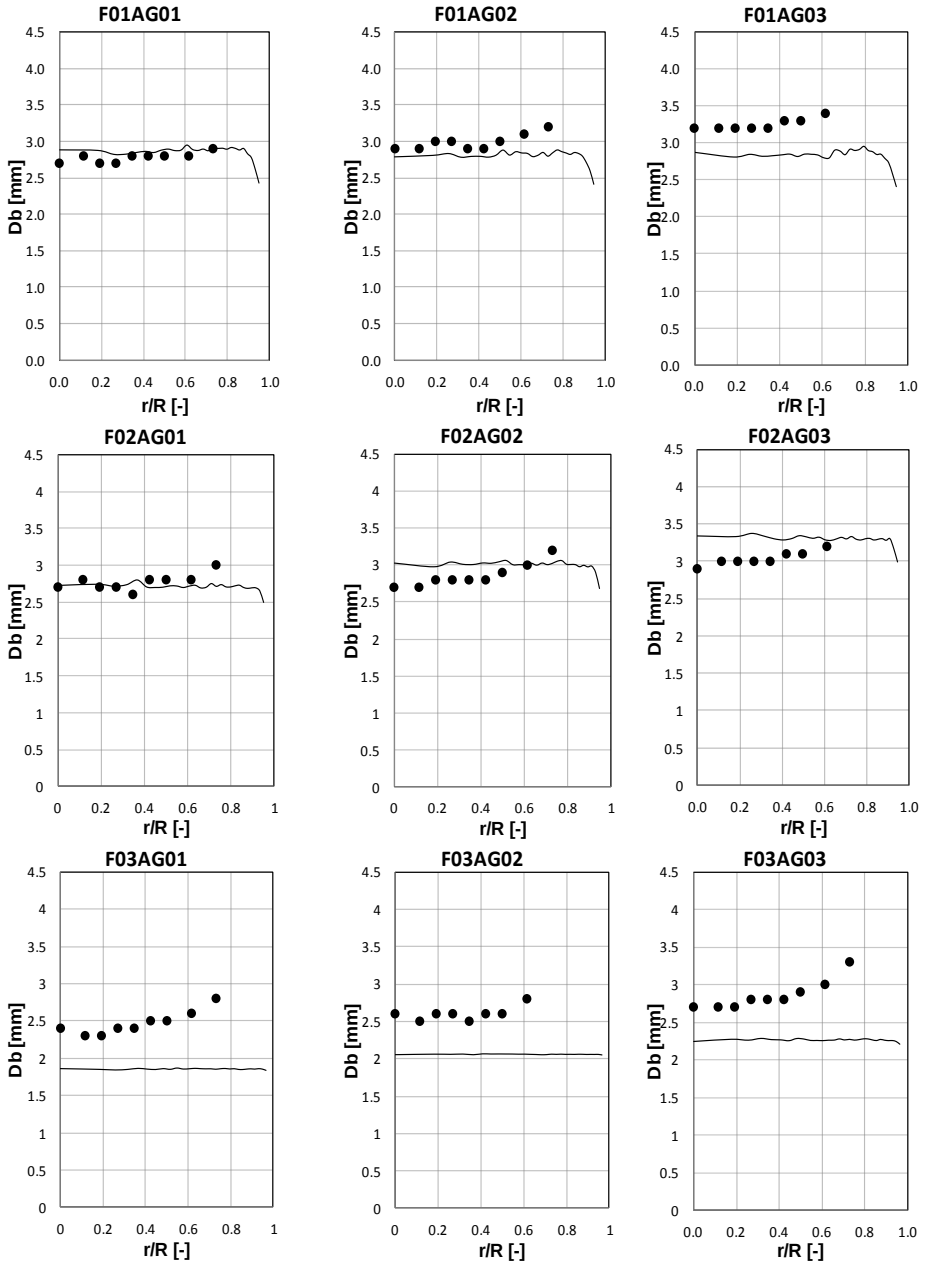

Figure 5.27. Average bubble diameter distribution for the relation $S_{BIT,k} = 0.5 * u_{rel} * D_b$.

5.2.5 Number of collisions density

Bubble-bubble collision is an important mechanism that controls bubbles motion and coalescence in bubbly flows. In order to identify coalescence process between two colliding bubbles, two processes and parameters are needed to be known. These are the collision between the two particles and coalescence efficiency of this collision. At this section the process of collisions is studied to identify the places at which collision occurs more frequently and hence there is bigger chance for coalescence between bubbles. Figure 5.28 shows the total collision number of the bubbles displayed as contours plot at the left side and as radial distribution at the right side. At the right side column, the normalized gas void fraction distribution on the secondary vertical axis was plotted to display the relative locations of the peaks in both profiles of void fraction and number of collisions. The contours data was calculated by counting the number of the collisions in each cell using equal cell areas. On the other hand, the radial distributions represented on the right side column were calculated counting the number of collisions in each radial sector with using 20 radial sectors of the same area. Both of the contour plot and the radial distribution were calculated for 5 vertical sectors of the pipe height to study the change of the variable with height. Each vertical sector is of 0.2m height. Figure 5.28 shows that the maximum number of collisions of the bubbles is in the lower part of the pipe, as the bubbles go upward, the number of collisions decreases. Also it can be observed that the radial position of the maximum number of collisions is fixed in the five vertical parts. This radial position is the location at which the wall peak of the gas void fraction is formed as can be seen from the void fraction profile. This is because the density of the bubbles in that place is high compared to the other radial locations.

In order to study why the collisions numbers is the maximum at the lower part, the radial distributions of the normalized void fraction was plotted at the secondary vertical axis and the radial gas velocity of the bubbles at the primary vertical axis at the left side as illustrated at figure 5.29.

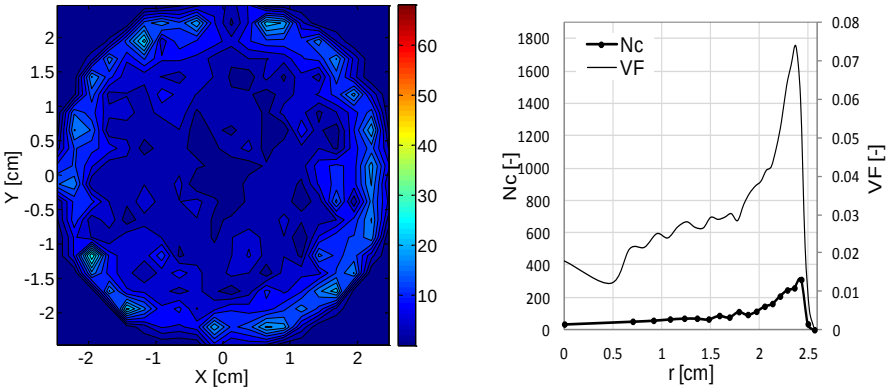
Y [cm]
X [cm]
Nc
VF
Nc [-]
VF [-]
r [cm]

(a)

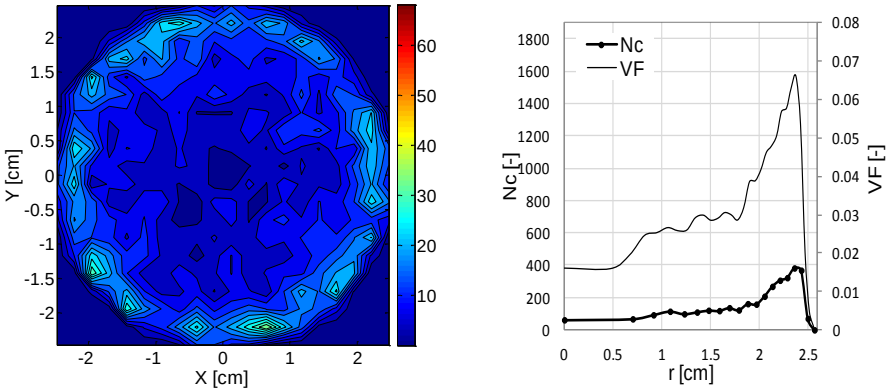
Y [cm]
X [cm]
Nc
VF
Nc [-]
VF [-]
r [cm]

(b)

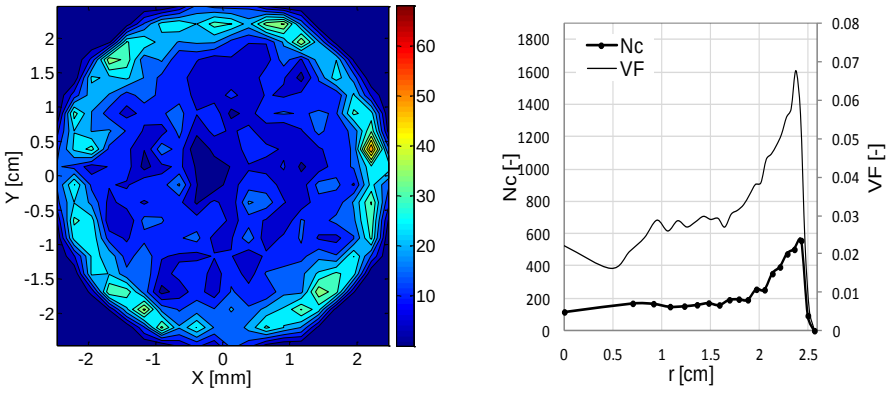
Y [cm]
X [mm]
Nc
VF
Nc [-]
VF [-]
r [cm]

(c)

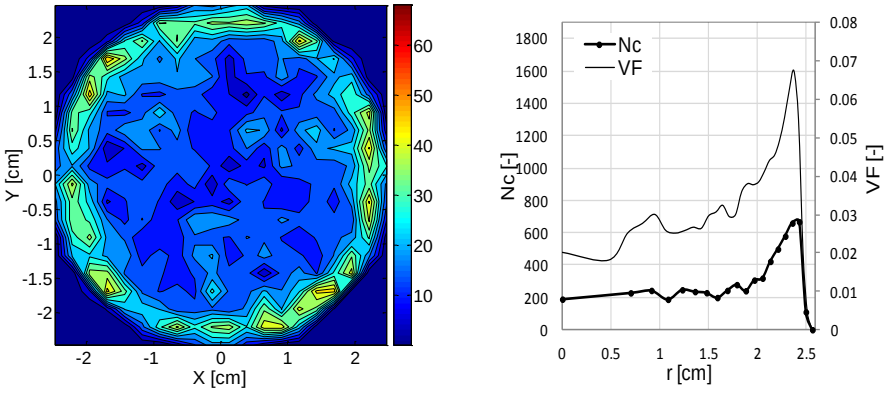

(d)

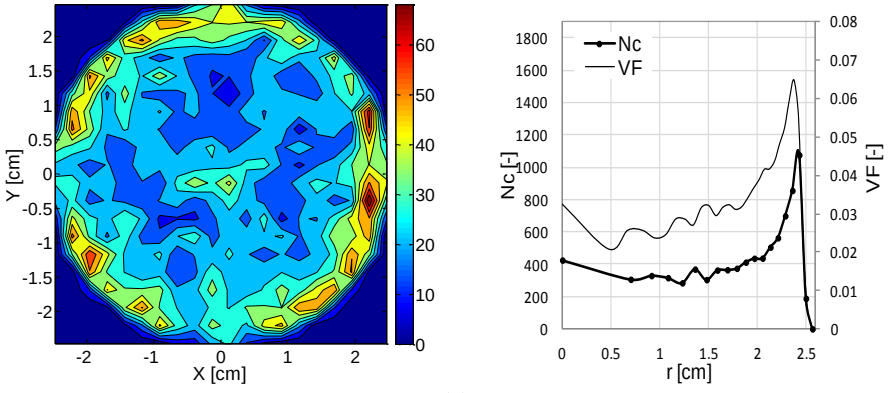

(e)

Figure 5.28. Total bubbles collisions number contours at the left and radial profile at the right. (a) For height 0.8m<z<1.0m, (b) For height 0.6m<z<0.8m, (c) For height 0.4m<z<0.6m, (d) For height 0.2m<z<0.4m, (e) For height 0.0m<z<0.2m.

At figure 5.29, Vgr refers to the average gas velocity at radial direction, VF refers to the gas void fraction, and r refers to the radial location. As it can be observed from figure 5.29 (a), the radial velocity of the bubbles beside the wall is directed to the center of the pipe, this negative velocity is located at the left of the wall peak value of the gas void fraction, which causes the bubbles at the negative gas velocity location to make collisions with much number of bubbles at the void fraction wall peak location in order to move to the pipe center. We can observe that this negative gas velocity have the maximum absolute value at the lower fifth of the pipe, so the number of collisions is higher in this fifth than the other ones.

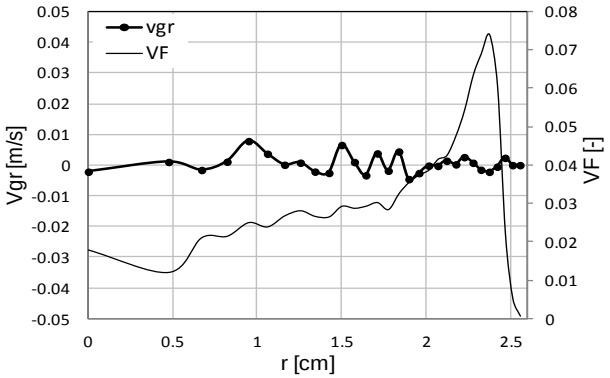

(a)

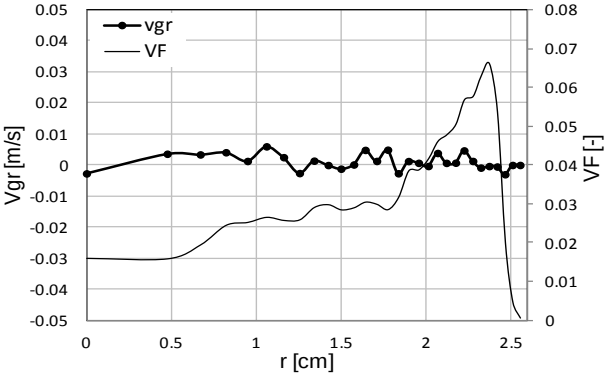

(b)

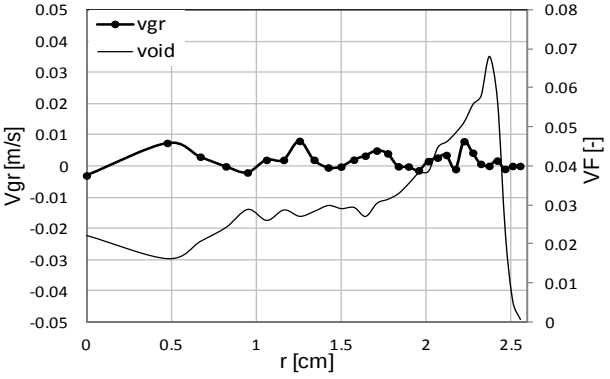

(c)

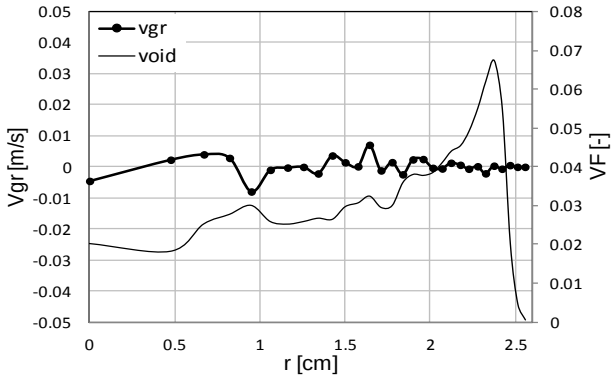

(d)

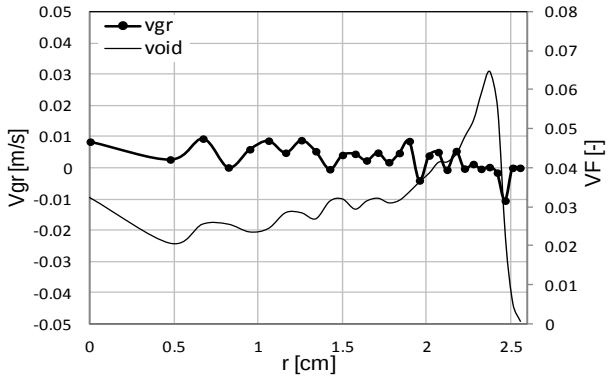

(e)

Figure 5.29. Radial distribution of the gas velocity at radial direction and gas void fraction. (a) For height 0.8m<z<1.0m, (b) For height 0.6m<z<0.8m, (c) For height 0.4m<z<0.6m, (d) For height 0.2m<z<0.4m, (e) For height 0.0m<z<0.2m.

Moving upward in the pipe, this negative gas velocity in the radial direction decreases and as shown at figure 5.28 the number of collisions decreases in the upward direction. Also we can observe from figure 5.29 that the radial location at the left wall peak of the void fraction has positive values of the radial gas velocity which push the bubbles towards the zone of the higher bubbles density and make collisions with them.

5.2.6 Effect of gas holdup on turbulence data

At this section, the effect of the gas existence and the influence of the gas holdup on the turbulence properties of the liquid are studied. Figure 5.30 illustrates the radial profiles of the liquid turbulence kinetic energy K, turbulence intensity I and Turbulence dissipation rate ε at five vertical positions of divisions H/5, such that H is the height of

the pipe. Four gas holdups was compared which are G00 with no gas, G01 with 5% gas, G02 with 10% gas and G03 with 15% gas for a liquid velocity of 0.5 m/s.

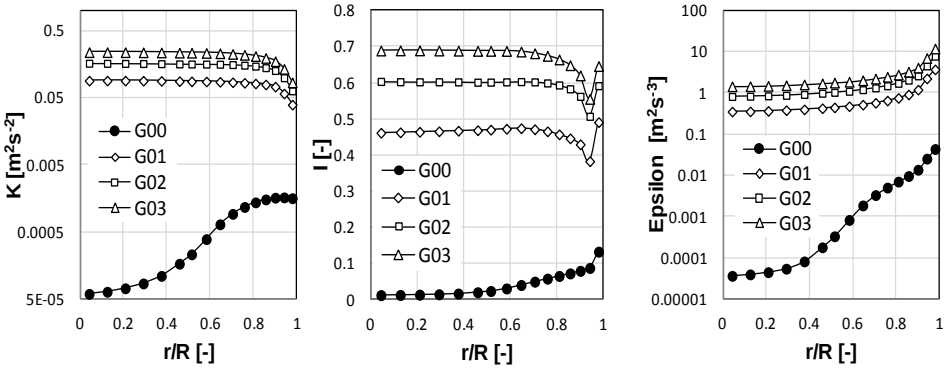

(a)

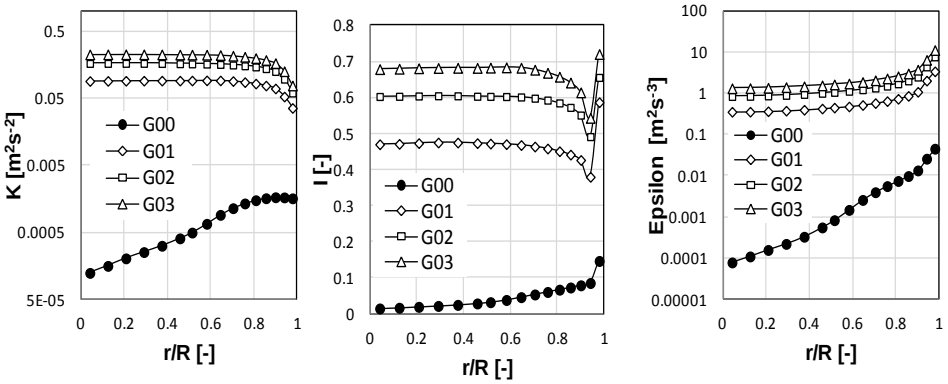

(b)

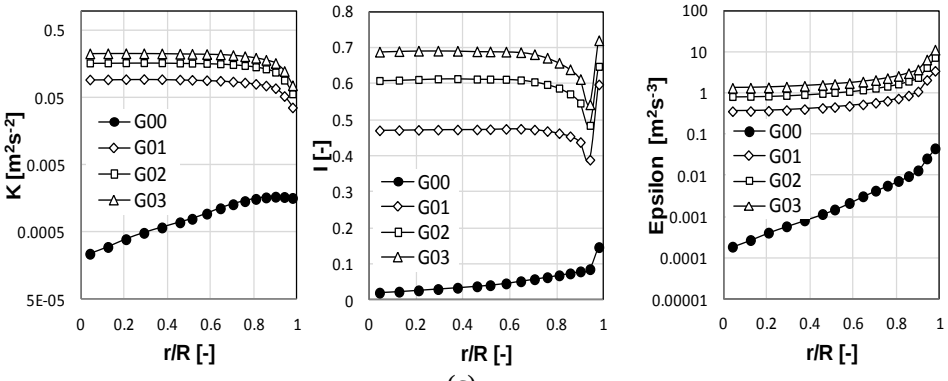

(c)

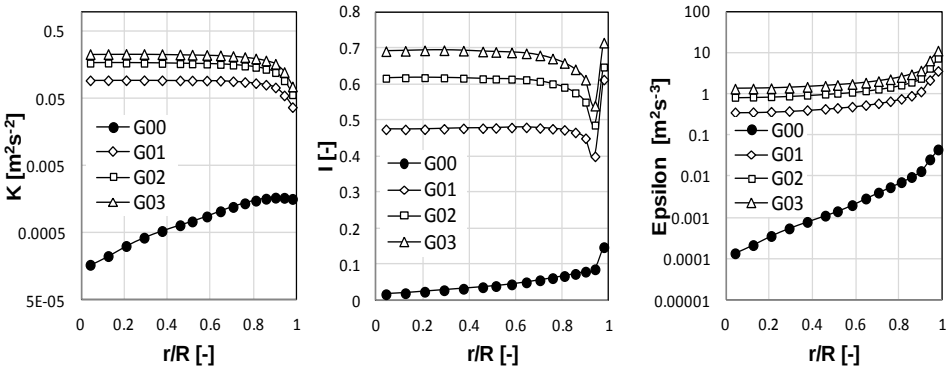

(d)

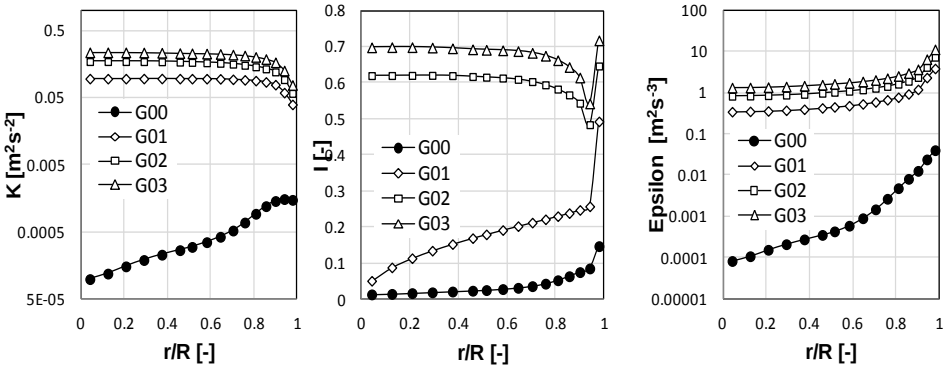

(e)

Figure 5.30. Radial distribution of liquid turbulence Kinetic energy k, turbulence intensity I, and turbulence dissipation rate ε. (a) For height z=5H/5, (b) For height z=4H/5, (c) For height z=3H/5, (d) For height z=2H/5, (e) For height z=H/5.

As it can be seen at figure 5.30, the gas affects extensively on the turbulence properties of the liquid. In general it can be concluded that the effect of the gas on the liquid phase is very important even if the percent of the gas is very low compared with the effect of the percent of the gas itself. This can be found out at the left and right columns of figure 5.30 of the k and ε. Also, it can be observed that the difference of the profiles of G01, G02, and G03 is very low compared to that of the case G00. Also at the center column of graphs which illustrates the profiles of the turbulence intensity I, the same conclusion is obtained. At the first level (e) the profile of the turbulence intensity of the case G01 seems to differ from the profiles of the cases G02 and G03. This is because the G01 case has lower effect on the bubble induced turbulence due to the low void fraction compared to the cases G02 and G03 which have higher void fraction and as a

result higher $S_{BIT,k}$ effect on the liquid turbulence at the entrance of the pipe. Also the entrance effect on the turbulence growth can be a cause for that.

5.2.7 Effect of considering bubbles coalescence

In this section the effect of adding the coalescence effect for the colliding bubbles is studied. The coalescence mechanism is considered in the Lagrangian simulation of the two-phase flow as a complementary step for the bubbles collision process, so it was not separated in a different area for explaining its effect, and we included it at this section of collision consideration.

Some differences will be considered in the code algorithm for the two-way coupling considering bubbles collision illustrated at figure 5.13 to account for the coalescence process. The time stepping mechanism will not change. The collision subroutine will have a little change. Simply, when the bubbles collision process is applied we test for the coalescence occurrence according to the calculation of the contact time t_{con} and the film drainage time t_{dr} for the two bubbles according to Chesters (1991) model as explained at chapter 2. When the film drainage time is less that the contact time, the coalescence will happen; else the colliding bubbles will bounce a way from each other's which is applied by the collision model used. When coalescence take place, one of the two bubbles is out from all the calculations and that is selected to be the bubble with the higher index. This deleted bubble is collected by their index in an array which is used in the other loops to ensure that the deleted bubbles will not enter in any calculation later. In order to test the effect of the bubbles coalescence, the test case F01AG01 only was used as the calculation time was very large as will be seen later. Figure 5.31 shows the void fraction distribution for the test case according to considering the coalescence of the colliding bubbles. At the legend, "Wot coalescence" refers to the simulation without coalescence and considering only collisions, on the other hand "With coalescence" refers to the simulations with considering both collisions and coalescence.

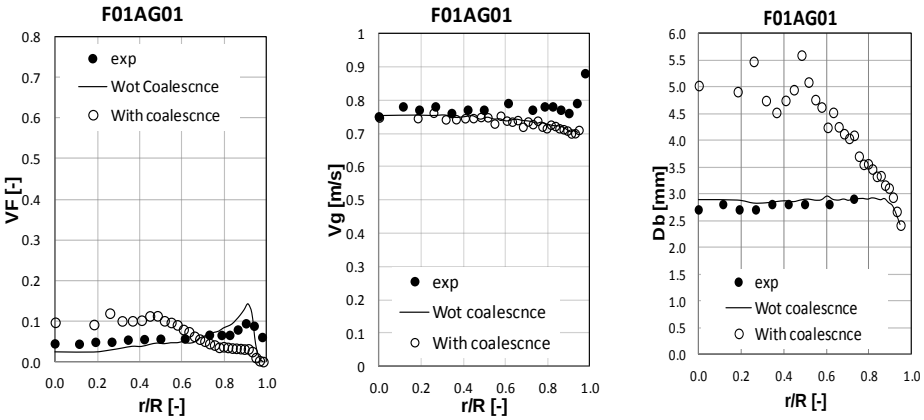

Figure 5.31. Gas void fraction (VF), Gas vertical velocity (Vg), and Bubble mean diameter (Db) radial distributions for considering coalescence mechanisms.

As can be observed in figure 5.31, the void fraction distribution is completely different from that of the experiment, if we see the bubble diameter distribution, we will understand the reason of that erroneous distributions as we consider only bubbles coalescence the bubbles are converted to bigger bubbles and as a result they are collected at the center of the pipe and make the pipe center peak for the gas void fraction. For the distribution of the gas velocity, it is found that the coalescence effect consideration does not affect much as the change of the bubbles diameter due to the coalescence did not affect much on the vertical forces on the bubble that accelerate the bubble so, the velocity of the bubbles does not change, also it can be deduced that from the distribution of the bubbles diameters as the bubbles at the center are bigger than that the ones beside the wall, the average gas velocity does not change much at these locations.

Now, it is important to see the effect of coalescence consideration on the bubble size distribution, this is illustrated at figure 5.32. Figure 5.32 shows the size of bubbles considering spherical shape at the inlet and the outlet of the pipe for a 0.08 m height window.

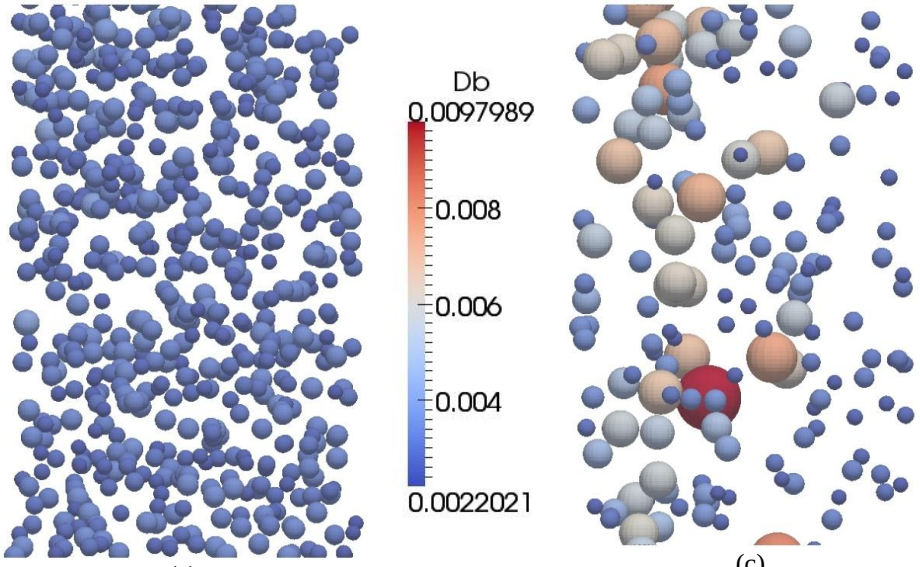

Figure 5.32. Coalescence effect on particle sizes at the pipe input and output for window of 0.08m height. Flow direction is upward. (a) Particles at pipe input, (b) Legend color map, (c) Particles at pipe outlet.

As we can see at figure 5.32 the bubbles size at the outlet reaches about 9.7mm although the range of bubble size at the inlet was 2.2mm to 3.3mm. as it is known, large bubbles migrate to the direction of the pipe center, this explains the center peak of the resulting void fraction distribution that disagree with experimental data for not taking in account the contrary interaction effect of the bubbles breakup which will be explained at the next section.

Finally, as illustrated at figure 5.31, considering only the coalescence effect without considering the breakup effect, only permit the bubble size to be larger and as a result the void fraction increases at the pipe center as the large bubbles migrate to the pipe center under the effect of the lift force. Although the disagreement found with the application of the coalescence, it could show the true migration of the large bubbles to the pipe center, the change of the bubbles size due to the coalescence consideration, and prepare the code to considering the breakup effect that will be explained at the next section.

5.3 Two way coupling considering bubble's collision, coalescence and Breakup

In this section, the change in the code to account for bubbles breakup mechanism is described. This includes the time stepping mechanism considered in case of applying the breakup with coalescence. For the code algorithm there will be some additions to apply the breakup mechanism. Then the simulation data resulting from considering the breakup mechanism when the coalescence is applied are presented with some discussion.

5.3.1 Time stepping

The time steps which are used in the code when considering both coalescence and breakup will be the same as that used for considering only bubbles collision which are illustrated at figure 5.12, only the value of the collision time step which is calculated automatically in the code will decrease due to the increase in the number of bubbles due to the breakup process. To account for these changes, the Eulerian time step should be decreased to account for the instantaneous changes of bubbles numbers and locations due to the interaction mechanisms.

5.3.2 Code algorithm

The code algorithm when considering all bubbles interaction mechanisms, including collision, coalescence and breakup is illustrated at figure 5.33. We can observe that this flow chart is very similar to that of figure 5.13. The difference between them is the test for the coalescence probability in the collision model, and the test for the breakup mechanism for all the bubbles which is handled every Lagrangian time step. As was mentioned before for the bubbles that had coalescence one of them is deleted from all the calculation and to care for the physical behavior of the coalescence mechanism. We record for every bubble that had coalescence a real number that represents the duration of the coalescence. This number is reduced by Lagrangian time step every Lagrangian time step and is used to prevent the bubble from coalescence or breakup at this duration tile the coalescence duration is ended. And so in the breakup, when the bubble have a probability for breakup, the same bubble index and a new bubble index are stored as the bubbles resulting from the breakup mechanism, also the breakup duration is recorded to prevent both bubbles from and coalescence or breakup during the breakup mechanism as they are still in a state of instability and to take in account the physical behavior of the bubble breakup.

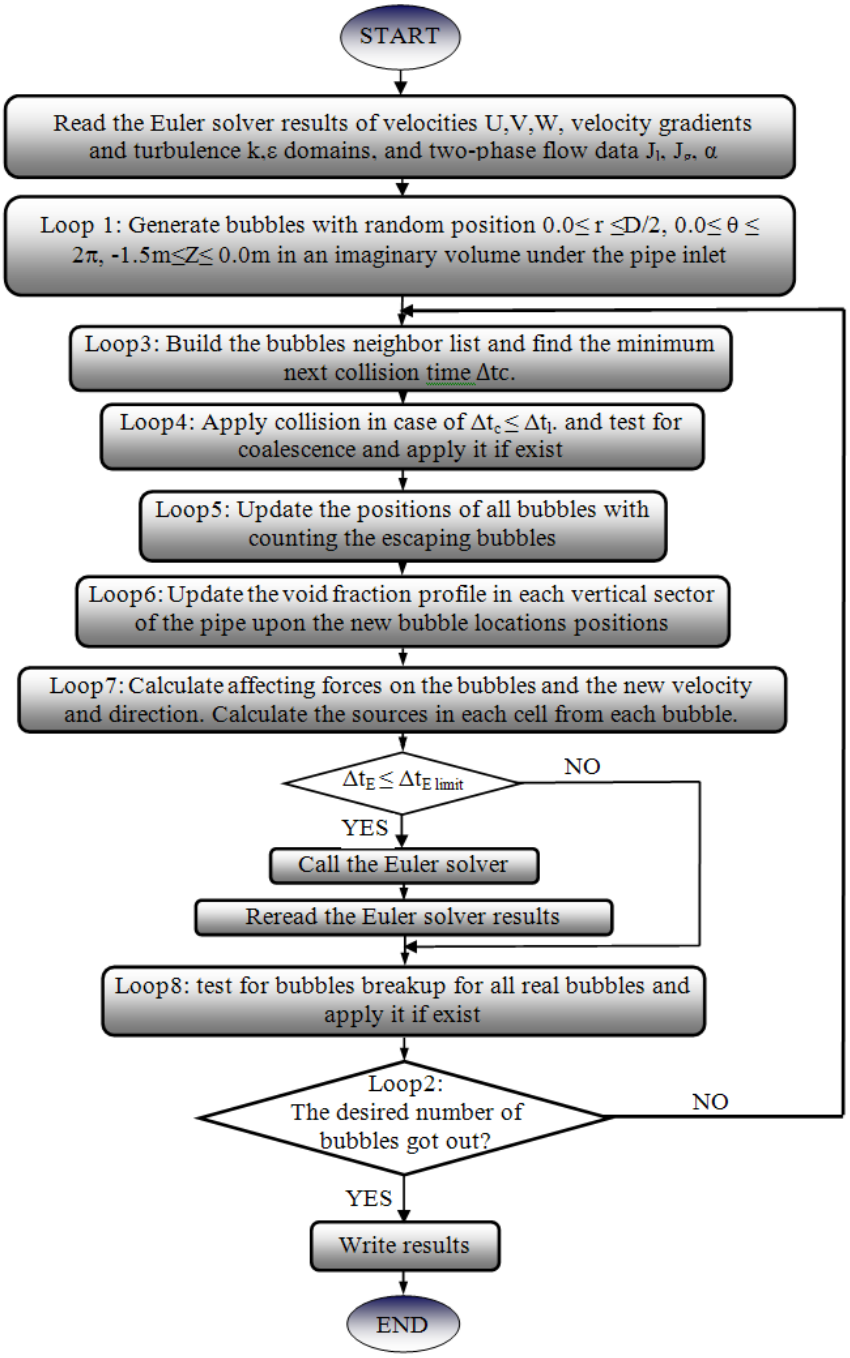

Figure 5.33. The flow chart for the Two-way coupling process considering bubbles collisions, coalescence and breakup.

5.3.3 Results and discussion

When considering both the coalescence and the breakup, the computational effort increases dramatically due to the test for the bubbles breakup and applying it at each Lagrangian time step, this will be explained in more details later at this chapter in the computational time discussion. So, only the case F01AG01 was simulated because it has the smallest gas hold up of 5%. During the simulation, the computational time indeed reached about one month only to get about 140 bubbles from the outlet of the pipe. So outlet profiles were considered for a height of 10 cm at the top of the pipe. In the current case, the displayed profiles are calculated at a specific instant and not averaged for lack of computational time that can cause some fluctuations in the profiles as will be shown. Figure 5.34 shows the simulation profiles of gas void fraction, gas velocity, gas IAC, and average bubble diameter compared with experimental data and the past simulation with collision only.

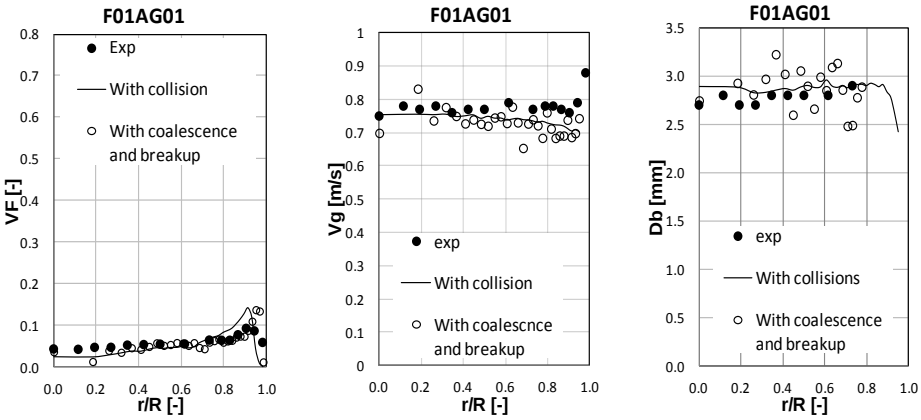

Figure 5.34. Gas void fraction (VF), Gas vertical velocity (Vg), and Bubble mean diameter (Db) radial distributions at considering both coalescence and breakup interaction mechanisms.

As shown at figure 5.34, the void fraction profiles seem to agree with the experimental one although we have instantaneous profile of void fraction. Also we can observe that the consideration of the breakup enhanced the void distribution at the gradient region near the wall. For the gas velocity profiles Vg, we can see that the average velocity of the simulated bubbles have a good agreement with the experimental data and the simulations of collision only. As was mentioned before, a small number of bubbles was used for calculating these profiles, which caused the profile to be irregular. For the averaged bubble diameter profile, we can find good agreement with the Sauter mean diameter represented by the experimental profile and with the collision simulations

with appearance of some peaks and bottoms caused by the averaging process and the variety of the bubble sizes. Generally, we can find that the tendency of the computed profiles are very good compared with the experimental data, which proves the good representation of the breakup and coalescence models used for the bubbles diameters.

As the profiles were calculated for the top 10cm of the bubbles, these results can be considered as a good agreement with the experimental data. Also as the simulation used here is unsteady, this need a lot of real simulated time tile at least 6000 bubbles exit from the outlet at the Monte Carlo simulations as the simulation cases presented before. At these simulations, only 140 bubbles got out and there were no opportunity to extend the simulation for longer time. To see the effect of the breakup and coalescence process on the bubbles diameter and also to see the unsteady effect of the simulation, figure 5.35 shows the bubbles near the entrance and the exit represented with its sizes of the bubbles.

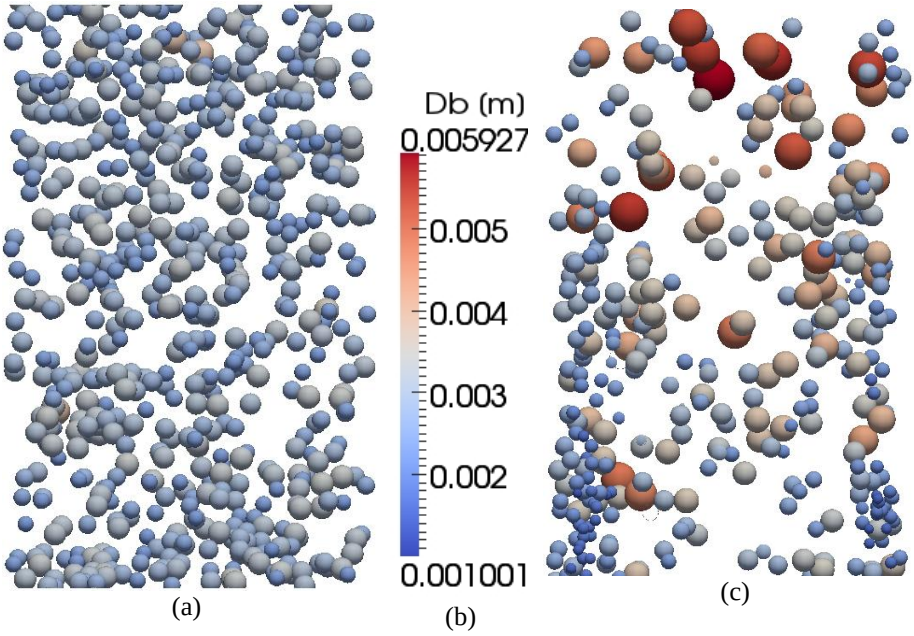

Figure 5.35. Breakup and coalescence effects on particle sizes at the pipe input and output for window of 0.08m height. Flow direction is upward. (a) Particles at pipe input, (b) Legend color map, (c) Particles at pipe outlet.

As we can see at figure 5.35, the effect of the breakup and coalescence effects is clear as at the outlet region appear smaller and larger bubbles in comparison with the bubble sizes at the inlet region.

As the Lagrangian simulations of bubbly flow tracks each bubble and calculates the acts over it like the velocity change, the coalescence and the breakup. This type of simulations could provide us with the number of the breakups and coalescences during the simulation. This ability is not available in many of the methods used for simulating bubbly flow problems. Figure 5.36 indicates the number of coalescences and breakups of the bubbles that occurred during this simulation at five different vertical levels of the pipe. We can observe from figure 5.36 the increase of the number of coalescences and breakups as the bubbles rise upward in the pipe. Also we can find clearly that the number of the breakups is much more than that of the coalescences. This can explain that as the number of breakups is more than that of coalescences, this in turn increases the rates of coalescences and breakups when the bubbles rise upward as the density of the bubbles increases. At the upper level, we can find that the number of coalescences and breakup starts to decrease. This is due to the insufficient calculation time that the number of the bubbles at the upper level is not as dense as that below it and hence the numbers of coalescences and breakups are lower.

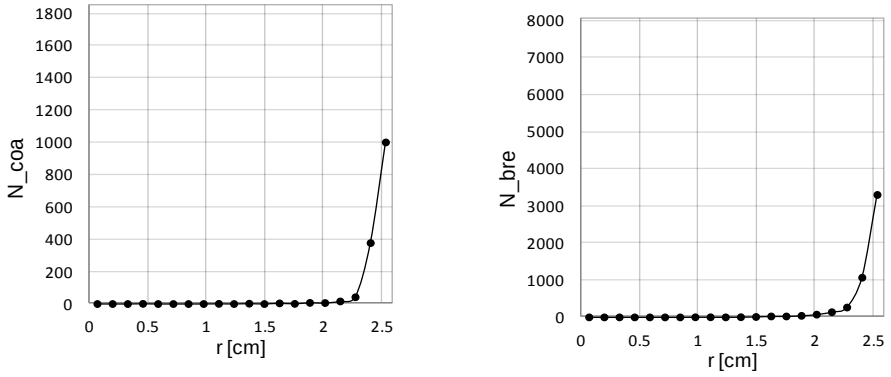

(a)

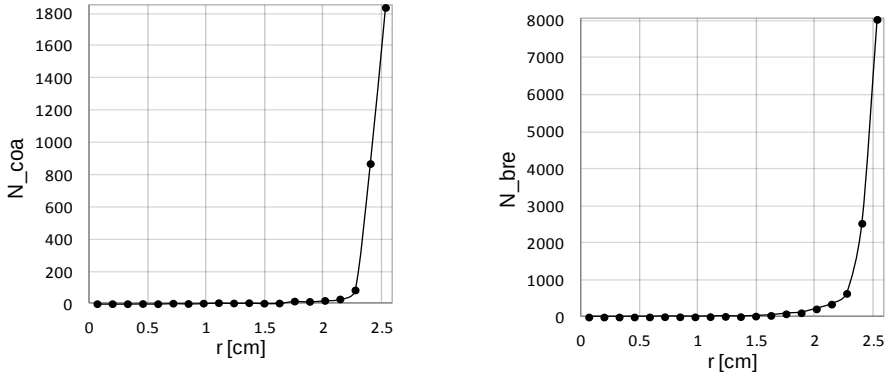

(b)

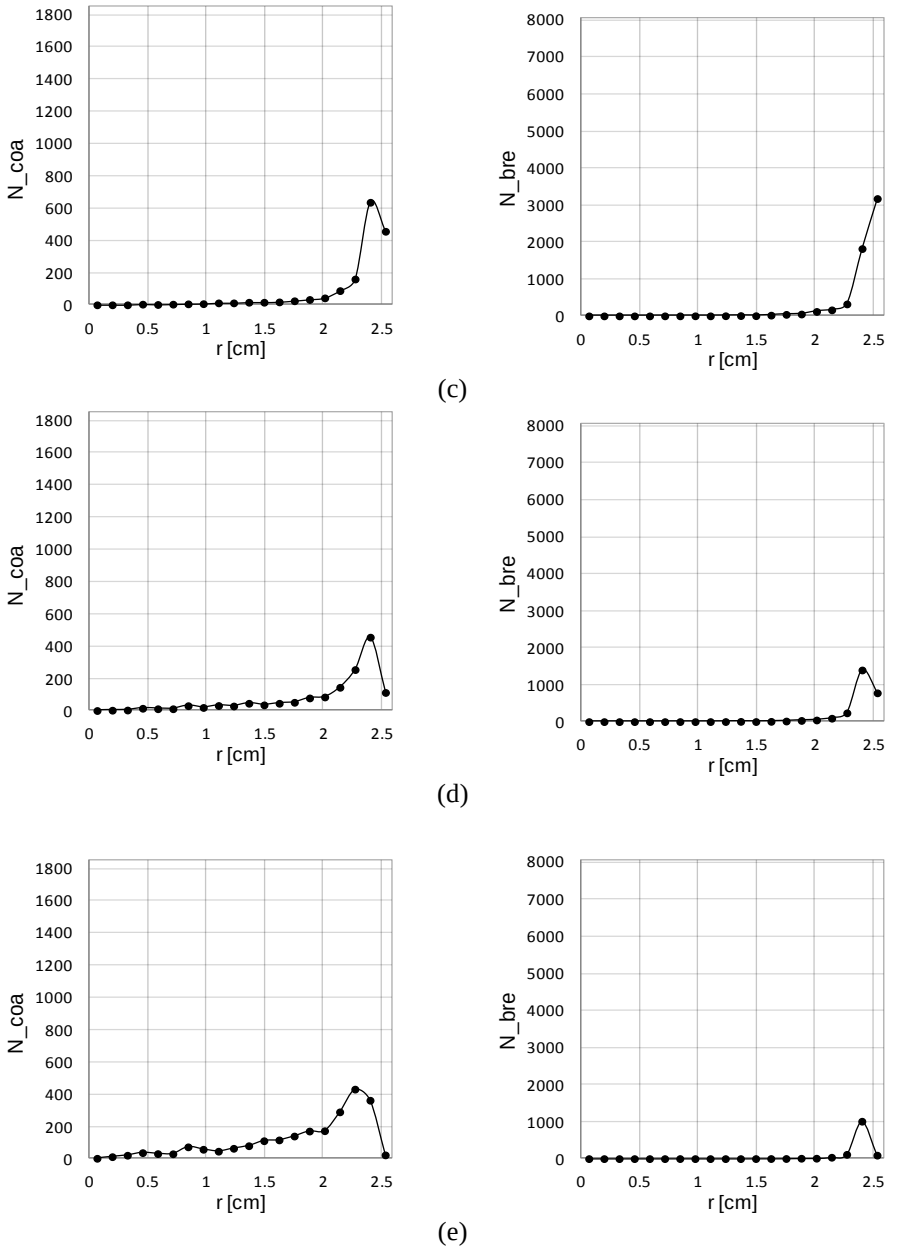

Figure 5.36. The radial distributions of the total number of coalescences at the left side and the total number of breakups at the right side during the simulation period of 1.353 seconds. (a) For height 0.8m<z<1.0m, (b) For height 0.6m<z<0.8m, (c) For height 0.4m<z<0.6m, (d) For height 0.2m<z<0.4m, (e) For height 0.0m<z<0.2m.

Figure 5.37 shows the radial profiles of the turbulence kinetic energy K and the turbulence dissipation rate ε at five vertical levels for the breakup simulation compared with the past simulation of considering collision only. This can show clearly the increase of the turbulence kinetic energy and the dissipation rate due to the increase in the bubbles density as the bubbles go upward.

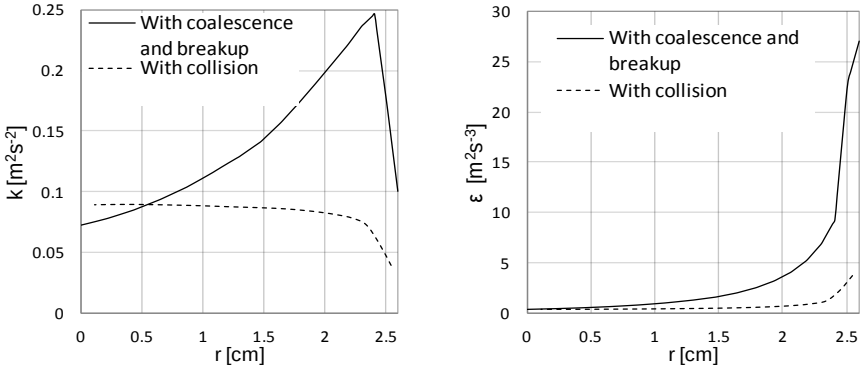

(a)

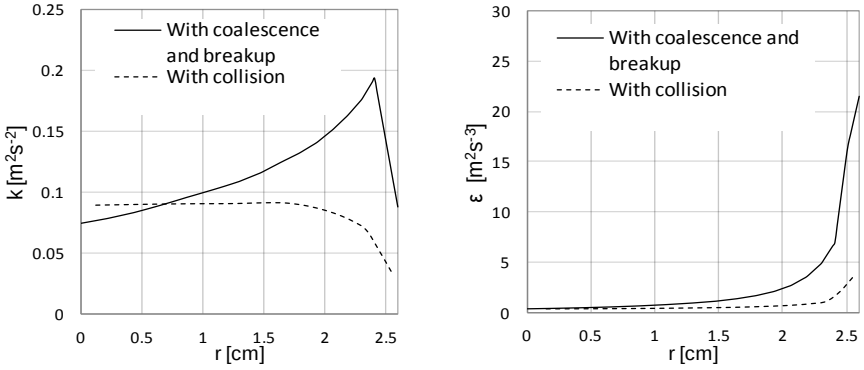

(b)

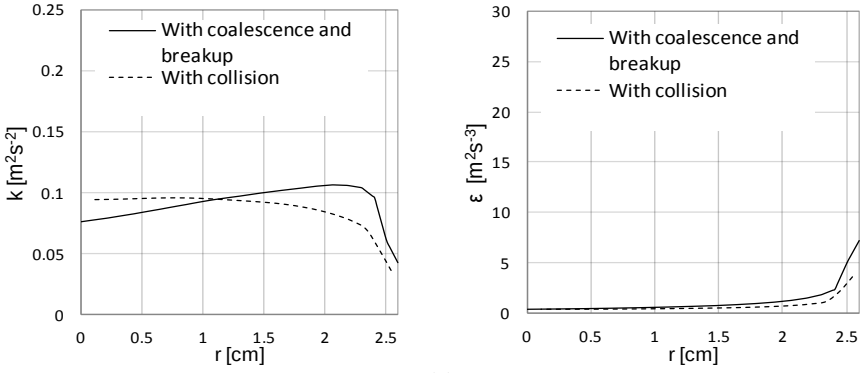

(c)

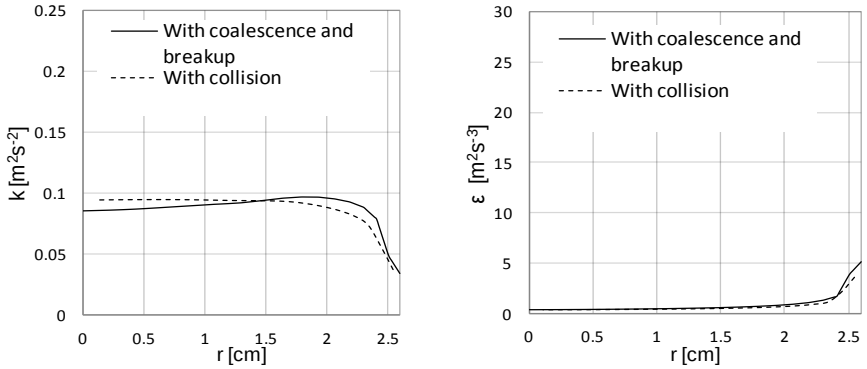

(d)

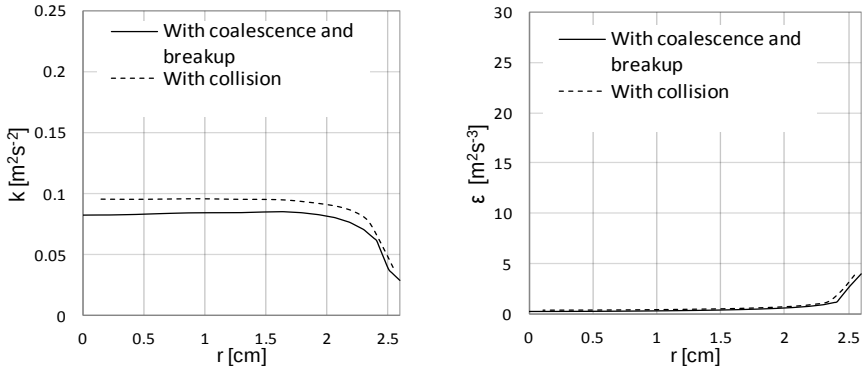

(e)

Figure 5.37. K at the left side and ε at the right side (a) For height z=0.9m, (b) For height z=0.7m, (c) For height z=0.5m, (d) For height z=0.3m, (e) For height z=0.1m.

For the lower level we can see no much difference between the two simulations. Moving upward in the pipe, both k and ε increase at the region close to the wall at which large numbers of small bubbles exist. This can explain the void fraction peak very close to the wall. With this new behavior arise the need for considering an induced turbulence due to the interaction mechanisms of collisions and breakups to simulate the physical behavior of the bubbles interactions. For the lack of experimental data about turbulence, the results could not be testes experimentally but we could see the agreement in the void fraction profiles and gas velocity.

For the simulation of the bubbly flow case F01AG01 when considering the interaction mechanisms between the bubbles including bubbles collisions, coalescences and breakups, the Lagrangian model under study could give a good agreement with the experimental data for the void fraction and the average bubble diameter distribution at the outlet of the pipe. The distribution of the gas vertical velocity is fluctuating due to the insufficient number of the bubbles which have been used for calculating this

distribution but in general the values coincide with the experimental data. We could also see clearly the effect of the applied models of coalescence and breakup in changing the bubbles diameter near the entrance and the exit of the pipe.

One important tool in the Lagrangian particle tracking models is that it can specify accurately the locations of collisions, coalescences and breakups of the bubbles which can give us an estimation of the locations at which this mechanism is predicted to occur with high or low frequency. As a final comment on the results of considering the breakup mechanism, the distributions were not very fine as the simulation time was not sufficient and the number of the exiting bubbles from the pipe was not sufficient to give a smooth distribution, especially that we are using a Monte Carlo statistical method. The computational time was the main obstacle which caused this problem. This is suggested to be solved by parallelizing the code as the computers used was already multi core that can be used with this option.

5.4 Calculation time discussion

In this section we will present a brief discussion for the time consumed in the calculations of the simulated cases. The computer used for the current calculations is a processor of type Intel Core 2 quad CPU Q9550 with 2.83Ghz cash and 12.00Gb of RAM. Table 5.1 shows the calculation time in hours for the two-way coupling process with different considerations.

Table 5.1. Computational time comparison between different runs in hours.

	clear	collision	coalescence	Coalescence & Breakup
F01AG01	10.66	19.35	318.32 for t_phy=1.286 s	586.35 for t_phy=1.353 s
F01AG02	-	-	-	-
F01AG03	11.61	33.17	-	-
F02AG01	15.25	45.61	-	-
F02AG02	-	-	-	-
F02AG03	15.66	40.78	-	-
F03AG01	30.15	57.77	-	-
F03AG02	39.72	-	-	-
F03AG03	56.86	-	-	-

In table 5.1, the title clear refers to the two-way coupling process clear from any interaction considerations, the title collision refers to the process when considering bubbles collisions, the title coalescence refers to considering collision and coalescence both, and finally the title Coalescence & Breakup refers to considering all the

interaction mechanisms of the bubbles including collision, coalescence and breakup. For the coalescence case, the physical time of the simulation period was of 1.286 seconds and for the coalescence & breakup case, the physical time of the simulation period was of 1.353 seconds. However the other simulations of the same case were calculated for 2.4 seconds of the real simulation time. We can observe that the increase in the calculation time between the different cases is exponential if we compared increasing the void fraction from G01 to G03 or adding more interaction mechanisms especially for high void fraction cases. The main mechanisms that increase the computational time dramatically are the coalescence and breakup as can be observed from the computational time durations in table 5.1. We plotted the calculation time for different cases for comparison between the clear and collision conditions in table 5.1. The plot is shown at figure 5.38.

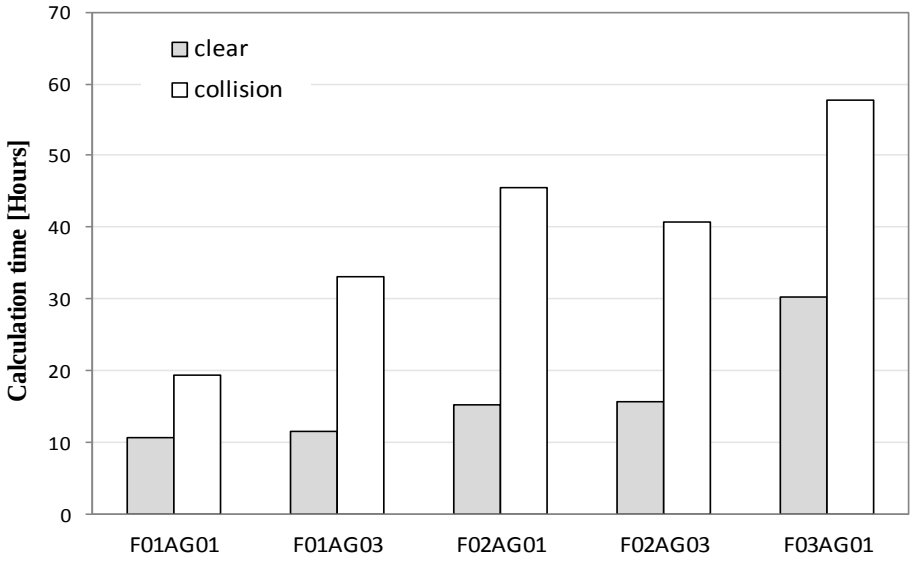

Figure 5.38. Calculation time comparison between two-way coupling with and without collision.

From figure 5.38, it is obvious that considering the collision process in the simulation take a great computational effort especially for higher gas hold up. And the percent of increase is exponential as the collision frequency depends on the density of the bubbles in a place which increases proportionally with the gas hold up. Also we can observe that as the liquid velocity increases, the computational time increases and the frequency of collisions between bubbles increase with the velocity of the bubble which is proportional to the liquid velocity.

6. Conclusions and Future Work

In this chapter, the general conclusions from the present research work are presented. Then the research area that needs more investigation in the future in the related work is introduced.

6.1 Conclusions from the present work

6.1.1 One-way coupling

- It was found that the k_{BIT} was necessary to be a function of the bubble properties like the relative velocity and diameter and moreover function of the void fraction of the gas at the location of the bubble. The best dependence on the gas void fraction was found to be a function of the absolute value of the gas void fraction gradient at the radial direction divided by the value of the gas void fraction. This relation found to give good agreement with experimental data for the one-way coupling process. On the other hand, the lift force coefficient developed by Tomiyama (1998) was found to give higher vales which causes high peak of the gas void fraction close to the pipe wall. A smaller constant lift coefficient of 0.07 was used that was found to fit the test cases under study. The presented test cases for the one-way coupling process ranged from liquid velocity of 0.5m/s to 2 m/s and gas hold up from 5% up to 15%.

6.1.2 Two-way coupling

- The vorticity of the liquid velocity decreased as a result of the two-way coupling application. It was necessary to increase the value of the lift force coefficient again taking the relation of Tomiyama (1998).

- Using the same relation of the $S_{BIT,k}$ proposed in the one-way coupling process, with different values for the $S_{BIT,k}$ coefficient C_{tb} of 0.02, 0.025, 0.035, and 0.06 were used to adjust the void fraction profiles. The value of C_{tb}=0.035 was found to give the best of all these values. However, it was found that although adjusting the values of C_{tb} changes the distribution beside the wall and can control the peak, however, it had no effect on the distribution of the gas void fraction at the pipe center which was lower than the experimental one. This problem thought to be caused by two factores. The first is the dependence of the $S_{BIT,k}$ on the gradient of the gas void fraction which normally has a zero value at the pipe center and as a result it does not give a considerable value for

the $S_{BIT,k}$ at the pipe center. The second and most important is that this dependence of the $S_{BIT,k}$ on the gas void fraction was considered in the one-way coupling process as the continuous phase does not feel the effect of the dispersed phase. However, in the two-way coupling, the effect of the bubbles is considered in the source terms and volume fraction of the conservation equations by the averaging introduced at equation (5.7). So, it was not necessary to consider the dependence of the $S_{BIT,k}$ relation on the void fraction in the two-way coupling process as it is already considered in the averaged interaction source term at equation 5.14. So we decided to delete the term of the void fraction dependence from the $S_{BIT,k}$ relation but before that, it was preferred to see the effect of the bubbles collision on the void fraction distribution. The Lagrangian code was modified for calculating the collisions between bubbles. It was found that for low gas holdups, the collision effect is negligible and for high hold ups it was very small. So, it was decided to make the study of the new $S_{BIT,k}$ relation on the code by considering bubbles collision.

- The $S_{BIT,k}$ relation was changed to be dependent only on the relative velocity of the bubble and the bubble diameter at relation (5.16). When the new $S_{BIT,k}$ relation had been used, it was found an enhancement in the gas void fraction distribution at the pipe center. Adjusting the coefficient C_{tb} for the new relation, it was found finally that the value of the coefficient C_{tb} should be 0.5 which gave good agreement with the cases under study for liquid velocities 0.5, 1.0, and 2.0m/s and for gas holdups of 5%, 10% and 15%.

- Considering the different interaction mechanisms including collisions, coalescences and breakup, there was no need to adjust the relations of the lift force coefficient or the $S_{BIT,k}$. And the results of considering the interaction mechanisms with the last proposed $S_{BIT,k}$ relation were successfully applied.

- It was found that considering the coalescence mechanism without the breakup mechanism causes the increase of the bubbles size dramatically and gives a peak in the void fraction profile distribution at the center of the pipe which does not agree with experimental data.

6.1.3 CRW model

- One of the principal new investigation points presented in this thesis is the use of the CRW model in the simulations of two phase bubbly flows. Following the work presented by Muñoz-Cobo et al (2012), we could apply the presented CRW model successfully to generate the fluctuation velocity of the bubble as a function of the turbulence properties of the liquid. For using the CRW model the turbulence dispersion force modeling was neglected as force acting on the bubble which does not give physical sense and needs adjustment with different cases. Using this model, we could recover the fluctuations of liquid phase that was lost in the RANSD averaging process and hence make use of it in getting a more physical behavior of the bubbles under the action of the different forces generated by the liquid phase.

- In this work, the $S_{BIT,k}$ was used as a relation that is convenient for both the k-ε turbulence model, and the CRW model. It was shown from results that the adjusted relation of the $S_{BIT,k}$ was successfully applied and the CRW was taking the total turbulence properties into account to generate the fluctuations.

6.1.4 New features in bubbly flow simulations

- The Euler-Lagrangian coupled model could display some important issues that are not available in many of the models for the bubbly flow simulations. This includes the ability of the Lagrangian models to show the locations at which collisions of bubbles occur, locations of bubbles coalescences and breakup individually with unsteady nature. This in turn adds a new tool for the bubble flow simulations with large number of bubbles. It was found that the number of collisions, coalescences and breakup increases with advancement upward in the pipe. This was due to the increase of the number of bubbles because normally the rate of the breakup is larger than that of coalescence and as the turbulence dissipation increases upward, then the breakup rate increases.

- Finally, this new model is considered as a 3D virtual laboratory that can show all the variables of the moving bubbles instantaneously. This includes the ability to have information about the different forces acting on each bubble, change of velocity and velocity fluctuations of the bubbles, interaction mechanisms among the bubbles. This ability is not available in many models that handle moderate number of bubbles at acceptable computational time that can be used in the market for some applications that needs information about the locations and times of different interaction mechanisms. This model can be considered a smart tool for testing different models for the physical behavior of the bubbles moving in a continuous phase.

6.2 Future Work

There are some areas that need further investigation in the current work which are as follows:

- One of the main problems found in the coupled Eulerian-Lagrangian simulation under study was the time consumed in the computation especially when considering the bubbles interaction mechanisms. So, this code need to be parallelized in order to minimize the calculation time especially as the computers nowadays have multi core processors.

- The CRW model under consideration needs some enhancement under considerations of the change of the particle size due to bubbles coalescence and breakup processes especially for changing the spherical bubble to account for the applications of slug and cap bubbles.

- The turbulence model used in the present simulations for the continuous phase was the standard $k-\varepsilon$ model which was not very good in solving the wall bounded flows. So, it needs some enhancement in the Euler solver model to be upgraded to the RNG-$k-\varepsilon$ model for example.

- One main point that needs extra investigation is that of the BIT effect to be adequate for larger range of experiments.

- Enhancement Study should be made for the lift force coefficient presented by Tomiyama that was made initially for single bubble and as a result of changing this; the bubble induced effect will be adjusted to a more correct one.

- The code presented at this work was capable of simulating the bubbly flow perfectly. This allows extending the code to account for the boiling and condensation problems which will consider the matter of the generating the vapor bubbles from the boiling surface and condensation of the vapor bubbles through the liquid.

Allen, M.P., Tildesley, D.J., 1987. “Computer Simulation of Liquids”. Oxford Science Publications, Oxford.

Alopaeus, V., Keskinen, K. I., Koskinen, J., Majander, J., Pitkänen, H., Holma, H., 2002a. Gas–liquid stirred tank reactor modeling with CFD and user subroutines. A.I.Ch.E. Annual Meeting, Indianapolis, IN, November 3–8.

Alopaeus, V., Koskinen, J., Keskinen, K. I., Majander, J., 2002b. Simulation of the population balances for liquid–liquid systems in a nonideal stirred tank. Part 2 Parameter fitting and the use of the multiblock model for dense dispersions. Chem. Eng. Sci. 57, 1815–1825.

Andrews, M.J., O'Rourke, P.J., 1996. The multiphase particle-in-cell (MF-PIC) method for dense particulate flows. Int. J. Multiphase Flows 22, 379-402.

Antal, S. P., Lahey, R. T., Jr., & Flaherty, J. E., 1991a. Analysis of phase distribution and turbulence in dispersed particle/liquid flows. Chemical Engineering Communications, 174, 85–113.

Antal, S.P., Lahey Jr, R.T. and Flaherty, J.E., 1991b. Analysis of Two Phase Flow Distribution in Fully Developped Laminar Bubbly Two-Phase Flow. Int. J. Multiphase Flow 17, 635-652.

Apte, S. V., Mahesh, K., Moin, P., Oefelein, J. C., 2003. Large-eddy simulation of swirling particle-laden flows in a coaxial-jet combustor. Int. J. Multiphase Flow 29 (8), 1311–1331.

Arnold, G.S., 1988. Entropy and objectivity as constraints upon constitutive equations for two-fluid modeling of multiphase flow. Ph.D. thesis, Rensselaer Polytechnic Institute, Troy, New York.

Auton, T.R., 1987. The Lift Force on a Spherical Body in a Rotational Flow. Journal of Fluid Mechanics, 183, 199-218.

Batchelor, G.K., 1956. “The Theory of Homogeneous Turbulence”. Cambridge University Press, London.

Bocksell, T.L., Loth, E., 2006. Stochastic modelling of particle diffusion in a turbulent boundary layer. Int. J. Multiphase Flow 32, 1234-1253.

Burns, A.D., Frank,T., Hamill, I., Shi, J.-M. 2004. The Favre averaged drag model for turbulence dispersion in Eulerian multi-phase flows. Fifth International Conference on

Multiphase Flow. ICMF (2004),Yokohama, Japan. 392.

Buwa, V. V., Deo, D. S., Ranade, V. V., 2006. Eulerian–Lagrangian simulations of unsteady gas–liquid flows in bubble columns. International Journal of Multiphase Flow, 32, 864–885.

Carrica, P.M., Drew, D., Bonetto, F., Lahey Jr, R.T., 1999. A polydisperse model for bubbly two-phase flow around a surface ship. International Journal of Multiphase Flow 25, 257–305.

CFX-solver modeling guide http://www.ansys.com

Chappelear, D.C., 1961. Models of a liquid drop approaching an interface. Journal of Colloid Science 16, 186–190.

Chatzi, E., 1983. Analysis of Interactions in Fluid-Fluid Dispersion Systems in Agitated Vessels. Cleveland State University Press, Cleveland, OH.

Chatzi, E., Gavrielides, A. D., Kiparissides, C., 1989. Generalized model for prediction of the steady-state drop size distributions in batch stirred vessels. Ind. Eng. Chem. Res. 28, 1704–1711.

Chatzi, E., Kiparissides, C., 1992. Dynamic simulation of bimodal drop size distributions in low-coalescence batch dispersion systems. Chem. Eng. Sci. 47, 445–456.

Chesters, A.K., 1975. The applicability of dynamic-similarity criteria to isothermal, liquid–gas, two-phase flows without mass transfer. International Journal of Multiphase Flow 2, 191–212.

Chesters, A.K., 1991. The modelling of coalescence processes in fluid-liquid dispersions: a review of current understanding. Trans. IchemE, 69, 259-270.

Chesters, A.K., Hofman, G., 1982. Bubble coalescence in pure liquids. Applied Scientific Research 38, 353–361.

Climent, E., Magnaudet, J., 1999. Large-scale simulations of bubble- induced convection in a liquid layer. Physical Review Letters, 82, 4827–4830.

Coffey, W. T., Kalmykov, Yu. P., Waldron, J. T., 2004. The Langevin Equation: With Applications To Stochastic Problems in Physics, Chemistry And Electrical Engineering". World Scientific Publishing Co. Pte. Ltd.

Coulaloglou, C.A., 1975. Dispersed phase interactions in an agitated flow vessel. Ph.D.

Dissertation, Illinois Institute of Technology, Chicago.

Coulaloglou, C.A., Tavlarides, L.L., 1977. Description of interaction processes in agitated liquid–liquid dispersions. Chemical Engineering Science 32, 1289–1297.

Crowe, C.T., Sharma, M.P., Stock, D.E., 1977. The particle-source-in-cell (PSI-cell) method for gas-droplet flows. J. Fluids Eng. 99, 325–332.

Csanady, G. T., 1973. "Turbulent Diffusion in the Atmosphere", D. Reidel Publ. Co., Dordrecht, Holland.

Cundall, P.A., Strack, O.D.L., 1979. A discrete numerical model for granular assemblies. Geotechnique, 29, 47–65.

Darmana, D., Deen , N.G., Kuipers, J.A.M., 2006. Parallelization of an Euler–Lagrange model using mixed domain decomposition and a mirror domain technique: Application to dispersed gas–liquid two-phase flow. Journal of Computational Physics 220, 216–248.

Das, P.K., Kumar, R., 1987. Coalescence of drops in stirred dispersion. A white noise model for coalescence. Chemical Engineering Science 42, 213–220.

Davis, R.H., Schonberg A. J., Rallison, M. J., 1989. The lubrication force between two viscous drops. Physics of Fluids A 1, 77–81.

Deen, N.G., Van Sint Annaland, M., Kuipers, J.A.M., 2004. Multi-scale modeling of dispersed gas–liquid two-phase flow. Chemical Engineering Science 59, 1853–1861.

Dehbi, A., (2008). Turbulent particle dispersion in arbitrary wall-bounded geometries: a coupled CFD-Langevin-equation based approach. Int. J. Multiphase Flow, 34, 819–828.

Delnoij, E., Lammers, F. A., Kuipers, J. A. M., Van Swaaij, W. P. M., 1996. Dynamic simulation of dispersed gas-liquid two-phase flow using a discrete bubble model. Chemical Engineering Science, 52, (9), 1429-1458.

Dolfyn input Guide, December 2008 "http://www.dolfyn.net/".

Doubliez, L., 1991. The drainage and rupture of a non-foaming liquid film formed upon bubble impact with a free surface. International Journal of Multiphase Flow 17, 783–803.

Drew, D. A., Lahey, R. T., Jr., 1979. Application of general constitutive principles to the derivation of multi-dimensional two-phase flow equation. International Journal of

Multiphase Flow, 5, 243–264.

Duineveld, P.C., 1994. Bouncing and coalescence of two bubbles in water. Ph.D. Dissertation, University of Twente, The Netherlands.

Durbin, P. A., 1980. A Random Flight Model of Inhomogeneous Turbulent Dispersion', Phys. Fluids 23, 2151-2153.

Eastwood, C., Cartellier, A., Lasheras, J.C., 2000. The break-up time of a droplet in a fully developed turbulent flow. In: Advances in Turbulence VIII, Proceedings of the Eight European Turbulence Conference. Barcelona, pp. 573– 576.

Einstein, A., Fürth, R. H.., 1954. Investigations on the Theory of the Brownian Movement, Methuen, London, 1926; reprinted Dover, New York,.

Elghobashi, S., Truesdell, G., 1993. On the two-way interaction between homogeneous turbulence and dispersed solid particles I: Turbulence modification. Physics of Fluids ,A 5, 1790–1801.

Ervin, E.A., Tryggvason, G., 1997. The rise of bubbles in a vertical shear flow. Journal of Fluids Engineering. 119, 443–449.

Farzpourmachiani, A., Shams, M., Shadaram, A., Azidehakb, F., 2011. Eulerian–Lagrangian3-Dsimulationsofunsteadytwo-phasegas–liquidflow in a rectangular column by considering bubble interactions. International Journal of Non-Linear Mechanics, 46 , 1049–1056.

Frank, Th., Shi, J. M., Burns, A. D., 2004. Validation of Eulerian Multiphase Flow Models for Nuclear Safety Applications. 3rd International Symposium on Two-Phase Flow Modelling and Experimentation, Pisa, Italy, 22-24, Sept. 2004.

Frank, Th., Zwart, P. J., Krepper, E., Prasser, H. -M. and Lucas, 2008. Validation of CFD models for mono- and polydisperse air-water two-phase flows in pipes. J. Nuclear Engineering & Design, 238, 647–659.

Garg, R., Narayanan, C., Lakehal, D., Subramaniam, S., 2007. Accurate numerical estimation of interphase momentum transfer in Lagrangian–Eulerian simulations of dispersed two-phase flows. International Journal of Multiphase Flow, 33, 1337–1364.

Grace, J. R., Wairegi, T. and Nguyen, T. H., 1976. Shapes and velocities of single drops and bubbles moving freely through immiscible liquids. Trans. Inst. Chem. Engin, 54, 167-173.

Guan, H. Y., and Jiyuan Tu, 2010. “Computational Techniques for Multi-phase Flows”. Elsevier Ltd, ISBN: 978-0-08046-733-7.

HAN Luchang , CAO Yang , WU Xuewen , BAI Ge , LIU Yuejin, 2010. The Effect of Eddy-bubble Interaction Model on the Turbulent Dispersion of Gas Bubbles in Stirred Tanks. Chinese Journal of Chemical Engineering, 18(1), 27-33.

Haselbacher, A., Najjar, F. M., Ferry, J. P., 2007. An efficient and robust particle-localization algorithm for unstructured grids. Journal of Computational Physics. 225 (2), 2198–2213.

Hasseine, A., Meniai, A.-H., Lehocine, M. B., Bart, H.-J., 2005. Assessment of drop coalescence and breakup for stirred extraction columns. Chemical Engineering and Technology 28, 552–560.

Hibiki, T., Ishii, M., 1999. Experimental study on interfacial area transport in bubbly two-phase flows. International Journal of Heat and Mass Transfer 42, 3019–3035.

Hibiki, T., Ishii, M., 2007. Lift force in bubbly flow systems. Chemical Engineering Science 62, 6457 – 6474.

Hibiki, T., Ishii, M., Xiao, Z., 2001. Axial interfacial area transport of vertical bubbly flows. International Journal of Heat and Mass Transfer 44, 1869–1888.

Hibiki, T., Situ, R., Mi, Y., Ishii, M., 2003. Local flow measurements of vertical upward bubbly flow in an annulus. International Journal of Heat and Mass Transfer 46, 1479–1496.

Hinze, J.O., 1955. Fundamentals of the hydrodynamic mechanism of splitting in dispersions processes. AICHE J,1(3), 289-295.

Hirt, C.W., Nichols, B.D., 1981. Volume of fluid (VOF) method for the dynamics of free boundaries". J. Comp. Phys. 39, 201–225.

Hoomans, B. P. B., Kuipers, J. A. M., Briels, W. J., Van Swaaij, W. P. M., 1996. Discrete Particle Simulation Of Bubble And Slug Formation In A Two-Dimensional Gas-Fluidised Bed: A Hard-Sphere Approach. Chemical Engineering Science, 51, (1),99-118.

Hosokawa, S., Tomiyama, A., Misaki, S., Hamada,T., 2002. Lateral migration of single bubbles due to the presence of wall. Proceedings of ASME Fluids Engineering Division Summer Meeting, Montreal, Quebec, Canada.

Howarth, W.J., 1964. Coalescence of drops in a turbulent flow field. Chemical Engineering Science 19, 33–38.

Hu, S. and Kintner, R. C, 1955. The fall of single liquid drops through water. AICHE Journal, 1, 42-50.

Huilin, L., Zhiheng, S., Ding, J., Xiang, L., Huanpeng, L., 2006. Numerical simulation of bubble and particles motions in a bubbling fluidized bed using direct simulation Monte-Carlo method. Journal of Powder Technology. 169, (3), 159-171.

Ishii, M., 1975. Thermo-fluid dynamic theory of two-phase flow. Collection de la Direction des Etudes et Recherches d'Electricite de France, Eyrolles, Paris, France.

Ishii, M., Zuber, N. 1979. Drag coefficient and relative velocity in bubbly, droplet or particulate flows. AIChE Journal, 25, 843–855.

Jeelani, S.A.K., Hartland, S., 1991. Effect of approach velocity on binary and interfacial coalescence. Chemical Engineering Research and Design: transactions of the institution of chemical engineers: Part A 69, 271–281.

Jeffreys, G.V., Davies, G.A., 1971. Coalescence of Liquid Droplets and Liquid Dispersion: Recent Advances in Liquid–Liquid Extraction, 1st ed Pergamon Press, Oxford, UK, p. 495.

John, K. E., 2009. Two-way coupled turbulence simulations of gas-particle flows using point-particle tracking. International Journal of Multiphase Flow, 35, 792–800.

Johnson, A. I., and Braida, L., 1957. The velocity of fall of oscillating and circulating liquid drops through quiescent liquid phases. Can. J. Chem. Eng., 35, 165-172.

Kallio, G.A., Reeks, M.W., 1989. A numerical simulation of particle deposition in turbulent boundary layers. Int. J. Multiphase Flow 3, 433–446.

Kamp, A.M., Chesters, A.K., 2001. Bubble coalescence in turbulent flows: A mechanistic model for turbulence-induced coalescence applied to microgravity bubbly pipe flow. International Journal of Multiphase Flow, 27, 1363–1396.

Kariyasaki, A., 1987. Behavior of a single gas bubble in a liquid Flow with a linear velocity profile. In. Proceedings of the 1987 ASME-JSME Thermal Engineering Joint Conference, 261-267.

Kataoka, I., Serizawa, A., 1989. Basic equations of turbulence in gas–liquid two-phase flow. International Journal of Multiphase Flow, 15, 843–855.

Kitagawa, A., Murai, Y., Yamamoto, F., 2001. Two-way coupling of Eulerian–Lagrangian model for dispersed multiph9ase flows using filtering functions, International Journal of Multiphase Flow 27 , 2129–2153.

Kolmogorov, A.N., 1949. On the breakage of drops in a turbulent flow. Dokl. Akad. Navk. SSSR 66, 825–828.

Konno, M., Matsunaga, Y., Arai, K., Saito, S., 1980. Simulations model for break-up process in an agitated tank. J. Chem. Eng. Jpn. 13, 67–73.

Krepper, E., Lucas, D., Prasser, H.M. 2005. On the modelling of bubbly flow in vertical pipes. Nucl. Eng. Des. 235, 597–611.

Krepper, E., Lucas. D., Schmidtke, M., 2010. Modelling of Turbulence in Bubbly Flows. ICMF 2010, Tampa, FL USA, May 30-June 4, 2010.

Laín, S., Broder, D., Sommerfeld, M., Goz, M.F., 2002. Modelling hydrodynamics and turbulence in a bubble column using the Euler–Lagrange procedure. International Journal of Multiphase Flow 28, 1381–1407.

Langevin, P., 1908. Sur la Theorie de Mouvement Brownien. C. R. Acad. Sci. Paris, 146, 530.

Lasheras, J.C., Eastwood, C., Martínez-Bazán, C., Montañes, J.L., 2002. A review of statistical models for the break-up of an immiscible fluid immersed into a fully developed turbulent flow. International Journal of Multiphase Flow, 28, 247–278.

Lau, Y. M., Deen, N. G., Kuipers, J. A. M. 2010 .Bubble Breakup in Euler-Lagrange Simulations of Bubbly Flow. 7th international conference on multiphase flow, Tampa, FL, May 30-June 4, 2010.

Launder, B.E., Spalding, B., (1972). “Mathematical Models of Turbulence”. Academic Press, New York.

Lee, C.H., Erickson, L.E., Glasgow, L.A., 1987a. Bubble breakup and coalescence in turbulent gas–liquid dispersions. Chem. Eng. Commun. 59, 65–84.

Lee, C.H., Erickson, L.E., Glasgow, L.A., 1987b. Dynamics of bubble size distribution in turbulent gas–liquid dispersions. Chem. Eng. Commun. 61, 181–195.

Lee, J.C., Hodgson, T.D., 1968. Film flow and coalescence–I Basic relations film shape and criteria for interface mobility. Chemical Engineering Science 23, 1375–1397.

Legg, B.J., Raupach, M.R., 1982. Markov-chain simulation of particle dispersion in

inhomogeneous flows: the mean drift correction induced by a gradient in the Eulerian velocity variance. Bound.-Layer Meteorol. 24, 3–13.

Lehr, F., Mewes, D., 1999. A transport equation for the interfacial area density in two-phase flow. In: Second European Congress of Chemical Engineering, October 5–7, Montpellier, France.

Lehr, F., Millies, M., Mewes, D., 2002. Bubble-size distributions and flow fields in bubble columns. A.I.Ch.E. J. 48, 2426–2443.

Levich, V.G., 1962. Physicochemical Hydrodynamics. Prentice Hall, Englewood Cliffs, NJ.

Liao, Y., Lucas, D., 2010, A literature review on mechanisms and models for the coalescence process of fluid particles, Chemical Engineering Science 65, 2851–2864

Liao, Y., Lucas, D., D., 2009. A literature review of theoretical models for drop and bubble breakup in turbulent dispersions. Chemical Engineering Science. 64. 3389 – 3406.

Liu, T.J., 1993. Bubble size and entrance length effects on void development in a vertical channel. International Journal of Multiphase Flow, 19, 99–113.

Löhner, R., 1995. Robust Vectorised Search Algorithms for Interpolation on Unstructured Grids. J. Comput. Phys. 118 (2), 380–387.

Lopez de Bertodano, M. 1998. Two-fluid model for two-phase turbulent jet. Nuclear Engineering and Design, 179, 65–74.

Lopez de Bertodano, M., 1992. Turbulent bubbly two-phase flow in a triangular duct PhD Dissertation, Rensselaer Polytechnic Institute, New York.

Lopez de Bertodano, M., Lahey Jr., R. T., Jones, O. C., 1994. Phase distribution in bubbly two-phase flow in vertical ducts. Int. J. Multiphase Flow, Vol. 20, (5), 805–818.

Loth, E., Taeibi-Rahni, M., Tryggvason, G., 1997. Deformable bubbles in a free shear layer. International Journal of Multiphase Flow 23, 977–1001.

Luo, H., 1993. Coalescence, breakup and liquid circulation in bubble column reactors. Ph.D. Dissertation, The Norwegian Institute of Technology, Trondheim

Luo, H., Svendsen, F., 1996. Theoretical model for drop and bubble break-up in

turbulent dispersions. AIChE J. 42, 1225–1233.

Mackay, G.D.M., Mason, S.G., 1963. The gravity approach and coalescence of fluid drops at liquid interfaces. Canadian Journal of Chemical Engineering 41, 203–212.

Malin, M. R., 1983. Calculations of intermittency in self-preserving, free turbulent jets and wakes. Imperial College Report CFDU Report CFD/83/10. London: University of London. (1983).

Malin, M. R., Spalding, D. B., 1984. A two-fluid model of turbulence and its application to heated plane jets and wakes. PhysicoChemical Hydrodynamics, 5, 339–362.

Marta Garcia, 2009. Développement et validation du formalisme Euler-Lagrange dans un solveur parallèle et non-structuré pour la simulation aux grandes échelles. Doctoral thesis in the University of Toulouse.

Martínez-Bazán, C., Montañes, J.L., Lasheras, J.C., 1999a. On the break-up of an air bubble injected into a fully developed turbulent flow. Part I: Break-up frequency. J. Fluid Mech. 401, 157–182.

Martínez-Bazán, C., Montañes, J.L., Lasheras, J.C., 1999b. On the break-up of an air bubble injected into a fully developed turbulent flow. Part II: Size pdf of the resulting daughter bubbles. J. Fluid Mech. 401, 183–207.

Martínez-Bazán, C., Rodríguez- Rodríguez, J., Deane, G. B.,J Montañes, J.L., Lasheras, J.C., 2010. Considerations on bubble fragmentation models. J. Fluid Mech. 661, 159–177.

Mattson, M.D., Mahesh, K. 2012. A one-way coupled Euler–Lagrangian simulation of bubble coalescence in a turbulent pipe flow. International Journal of Multiphase Flow 40, 68–82.

Maxey, M. R., Chang, E. J., Wang, L. P. 1994. Simulation of interactions between microbubbles and turbulent flows. Appl. Mech. Rev. 47, No 6S, S70–S74.

Mendez Diaz, S., 2008. Medida Experimental De La Concentración De Area Interfacial , PhD Thesis, Universidad Politécnica de Valencia, Spain.

Meneveau, C., Lund, T.S., Cabot, W. H., 1996. A Lagrangian dynamic subgrid-scale model of turbulence. Journal of Fluid Mechanics, 319, 353–385.

Michael D. L., Mark J. M., 2009. Modeling of bubble coalescence in bubbly co-current

flows restricted by confined Geometry. Chemical Engineering Science 64, 4060 - 4067.

Michaelides, E. E., 2006. "Particles, Bubbles &Drops, Their Motion, Heat and Mass Transfer". World Scientific Publishing, Singapore.

Moraga, F. J., Larreteguy, A. E., Drew, D. A., Lahey Jr, R. T., 2003. Assessment of turbulent dispersion models for bubbly flows in the low Stokes number limit. International Journal of Multiphase Flow, 29, 655–673.

Moraga, F.J., Bonetto, F.J., Lahey, R.T., 1999. Lateral forces on spheres in turbulent uniform shear flow. International Journal of Multiphase Flow 25, 1321-1372.

Mortensen, G.A., Trapp, J.A. 1992. Particle-fluid two-phase flow modeling. Proc. Japan-US Seminar on two-phase flow dynamics, Berkley, USA, 85–102.

Movahedirad, S., Ghafari, M., Dehkordi, A. M., 2012. Discrete Bubble Model for Prediction of Bubble Behavior in 3D Fluidized Beds. Chemical Engineering and Technology, 35, (5), 929–936.

Muñoz-Cobo, J. L., Chiva, S., Ali Abdelaziz, M., Mendez, S., 2012. Simulation of bubbly flow in vertical pipes by coupling Lagrangian and Eulerian models with 3D random walks models: Validation with experimental data using multi-sensor conductivity probes and Laser Doppler Anemometry. Nuclear Engineering and Design, 242, 285– 299.

Narsimhan, G., Gupta, J.P., 1979. A model for transitional breakage probability of droplets in agitated lean liquid–liquid dispersions. Chem. Eng. Sci. 34, 257–265.

Nelson, E., 1967. Dynamical Theories of Brownian Motion, Princeton University Press, Princeton.

Oolman, T.O., Blanch, H.W., 1986. Bubble coalescence in stagnant liquids. Chemical Engineering Communications 43, 237–261.

Pang, M., Wei, J., Yu, B., 2010. Numerical study of bubbly upflows in a vertical channel using the Euler–Lagrange two-way model. Chemical Engineering Science 65, 6215–6228.

Patanker, N.A., Joseph, D.D., 2001. Lagrangian Numerical Simulation of Particulate flows. International Journal of Multiphase Flows, 27, 1685-1706.

Peskin, C.S., 1977. Numerical analysis of blood flow in the heart, Journal of Computational Physics, 25, 220–252.

Pozorski, J., Minier, J. P., 1998. On the Lagrangian turbulent dispersion models based on the Langevin equation, International Journal of Multiphase Flow, 24, 913-945.

Prandtl, L. (1925), "Über die ausgebildete Turbulenz," ZAMM, Vol. 5, pp. 136-139.

Press, W. H., Teukolsky, S. A., Vetterling, W. T., Flannery, B. P., (1996) Numerical recipes in Fortran 90 (second edition): the art of parallel scientific computing. New York, NY, USA: Cambridge University Press.

Press, W. H., Teukolsky, S. A., Vetterling, W. T., Flannery, B. P., (2003) Numerical Recipes in Fortran 77, The Art of Scientific Computing, second edition. Cambridge: Cambridge University Press.

Prince, M.J., Blanch, H.W., 1990. Bubble coalescence and break-up in air-sparged bubble columns. AIChE Journal 36, 1485–1499.

Rüger, M., Hohmann, S., Sommerfeld, M., Kohnen, G., 2000. Euler/Lagrange Calculations of Turbulent Sprays: the effect of droplet collisions and coalescence. Atomization and Sprays, 10, 47-81.

Ross, S.L., 1971. Measurements and models of the dispersed phase mixing process, Ph.D. Dissertation, The University of Michigan, Ann Arbor.

Sagert, N.H., Quinn, M.J., 1976. The coalescence of H2S and CO2 bubbles in water. The Canadian Journal of Chemcial Engineering 54, 392–398.

Sato, Y., Sadatomi, M., Sekoguchi, K., 1981. Momentum and heat transfer in two-phase bubbly flow-I. International Journal of Multiphase Flow, 7, 167-178.

Sato, Y., Sekoguchi, K., 1975. Liquid velocity distribution in two-phase bubble flow. International Journal of Multiphase Flow, 2, 79-95.

Schiller, L. and Nauman, A., 1933. Uber die grundlegende Berechnung bei der Schwekraftaufbereitung. Ver. Deutch Ing., 44, 318-320.

Seldner, D., Westermann, T., 1988. Algorithms for Interpolation and Localization in Irregular 2D Meshes. J. Comput. Phys. 79 (1), 1–11.

Serizawa, A., Kataoka, I., 1987. Phase distribution in two phase Flow. In: ICHMT Int. Seminar on Transient Phenomena in Multiphase Flow. Dubrovnik, Yugoslavia, 179-224.

Serizawa, A., Kataoka, I., 1988. Phase Distribution in Two-phase Flow. Transient

Phenomena in Multiphase Flow. Hemisphere, Washington, DC. 179–224.

Serizawa, A., Kataoka, I., 1994. Dispersed flow I. Multiphase Science and Technology. vol. 8. Begell House Inc., New York. pp. 125–194.

Shams, E., Finn, J., Apte, S. V., 2010. A Numerical Scheme for Euler-Lagrange Simulation of Bubbly Flows in Complex Systems. International Journal For Numerical Methods In Fluids, 67, 1865–1898.

Shinnar, R., Church, J.M., 1960. Predicting particle size in agitated dispersions. Industrial and Engineering Chemistry, 52, 253–256.

Simon, M., 2004. Koaleszenz von Tropfen und Tropfenschw¨ armen, Ph.D. Dissertation, die Teschinschen Universtit ¨ at Kaiserslautern.

Simonin, O., Viollet, P. L., 1988. On the computation of turbulent two-phase flows in the Eulerian formulation. Toulouse, France. EUROMECH, 234.

Smith, B. L., 1998. On the modeling of bubble plumes in a liquid pool. Applied Mathematical Modeling, 22, 773–797.

Smoluchowski, C., 1943. Stochastic Problems in Physics and Astronomy, Rev. Mod. Phys. 15, (1).

Sommerfeld, M., 2000. Overview and fundamentals, in: V.K.I. for Fluid Mechanics, Theoretical and Experimental Modelling of Particulate Flow. Lecture Series No. 2000-6, 2000, pp. 1–62.

Sommerfeld, M., 2001. Validation of a Lagrangian Modelling Approach for Inter-particle Collisions in Homogeneous Isotropic Turbulence. Int. J. Multiphase Flows, 27, 1828–1858.

Sommerfeld, M., Bourloutski, E., Bröder, D., 2003. Euler/Lagrange Calculations of Bubbly Flows with Consideration of Bubble Coalescence. The Canadian Journal of Chemical Engineering, 81(3-4), 508-518.

Spelt, P. D. M., Biesheuvel, A., 1997. On the motion of gas bubbles in homogeneous isotropic flow. J. Fluid Mech. 336, 221–244.

Squires, K., Eaton, J., 1990. Particle response and turbulence modification in isotropic turbulence. Physics of Fluids, A 2, 1191–1203.

Sridhar, G., Katz, J., 1995. Drag and lift forces on microscopic bubbles entrained by a

vortex. Physics of Fluids 7, 389–399.

Sungkorn, R., Derksen, J.J., Khinast, J.G., 2011. Modeling of turbulent gas–liquid bubbly flows using stochastic Lagrangian model and lattice-Boltzmann scheme. Chemical Engineering Science 66, 2745–2757.

Swift, D.L., Friedlander, S.K., 1964. The coagulation of hydrosols by Brownian motion. Journal of Colloid Science 19, 621–647.

Takagi, S., Matsumoto, Y., 1995. Three dimensional calculation of a rising bubble. Proceedings of the Second International Conference on Multiphase Flow, Kyoto Japan, 1, PD2-9-PD2-16.

Takagi, S., Matsumoto, Y., 1998. Numerical study on the forces acting on a bubble and particle. In: Proceedings of the third international conference on multiphase flow, Lyon, France.

Tomiyama, A., 1998. Struggle with computational Dynamics. Third International Conference on Multiphase Flow. ICMF 98. Lyon. France.

Tomiyama, A., 2004. Drag, lift and virtual mass forces acting on a single bubble. Proceedings of the Third International Symposium on Two-Phase Flow Modeling and Experimentation, Pisa, Italy.

Tomiyama, A., Matsuoka, T., Fukuda, T., Sakaguchi, T., 1995a. A simple numerical method for solving an incompressible two-fluid model in a general curvilinear coordinate system. In: Serizawa, A. (Ed.), Advances in Multiphase Flow, Elsevier, Amsterdam, pp. 241–252.

Tomiyama, A., Sou, A., Yoshikawa, H., Sakaguchi, T., 1994a, Three-dimensional detailed numerical simulation of bubbly flow in vertical square duct. Trans. JSME B 60 (576), 2678–2685.

Tomiyama, A., Sou, A., Žun, I., Kanami, N., Sakaguchi, T., 1995b. Effects of Eötvös number and dimensionless liquid volumetric flux on lateral motion of a bubble in a laminar duct flow. Advances in Multiphase Flow. Elsevier, 3–15.

Tomiyama, A., Sou, A., Žun, I., Sakaguchi, T., 1994b. Three dimensional detailed numerical simulation of bubbly upflow in a vertical square duct. KfK-5389. Proc. German-Japanese Symposium on Multiphase Flow, Karlsurhe, Germany, pp. 487–498.

Tomiyama, A., Tamai, H., Žun, I., Hosokawa, S., 2002. Tranverse migration of single

bubbles in simple shear flows. Chemical Engineering Science, 57, 1849-1858.

Tomiyama, A., Žun, I., Higaki, H., Makino, Y., Sakaguchi, T., 1997. A three dimensional particle tracking method for bubbly flow simulation. Nuclear Engineering and Design, 175, 77-86.

Tomiyama, A., Žun, I., Sou, A., Sakaguchi, T., 1993. Numerical analysis of bubble motion with the VOF method. Nuclear Engineering Design 141, 69–82.

Tsouris, C., Tavlarides, L. L., 1994. Breakage and Coalescence Models for Drops in Turbulent Dispersions. AIChE Journal. Vol. 40, (3), 395-406.

Van den Hengel, E. I. V., Deen, N. G., Kuipers, J. A. M., 2005. Application of Coalescence and Breakup Models in a Discrete Bubble Model for Bubble Columns. Ind. Eng. Chem. Res, 44, 5233-5245.

Veenman, M.P.B., (2004). Statistical analysis of turbulent flow. Ph.D. Thesis. University of Eindhoven.

Wachem, B.v., Yu, X., Hsu, T.J., 2010. A 3D Eulerian-Lagrangian Numerical Model for Sediment Transport. 7th international Conference on Multiphase Flow, ICMF 2010.

Wang, L. P., Maxey, M. R. 1993a. The motion of microbubbles in a forced isotropic and homogeneous turbulence. Applied Scientific Research 51, 291–296.

Wang, L., Maxey, M. 1993b. Settling velocity and concentration distribution of heavy particles in homogeneous isotropic turbulence. J. Fluid Mech. 256, 27–68.

Wang, M. C., Uhlenbeck, G. E., 1945. On the Theory of the Brownian Motion II, Rev. Mod. Phys, 17, 323-342.

Wang, S.K., Lee, S.J., Jones Jr., O.C., Lahey Jr., R.T., 1987. 3-D turbulence structure and phase distribution measurements in bubbly two-phase flows. International Journal of Multiphase Flow, 13, 327–343.

Wang, T., Wang, J., Jin, Y., 2003. A novel theoretical breakup kernel function for bubbles/droplets in a turbulent flow. Chem. Eng. Sci. 58, 4629–4637.

Wang, T.F., Wang, J., Jin, Y., 2005a. Theoretical prediction of flow regime transition in bubble columns by the population balance model. Chemical Engineering Science 60, 6199–6209.

Wang, T.F., Wang, J., Jin, Y., 2005b. Population balance model for gas–liquid flows: Influence of bubble coalescence and breakup models. Industrial and Engineering

Chemistry Research 44, 7540–7549.

Wellek, R.M., Agrawal, A.K., Skelland, A.H.P., 1966. Shape of liquid drops moving in liquid media. AIChE J. 12, 854–862.

Westermann, T., 1992. Localization schemes in 2D boundary-fitted grids. J. Comput. Phys. 101 (2), 307–313.

Wilcox, D. C., 1994. "Turbulence Modeling for CFD", DCW Industries, Inc.

Yang, C., Lei, U., 1998. The role of the turbulent scales in the settling of heavy particles in homogeneous isotropic turbulence. J. Fluid Mech. 371, 179–205.

Yao, W., Morel, C., 2004. Volumetric interfacial area prediction in upwards bubbly two-phase flow. International Journal of Heat and Mass Transfer, 47, 307–328.

Zaruba, A., Lucas, D., Prasser, H-M., Höhne, T., 2007. Bubble-wall interaction in a vertical gas-liquid flow: Bouncing, sliding and bubble deformations. Chemical Engineering Science, 62, 1591-1605.

Zhao, H., Ge, W., 2007. A theoretical bubble breakup model for slurry beds or three-phase fluidized beds under high pressure. Chem. Eng. Sci. 62, 109–115.

Ziqi CAI, Yuyun BAO, Zhengming GAO., 2010. Hydrodynamic Behavior of a Single Bubble Rising in Viscous Liquids. Chinese Journal of Chemical Engineering, 18(6) 923—930.

Žun, I., 1985. The role of void peaking in vertical two-phase bubbly Flow. In: Proc. of the 2nd Int. Conf. on Multiphase Flow, London, England, 127-139.

Žun, I., 1998. Transition from wall void peaking to core void peaking in turbulent bubbly flow. Transient Phenomena in Multiphase Flow. Hemisphere, Washington, DC. (1998) 225-245.

Žun, I., Kljenak, I., Moze, S., 1993. Space-time evolution of the non homogeneous bubble distribution in upward flow. Int. J. Multiphase Flow 19, 151–172.

A. Bubbles acceleration for cylindrical coordinates.

At this section, we will describe the form of the bubble acceleration that is used in cylindrical coordinates.

The components of the velocity of the bubble in cylindrical coordinates are denoted by$(u_r, u_\theta, u_z) = (\dot{r}, r\dot{\theta}, \dot{z})$. In order to get the acceleration terms in cylindrical coordinates we get the relation between the Cartesian coordinates and cylindrical coordinates and then make the derivatives in order to get the final acceleration terms.

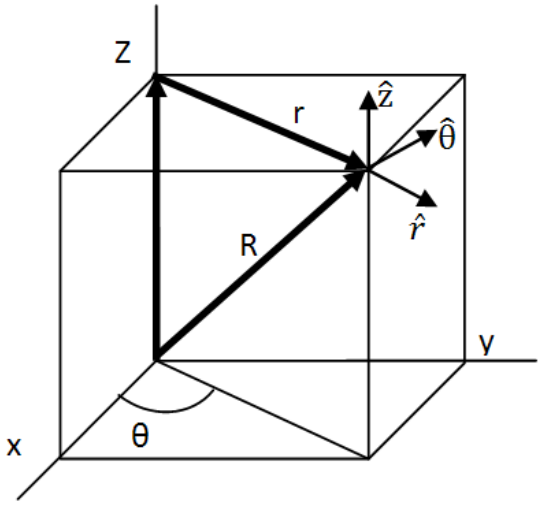

Figure A.1. Point coordinates in cylindrical coordinates system.

Considering the relation between the cylindrical coordinates and the Cartesian coordinates, and from figure A.1, we can write these relations as follows:

$$r = \sqrt{x^2 + y^2} \qquad (A.1)$$

$$\theta = arctan\left(\frac{y}{x}\right) \qquad (A.2)$$

$$z = z \qquad (A.3)$$

We can find the three unit vectors for the cylindrical coordinates as follows:

$$\hat{e}_r = \frac{\hat{r}}{r} = \frac{x\hat{\imath} + y\hat{\jmath}}{r} = \frac{rcos\theta\hat{\imath} + rsin\theta\hat{\jmath}}{r} = cos(\theta)\,\hat{\imath} + sin(\theta)\,\hat{\jmath} \quad (A.4)$$

$$\hat{e}_z = 1$$

$$\hat{e}_\theta = \hat{e}_z \times \hat{e}_r = \begin{vmatrix} \hat{\imath} & \hat{\jmath} & \hat{k} \\ 0 & 0 & 1 \\ cos\,(\theta) & sin\,(\theta) & 0 \end{vmatrix} = -sin(\theta)\,\hat{\imath} + cos(\theta)\,\hat{\jmath} \quad (A.5)$$

And the derivatives for each vector are as follows

$$\frac{d\hat{e}_r}{dr} = 0, \quad \frac{d\hat{e}_r}{d\theta} = -sin(\theta)\,\hat{\imath} + cos(\theta)\,\hat{\jmath}\ , \quad \frac{d\hat{e}_r}{dz} = 0 \quad (A.6)$$

$$\frac{d\hat{e}_\theta}{dr} = 0, \quad \frac{d\hat{e}_\theta}{d\theta} = -cos(\theta)\,\hat{\imath} - sin(\theta)\,\hat{\jmath}, \quad \frac{d\hat{e}_\theta}{dz} = 0 \quad (A.7)$$

$$\frac{d\hat{e}_z}{dr} = 0, \quad \frac{d\hat{e}_z}{d\theta} = 0\ , \quad \frac{d\hat{e}_z}{dz} = 0 \quad (A.8)$$

Also we will need the time derivative of the three coordinates. Using the chain rule for derivation, the time derivatives will be as follows:

$$\dot{\hat{e}}_r = \frac{d\hat{e}_r}{dr}\frac{dr}{dt} + \frac{d\hat{e}_r}{d\theta}\frac{d\theta}{dt} + \frac{d\hat{e}_r}{dz}\frac{dz}{dt} = \dot{\theta}\hat{e}_\theta \quad (A.9)$$

$$\dot{\hat{e}}_\theta = \frac{d\hat{e}_\theta}{dr}\frac{dr}{dt} + \frac{d\hat{e}_\theta}{d\theta}\frac{d\theta}{dt} + \frac{d\hat{e}_\theta}{dz}\frac{dz}{dt} = -\dot{\theta}\hat{e}_r \quad (A.10)$$

$$\dot{\hat{e}}_z = \frac{d\hat{e}_z}{dr}\frac{dr}{dt} + \frac{d\hat{e}_z}{d\theta}\frac{d\theta}{dt} + \frac{d\hat{e}_z}{dz}\frac{dz}{dt} = 0 \quad (A.11)$$

Velocity and acceleration derivation

As the principal position vector of the point under consideration is $\hat{R}$ as shown at figure A.1, can be expressed as:

$$\hat{R} = r\hat{r} + z\hat{z} \quad (A.12)$$

Then the velocity vector can be expressed as

$$\hat{U} = \dot{\hat{R}} = (\dot{r}\hat{e}_r) + (\dot{z}\hat{e}_z) = \dot{r}\hat{e}_r + r\dot{\hat{e}}_r + \dot{z}\hat{e}_z + z\dot{\hat{e}}_z$$

$$= \dot{r}\hat{e}_r + r\dot{\theta}\hat{e}_\theta + \dot{z}\hat{e}_z \qquad (A.13)$$

The velocity components at the three directions will be expressed as :

$$U_r = \dot{r}, \qquad U_\theta = r\dot{\theta}, \quad U_z = \dot{z} \qquad (A.14)$$

And the acceleration vector will be as follows:

$$\hat{a} = \dot{\hat{V}} = \ddot{r}\hat{e}_r + \dot{r}\dot{\hat{e}}_r + r\ddot{\theta}\hat{e}_\theta + \dot{r}\dot{\theta}\hat{e}_\theta + r\dot{\theta}\dot{\hat{e}}_\theta + \ddot{z}\hat{e}_z + \dot{z}\dot{\hat{e}}_z =$$

$$= \left(\ddot{r} - r\dot{\theta}^2\right)\hat{e}_r + \left(r\ddot{\theta} + 2\dot{r}\dot{\theta}\right)\hat{e}_\theta + \ddot{z}\hat{e}_z \qquad (A.15)$$

The acceleration components at the three directions will be expressed as :

$$a_r = \ddot{r} - r\dot{\theta}^2, \qquad a_\theta = r\ddot{\theta} + 2\dot{r}\dot{\theta}, \quad a_z = \ddot{z} \qquad (A.16)$$

Then the final expression of the velocity time derivative can be expressed as follows:

$$\frac{d\hat{U}}{dt} = \left(\frac{dU_r}{dt} - \frac{U_\theta^2}{r}\right)\hat{e}_r + \left(\frac{dU_\theta}{dt} - \frac{U_r U_\theta}{r}\right)\hat{e}_\theta + \frac{dU_z}{dt}\hat{e}_z \qquad (A.17)$$

So, we can find that each the components of acceleration at $\hat{e}_r$ and $\hat{e}_\theta$ directions have excess terms that should be considered when calculating the acceleration as a function of the velocity variation.

B. Data Structure

In this appendix, we will present the data structure used in the Lagrangian framework and the data structure of the common data that is used in both Euelrian and Lagrangian codes.

B.1 Lagrangian variables

Some of the Lagrangian variables are important to be stored for both one way and two way coupling processes. And others will be important for two-way coupling only. So we will divide the variables of the particle to Basic variables and secondary variables. We will start exploring the basic variables and then the secondary ones. The basic data types are:

- The bubble identifier id_p: this integer number is used to label the particle during the hole simulation and is necessary for tracking the bubble during the integration among different time steps. It is considered as a basic data type.

- The bubble cell number Bcell(:): it is an integer array of a dimension equal to the total number of particles in the domain. This variable identify the cell index at which the bubble is located. This variable is changed each time step after the re allocation of the bubble.

- The bubble position Coo_cyl(:,3): it is a real type array of dimensions $N_{particles} \times 3$ to store the position of the particle in the cylindrical coordinates r, θ, z respectively. This array is updated each time step of the simulation. It is considered a secondary variable that is important in the two way coupling and one way coupling with collision consideration.

- The bubble velocity vg(:,3): this array is a real type with dimensions $N_{particles} \times 3$ to store the velocity of the bubble at cylindrical coordinates v_r,v_θ, v_z. this array is updated also each time step of the simulation. It is also a secondary type data that is important only for use in two way coupling process and one-way coupling with collision consideration.

- The bubble diameter d_b( ) : this array is a real type of dimension $N_{particles}$ that stores the diameter of each particle in the domain. This array is modified each time step depending on expansion that will happen to the bubble due to the change of height. This is a secondary data type.

- The particle fluctuation velocity vfedd(:,3): this is a real type of dimensions $N_{particles}\times 3$. In this array, the fluctuating velocity components for each bubble in cylindrical coordinates V_f^r, V_f^θ and V_f^z. This is because the CRW model uses the past value of fluctuating velocity to generate the present one.

- The Bubble Neighbor list bubblenbr(:,:): this is an integer data type of dimensions $N_{particles}\times 300$. In this array, we store the neighbor bubbles of each bubble to save the time required for calculating the collision between each bubble and all the others in the domain. In this array we store only the bubble which are in a constant distance from the bubble under consideration. The second dimension of the array which is 300 in our case and the distance at which neighbors are specified are dependent on each case. This array is considered as a secondary data type.
- The cells Neighbor lists Cellnbrs(:,),Cellnbrs2(): these are integer arrays of dimensions of $N_{cells}\times 26$ and $N_{cells}\times 98$ respectively. The first one Cellnbrs() is used to store the first level of the cell neighbor for each cell in the domain which are 26 neighbor cells, and the second one Cellnbrs2() is used to store the second level of cell neighbors which are 98 neighbor cells as can be seen in figure 2.17. These arrays are created only in the start of all the simulation and then used in re allocating the bubbles in the cells for which the cell of the last time step is known. This is a secondary variable. The number of neighbors is related to the type of mesh that we are using which is shown in figure 2.16.

B.1.1 Data structure applied for bubbles coalescence

In the coalescence process, we consider that when coalescence take place between two bubbles of indexes i and j. then the bubbles of the higher index from i and j is deleted from the list of real bubbles and the other bubbles index stores the data of the new bubble resulting from the coalescence process. The arrays used for this purpose are:

- Deleted(): this array stores the indexes of the deleted bubbles due to the coalescence process in order to re use it on the program not to account for the bubbles of these indexes
- Coal_new(:,2): this array contains number of rows equal to the number of the deleted bubbles due to the coalescence process, and contains two columns. The array stores the in the first column Coal_new(:,1) the index of the bubble resulting from the coalescence process, and in the second column Coal_new(:,2) it stores the time duration for the coalescence process to take place. This is important for us as we consider the real times for the coalescence duration and not to permit further breakups or coalescences for the bubbles that already did not finalize the coalescence process.

B.1.2 Data structure applied for bubbles breakup

In the breakup process, we consider that the bubble under breakup will produce only two daughter bubbles. The index of the first one will be the same as the mother bubble. The index of the second daughter bubble will be a new one that is greater than the total number of real bubbles by one. The array used for handling this process is:

- Added_b(:,3): this array contains number of rows equal to the number of the added bubbles due to the breakup process, and contains three columns. At the first column, the index of the mother bubble is stored which will be the same as one of the daughter bubbles. At the second column, the index of the other daughter bubbles is stored, and at the third column, the time duration of the breakup process is stored in order to use it in no permitting further breakups or coalescences for the bubbles that already did not complete the breakup process.

B.2 Common data variables

The common data variable are the variables which are used in both solvers Lagrangian and Eulerian one for the purpose of interaction source terms in the two way coupling process. These variables are:

- The cell momentum sources soru(), sorv(), and sorw(): these are real variables of dimension N_{cells}. This three variables are updated each Lagrangian time step and collision time step to account for the effect of the bubbles on the momentum of the continuous phase as explained in the two-way coupling process. After completing one Eulerian time step, these source terms are added to the momentum equation of the continuous phase and solve it for the new variation of momentum

- The cell void fraction sorvf(): the same dimension as the momentum source terms. This variable is used for calculating the volume of the cell available for calculation as the cell contains a bubble or a portion of it. Also it is calculated each time step smaller than the Eulerian one, and when reaching the Eulerian time it is multiplied by the density of the terms in the momentum and turbulent energy equations.

- The cell turbulent kinetic energy K and dissipation rate ε sources sork(), sorEps(): these arrays have the same dimension as the momentum source terms. These are the source terms added for the conservation equations of the k and ε respectively.

Publications from the present research

Participations in conferences

José L. Muñoz-Cobo, Sergio Chiva, Santos Mendez, Mohamed Ali Abdelaziz, coupled lagrangian and eulerian simulation of bubbly flows in vertical pipes: validation with experimental data using multi-sensor conductivity probes and laser doppler anemometry, CFD4NRS-3, Septembre 14-16, 2010, Bathesda, Maryland, USA.

José L. Muñoz-Coboa, Sergio Chiva, Mohamed Aliabdelaziz Essaa, Santos Mendez. 2011, simulation of bubbly flow in vertical pipes by coupling lagrangian and eulerian models with 3d random walks models: validation with experimental data using multi-sensor conductivity probes and laser doppler anemometry, NURETH-14, Toronto, Ontario, Canada, September 25-30, 2011.

Publications in Journals

José L. Muñoz-Cobo, Sergio Chiva, Mohamed Ali Abd El Aziz Essa, Santos Mendez, simulation of bubbly flow in vertical pipes by coupling lagrangian and eulerian models with 3d random walks models: validation with experimental data using multi-sensor conductivity probes and laser doppler anemometry, Nuclear Engineering and Design, 242 (2012) 285–299

José L. Muñoz-Cobo,, Sergio Chiva, , Mohamed A. Abdelaziz, Santos Mendez , "Experiments performed with bubbly flow in vertical pipes at different flow conditions covering the transition region: simulation by coupling Eulerian, Lagrangian and 3D random walks models", archives of thermodynamics Vol. 32(2012), No. 1, 163–199.

José L. Muñoz-Cobo, Sergio Chiva, Mohamed Ali Abd El Aziz Essa, Santos Mendez , tracking of bubble trajectories in vertical pipes in bubbly flow regime by coupling lagrangian, eulerian and 3d random walks models: validation with experimental data, Jornal of computational Multiphase flows, vol. 4 (under publication).